Author:
Branfoot, Callum

Title:
Covalent adaptable networks

from dynamic bonds to sustainable composites

Covalent Adaptable Networks: from Dynamic Bonds to Sustainable Composites

Callum Branfoot

Department of Aerospace Engineering

University of Bristol

May 2021

A dissertation submitted to the University of Bristol in accordance with the requirements for award of the degree of Doctor of Philosophy in the Faculty of Engineering.

Word count: 78500

Abstract

In this thesis, covalent adaptable networks (CANs) are investigated as novel matrices for fibre-reinforced polymer composites (FRPs). A new generation of previously reported Diels-Alder epoxies are prepared and extensively characterised (Chapter 2). These materials are then used to prepare GFRP laminates via a vacuum-assisted compression moulding technique, imbuing them with functionality courtesy of the intrinsic dynamic chemistry (Chapter 3). These composites are characterised and tested in terms of healing and recycling with a view to creating more sustainable composites. Two additional sub-projects concerning diselenides (Chapter 4) and diphosphanes (Chapter 5) are also investigated to explore the viability of these dynamic chemistries as more reactive alternatives to disulfides (in CANs). Chemical synthesis and mechanistic investigations dominate both of these chapters, although some preliminary investigations concerning new diselenide-containing polymers are introduced in the former.

Acknowledgements

First of all I would like to give my special thanks to my primary supervisors, Ian Bond and Paul Pringle for their generous support over the last four years, we got there in the end. That you both found the time to provide so much support despite the heavy workloads has not gone unnoticed. Thanks also to my secondary supervisors, Duncan Wass and Tim Coope for their assistance particularly in the early stages of this work. My gratitude also extends to Hartmut Fischer and Henk van Bracht for hosting me in Eindhoven and facilitating the Diels-Alder sub-project. Thanks also to Ian Hamerton as my annual reviewer for providing valuable insights.

The interdisciplinary nature of this PhD thesis means there are a large number of support staff to whom I must also extend my gratitude at the University and beyond: Tony Rogers (Chem), Paul Lawrence (Chem), Paul Gates (Chem), Ian Chorley (Eng), Steve Rae (Eng), Kris Avery (NCC) and the Faculty of Engineering workshop technicians.

My thanks also extend to Rob Iredale for the advice and support in my early years as a fellow chemist in engineering and also to Rich Wingad for the chemistry tips way back at the beginning; I know all the Pringles felt the loss when you moved with Duncan to Cardiff.

Thanks to my Manor Park boys Riccardo Mega and Kilian Grübler for the comradery at home, to the lads from football, to everyone from Karate (particularly Sensei Smiley), to Lourens Blok and Hugh Hamilton for the Squash—all things to take the edge off the long days in the lab. My thanks also extend to all my friends and family, and to Elis James, John Robins & Dave Masterman, for providing the top quality content that has helped to make it all seem worthwhile!

Thanks to all of the Pringles past and present, for suffering me through the years: to Adam for teaching me the way of phosphorus chem. To the hoarder Wise Dan, that you still enjoy synthetic chemistry after all these years is testament to your positive attitude; apt that you managed to get your thesis finished first. To Ailis and Lexy, my thanks for taking me under your collective wing. To Ash, you have been, and continue to be ridiculous, thank you! To Sarah and the Nut, my thanks for putting up with my crap for so long—it is greatly appreciated. To Tim, Hubert, Charly, Daniel, Krishna, and more recently Derek and Maddie, thank you too. Finally, to Rachel Doyle/Lamb, thanks for being there for me, both literally there, one whole fumehood away through most of my PhD, and emotionally there, even through all of *your* early year tears. How you could put up with me from such close range is truly something, you have been a great help and are undoubtedly a better chemist than me!

Author’s declaration

I declare that the work in this dissertation was carried out in accordance with the requirements of the University's *Regulations and Code of Practice for Research Degree Programmes* and that it has not been submitted for any other academic award. Except where indicated by specific reference in the text, the work is the candidate's own work. Work done in collaboration with, or with the assistance of, others, is indicated as such.

Any views expressed in the dissertation are those of the author.

SIGNED:  DATE: 04/05/2021

Table of contents

List of figures, schemes and tables

Chapter 1

Chapter 2

Chapter 3

Chapter 4

Chapter 5

Chapter 6

List of abbreviations

[BnSe]$_2$ – dibenzyl diselenide

[BuSe]$_2$ – di-*n*-butyl diselenide

[PhSe]$_2$ – diphenyl diselenide

12plyDA0.5 – GFRP prepared from 12 plies of crossply standard weave glass fabric and DA0.5

1MI – 1-methylimidazole

3pb – three-point bending

4pb – four-point bending

8plyDA1 – GFRP prepared from 8 plies of crossply standard weave glass fabric and DA1

A$_2$ – tetraphenyldiphosphane

ADS – aniline diselenide

AE – 1,1-diphenyl-2,2-di-o-tolyldiphosphane

APCI – atmospheric pressure chemical ionisation

APDS – aminopropyl diselenide

aq. – aqueous

Ar$_2$P• – phosphinyl radical

b.p. – boiling point

B$_2$ – tetra(*p*-tolyl)diphosphane

BCA – biscitraconamic acid

BCI – biscitraconimide

BDE – bond dissociation energy

BII – bisitaconimide

BMC – bulk moulding compound

BMI – bismaleimide

BMI1 – 1,1‘-(methylenedi-4,1-phenylene)bismaleimide

BMI2 – N,N’-(4-methyl-m-phenylene)-bismaleimide

BMI3 – 3,4’-bismaleimidodiphenyl ether

BnSeBn – dibenzyl selenide

BOC – *tert*-butyl carbamate

BOCDS – BOC-diselenide

BVID – barely visible impact damage

C1 – first cooling cycle

C$_2$ – tetra(*p*-anisyl)diphosphane

CAI – compression after impact

CANs – covalent adaptable networks

CDS – [3,3’-diselanediyldipropionic acid]

CF – carbon fibre

CFRP – carbon fibre reinforced polymer

CI – chemical ionisation

CTE – thermal expansion coefficient

Ctrl1 – control epoxy 1

Ctrl2 – control epoxy 2

D$_2$ – bis(3,5-trifluoromethl(phenyl)diphosphane

DA – Diels-Alder

Da – Dalton

DA0.5 – Diels-Alder polymer 0.5

DA1 – Diels-Alder polymer 1

DA2 – Diels-Alder polymer 2

DA3 – Diels-Alder CAN prepared from PreDA1 and BMI3

DAN – 1,8-diaminonaphthalene

DCB – double cantilever beam

DCC – dynamic covalent chemistry

DCM – dichloromethane, CH_2Cl_2

DCNPs – dynamic covalent network polymers

DCPD – dicyclopentadiene

DFT – density functional theory

DGEBA – digylcidyl ether of bisphenol A

DGGO – N,N-diglycidyl-4-glycidyloxyaniline

DI – deionised

DMA – dynamic mechanical analysis

DMF – dimethylformamide

DMSO – dimethylsulfoxide

DSC – differential scanning calorimetry

DTDA – dithiodianline

E' – storage modulus

E'' – loss modulus

E_2 – tetra(*o*-tolyl)diphosphane

E_A – activation energy

EDA – ethylene dianiline

EDG – electron donating group

EG – ethylene glycol

EI – electron ionisation

EMAA – ethylene methacrylic acid

EOL – end-of-life

EpxSeSe1 – the polymer prepared from APDS and DGEBA

EpxSeSe2 – the polymer formed from reaction of BOCDS and DGEBA

EpxSeSe3 – the polymer formed from reaction of CDS and DGEBA

EpxSS1 – the disulfide CAN prepared from DTDA and DGEBA

EpxSS2 – the polymer formed from reaction of dithiopropionic acid, citric acid and DGEBA

eq. – equivalents

eqm. – equilibrium

ESI – electrospray ionisation

Et_2O – diethyl ether

EtOAc – ethyl acetate

EtOH – ethanol

EWG – electron withdrawing group

FMOC – fluorenylmethyl carbamate

FRP – fibre-reinforced polymer composite

FTIR – Fourier-transform infrared spectroscopy

GFRP – glass fibre–reinforced polymer

GPC – gel permeation chromatography

H1 – first heating cycle

H2 – second heating cycle

HDCN – hemiaminal dynamic covalent network

HGFs – hollow glass fibres

HOMO – highest occupied molecular orbital

HP – homopolymerisation

HR-MS – high resolution mass spectrometry

HT – high temperature

K – equilibrium constant

LUMO – lowest unoccupied molecular orbital

m.p. – melting point

m/z – mass to charge ratio

MeOH – methanol

MALDI – matrix-assisted laser desorption/ionisation mass spectrometry

MC – microcapsule

M_n – number average molecular weight

MOM – methoxymethyl ether

MS – mass spectrometry

MW – molecular weight

M_w – weight average molecular weight

NaO^{t}Bu – sodium *tert*-butoxide

NaSEt – sodium ethanethiolate

nbd – norbornadiene

NBS – N-bromosuccinimide

^{n}BuLi – *n*-butyllithium

NCC – National Composites Centre

NHC – N-heterocyclic carbene

NMR – nuclear magnetic resonance

NOE – nuclear Overhauser effect

obs. – observed

OOA – out of autoclave

PA – polyamide

PDI – polydispersity index (**Đ**, dispersity)

PEDS – phenolethyl diselenide

PEEK – polyether ether ketone

PES – polyethersulfone

PET – polyethylene terephthalate

PGMEA – propylene glycol monomethyl ether acetate

PhMe – toluene

PI – polyimide

PLA – poly(lactic acid)

ppm – parts per million

PreDA0.5 – Diels-Alder prepolymer 0.5

PreDA1 – Diels-Alder prepolymer 1

PreDAx – Longer-chain Diels-Alder prepolymer

PreDAy – thiol end-capped Diels-Alder prepolymer

PS – polystyrene

PTFE – poly(tetrafluoroethene)

***p*-TsOH** – *para*-toluenesulfonic acid

PU – polyurethane

rDA – retro Diels-Alder

ROMP – ring-opening metathesis polymerisation

RS• – sulfanyl radicals

RSeH – selenol

RSeR – selenide

RSeSeR – diselenide

RSeSeSeR – triselenide

RSeSeSeSeR – tetraselenide

RT – room temperature

RTM – resin transfer moulding

S_0 – ground state

S_1 – first singlet state

S_2 – second singlet state

SBS – short beam shear

SD – standard deviation

SEC – size-exclusion chromatography

SEM – standard error of the mean

SH – self-healing

SHM – structural health monitoring

SMC – sheet moulding compound

T_1 – longitudinal relaxation time

T_1 – first triplet state

TBAF – tetrabutylammonium fluoride

TBD – triazabicyclodecene

TEMPO – (2,2,6,6-Tetramethylpiperidin-1-yl)oxyl

T_{end} – end temperature

TFA – trifluoroacetic acid

T_g – glass transition

THF – tetrahydrofuran

T_m – melt temperature

TM – transition metal

TMSBr – trimethylsilyl bromide

TMSCl – trimethylsilyl chloride

TMSI – trimethylsilyl iodide

TOF – time-of-flight

T_{on} – onset temperature

TRL – technology readiness level

TTBP – 2,4,6-tri-*tert*-butylphenol

T_v – topological freezing temperature

VACM – vacuum assisted compression moulding

V_f – fibre volume fraction

VT – variable temperature

η – healing efficiency

-ve – negative

+ve – positive

Chapter 1: Background and introduction

1.1 Motivation

Conventional fossil-fuel based polymer composites are intrinsically unsustainable: in their manufacture high-energy processes are required and the presence of defects and offcuts leads to waste material. The inherent brittleness of composites and their sensitivity to defects can also lead to reduced durability and service life. Furthermore, the vast majority of composites components currently use thermoset polymer matrices, and as such, are either subject to landfill or incineration at end-of-life. In combination, these features make fibre-reinforced polymer composites (FRPs) less sustainable than they could be. By exploiting dynamic chemistry, covalent adaptable networks (CANs) present an opportunity to create more sustainable thermoset-like polymers and composites.

1.2 Fibre-reinforced polymer composites

1.2.1 Background

Fibre-reinforced polymer composites are materials comprising a polymer matrix with fibre reinforcement. The matrix may feasibly be any polymer capable of transferring load between the fibres; both of the major categories of polymer—thermoset and thermoplastic—are widely used. The key prerequisites are fibre adhesion and the inherent mechanical properties of stiffness, strength and toughness. The reinforcement (fibre) has historically been one of carbon, glass or aramid (such as Kevlar®), though mineral fibres such as basalt have also been used,[1] and sustainable plant-based fibres including hemp,[2,3] flax,[4–6] and jute,[7,8] are now the subject of substantial interest.[9] Moreover, combinations of different fibre types have also demonstrated their utility.[10–12] FRPs are generally used as either semi-structural or structural, load-bearing materials, typically in high performance applications. High performance FRPs fall within the category of so-called ‘advanced composites’ which are usually defined as having a high fibre volume fraction (>50%) and continuous fibres, though the use of short fibre FRPs is common in less demanding, semi-structural applications.[13] Furthermore, several researchers have recently demonstrated the potential of highly aligned short fibres to compete with the mechanical performance of conventional continuous fibre composites.[14–18]

High performance FRPs and advanced composites are important structural materials because they exhibit extremely high specific stiffness and strength.[19] Consequently, FRPs are ideal for weight-critical applications. Beyond strength and stiffness, the versatility in terms of design space (fibre type, fibre orientation, matrix type etc.) affords an additionally advantageous level of application-specific tailorability.

The aerospace sector has been the major driving force behind the development and implementation of FRPs. Modern passenger aircraft are one of the major applications of FRPs, with composites taking an ever-increasing share of airframe mass, as exemplified by the Airbus A350 XWB, which is purportedly >52% carbon fibre.[20] Use of composites by the automotive industry has traditionally been limited to (low production volume) high performance sports cars where the high material cost can be justified.[21–24] However, in recent years—in no small part due to emissions-reducing legislation from the EU, US and others—there has been a significant drive towards 'lightweighting' the automotive industry, which in turn has led to increased composites deployment in more mainstream vehicles.[25] Lightweighting is the main driving force behind the use of composites more generally; it is the act or process of replacing conventional materials and structures with lower mass alternatives. Using the automotive example, a more lightweight vehicle can expect greater overall efficiency: reduced fuel consumption, increased range and increased performance.[26] Today, FRPs also find significant utility in marine structures,[27] sports equipment,[28] and energy applications, most notably in wind turbines,[29] where the push towards increasing blade size has necessitated the use of extremely high stiffness-to-weight ratio materials; hence the widespread adoption of high performance CFRP.

Despite recent success and signs of substantial growth in uptake,[30] FRPs are not without their drawbacks. Chief among these is the often-quoted low toughness (brittleness) of composites, which in combination with poor transverse (out-of-plane) mechanical properties (a function of their laminated configuration), makes composites susceptible to damage which can result in their premature failure. Furthermore, in addition to often being expensive and complicated to manufacture,[31] FRPs are also notorious for their limitations in the context of repair[32] and recycling.[33]

1.2.2 Sustainability and the composite lifecycle

From cradle-to-grave, the lifecycle of a typical FRP structure can be separated into four major categories: materials, manufacture, service and end-of-life. Each category is associated with its own challenges surrounding sustainability and ongoing research designed to improve the situation.

Materials. Typically, the polymer matrix starts life from oil-derived precursors. This is also true of some reinforcement fibres, notably aramids and carbon, though glass fibres are a major exception. Most of these materials, particularly the fibres, require highly energy-intensive processes to give the finished product. The dependency on oil and high-energy processes has led to considerable research into alternative bio-derived fibres and bio-derived (green) resins.[34–37] This is set against a backdrop of wider research into the use of greener feedstocks in the chemical industry,[38] which show great potential for increasing composite sustainability and reducing the environmental impact associated with the

constituent materials. In addition, the transportation of all the materials involved is another factor to be considered in the sustainability of this part of the composite lifecycle (and each of the other stages).

Manufacture. All FRP materials and structures involve multiple manufacture stages—in which the composite is formed from its constituent materials. These are the processes involving the moulding, manufacture and machining of the composite, as well as its assembly into the final structure. A wide variety of manufacturing processes are used to prepare composites, which can be broadly separated into traditional autoclave, prepreg-based (pre-impregnated composite ply) processes and so-called 'out-of-autoclave' (OOA) processes. These OOA processes cover a huge variety of different techniques, from pultrusion and filament winding to resin transfer moulding and additive manufacturing.[39–41] One commonality amongst all of these processes is that they require a heating step and often consolidation by applying pressure, and both of these processes can require significant energy expenditure. Each of these manufacturing techniques, also results in material waste, ranging from small off-cuts (from machining) to entire scrapped parts (due to manufacturing defects). This is a particular problem in thermoset polymer composites because they cannot be reprocessed: there is only one chance to get it right. Both of these factors (energy and material wastage) are major concerns and motivations in composites manufacture.

In service. In service contributions to the composite lifecycle include transportation, maintenance and repair. The key sustainability factor here is the combination of damage susceptibility and inefficient repair, which can result in significant waste material, both from scrapped parts and from replacement of damaged material. Maintenance and inspection (looking for damage) are also labour intensive and thus indirectly reduce the efficiency of the composite's lifecycle. Accordingly, there is significant ongoing research into composite repair (discussed at length in Sections 1.2.3 and 1.3) and damage inspection, notably in the form of structural health monitoring (SHM).[42–45]

End-of-life. Numerous end-of-life (EOL) treatments for FRPs exist including incineration, pyrolysis, hydrolysis, chemical recycling and milling. However, many of these processes recover fibres but not the polymer matrix, instead resorting to burning the polymer as a fuel. Worse still, most composite is simply discarded in landfill. Pyrolysis, hydrolysis, chemical recycling and milling can produce 'useful' products for reuse, although they only account for a relatively small proportion of FRP end-of-life. Furthermore, most of these processes require further processing steps before the resulting product is ready for reuse. Even when the composite is recycled into useful products, these are usually unsuitable for replacing the pristine/virgin material and are instead used in lower grade applications. Currently, composite recycling and EOL processing is in its infancy and is one of the major impediments to the

wider employment of composite materials.[46,47] Composite recycling will be reviewed in more detail in Section 1.4.

In summary, the key sustainability challenges include non-renewable constituent materials (both matrix and reinforcement), scrap material from manufacture, scrap material due to damage, down time (from damage inspection) and non-recyclability (EOL), Figure 1.1.

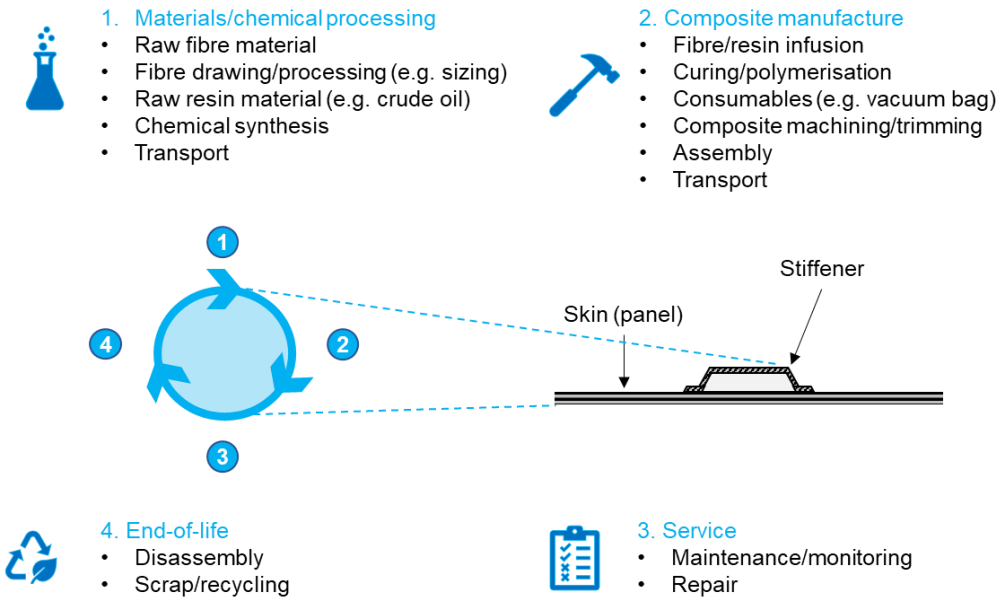

Figure 1.1. The lifecycle of a simple FRP (skin-stiffener) structure.

1.2.3 Composite damage and repair

Since the aerospace industry has pioneered the large-scale usage of composites, it is predominantly aircraft which feature in the literature surrounding composite damage and repair,[32,48–50] though much of the research and methodology may be equally applicable to other large in-service structures where part replacement is either very costly or impractical, e.g. ships and wind turbines.

Courtesy of their heterogeneity and anisotropy, the damage and failure behaviour of FRPs is complex; simply put, the fibres, matrix, interface and any combination thereof can be damaged in multiple ways and at multiple length scales from any single initiation event. Impacts (e.g. collisions, dropped tools and bird strikes) are the most common mechanism of damage initiation, but this mechanism can and does result in a complex combination of damage types, including surface blistering and puncturing, matrix microcracking, delamination, internal voids, holes and fibre breakage, see Figure 1.2. Critically, many impact events can result in so-called 'barely visible impact damage' (BVID), where much of the damage is invisible to the naked eye.[51,52] Naturally, this results in significant challenges associated with damage detection, though this is beyond the scope of this research. Aside from impacts, much of the damage to composite structures originates from manufacturing defects (e.g. porosity/voids, fibre

misalignment and microcracking from machining),[53] or environmental conditions such as rain erosion.[54]

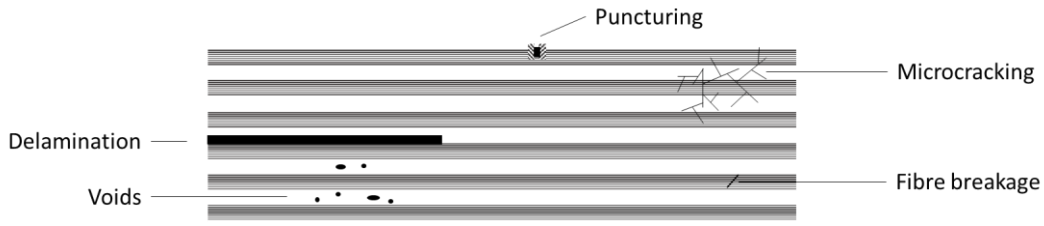

Figure 1.2. The common damage categories of FRPs.

Generally, the objective of repair in any structural part is to restore mechanical performance to as-designed levels and ideally restore any further functionality (such as aerodynamic profile) in the most robust and cost-effective manner possible. Historically, this has most often been achieved with the use of composite patches. These patches can take a variety of forms but most commonly fall into the three categories of scarf (including stepped scarf), single- and double-sided doubler, Figure 1.3.[50] Scarf joints are often the preferred joint for patch repair, since they result in a load distribution which most closely follows the original structure, and have the additional advantage that with a minimum of extraneous material, they tend to have a minimal effect on the aerodynamic profile of lifting surfaces. However, such repairs require the removal of relatively large volumes of undamaged material in order to achieve the large length-to-depth ratios required for an efficient scarf joint, to minimise shear and peel stresses.[49] Doublers are generally a much quicker and simpler type of patch to use, primarily because they do not require the removal of material from the original structure. However, in contrast to scarfing, a significant amount of material is added on top of the original composite surface and this results in both a poor aerodynamic profile and some loading eccentricity. Double-sided doublers can improve on single-sided doublers to an extent by mitigating this eccentricity, better balancing the load distribution; however, it is often impossible to access both laminate surfaces within a built-in structure. Ergo, in many cases double-sided doublers cannot be used.

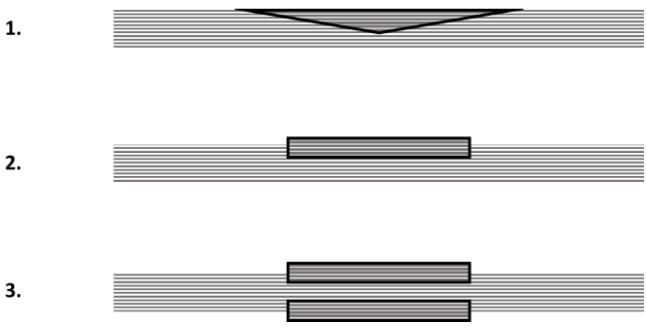

Figure 1.3. Patch repair in FRPs. 1 – scarf, 2 – single doubler and 3 – double doubler.

There are multiple methods of using any one of these patches dependent upon the type of material and processing conditions used. Hard patches, where composite (often prepreg) is pre-cured and then affixed to the joint can be used, as well as uncured (β-staged) prepreg or even wet lay-ups. Generally, prepreg repairs are preferred when an autoclave is available for curing since this usually results in a maximum of fibre volume fraction and minimum of porosity (void volume). However, in many circumstances, particularly with large structures while in service, autoclaves are often not available or indeed practical. This may necessitate the use of wet lay-ups which are typically associated with inferior mechanical performance (due to void content and low V_f). With hard patches there is the additional consideration of attachment mechanism. Mechanical fasteners (bolts) are widely used in large structures with thick laminates, though must be avoided in thin laminates—where the stress concentration associated with the holes is particularly significant.[48,49]

These patching methods can be highly effective,[50,52] in some cases purportedly fully restoring mechanical performance. However, the most effective processes are expensive by virtue of equipment costs and being both labour intensive and time consuming. One of the most mature alternatives to patching is liquid resin injection/infiltration.[32,55] This process involves injecting low viscosity resin into pre-drilled holes within a damaged area of composite, it is typically performed under vacuum which helps to close fracture surfaces and help resin infiltration. The part may be pre-heated to further aid infiltration. When infiltration is complete the resin is cured in place. Although arguably still not a straightforward process, resin injection is generally considered to be simpler and cheaper than patching methods, Figure 1.4. Resin injection repair relies upon the fact that most damage to composite parts is low-energy impact damage, where low-energy is broadly <10 J, though this is not strictly defined; some authors define up to 30 J as 'low energy'.[56] Low-energy impacts typically result in minimal fibre damage: the dominant forms of damage here are matrix cracking and delamination, which—in contrast to fibre damage—can be repaired through 'manipulation' of the matrix. Matrix manipulation in this case simply means the addition of more resin/matrix. Accordingly, this type of repair is touted as having greater potential in the automotive sector where due to the high volumes of parts involved, speed and cost of repair are more likely to encourage compromise with respect to mechanical performance.[57] This is in contrast to aerospace, which has strict certification protocols that currently prevent the use of such repair processes. Beyond resin injection, much of the modern research into alternative composite repair methods concerns bestowing a degree of 'self-healing'.

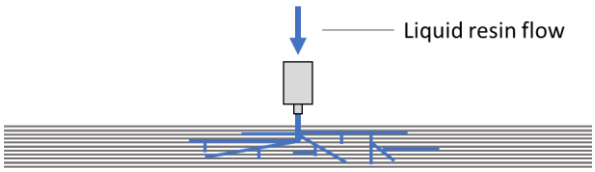

Figure 1.4. Resin injection repair of FRPs. Liquid resin infiltrates cracks with a composite laminate and is cured *in situ*.

1.3 Self-healing FRPs

This section extensively cites the 2018 paper in *Advanced Materials: Interfaces*, 'Progress in Self-Healing Fiber-Reinforced Polymer Composites', written by this author and co-workers.[58]

1.3.1 Background

Biological structures and materials are subject to damage and wear in much the same fashion as manmade materials. However, materials from nature tend to exhibit an ability to repair themselves, as exemplified by the repair of bone.[59] Inspired by nature, the concept of self-healing (SH) has been developed by researchers over the last few decades as an *in situ* repair method, part of the wider push towards so-called 'smart materials'. The principal goal of SH is demonstration of fully autonomous damage recovery. That is, after a structure is damaged it is capable of 'sensing' and responding in such a way that the original mechanical performance of the structure is fully restored. In practice, few SH materials have been demonstrated that are capable of full recovery after significant damage, with even fewer (if any) achieving this in a truly autonomous manner—i.e. recovery with no external intervention. Accordingly, non-autonomous self-repair systems often fall under the SH umbrella. A more practical definition of SH materials is 'materials which are designed to be repaired with minimal (reduced) human intervention'.

Due to their poor out-of-plane properties and low fracture toughness, FRPs are easily damaged. Since repair can be both complex and expensive, FRPs are ideal candidates for applying a SH concept. A variety of SH technologies have been developed by researchers during the last 20 years and each broadly falls within one of two major classifications: extrinsic or intrinsic. Extrinsic SH systems are implemented via the incorporation of additional functional materials or structures within the laminates. After a damaging event, rupture of the additive structures (microcapsules, hollow fibres, vasculature etc.), leads to the release of entrained fluids (e.g. liquid monomer) which fill the fractures and upon solidification (i.e. polymerisation) restore load bearing capability at the damaged site, thus restoring mechanical performance. In intrinsic systems, a matrix additive (e.g. thermoplastic phase) or matrix dynamic chemistry (e.g. CANs/vitrimers) allows the matrix itself to flow and repair cracks. However, invariably these systems require an external stimulus (usually heat) to initiate repair. Figure 1.5 illustrates each of these common concepts for SH composites.

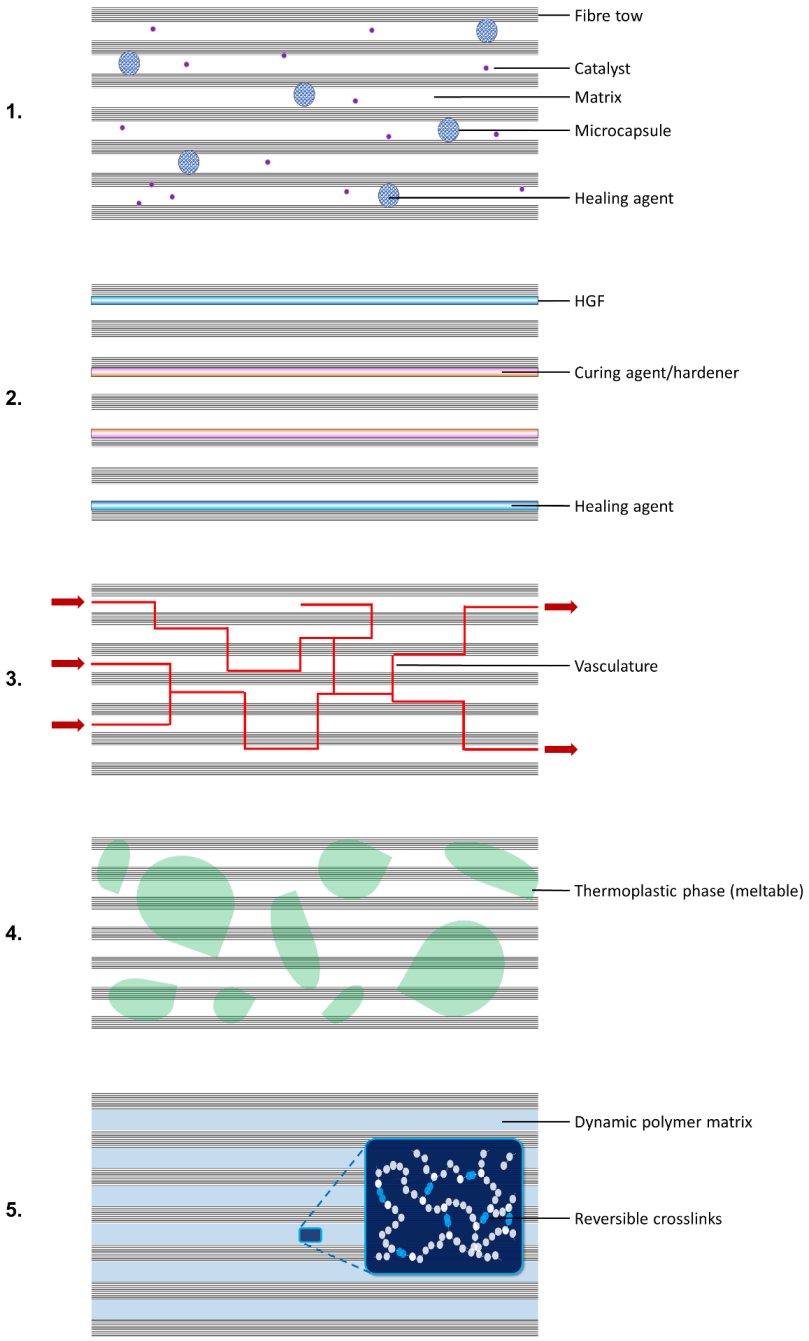

Figure 1.5. Concepts in SH composites. 1 – microcapsules, 2 – hollow fibres, 3 – vasculature, 4 – thermoplastic phases and 5 – CANs/dynamic chemistry.

1.3.2 Extrinsic systems

Microcapsules. This approach typically employs either a single or dual microcapsule (MC) archetype. Generally, single-MC systems rely upon activation post-release by a catalyst distributed throughout the matrix which initialises polymerisation. For dual MC systems, an appropriate hardener material is entrained within separate capsules distributed alongside the monomer capsules throughout the matrix; repair in this case is thus strongly dependent upon the efficient mixing of the two encapsulated agents.

Much of the pioneering work in microencapsulated SH utilises the ring-opening metathesis polymerisation (ROMP) of dicyclopentadiene (DCPD) by Grubbs' catalyst. As is often the case in the field of SH polymers, most of the research with this system has been performed in neat (non-reinforced) polymer,[60–63] though a notable exception is the work of Patel and co-workers,[64] in which they employed a DCPD-Grubb's–based wax microcapsule system in a GFRP laminate and explored healing behaviour with compression after impact (CAI) testing. Although the authors reported good healing efficiency compared to laminates containing wax capsules without the healing agents, a comparison of compressive strength with a conventional, control laminate, which would indicate any disruptive effect on fibre architecture, was notably absent. The longer crack lengths observed in the modified laminates are illustrative of a widespread concern in SH research—the embedded healing additives or structures compromise baseline mechanical performance.

Although the DCPD-Grubbs' system is in many respects an excellent healing system since polymerisation is both rapid and highly efficient, it is not without several drawbacks. These include the cost, toxicity and dispersal of the Ru catalyst, as well as the limited thermal stability of the system, which means the healing ability may be compromised during any heat treatment (e.g. cure) of the host FRP. Coope *et al*.[65] explored the use of alternatives to the Grubbs' catalysts, with scandium triflate being the most promising candidate. Although this system improved on some features (including cost and thermal stability), the overall healing performance was more modest. Another notable single MC system is that reported by Yin *et al.*,[66–68] which employed epoxy resin filled capsules with a copper catalyst dispersed through the matrix.

Dual capsule systems are often based on epoxy-amine polymerisations or similar reactions and thus tend to avoid the use of expensive metal catalysts. However, encapsulation of these agents is not trivial and has been the subject of recent research.[69] In neat polymers, both types of MC system have been demonstrated to work very well. However, there is limited literature concerning application in FRPs. Evidently, a major challenge with MCs in FRPs is overcoming the deleterious effect their inclusion has upon the baseline mechanical performance of the host structure.

Hollow fibres. The hollow-fibre approach to self-healing was developed primarily to overcome the mechanical detriment associated with the inclusion of microcapsules in FRPs. Hollow fibres with healing agents sequestered within, are interleaved within the layers of a laminate and otherwise function in much the same way as microcapsular systems; with rupture followed by egress of entrained healing agent. These fibres are most commonly hollow glass fibres (HGFs),[70–72] though the utility of plastic-shelled alternatives has also been demonstrated.[73] The principal advantage of these systems over microcapsules is that they have a much less disruptive effect on the fibre architecture,

since they sit parallel to the reinforcement fibres. In contrast, the large diameter of microcapsules causes significant curvature and displacement of reinforcement fibres. Researchers including Bleay *et al.*,[70] Pang and Bond,[71,72] Trask and Bond,[74] Williams *et al.*,[75,76] pioneered the use of HGFs in SH composites, in some cases reporting excellent recoveries (>80%). The polypropylene fibres reported by Zhu and co-workers,[73] which contained epoxy/mercaptan healing agents and were cured into a GFRP laminate demonstrated similarly impressive recoveries of up to 62% in terms of flexural strength (after simulated impact damage). In this example and indeed most of the HGF examples, the healing was initiated by a thermal curing event, and thus it was non-autonomous.

Despite the aforementioned success, several challenges associated with this type of system have thus far prevented industrial application. The major challenges here concern the nature of the healing agent and manufacture of the laminate. The healing agent, as for microcapsule systems, is at risk of degradation or complete loss of functionality if it is included in the hollow fibres prior to curing of the laminate (unless unusually low temperature curing cycles are used). Furthermore, if this agent is delivered in a two-part system then efficient mixing is generally required, which broadly means the healing agents need to be of very low viscosity. Whether the healing agent is added before or after cure of the host laminate, this adds significant complexity to the manufacturing process and is clearly incompatible with many composite manufacture techniques. The volume and distribution of hollow fibres are also significant factors that require exploration to achieve effective healing.

Vascular networks. The third category of extrinsic approaches to FRP self-healing is the use of vascular networks. In principle, this methodology is very similar to the hollow fibre approach. Inspired by the transport networks of plants (e.g. xylem and phloem) and animals, notably the circulatory system, channels within a composite can allow the direct distribution of healing agents to damaged areas. When cracks form within the laminate, they eventually intersect with the vascular network, allowing those cracks to be filled and the damage remediated. The primary difference between this and the hollow-fibre approach is the interconnectivity of the network. Accordingly, vascular networks allow a more thorough distribution through the laminate and also presents the possibility of repeated healing events (by adding more healing agent) or even using a continuous circulation of healing agent.

The experiments of Williams *et al.*,[77,78] in which a GFRP sandwich panel, comprising a vascular network with the foam core, revealed exceptional healing performance in some cases, with healing efficiencies (as determined by compression after impact testing) significantly above 100%. The improved mechanical performance was attributed to the densification of the core material by the healing agent (low-viscosity epoxy). However, much poorer results were observed when the epoxy resin and hardener were injected at low pressure without premixing. Poor mixing of the healing agent

constituents resulted in incomplete cure, and poor healing. Norris *et al*.[79] prepared vascular networks within CFRP laminates using a 'lost wax' process. In this procedure, a low melting solder wire network was added to the laminate during lay-up, which was readily removed after cure. Via manual addition of an epoxy healing agent and compression after impact (low energy ~10 J), excellent recoveries approaching 100% were observed. However, the manual addition of healing agent and added complexity in manufacture may negate the benefits of this type of process relative to conventional composite repair.

Other researchers have reported different methods of producing vascular networks, including Patrick and co-workers,[80] who used sacrificial PLA (polylactic acid) fibres (and demonstrated >100% healing efficiencies after multiple cycles of double cantilever beam (DCB) Mode I testing), and Luterbacher *et al*.,[81] who used PTFE-coated nickel chromium wires, manually pulled-out after laminate cure. Despite their consistently high healing efficiencies and the previously mentioned advantages over the other extrinsic systems, vascular networks also have their drawbacks: complexity in manufacture, degradation in baseline mechanical performance—which is arguably worse than hollow-fibres but better than microcapsules—and the manual delivery of healing agent (resin), which is analogous to resin injection repair (Section 1.2.3).

1.3.3 Intrinsic systems

Healable matrices. In terms of intrinsically healable polymers, the most important are those which incorporate dynamic covalent chemistry (DCC) in some capacity. Historically the most common chemistries in this area were disulfides and the Diels-Alder (DA) reaction. Although a wide variety of functional chemistries exist—as will be discussed in Section 1.5—few have been applied to make healable composites. One such example is the disulfide system reported by Post *et al*.[82] in which the authors prepared, via vacuum infusion, a GFRP laminate of good mechanical performance (modulus ~1 GPa) that was capable of repeated delamination healing at modest temperatures (70–85 °C). The healing performance of this composite was thoroughly characterised using a combination of 3-point-bending (3pb), DCB and low-velocity impact testing. From these experiments, long healing regimes (16 h) at the aforementioned modest healing temperatures were shown to give very effective recovery (80% strength, 100% fracture toughness) when the damage was localised in the matrix or fibre-matrix interface. However, it is worth noting that significant pressures (up to 20 bar) were applied with a hot press in order to achieve this. The repeated nature of healing here is a significant advantage over some extrinsic systems. A similar disulfide-containing composite was reported by Ruiz de Luzuriaga *et al*.[83] prepared from the epoxy-amine combination of diglycidyl ether of bisphenol A (DGEBA) and dithiodianiline (DTDA) with either glass or carbon fibre. However, neither the healing efficiency nor the recycling efficiency of the prepared composites were quantified.

The DA/retro-Diels-Alder (rDA) reaction has been used to similar effect by Park *et al*.,[84] who created a CFRP (of V_f ~40%) with a mendomer 401 matrix. The mendomer series of monomers are in essence a tethered pair of cyclopentadiene units with a linker in between, in which one cyclopentadiene is pre-reacted as the diene and the other as the dieneophile in an *intra*molecular DA reaction. When the material is heated, the rDA reaction occurs, causing dissociation of the monomer which facilitates *inter*molecular reaction to form linear polymers. In this case, the authors tested the composite in 3pb and demonstrated healing via strain energy recovery of ~90% in up to three successive damage cycles after thermal repairs at 150 °C (via resistive heating). However, in this research the authors did not quantify the damaged state, thus it is unclear how damaged the specimens were. Heo and Sodano successfully prepared and tested CFRP short-beam-shear (SBS) specimens infused with a DA-PU.[85] With this composite, the researchers managed to achieve excellent (strength) healing efficiencies after both the first and second thermal healing cycles, 85% and 73% respectively. The healing cycle in this case was specifically designed to maximise the efficiency of the rDA and DA reactions, with an initial heating of 135 °C for 2 h (rDA) and a subsequent heating step of 90 °C for a further 2 h (DA). This healing procedure was specifically designed based upon the results of variable temperature (VT) ^{13}C NMR experiments which revealed the optimal temperatures via the direct observation of association and dissociation in the monomer. In each of these articles, healing is in essence effected by a process akin to thermoplastic welding: melting of the matrix allows the polymer chains within it to flow and repair cracks.

Non-covalent interactions. Numerous researchers have explored the use of non-covalent/supramolecular interactions as alternatives to DCC, which has been thoroughly reviewed by Herbst *et al*.[86] Such interactions include hydrogen bonding, metal (coordination) bonding, π-stacking and ionic bonding (as seen in ionomers). Generally, non-covalent interactions are significantly weaker than conventional covalent bonds. Accordingly, where polymer networks are held together principally by such interactions, they are not mechanically robust. This weakness is then compounded by the low stiffness and very high polymer mobility (low T_g) of the backbones which are used, which are often elastomers. This is intentional and is done to facilitate exchange of the non-covalent interactions but precludes the use of such materials in structural FRP applications.

Thermoplastic blends. Thermoplastics, courtesy of their lack of crosslinks, can melt. Although engineering thermoplastics melt at high temperatures (often in excess of 300 °C), a vast array of thermoplastics can be designed to melt at any temperature imaginable. With sufficient pressurisation, thermoplastics can thus be repaired when molten. However, the lack of crosslinking often makes such materials less stiff than thermosets, while also making them susceptible to solvents and prone to creep. To create a compromise between these properties (and imbue thermosets with self-healing

characteristics), researchers have blended both miscible and immiscible thermoplastic-thermoset combinations. The GFRP laminates prepared by Hayes *et al*.[87,88] are an excellent example of the former, in which an anhydride-cured DGEBA epoxy system was used as the host thermoset, and linear DGEBA-based resin as the thermoplastic (10 wt%). Although good healing efficiencies were reported for the neat polymer, the composite's healing efficiency was not mechanically tested. The researchers noted that a system of 10 wt% thermoplastic was chosen 'as it had been shown to give an acceptable compromise between healing efficiency and resin viscosity'. Herein lies one of the major practical limitations of thermoplastic blending: usually only a small fraction of thermoplastic can be added to the uncured thermoset without compromising its processability.

One of the most promising systems for immiscible thermoplastic blending is the ionomeric copolymer, ethylene methacrylic acid (EMAA). EMAA blends into epoxy resins efficiently, with excellent adhesion between the two phases courtesy of the reaction between its carboxylic acid groups and epoxides, forming strong covalent bonds. Pingkarawat *et al*.[89] prepared CFRP composite using such a system and via DCB testing confirmed a massive improvement (~200%) in baseline mode I interlaminar fracture toughness when compared to a conventional epoxy. With healing performed at 150 °C, healing efficiency (toughness) was 82% and this was improved further to 114% at 200 °C. The researchers explained this >100% healing efficiency on the changes to the EMAA morphology during repair. Prior to healing, the thermoplastic was evenly distributed as particles throughout the matrix. After healing, the EMAA was observed to have migrated into the crack, in effect becoming a thin film of adhesive binding the fracture surfaces together. Such a film might be expected to have a higher delamination resistance than the virgin material. In a similar fashion to EMAA, the thermal expansion of polycaprolactone (PCL) has been exploited in epoxy blends to create mendable matrices. Full recovery of GFRP laminates comprising such systems has been demonstrated after impacts of up to 8.5 J.[90]

1.3.4 Evaluating healing systems

One of the major challenges surrounding SH polymers is reliably quantifying healing in a consistent manner. Generally, healing efficiency is defined by one of two equations:

$$\eta = 100 * [\frac{\text{healed property}}{\text{pristine property}}] \quad \text{Eq. 1.1}$$

$$\eta = 100 * [\frac{\text{healed property} - \text{damaged property}}{\text{pristine property} - \text{damaged property}}] \quad \text{Eq. 1.2}$$

Equation 1.1 is derived from 1.2 with the damaged property set to zero. This is an important distinction to make. Eq. 1.1 is only truly appropriate when the property has no residual value, which is sometimes the case, e.g. tensile and DCB tests, where clean separation occurs through the tested cross-section of the material; however, some researchers have employed Eq. 1.1 and consequently published less

meaningful data than they might have otherwise using Eq. 1.2. Beyond the choice of equation, the choice of 'property' in question also adds to the freedom of the SH researcher and the inconsistency of the SH literature. The most widely used methods of quantifying recovery with FRPs include Mode I DCB, CAI and 3pb/4pb after impact. Importantly, due to the complex heterogeneous nature of FRPs, each of these test methods results in a complex array of damage- and failure-modes which precludes their like-for-like comparison. Nevertheless, with each of these methodologies it is possible to introduce the key types of damage (matrix and interfacial) which are sensible targets of healing. After all, it is matrix and interfacial damage which dominates (low energy) damaging events in these out-of-plane test methodologies. For this reason, and the intrinsic poor out-of-plane properties of FRPs, which makes FRPs naturally susceptible to similar damage in service, these are all good, if not relatively complex assessment methods. However, it would be desirable to develop a more consistent, unified approach to SH characterisation around a single simplified experiment.

Inconsistency in host composite, manufacture method and healing procedure also generates further uncertainty when comparing data in the SH literature. Together, these inconsistencies are undoubtedly a contributing factor to the current lack of higher TRL (technology readiness level) SH materials and strategies.

1.3.5 Implementation of SH strategies

Presently, little if any SH research has been sufficiently transitioned into industry to find real-world application. The vast majority of research is at TRL 1–2, with most testing at the coupon level. Two particularly important conclusions from the aforementioned progress paper are: (1) focus on upscaling and testing demonstrator parts (to prove value). (2) investigated targeted healing strategies.[58] In general, in most SH research it is implied that entire structures would be made of the fully self-healing material in question. However, as a consequence of design, composite structures have known susceptible features which present an opportunity for more targeted, local application. In general, any position where matrix damage or delamination occurs is an ideal target, thus SH material might be best applied at 'design features' such as section changes, ply drops, stringer run-outs, holes and joints. Application of healing technology at joints also introduces questions surrounding the nature of the joint, since healing agents could in some cases also serve as reversible adhesives.

1.4 FRP recycling

As a consequence of the wide range of constituent matrices and reinforcements, as well as the breadth of their applications, composites are subject to a broad range of End-of-life (EOL) treatments as introduced in Section 1.2.2. Historically, the majority of composite products and scrap have ended up

in landfill. This is in no small part due to the challenges associated with the heterogeneous nature of composites; for efficient recycling, the different phases must be separated. Clearly, landfill and incineration (the next most popular treatment) are not sustainable options for a growing composites industry.

One of the simplest definitions of recycling is 'the act or process of converting waste into reusable material'. By this definition, many current composite end-of-life solutions fall under this category including pyrolysis, hydrolysis, chemical recycling and milling/grinding (mechanical recycling), though incineration which recovers energy, does not constitute recycling because no usable material is recovered.

Because of their intrinsic capacity to melt, thermoplastic composites are capable of reshaping and can in theory be directly recycled into 'new' products with minimal treatment. Despite their dominance in the (unreinforced) polymer market, thermoplastics currently hold a limited but rapidly growing share of the market for FRP composites.[91–93] This is in large part due to manufacturing challenges, the high viscosity of thermoplastics compared to thermosets makes fibre wetting and penetration (impregnation) problematic. Historically, this has resulted in considerably less research into methodologies surrounding the recycling of thermoplastic composites, despite the fact that these materials have an intrinsically higher capacity for recycling than their thermoset counterparts. The most common method of recycling unreinforced thermoplastics is a combination of shredding (mechanical recycling) and melting (thermal recycling): a plastic is shredded into granules and melted for further use. However, although this works well with commodity plastics with relatively low melting points such as polyethylene, polypropylene and polyethylene terephthalate (PET), such processes are much less efficient with engineering thermoplastics (i.e. those used to make high performance thermoplastic composites) such as polyether ether ketone (PEEK), polyethersulfone (PES), polyamides (PA) and polyimides (PI), because these materials typically melt at prohibitively high temperatures (*ca*. 250–400 °C). Thus, although in theory thermoplastic composites can melt, and the polymer may be separable from the fibres, in practice this may not be economically achievable without favourably low viscosities and melting temperatures.

1.4.1 Mechanical recycling

Multiple organisations have developed processes for mechanical recycling of thermoset composites. In general, the waste substrate (often bulk moulding compound, BMC or sheet moulding compound, SMC, which are usually glass-fibre reinforced polyesters) is shredded, pulverised and fractionated by companies including ERCOM and Phoenix Fibreglass.[47] The product recyclates are typically used as fillers in virgin composite (BMC/SMC), though have a low overall value since there is limited demand.

Research is ongoing to find alternative applications for these recyclates, particularly the coarser (higher fibre content) grades which are less appropriate as fillers.[94] Thermoplastic composites are just as easily mechanically recycled as their thermoset cousins; however, they have the advantage that the recyclate products (granules, pellets etc.) are to some extent meltable and accordingly have a higher value. Meltable materials may be moulded into new structures in their own right. Nevertheless, the mechanical processing does significantly erode the performance of both thermoplastics and thermosets, principally by greatly reducing the length (and alignment) of the reinforcement fibres.

1.4.2 Pyrolysis/thermal recycling

The most common form of thermal recycling involves combustion of the polymer matrix (as an energy source) and recovery of the incombustible fibres. However, in these processes the incombustible fraction (fibres) is again a low value product, principally used as a cement filler.[94] Fluidised bed processes offer a potential alternative which can lead to the recovery of intact fibres. The principle here is relatively simple: a stream of hot air passing through a bed of sand can break up small sections of composite, fully volatilising the polymer and thus efficiently separating the continuous and discontinuous phases of the composite. The fibres are then carried by the gas stream to a collection chamber and the volatile gases burned as a fuel. The high temperatures (~500 °C) can result in a significant deterioration of strength in glass fibres. A similar but much less significant effect is seen with carbon fibres. In any case, the recovered fibres are of sufficient quality to be used as reinforcement in 'new' short fibre composites.[95]

Pyrolysis is the anoxic thermal decomposition of materials at elevated temperatures. Under these conditions, the polymer is broken down into lower molecular weight organic species which can be condensed and used as chemical feedstocks. Low-value products, chars, fibres and inorganic fillers are also isolated and can be reused as fillers. Dependent upon the composite input, temperature and the presence of a catalyst, it appears some pyrolysis methods can yield higher quality fibres which have potential in higher value applications. Usually a post-pyrolysis oxidative process is required to clean the fibres to an extent that they are appropriate for reuse. Again, high temperature treatments have been observed to degrade the strength of carbon fibres to an appreciable level (often up to 20%) and glass fibres significantly more (often up to 50%), temperature dependent. The advantage of pyrolysis over most of the other recycling methods discussed thus far is that it has the potential to give reasonably valuable products from both the matrix and reinforcement, particularly with carbon fibre.[94,96]

1.4.3 Hydrolysis, solvolysis and chemical recycling

In general, chemical recycling (solvolysis) methods use agents to dissolve or depolymerise the matrix to liberate free fibres. Ideally, the polymer is then precipitated from solution prior to further processing and reuse. In contrast to thermal and mechanical processes, chemical processes are much more sensitive to the functionality present in the polymer matrix. For example, a process which works well for anhydride-cured epoxies may not work at all for polyurethanes. Agents including alkali metal hydroxides in supercritical water (used up to 375 °C),[97] and solutions of titanium (IV) *n*-butoxide in diethyleneglycol (245 °C),[98] have been shown to be effective at depolymerising amine- and anhydride-cured epoxies respectively. The latter process uses the cleavage of ester linkages via transesterification to degrade the network, a process which has also been successfully demonstrated with polycarbonates,[99] and polyesters including PET.[100] The former process with supercritical water was also reported to operate via transesterification; however, no esters should be present in the tested polymer since it was a simple amine-epoxy system, hence the true mode of degradation is unclear. Both cases yielded high quality fibres and could be extended to the recovery of much longer fibres than is possible with thermal-mechanical recycling processes; however, more work is required in terms of the further treatment and application of the recovered depolymerisation products. Aqueous solutions of concentrated nitric acid have also been demonstrated to depolymerise amine-cured bisphenol F–derived epoxy resins sufficiently well to enable the product monomers to be re-polymerised into robust materials.[101] Although this process is much slower than the aforementioned alternatives, with nitric acid digestion taking approximately 2 weeks (in contrast to a few hours), it required much more modest temperatures (80 °C).

Similar processes have also been developed for PU composites, with a notable example being glycerol-based glycolysis.[102] These authors managed to recover high purity polyol (71%) and microcapsules separately from PU foam core materials.

As with each of the other recycling categories, thermoplastics have a theoretical advantage over thermosets; the absence of crosslinks typically makes thermoplastics more susceptible to chemical attack. However, most thermoplastics like thermosets are not readily ‘de-polymerised’ into their constituent monomers—the ‘holy grail’ of polymer recycling—after all, engineering polymers are designed for the opposite, to be stable. The key exceptions are polylactic acid (PLA) and polycaprolactone, though neither of these polyesters are significantly used in FRPs. Accordingly, there is a case to suggest a paradigm shift is needed to bring the design of polymers towards a more sustainable future, by design for recycling.

1.4.3 Evaluating recycling processes

The major recycling processes discussed in this section are summarised in Table 1.1.

Table 1.1. A summary of recycling processes for FRP composites.

Category	Process	Substrate	Conditions	Products	Advantages	Disadvantages
Mechanical	Shredding, grinding, milling	Any	No external heating or pressurisation required	Fine filler powder, coarser filler	Relatively simple, any substrate, minimal treatment or heating required	Low value products, blades require frequent treatment or replacement
Thermal	Combustion	Any	High temperatures, though the substrate is the fuel	Fibrous filler, thermal energy	Simple, compatible with any substrate	Low value products, increasingly restricted due to emissions legislature
	Fluidised bed	CFRP preferred to GFRP	High temperatures required, though volatile gases from matrix degradation used as fuel	Short fibres, thermal energy	Fibres and matrix are efficiently separated, recovered short fibres have potential value	Significant degradation of glass fibre properties precludes the use of GFRP substrates, the matrix is not recovered, relatively expensive
	Pyrolysis	CFRP preferred to GFRP	High temperatures, catalysts	Short fibres, low molecular weight organics	Fibres and matrix are efficiently separated, both short fibres and organic products have potential value	Significant degradation of glass fibre properties, some degradation of carbon fibre properties, often post-processing is required to clean fibres, relatively expensive
Chemical	Solvolysis (including hydrolysis, glycolysis and acid digestion)	Process specific	High temperatures, solvents, catalysts and sometimes high pressures	Short (potentially long) fibres, low molecular weight organics	Fibres and matrix are efficiently separated, both short fibres and organic products have potential value	Highly specific processes, potentially harmful solvents and catalysts required, slow/long residence times possible, relatively expensive

Evidently, not all recycling processes can be fairly compared. There are different ways of ranking different processes against each other. Processes which produce higher value products (recyclates) are clearly better than those which produce lower value products, all else being equal. Similarly, processes which transform a higher proportion of the material into new products are better than those which transform a lower proportion of material, since the overall volume of waste is lower. Ideally, any recycling process should be quantified on these two metrics: the value of the products it generates and the fraction of material that is wasted. These are the primary targets researchers can use to develop improved recycling methodologies, though clearly other factors including broadness of applicability, environmental impact and scalability are also important for industrial application.

In summary, conventional FRPs can often be recycled to a limited extent; however, the simplest and most benign processes tend to give products of very low value (mechanical processing) and processes which give higher value products are often situation specific and energy intensive. Overall, this means relatively little FRP is currently recycled. Thermoplastic composites offer improved potential for recycling relative to conventional thermoset composites, though due to their limited usage they have been subject to less research. Considerable research needs to be carried out to improve existing processes, to establish a market for the recyclates and to make composite recycling cost-effective.

1.5 Dynamic materials, CANs and Vitrimers

1.5.1 Dynamic chemistry

The field of dynamic chemistry evolved from the pioneering research of Lehn and co-workers into supramolecular chemistry, the chemistry of molecular systems, in the late 1980s.[103] Supramolecular systems are groups of molecules held together by non-covalent interactions, including hydrogen bonds, π-stacking, ionic interactions and many more. These interactions are intrinsically dynamic in nature due to their weakness, with molecular exchange typically facile. Dynamic covalent chemistry (DCC) is principally similar to supramolecular chemistry, but concerns dynamic behaviour *within* molecules, i.e. the making and breaking of (stronger) covalent bonds. Where, as is typical, the systems in question are under thermodynamic control, these fields are collectively referred to as dynamic combinatorial chemistry. Confusingly, this is also often abbreviated as DCC; however, since the research described in this thesis exclusively concerns covalent systems, DCC will continue to be referred to as covalent chemistry throughout. Dynamic chemical systems of both covalent and supramolecular flavours have found applications in areas as diverse as molecular recognition (receptors/sensors), molecular machines, catalysis, self-assembly and functional polymers.[104]

1.5.2 Polymeric materials: thermosets and thermoplastics

As previously noted, engineering polymers can be broadly separated into one of two categories, thermosets and thermoplastics. At this stage, it is important to distinguish their differences, prior to the introduction of an intermediate third category. As a field that is more than a century old, polymer chemistry has been extensively researched and consequently there are numerous examples of polymers which contradict the rules and observed trends concerning their properties. Despite the fact this research concerns only polymers of engineering relevance (structurally robust, stiff materials), this is still true. However, with this caveat, there are broad property generalisations which can be made as summarised in Table 1.2.

Table 1.2. Qualitative differences between the properties of thermosets and thermoplastics**.**

Property	Thermosets	Thermoplastics
Fibre impregnation	*Easy impregnation/processing*. With monomer blends usually in the form of liquid resins at room temperature.	*Poor fibre impregnation, wetting and penetration*. Thermoplastics are usually fully polymerised at the point of composite manufacture and are thus usually high melting point solids.
Chemical resistance	*High resistance*. Crosslinking minimises solvent ingress.	*Lower resistance*. Solvent resistance varies, but the lack of crosslinks can result in partial to complete dissolution of the material.
Thermal resistance	*Higher resistance*. Thermal stability varies substantially based on the chemical structure, but the crosslinks prevent melting.	*Lower resistance*. Thermal stability varies based on the chemistry, but most thermoplastics undergo a melt prior to degradation
Stiffness	*Variable*. Crosslinks certainly reduce creep and imbue stiffening properties, but engineering thermoplastics have comparable stiffness.	*Variable*. Some engineering thermoplastics have comparable stiffness to thermosets. However, thermoplastics are much more susceptible to creep.
Strength	*Variable*. Commodity thermosets have improved strength relative to thermoplastics. However, engineering thermoplastics have comparable strengths.	*Variable*. Commodity thermosets have improved strength relative to thermoplastics. However, engineering thermoplastics have comparable strengths.
Toughness	*Low toughness.* Thermosets are usually much more brittle than thermoplastics.	*Higher toughness*. Thermoplastics can more readily access plastic deformation modes and thus exhibit improved crack resistance.
Repairability	*Difficult to repair.* Since they cannot be re-worked, thermosets are difficult to repair.	*Easier to repair*. Melting makes techniques such as thermoplastic welding possible, localised melting can aid repair.
Recyclability	*Difficult to recycle*. An inability to melt courtesy of permanent crosslinks makes recycling challenging.	*Easier to recycle*. Reduced solvent resistance and melting make recycling theoretically easier.
Reformability	*Impossible to reshape*. Melting is not possible.	*Reformable*. Melting allows thermoplastics to be re-worked.

These factors are further complicated when these polymers are fibre-reinforced, though it is evident that it would be advantageous to have a balance of the positive properties of both categories.

1.5.3 Dynamic polymers (dynamers), CANs and vitrimers

Through careful design, DCC (reversible bonds) can be integrated into polymeric networks to create stimuli-responsive materials. Multiple strategies exist to achieve this, and each can result in significantly different behaviour. Polymers containing some form of dynamic chemistry are generally referred to as the abbreviation of dynamic polymers, ‘dynamers’. Dynamers may refer to both linear or network polymers. In general, for the material to be as responsive as possible, the density of dynamic linkages should be maximised such that when activated (and the linkage is broken) the polymer chain or network is broken down into the smallest sections possible. When dynamic covalent chemistry is applied to polymer *networks*, the reversible bonding can produce polymers which have intermediate properties between thermosets and thermoplastics.

The term ‘covalent adaptable network’ or ‘CAN’ was first defined by Bowman *et al*.[105] in 2010 as ‘networks which contain a sufficient number and topology of reversible covalent bonds as to enable the cross-linked network structure to respond chemically to an applied stimulus.’ Also referred to as dynamic covalent network polymers (DCNPs), CANs can be broadly separated into two distinct categories based on the mechanism of the dynamic behaviour: associative or dissociative, Figure 1.6. Associative CANs are more widely known as ‘vitrimers’, a term coined by Leibler and co-workers,[106] reflecting the Arrhenius-type kinetics of flow behaviour which is reminiscent of glasses. In these systems, chemistries such as Leibler’s transesterification vitrimers,[107] and Du Prez’s vinylogous urethane vitrimers,[108] maintain a constant number of crosslinks after activation (i.e. crosslink density is maintained during dynamic exchange). This means that the exchange reactions and thus mechanical behaviour of these materials is under kinetic control. As a result, associative CANs (vitrimers) are reasonably robust, maintaining mechanical integrity (not melting) when activated. This lends itself to more subtle, controlled behaviour than is observed of their dissociative counterparts.

Dissociative CANs, in contrast, as exemplified by the Diels-Alder polymers of Chen *et al.*,[109] Adzima *et al.*,[110] and Turkenburg and Fischer,[111] lose mechanical integrity while going through a true ‘de-crosslinking’ process. Typically, this is manifested as a broad melting event, where the glassy solid transitions into a viscoelastic liquid. Accordingly, care must be taken to prevent the compromise of structural integrity with such systems; however, the melt presents an opportunity for faster response: quicker repair and easier recycling. In theory, a wide variety of stimuli can be used to activate CANs, dependent on the underlying chemistry, including acid,[112] stress (mechanochemistry),[113] visible light,[114] ultraviolet light,[115–117] and heat, the conventional stimulus. In practice, most systems require some heating in order to give the polymer chains sufficient segmental motion (i.e. overcome the glass transition) to react.

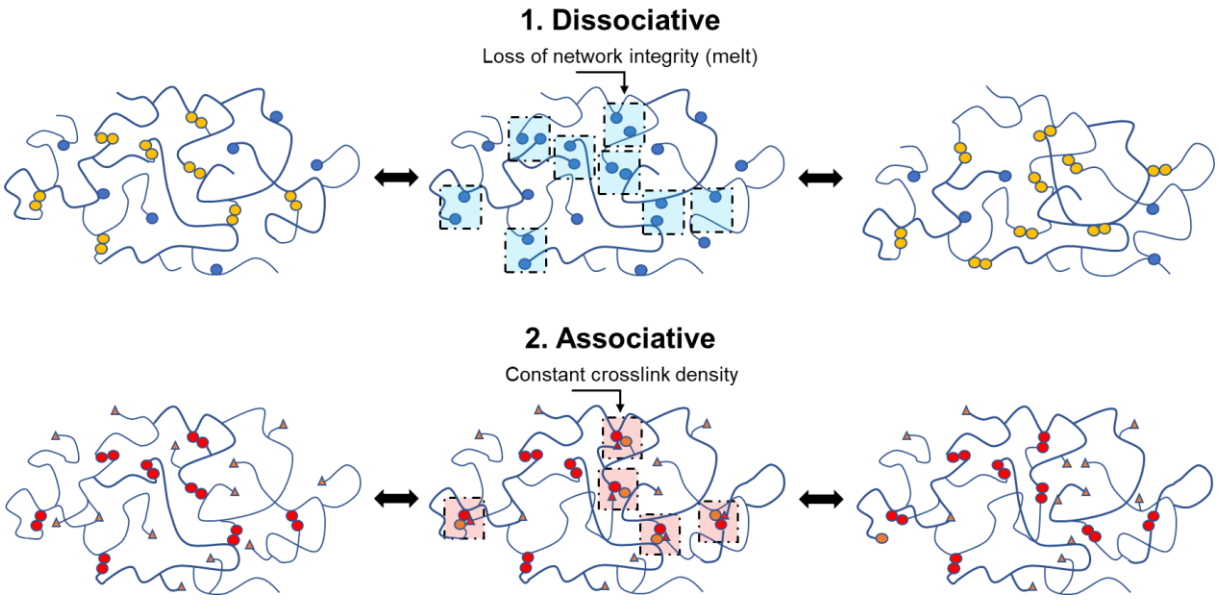

Figure 1.6. Covalent adaptable networks, CANs.

Historically, much of the early work concerning dynamic polymers was derived from either DA/rDA chemistry or disulfides, which have long been observed to play a crucial role as reversible covalent linkages in nature, principally in protein chemistry.[118,119] In recent years, particularly since the formal definitions of CANs and vitrimers, a huge range of functional groups have been developed as reversible bonds in CANs, as shown in Figure 1.7.

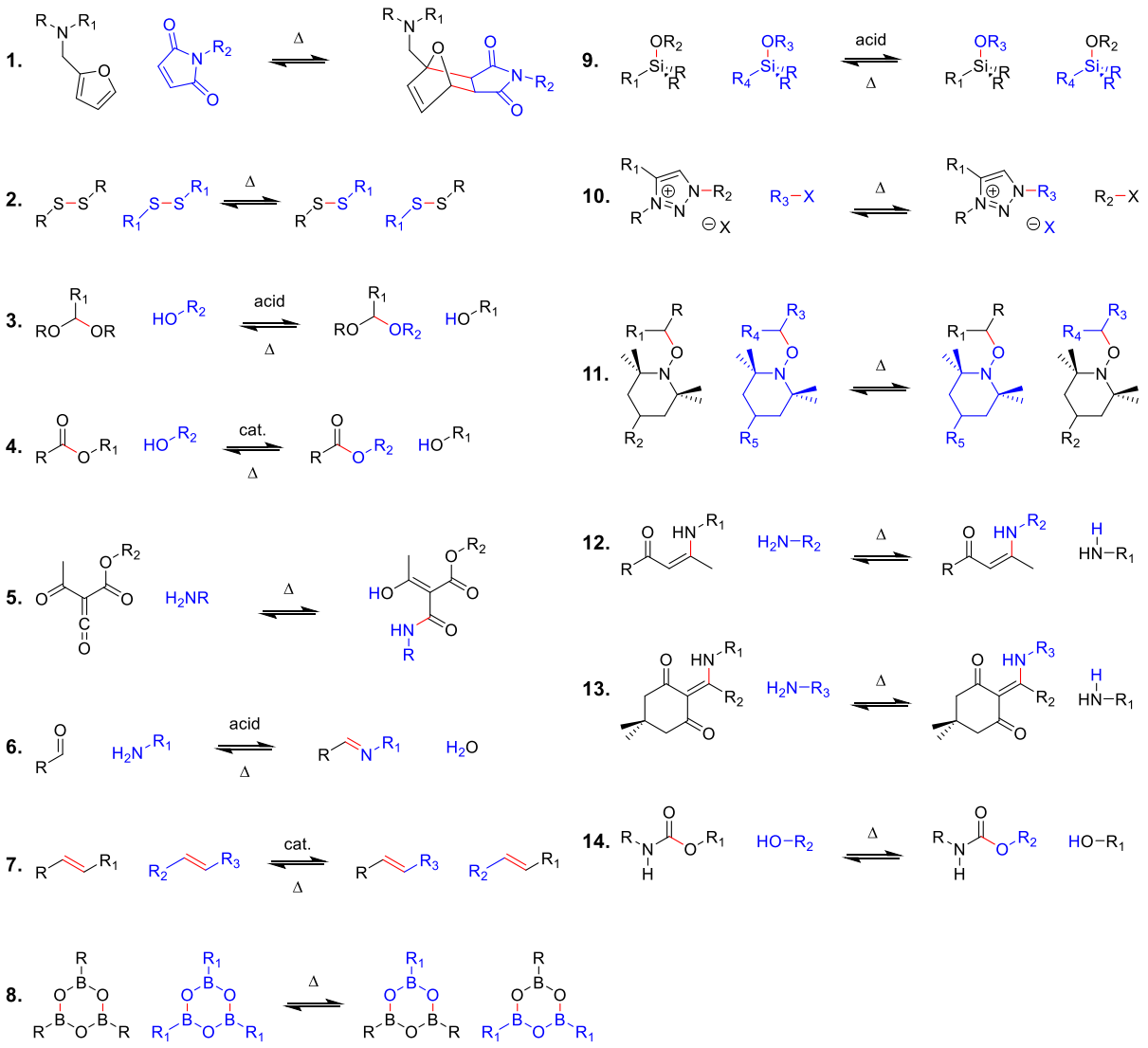

Figure 1.7. A list of some of the most important DCCs used in CANs. The key dynamic (breaking) bonds are coloured red for clarity. 1 – Diels-Alder,[109] 2 – disulfides,[120] 3 – acetals,[121] 4 – transesterification,[122,123] 5 – amides,[124] 6 – imines,[125–127] 7 – olefin metathesis,[128] 8 – boronic esters/acids,[129,130] 9 – silyl ethers,[131] 10 – transalkylation,[132,133] 11 – alkoxyamines,[134,135] 12 – vinylogous urethanes,[108,115,136] 13 – diketoenamines,[112] and 14 – transcarbamoylation.[137]

For the sake of brevity, the precise synthetic procedures and mechanistic behaviours of each of these systems will not be further discussed here, though the reader is directed to the specific articles referenced above and the progress reports and minireviews of Podgórski *et al.*,[138] Denissen *et al.*,[139] and Zou *et al*.[140] Instead, the nature of those chemistries which are investigated in this thesis will be more thoroughly examined in the opening sections of their respective chapters. Such a plethora of different systems presents a treasure trove of opportunity and unsurprisingly, this is presently a highly active field of research.

Recent progress in CANs. Guo and co-workers,[141] through experiments varying the crosslink density of an imine vitrimer, observed that faster stress relaxation occurs in networks with lower crosslink density but surprisingly discovered that the activation energy to polymer flow was also increased with lower crosslink density. This was rationalised in terms of a reduced number of bonds required to effect topology change (faster relaxation), but a decrease in the concentration of dynamic groups hinders the reaction kinetics (affects E_A).

Spiesschaert and co-workers systematically varied the backbone structure, molecular weight and crosslink density of vinylogous urethane vitrimers (transamination chemistry) and observed very different viscoelastic and kinetic behaviour.[142] In contrast to the previously referenced work of Guo *et al*., Spiesschaert *et al*. observed faster stress relaxation in shorter-backbone polymers (with higher crosslink density); however, this effect was only significant with poly-THF backbones—no substantial difference was observed with analogous vitrimers with poly(propylene glycol) backbones. Evidently, backbone structures play an important, but not easily predictable, role in determining the (high temperature) viscoelastic properties of vitrimers. A significant backbone influence on relaxation time was also observed between different backbone structures: branched backbones resulted in an relaxation time increase of up to 20-fold compared with analogous linear polymers. The reduced rate of the branched, more sterically encumbered polymer was attributed to the 'reduced chain-end mobility'.

One of the latest examples of multi-mechanism CANs was recently reported by Podgórski *et al*.[143] based on thiol–succinic anhydride chemistry. By varying the stoichiometry of reactive groups and the nature of the catalyst, the researchers were able to favour or disfavour two distinct dynamic mechanisms: one associative, thiol-thioester substitution and one dissociative, thiol-anhydride ring-opening/closing. Such materials present an opportunity to tune the material based on the requirements of specific applications.

The recent study of Van Herck *et al*.,[144] in which the authors studied the exchange kinetics of a thiol-yne dissociative CAN system, highlighted the fact that the activation energy of their network polymers was much higher than that of the model (small-molecule) systems they investigated. This serves as an important reminder that exchange mechanisms are often complicated by the host network; it is never certain that dynamic behaviour on the molecular level will translate to the expected activity within networks.

1.6 CANs and composites

This following section is a short literature review, detailing the state-of-the-art with respect to CANs in composites.

CANs present numerous opportunities to improve composite sustainability. In manufacture, if a defective part is produced, in many cases it may be possible to reprocess the material, using the de-crosslinking reaction to have a second (or third) attempt. This is otherwise impossible with traditional FRPs. In service, if a CAN-composite part is damaged by low-energy impact such that there is extensive matrix cracking and delamination, but minimal fibre damage, it could be rapidly repaired via controlled heat application (assuming it is thermally activated), potentially fully restoring mechanical performance without removal or addition of material. This would potentially be a much faster and cheaper method of repair. During decommissioning, a structure of multiple CAN parts may be disassembled into smaller sections for recycling, if the matrix is also used as a reversible adhesive. De-crosslinking could then facilitate much more efficient recycling than is currently possible, yielding both matrix and fibres for further use in structural applications.

The main advantages of thermosets over thermoplastics in composites are creep resistance, solvent resistance, high T_g (though transitions of ~250 °C are typical of high performance thermoplastics) and easy fibre impregnation. Conversely, the advantage of thermoplastics is that they can melt and thus have an intrinsically higher potential for healing and reprocessability (which contributes to improved sustainability potential). CANs aim to maintain some of the benefits of both categories. Typically, T_g is viewed as simple metric in polymeric materials, the higher the better. However, since the principle benefit of CANs is their dynamic behaviour and the associated low T_v and softening point (which facilitates healing, recycling and reprocessing), a high T_g is not a desirable characteristic of a CAN. Nevertheless, for operating temperatures in the room temperature and wider 0–50 °C region, the T_g still needs to be >70 °C and ideally as close as possible to T_m/T_v such that the CAN goes from a robust solid to a highly processable material within a small window. In addition, CANs should have good solvent and creep resistance but this is only significant *below* T_g and T_v. Accordingly, the crucial characteristics CANs should share with thermosets are (low temperature) fatigue resistance and low processing viscosity (for fibre impregnation). Moreover, to present a significant advantage over thermoplastics, CANs should offer lower reprocessing temperatures, whether this temperature is a T_m, a T_v or otherwise. Commodity thermoplastics such as PP have processing temperatures as low as 200 °C, but most engineering thermoplastics (e.g. polyamides, polyimides, polysulfones and PEEK) require processing at >250 °C.

To date, there have been few examples of CANs being applied as FRP matrices, though in recent years there has been significant progress in this area.

In 2017, Post and co-workers reported a GFRP composite comprising a disulfide-containing matrix, specifically designed as an intrinsically self-healing material.[82] This healable epoxy matrix is not a CAN in the strictest sense as it comprises a dual network of both conventional (permanent) crosslinks and the dynamic disulfide moieties. In principle, this 'dual network' approach can overcome one of the historic limitations of CANs and CAN-like systems: poor mechanical properties (particularly stiffness and strength). Many dynamic chemistries can result in polymers with near 100% strength recovery, but much of that literature concerns elastomers or other low stiffness (non-structural) materials. The authors successfully vacuum-infused dry glass fabric with their disulfide resin system, curing the laminate at 100 °C for 60 h. Using a combination of 3pb, DCB and low-velocity impact testing, the mechanical performance and healing behaviour of the laminate was characterised. Healing was tested at different temperatures and pressures by heating in an oven or hot press for 16 h. Composite flexural moduli of the order of 10 GPa and yield strengths of 55 MPa were reported. Curiously, the researchers own curing study suggests that the curing regime they used results in only a partially crosslinked material—higher temperature (140+ °C) cures resulted in much stiffer materials (10x). However, instead of using higher curing temperatures, extended cure times of 60 h were used which gave a compromise on mechanical performance. Presumably, this regime was chosen because fully cured laminates did not exhibit good healing performance. Nonetheless, good fibre volume fractions (V_f ~ 50%) and respectable healing was reported (3pb: 50% strength recovery at 70 °C, and >70% at 85 °C). As will be discussed in Chapter 4, disulfide exchange and therefore healing, can operate via several mechanisms. In this case, the authors used base-catalysed thiol substitution (adding both thiols and free triethylamine to the matrix).

Ruiz de Luzuriaga *et al*.[83] prepared one of the first examples of a true CAN composite using a very simple resin system: DGEBA (Araldite® LY 1564) and DTDA. This system was cured in two steps at 120 and 150 °C. Good mechanical performance was observed of the neat polymer, with strength, stiffness and fracture toughness all in the same region as conventional DGEBA-based epoxies. By using DMA to investigate stress relaxation, the authors confirmed that the resin had vitrimeric behaviour and was capable of extremely rapid stress relaxation (~20 s) at 200 °C. Qualitative healing experiments confirmed that both healing and reprocessing (milling and hot pressing into films) were successful at this temperature. The authors went on to prepare what they called 'enduring prepregs' by infusing this vitrimeric resin into single sheets of FRP and then compressing these individual layers together into complete laminates (in a hot press under 100 bar). This process was very effective, yielding laminates with excellent mechanical performance which bested their control laminate in terms of

compressive strength (292 *vs.* 242 MPa), interlaminar shear strength (37 *vs.* 29 MPa), flexural strength (595 *vs.* 557 MPa) and impact strength (194 *vs.* 159 MPa). However, good though these values are, it is likely that the control laminate values are lower due to the different manufacture conditions (hot press *vs*. oven cure) giving rise to different fibre volume fractions. The authors were even able to demonstrate the recycling potential of these laminates by dissolving the resin in a DMF-thiol solution. This paper clearly demonstrates the potential of CANs in composites and only really suffers from one key drawback: the 200 °C reprocessing temperature. At such high temperatures we begin to approach the melting temperature of some engineering thermoplastics and accordingly CANs present less value. However, 200 °C is still below this region and if the resin is of very low viscosity (not reported in this study) at this temperature, this material may be of commercial value. Interestingly, another study by the same researchers revealed that this resin is mechanochromic—when struck by a hammer it turns from orange to green and then slowly returns to its original colour.[145] This is attributed to cleavage of the disulfide bonds to give their respective sulfanyl radicals.

More recently, Si and co-workers extended the concept of using disulfide CANs in composites, with an epoxy resin in which both components (epoxy and amine hardener) contained a disulfide bond.[146] This led to enhanced stress relaxation and recycling performance (neat resin was mechanically recycled without any detriment to the mechanical properties). The product composite had good mechanical performance and a high T_g (~140 °C), as well as good solvent resistance, though when heated (90 °C) in thiol solution, the composite was readily recycled. The recycled composite also exhibited good mechanical performance. The only major limitations of this study are that the composite was manually infused, hence the resin may not be compatible with conventional composite manufacturing conditions (though it seems possible), and more importantly, that the minimum exchange temperature is 170 °C, though the authors used ≥180 °C temperatures throughout. Although this is high, the properties of this material still present significant advantages over some thermoplastics; there appears to be value in developing this disulfide CAN system further.

In 2016 Qi and co-workers published an article concerning a carbon fibre composite with ‘near 100% recyclability’.[147] This composite uses a modified epoxy resin which is capable of transesterification, the prototypical example of vitrimer chemistry. A combination of natural fatty acids are used to crosslink DGEBA in the presence of zinc acetate (catalyst) which results in a crosslinked epoxy with many free hydroxyls and carboxylic acid groups which can participate in transesterification (see Figure 1.7, 4). In this paper the authors go on to exploit the transesterification reaction for recycling by using ethylene glycol (EG) as a solvent. The free hydroxyl groups of EG in conjunction with its high boiling point allow it to reversibly dissolve the CAN (vitrimer), with near complete dissolution within 3 h at 180 °C (well below the thermal degradation temperature). By allowing EG evaporation, the polymer can even be

repolymerised. Impressively, when CFRP specimens (pristine and recycled) were tested under uniaxial tension, the recycled specimens maintained both stiffness and strength equal to the pristine samples (within experimental error) even up to four recycling generations. A truly impressive achievement. However, this resin has such a low T_g (< 30 °C) that this will limit the potential application of this particular system; the storage modulus begins to sharply decline around 15 °C, even at ambient temperature the modulus has fallen from *ca*. 2 GPa, to <100 MPa.[148]

Chabert *et al*.,[149] used a similar transesterification vitrimer system, with the same zinc acetate catalyst, but prepared their laminates via an RTM process. In this article the authors focused on the adhesive property of the matrix, which allows multiple laminates to be glued or 'welded' together. Lap-shear experiments revealed good adhesive strengths, with a relatively consistent load at break of around 500 N (~ 2 MPa). Critically this welding process was repeatable and did not result in a consistent decrease in lap-shear strength. A more recent article by Yu and co-workers explored a powder-based composite manufacture process using a pre-cured vitrimer resin that was also based on transesterification chemistry (zinc acetate catalysed).[150] In this work the authors produced high quality composite rapidly (~1 min) by using a hot-press technique and justifiably claim that such fast processing may enable the use of CANs in the automotive sector. However, as with the study by Qi *et al*.,[147] the T_g is prohibitively low (~30 °C).

In the study of Denissen *et al*.,[151] the authors were aiming to specifically address the limitations of some of the previously discussed articles, by preparing CAN (vitrimer) composites with reasonably high glass transition temperatures. In this work, the authors used a vinylogous urea vitrimer (which is chemically similar to vinylogous urethanes see Figure 1.7, 12) with a useful T_g (*ca*. 110 °C) and thermal decomposition temperature >200 °C. When exchange was catalysed by *p*-TsOH (an organic acid), extremely fast exchange reactions were observed with relaxation times of 13.9 s at 140 °C and 2.4 s at 170 °C. Mechanical recycling of the neat polymer was highly effective; milling and compression moulding of specimens at 180 °C resulted in similar mechanical properties to the pristine specimens. In a fashion akin to the previously mentioned 'enduring prepregs'. Denissen *et al*.[151] went on to manually impregnate glass fabric with a solution of their resin, prior to curing these individual layers in a vacuum oven, and finally hot pressing the layers into a single laminate at 200 bar (170 °C). This resulted in good quality GFRP (V_f ~ 57%) with no observable defects or porosity, though a variety of other curing conditions were explored previously with less success. This composite had mechanical performance comparable to a reference epoxy composite, with equivalent Young's modulus and 84% of the tensile strength. Though neither healing nor recycling were quantified, qualitative recycling experiments indicate complete matrix dissolution in amine solutions within 15 min at 100 °C. Evidently

this system has potential as both a recyclable and repairable composite matrix, though more testing is required.

In 2020 Cui *et al*.[152] published a study concerning polythiourethane CANs, which they prepared at room temperature via the reaction of polythiols and diisocyanates (with 0.1% amine catalyst). The stress relaxation behaviour appears to fit the Arrhenius equation, indicative of vitrimer-type behaviour, although only four data points were plotted. In this article the authors focus primarily on the application of this CAN as a reversible/reworkable adhesive, though the excellent mechanical performance and processability of the resin system allowed them to go on and prepare FRP laminates. In this particular case, the properties of the product CFRP composite were not thoroughly tested, though a qualitative experiment indicated that solutions of polythiol could lead to full dissolution of the CAN, demonstrating the potential of this system in composite recycling.

In their 2019 review paper,[153] McBride and colleagues summarised recent progress in CANs. One particularly valuable insight from their paper that has not yet been discussed in this chapter, is the concept of shrinkage stress. Amongst many valuable insights, the authors identified this as a further area (in addition to recycling and healing) in which CANs present an opportunity in composites—many conventional resin systems generate significant stresses during cure which can result in premature composite failure. Where dynamic chemistry takes place concomitantly with cure, these stresses can be avoided, resulting in higher quality composite.

1.7 Summary

Repair of conventional composites is often both expensive and time consuming. Though this is generally performed with patches, resin injection processes can be used in cases of more minor damage.

Many composite recycling processes have been reported in the academic literature. Although some commercial ventures are attempting to industrialise these processes, presently there has been little progress toward recycling composites on a significant scale. This is principally because there is little in the way of a market for the low-value recyclates which are usually produced.

CANs are de-crosslinkable polymers. In recent years a wide variety of systems have been developed though most exist at a very low TRL (1–2). There are several parts of the composite lifecycle in which CANs could be used to increase sustainability courtesy of their dynamic behaviour.

To compete with conventional thermosets and thermoplastics for application as FRP matrices, CANs should exhibit the following characteristics:

- Processing temperature (T_m/T_v) significantly below thermoplastic processing temperatures <200 °C (competitive with thermoplastics)
- Good low temperature (below $T_m/T_v/T_g$) mechanical performance, including creep resistance (competitive with thermosets)
- Excellent fibre impregnation (wetting and penetration), which equates to low viscosity (competitive with thermosets)

At the time this research project was started, there were very few examples of CAN use in composites despite their great potential. Though more examples have since been reported, and the value of CANs in composites has been demonstrated, more work is needed to create robust systems and realise their true potential in real-world structures.

1.8 Research objectives

In this project, the overarching objective was to demonstrate the utility of CANs in FRP composites with a view to developing more sustainable materials. With this in mind, the research will primarily focus on two main strands:

- Expand upon the research concerning the Diels-Alder epoxy CANs developed by Fischer *et al*.[111] principally through exploring their use as healable and recyclable composite matrices (Chapters 2 and 3). In the previous works there has been limited thermomechanical characterisation.
- Develop new dynamic chemistries as more reactive alternatives to disulfides, namely, diselenides (Chapter 4) and diphosphanes (Chapter 5).

1.9 References

1 V. Fiore, T. Scalici, G. Di Bella and A. Valenza, *Compos. Part B Eng.*, 2015, **74**, 74–94.

2 A. Pappu, K. L. Pickering and V. K. Thakur, *Ind. Crops Prod.*, 2019, **137**, 260–269.

3 A. C. Corbin, D. Soulat, M. Ferreira, A. R. Labanieh, X. Gabrion, P. Malécot and V. Placet, *Compos. Part B Eng.*, 2020, **181**, 107582.

4 N. Cuinat-Guerraz, M. J. Dumont and P. Hubert, *Compos. Part A Appl. Sci. Manuf.*, 2016, **88**, 140–147.

5 A. O'Donnell, M. A. Dweib and R. P. Wool, *Compos. Sci. Technol.*, 2004, **64**, 1135–1145.

6 L. Pil, F. Bensadoun, J. Pariset and I. Verpoest, *Compos. Part A Appl. Sci. Manuf.*, 2016, **83**, 193–205.

7 E. Gogna, R. Kumar, Anurag, A. K. Sahoo and A. Panda, Springer, Singapore, 2019, pp. 459–467.

8 M. Delgado-Aguilar, H. Oliver-Ortega, J. Alberto Méndez, J. Camps, F. X. Espinach and P. Mutjé, *Int. J. Biol. Macromol.*, 2018, **116**, 299–304.

9 K. L. Pickering, M. G. A. Efendy and T. M. Le, *Compos. Part A Appl. Sci. Manuf.*, 2016, **83**, 98–112.

10 C. Sergi, J. Tirillò, M. C. Seghini, F. Sarasini, V. Fiore and T. Scalici, *Polymers (Basel).*, 2019, **11**, 603.

11 F. Ribeiro, J. Sena-Cruz, F. G. Branco and E. Júlio, *Constr. Build. Mater.*, 2018, **171**, 871–890.

12 D. K. Rathore, R. K. Prusty, S. C. Mohanty, B. P. Singh and B. C. Ray, *Mech. Mater.*, 2017, **105**, 99–111.

13 U. N. Gandhi, S. Goris, T. A. Osswald and Y.-Y. Song, in *Discontinuous Fiber-Reinforced Composites*, Hanser, 2020, pp. 1–27.

14 K. W. Gan, Y. W. Ho, Z. Y. Ow, H. A. Israr and K. J. Wong, *J. Compos. Mater.*, 2019, **53**, 3893–3907.

15 M. L. Longana, N. Ong, H. Yu and K. D. Potter, *Compos. Struct.*, 2016, **153**, 271–277.

16 J. Henry and S. Pimenta, *Compos. Sci. Technol.*, 2017, **144**, 230–244.

17 K. L. Pickering and T. M. Le, *Compos. Part B Eng.*, 2016, **85**, 123–129.

18 J. Tierney, A. Vanarelli, D. Heder, S. Yarlagadda and J. Gillespie, WO Pat., 2019032401, 2018.

19 M. Ashby, H. Shercliff and D. Cebon, *Materials: engineering, science, processing and design*, Elsevier, Cambridge, UK, 3rd edn., 2014.

20 G. Marsh, *Reinf. Plast.*, 2007, **51**, 26–29.

21 S. Das, *The cost of automotive polymer composites: a review and assessment of DOE's lightweight materials composites research*, Oak Ridge, 2001.

22 P. Beardmore and C. F. Johnson, *Compos. Sci. Technol.*, 1986, **26**, 251–281.

23 K. K. Chawla and N. Chawla, in *Wiley Encyclopedia of Composites*, John Wiley & Sons, Inc., Hoboken, NJ, USA, 2012, pp. 1–6.

24 J. Osborne, *Met. Finish.*, 2013, **111**, 26–30.

25 R. N. Yancey, *Light. Compos. Struct. Transp.*, 2016, 35–52.

26 A. Taub, E. De Moor, A. Luo, D. K. Matlock, J. G. Speer and U. Vaidya, *Annu. Rev. Mater. Res.*, 2019, **49**, 327–359.

27 P. Davies, *Philos. Trans. R. Soc. A Math. Phys. Eng. Sci.*, 2016, **374**, 20150272.

28 M. Strangwood, in *Materials in Sports Equipment*, Woodhead Publishing, 2019, pp. 3–35.

29 L. Mishnaevsky, K. Branner, H. Petersen, J. Beauson, M. McGugan and B. Sørensen, *Materials (Basel).*, 2017, **10**, 1285.

30 S. Das, J. Warren, D. West and S. M. Schexnayder, *Global Carbon Fiber Composites Supply Chain Competitiveness Analysis*, 2016.

31 M. G. Bader, *Compos. Part A Appl. Sci. Manuf.*, 2002, **33**, 913–934.

32 M. Hautier, D. Lévêque, C. Huchette and P. Olivier, *Plast. Rubber Compos.*, 2010, **39**, 200–207.

33 S. Pimenta and S. T. Pinho, *Waste Manag.*, 2011, **31**, 378–392.

34 S. K. Bobade, N. R. Paluvai, S. Mohanty and S. K. Nayak, *Polym. Plast. Technol. Eng.*, 2016, **55**, 1863–1896.

35 H. S. S. Shekar and M. Ramachandra, *Mater. Today Proc.*, 2018, **5**, 2518–2526.

36 K. Jha, R. Kataria, J. Verma and S. Pradhan, *AIMS Mater. Sci.*, 2019, **6**, 119–138.

37 G. S. Mann, L. P. Singh, P. Kumar and S. Singh, *J. Thermoplast. Compos. Mater.*, 2018, 1–27.

38 G. Fiorentino, M. Ripa and S. Ulgiati, *Biofuels, Bioprod. Biorefining*, 2017, **11**, 195–214.

39 S. G. Advani and K.-T. Hsiao, *Manufacturing techniques for polymer matrix composites (PMCs)*, Woodhead Pub, 2012.

40 P. Boisse, *Advances in composites manufacturing and process design*, Woodhead Publishing, 2015.

41 P. Parandoush and D. Lin, *Compos. Struct.*, 2017, **182**, 36–53.

42 K. Diamanti and C. Soutis, *Prog. Aerosp. Sci.*, 2010, **46**, 342–352.

43 V. Memmolo, E. Monaco, N. D. Boffa, L. Maio and F. Ricci, *Compos. Struct.*, 2018, **184**, 568–580.

44 A. Güemes, A. Fernández-López, P. Díaz-Maroto, A. Lozano and J. Sierra-Perez, *Sensors*, 2018, **18**, 1094.

45 Y. Wang, Y. Wang, B. Wan, B. Han, G. Cai and Z. Li, *Compos. Struct.*, 2018, **200**, 669–678.

46 Y. S. Song, J. R. Youn and T. G. Gutowski, *Compos. Part A Appl. Sci. Manuf.*, 2009, **40**, 1257–1265.

47 Y. Yang, R. Boom, B. Irion, D.-J. van Heerden, P. Kuiper and H. de Wit, *Chem. Eng. Process. Process Intensif.*, 2012, **51**, 53–68.

48 C. N. Duong and C. H. Wang, *Composite Repair: Theory and Design*, Elsevier, 2010.

49 M. Mahler and H. T. Hahn, in *Adaptive Structures, Eighth Japan/US Conference Proceedings*, ed. G. M. Newaz, CRC Press, 1998, pp. 53–59.

50 K. B. Katnam, L. F. M. Da Silva and T. M. Young, *Prog. Aerosp. Sci.*, 2013, **61**, 26–42.

51 P. Kumar and B. Rai, *Compos. Struct.*, 1993, **23**, 313–318.

52 H. Park and C. Kong, *Aerosp. Sci. Technol.*, 2013, **29**, 363–372.

53 M. H. Hassan, A. R. Othman and S. Kamaruddin, *Int. J. Adv. Manuf. Technol.*, 2017, **91**, 4081–4094.

54 M. H. Keegan, D. H. Nash and M. M. Stack, *J. Phys. D. Appl. Phys.*, 2013, **46**, 383001.

55 A. J. Russell, C. P. Bowers and A. J. Moss, in *Composite Structures*, Springer Netherlands, Dordrecht, 1991, pp. 145–159.

56 E. Panetettieri, D. Fanteria, M. Montemurro and C. Froustey, *Compos. Part B Eng.*, 2016, **107**, 9–21.

57 R. S. Pierce, W. C. Campbell and B. G. Falzon, in *ICCM International Conferences on Composite Materials*, 2017, vol. 21.

58 A. Cohades, C. Branfoot, S. Rae, I. Bond and V. Michaud, *Adv. Mater. Interfaces*, 2018, **5**, 1800177.

59 J. Kular, J. Tickner, S. M. Chim and J. Xu, *Clin. Biochem.*, 2012, **45**, 863–873.

60 E. N. Brown, S. R. White and N. R. Sottos, *Compos. Sci. Technol.*, 2005, **65**, 2474–2480.

61 S. R. White, N. R. Sottos, P. H. Geubelle, J. S. Moore, M. R. Kessler, S. R. Sriram, E. N. Brown and S. Viswanathan, *Nature*, 2001, **409**, 794–797.

62 J. D. Rule, N. R. Sottos and S. R. White, *Polymer*, 2007, **48**, 3520–3529.

63 E. L. Kirkby, V. J. Michaud, J. A. E. Månson, N. R. Sottos and S. R. White, *Polymer*, 2009, **50**, 5533–5538.

64 A. J. Patel, N. R. Sottos, E. D. Wetzel and S. R. White, *Compos. Part A Appl. Sci. Manuf.*, 2010, **41**, 360–368.

65 T. S. Coope, U. F. J. Mayer, D. F. Wass, R. S. Trask and I. P. Bond, *Adv. Funct. Mater.*, 2011, **21**, 4624–4631.

66 T. Yin, L. Zhou, M. Z. Rong and M. Q. Zhang, *Smart Mater. Struct.*, 2008, **17**, 015019.

67 T. Yin, M. Z. Rong, M. Q. Zhang and G. C. Yang, *Compos. Sci. Technol.*, 2007, **67**, 201–212.

68 T. Yin, M. Z. Rong, M. Q. Zhang and J. Q. Zhao, *Smart Mater. Struct.*, 2009, **18**, 074001.

69 I. Lee Hia, E.-S. Chan, S.-P. Chai and P. Pasbakhsh, *J. Mater. Chem. A*, 2018, **6**, 8470–8478.

70 S. M. Bleay, C. B. Loader, V. J. Hawyes, L. Humberstone and P. T. Curtis, *Compos. Part A Appl. Sci. Manuf.*, 2001, **32**, 1767–1776.

71 J. W. C. Pang and I. P. Bond, *Compos. Part A Appl. Sci. Manuf.*, 2005, **36**, 183–188.

72 J. W. C. Pang and I. P. Bond, *Compos. Sci. Technol.*, 2005, **65**, 1791–1799.

73 Y. Zhu, X. J. Ye, M. Z. Rong and M. Q. Zhang, *Compos. Sci. Technol.*, 2016, **135**, 146–152.

74 R. S. Trask and I. P. Bond, *Smart Mater. Struct.*, 2006, **15**, 704–710.

75 G. J. Williams, I. P. Bond and R. S. Trask, *Compos. Part A Appl. Sci. Manuf.*, 2009, **40**, 1399–1406.

76 G. Williams, R. Trask and I. Bond, *Compos. Part A Appl. Sci. Manuf.*, 2007, **38**, 1525–1532.

77 I. P. Bond, R. S. Trask and H. R. Williams, *MRS Bull.*, 2008, **33**, 770–774.

78 H. R. Williams, R. S. Trask and I. P. Bond, *Compos. Sci. Technol.*, 2008, **68**, 3171–3177.

79 C. J. Norris, G. J. Meadway, M. J. O'Sullivan, I. P. Bond and R. S. Trask, *Adv. Funct. Mater.*, 2011, **21**, 3624–3633.

80 J. F. Patrick, K. R. Hart, B. P. Krull, C. E. Diesendruck, J. S. Moore, S. R. White and N. R. Sottos, *Adv. Mater.*, 2014, **26**, 4302–4308.

81 R. Luterbacher, R. S. Trask and I. P. Bond, *Smart Mater. Struct.*, 2016, **25**, 15003.

82 W. Post, A. Cohades, V. Michaud, S. van der Zwaag and S. J. Garcia, *Compos. Sci. Technol.*, 2017, **152**, 85–93.

83 A. Ruiz de Luzuriaga, R. Martin, N. Markaide, A. Rekondo, G. Cabañero, J. Rodríguez and I. Odriozola, *Mater. Horizons*, 2016, **3**, 241–247.

84 J. S. Park, H. S. Kim and H. Thomas Hahn, *Compos. Sci. Technol.*, 2009, **69**, 1082–1087.

85 Y. Heo and H. A. Sodano, *Compos. Sci. Technol.*, 2015, **118**, 244–250.

86 F. Herbst, D. Döhler, P. Michael and W. H. Binder, *Macromol. Rapid Commun.*, 2013, **34**, 203–220.

87 S. A. Hayes, F. R. Jones, K. Marshiya and W. Zhang, *Compos. Part A Appl. Sci. Manuf.*, 2007, **38**, 1116–1120.

88 S. A. Hayes, W. Zhang, M. Branthwaite and F. R. Jones, *J. R. Soc. Interface*, 2007, **4**, 381–387.

89 K. Pingkarawat, C. Dell'Olio, R. J. Varley and A. P. Mouritz, *Polymer*, 2016, **92**, 153–163.

90 A. Cohades and V. Michaud, *Compos. Struct.*, 2017, **180**, 439–447.

91 U. K. Vaidya and K. K. Chawla, *Int. Mater. Rev.*, 2008, **53**, 185–218.

92 K. Friedrich, in *AIP Conference Proceedings*, 2016.

93 L. Sorrentino, D. Silva de Vasconcellos, M. D'Auria, J. Tirillò and F. Sarasini, *Polym. Compos.*, 2018, **39**, 2942–2951.

94 S. J. Pickering, *Compos. Part A Appl. Sci. Manuf.*, 2006, **37**, 1206–1215.

95 S. J. Pickering, R. M. Kelly, J. R. Kennerley, C. D. Rudd and N. J. Fenwick, *Compos. Sci. Technol.*, 2000, **60**, 509–523.

96 S. R. Naqvi, H. M. Prabhakara, E. A. Bramer, W. Dierkes, R. Akkerman and G. Brem, *Resour. Conserv. Recycl.*, 2018, **136**, 118–129.

97 R. Piñero-Hernanz, C. Dodds, J. Hyde, J. García-Serna, M. Poliakoff, E. Lester, M. J. Cocero, S. Kingman, S. Pickering and K. H. Wong, *Compos. Part A Appl. Sci. Manuf.*, 2008, **39**, 454–461.

98 K. El Gersifi, G. Durand and G. Tersac, *Polym. Degrad. Stab.*, 2006, **91**, 690–702.

99 R. Piñero-Hernanz, J. García-Serna and M. J. Cocero, *AIChE J.*, 2006, **52**, 4186–4199.

100 M. Genta, T. Iwaya, M. Sasaki, M. Goto and T. Hirose, *Ind. Eng. Chem.*, 2005, **44**, 3894–3900.

101 W. Dang, M. Kubouchi, H. Sembokuya and K. Tsuda, *Polymer*, 2005, **46**, 1905–1912.

102 D. Simón, J. F. Rodríguez, M. Carmona, A. Serrano and A. M. Borreguero, *Chem. Eng. J.*, 2018, **350**, 300–311.

103 J.-M. Lehn, *Angew. Chem. Int. Ed.*, 1988, **27**, 89–112.

104 Y. Jin, C. Yu, R. J. Denman and W. Zhang, *Chem. Soc. Rev.*, 2013, **42**, 6634–6654.

105 C. J. Kloxin, T. F. Scott, B. J. Adzima and C. N. Bowman, *Macromolecules*, 2010, **43**, 2643–2653.

106 M. Capelot, D. Montarnal, F. Tournilhac and L. Leibler, *J. Am. Chem. Soc.*, 2012, **134**, 7664–7667.

107 A. Demongeot, R. Groote, H. Goossens, T. Hoeks, F. Tournilhac and L. Leibler, *Macromolecules*, 2017, **50**, 6117–6127.

108 W. Denissen, G. Rivero, R. Nicolaÿ, L. Leibler, J. M. Winne and F. E. Du Prez, *Adv. Funct. Mater.*, 2015, **25**, 2451–2457.

109 X. Chen, M. A. Dam, K. Ono, A. Mal, H. Shen, S. R. Nutt, K. Sheran and F. Wudl, *Science*, 2002, **295**, 1698–1702.

110 B. J. Adzima, H. A. Aguirre, C. J. Kloxin, T. F. Scott and C. N. Bowman, *Macromolecules*, 2008, **41**, 9112–9117.

111 D. H. Turkenburg and H. R. Fischer, *Polymer*, 2015, **79**, 187–194.

112 P. R. Christensen, A. M. Scheuermann, K. E. Loeffler and B. A. Helms, *Nat. Chem.*, 2019, **11**, 442–448.

113 K. Imato, T. Kanehara, S. Nojima, T. Ohishi, Y. Higaki, A. Takahara and H. Otsuka, *Chem. Commun.*, 2016, **52**, 4–7.

114 Y. Amamoto, H. Otsuka, A. Takahara and K. Matyjaszewski, *Adv. Mater.*, 2012, **24**, 3975–3980.

115 T. Wright, T. Tomkovic, S. G. Hatzikiriakos and M. O. Wolf, *Macromolecules*, 2019, **52**, 36–42.

116 B. T. Michal, E. J. Spencer and S. J. Rowan, *ACS Appl. Mater. Interfaces*, 2016, **8**, 11041–11049.

117 H. Y. Park, C. J. Kloxin, T. F. Scott and C. N. Bowman, *Dent. Mater.*, 2010, **26**, 1010–1016.

118 T. J. Bechtel and E. Weerapana, *Proteomics*, 2017, **17**, 1600391.

119 C. Czaplewski, S. Ołdziej, A. Liwo and H. A. Scheraga, *Protein Eng. Des. Sel.*, 2004, **17**, 29–36.

120 D. J. Fortman, R. L. Snyder, D. T. Sheppard and W. R. Dichtel, *ACS Macro Lett.*, 2018, **7**, 1226–1231.

121 T. Hashimoto, H. Meiji, M. Urushisaki, T. Sakaguchi, K. Kawabe, C. Tsuchida and K. Kondo, *J. Polym. Sci. Part A Polym. Chem.*, 2012, **50**, 3674–3681.

122 T. Liu, C. Hao, S. Zhang, X. Yang, L. Wang, J. Han, Y. Li, J. Xin and J. Zhang, *Macromolecules*, 2018, **51**, 5577–5585.

123 Z. Ding, L. Yuan, Q. Guan, A. Gu and G. Liang, *Polymer*, 2018, **147**, 170–182.

124 Z. Liu, C. Yu, C. Zhang, Z. Shi and J. Yin, *ACS Macro Lett.*, 2019, **8**, 233–238.

125 H. Memon, H. Liu, M. A. Rashid, L. Chen, Q. Jiang, L. Zhang, Y. Wei, W. Liu and Y. Qiu, *Macromolecules*, 2020, **53**, 621–630.

126 P. Taynton, H. Ni, C. Zhu, K. Yu, S. Loob, Y. Jin, H. J. Qi and W. Zhang, *Adv. Mater.*, 2016, **28**, 2904–2909.

127 S. Zhao and M. M. Abu-Omar, *Macromolecules*, 2018, **51**, 9816–9824.

128 Y. X. Lu, F. Tournilhac, L. Leibler and Z. Guan, *J. Am. Chem. Soc.*, 2012, **134**, 8424–8427.

129 S. Wu, H. Yang, S. Huang and Q. Chen, *Macromolecules*, 2020, **53**, 1180–1190.

130 S. Wu, Z. Yang, S. Fang, Z. Tang, F. Liu and B. Guo, *J. Mater. Chem. A*, 2019, **7**, 1459–1467.

131 C. A. Tretbar, J. A. Neal and Z. Guan, *J. Am. Chem. Soc.*, 2019, **141**, 16595–16599.

132 A. Jourdain, R. Asbai, O. Anaya, M. M. Chehimi, E. Drockenmuller and D. Montarnal, *Macromolecules*, 2020, **53**, 1884–1900.

133 M. M. Obadia, A. Jourdain, P. Cassagnau, D. Montarnal and E. Drockenmuller, *Adv. Funct. Mater.*, 2017, **27**, 1–10.

134 H. Otsuka, *Polym. J.*, 2013, **45**, 879–891.

135 K. Imato, A. Takahara and H. Otsuka, *Macromolecules*, 2015, **48**, 5632–5639.

136 A. Erice, A. Ruiz de Luzuriaga, J. M. Matxain, F. Ruipérez, J. M. Asua, H.-J. Grande and A. Rekondo, *Polymer*, 2018, **145**, 127–136.

137 S. Hu, X. Chen and J. M. Torkelson, *ACS Sustain. Chem. Eng.*, 2019, **7**, 10025–10034.

138 M. Podgórski, B. D. Fairbanks, B. E. Kirkpatrick, M. McBride, A. Martinez, A. Dobson, N. J. Bongiardina and C. N. Bowman, *Adv. Mater.*, 2020, 1906876.

139 W. Denissen, J. M. Winne and F. E. Du Prez, *Chem. Sci.*, 2016, **7**, 30–38.

140 W. Zou, J. Dong, Y. Luo, Q. Zhao and T. Xie, *Adv. Mater.*, 2017, **29**, 1606100.

141 Y. Liu, Z. Tang, J. Chen, J. Xiong, D. Wang, S. Wang, S. Wu and B. Guo, *Polym. Chem.*, 2020, **11**, 1348–1355.

142 Y. Spiesschaert, C. Taplan, L. Stricker, M. Guerre, J. M. Winne and F. E. Du Prez, *Polym. Chem.*, 2020, 5377–5385.

143 M. Podgórski, N. Spurgin, S. Mavila and C. N. Bowman, *Polym. Chem.*, 2020, 5365–5376.

144 N. Van Herck, D. Maes, K. Unal, M. Guerre, J. M. Winne and F. E. Du Prez, *Angew. Chem. Int. Ed.*, 2020, **59**, 3609–3617.

145 I. Azcune and I. Odriozola, *Eur. Polym. J.*, 2016, **84**, 147–160.

146 H. Si, L. Zhou, Y. Wu, L. Song, M. Kang, X. Zhao and M. Chen, *Compos. Part B Eng.*, 2020, **199**, 108278.

147 K. Yu, Q. Shi, M. L. Dunn, T. Wang and H. J. Qi, *Adv. Funct. Mater.*, 2016, **26**, 6098–6106.

148 K. Yu, P. Taynton, W. Zhang, M. L. Dunn and H. J. Qi, *RSC Adv.*, 2014, **4**, 10108–10117.

149 E. Chabert, J. Vial, J.-P. Cauchois, M. Mihaluta and F. Tournilhac, *Soft Matter*, 2016, **12**, 4838–4845.

150 L. Yu, C. Zhu, X. Sun, J. Salter, H. Wu, Y. Jin, W. Zhang and R. Long, *ACS Appl. Polym. Mater.*, 2019, **1**, 2535–2542.

151 W. Denissen, I. De Baere, W. Van Paepegem, L. Leibler, J. Winne and F. E. Du Prez, *Macromolecules*, 2018, **51**, 2054–2064.

152 C. Cui, X. Chen, L. Ma, Q. Zhong, Z. Li, A. Mariappan, Q. Zhang, Y. Cheng, G. He, X. Chen, Z. Dong, L. An and Y. Zhang, *ACS Appl. Mater. Interfaces*, 2020, **12**, 47975–47983.

153 M. K. McBride, B. T. Worrell, T. Brown, L. M. Cox, N. Sowan, C. Wang, M. Podgorski, A. M. Martinez and C. N. Bowman, *Annu. Rev. Chem. Biomol. Eng.*, 2019, **10**, 175–198.

Chapter 2: Diels-Alder epoxies 1

2.1 Introduction

2.1.1 Diels-Alder chemistry

Discovered by the German chemists Otto Diels and Kurt Alder in the late 1920s, the Diels-Alder (DA) reaction is the concerted [4+2] cycloaddition between a diene and a dienophile, which generates cyclohexene rings, Figure 2.01.[1] This reaction is of such great utility in synthetic chemistry—not least because of its simplicity and highly predictable selectivity—that Diels and Alder were awarded the Nobel prize in chemistry in 1950. Due to having both negative values of enthalpy (ΔH) and entropy (ΔS), at sufficiently high temperatures the reverse (or *retro*) reaction dominates, which has led to the widespread use of DA/rDA systems in DCC (dynamic covalent chemistry). However, although the DA reaction is versatile and compatible with a wide range of structures, the feasibility of the reverse reaction is highly limited—only specific structural features support the reverse reaction.

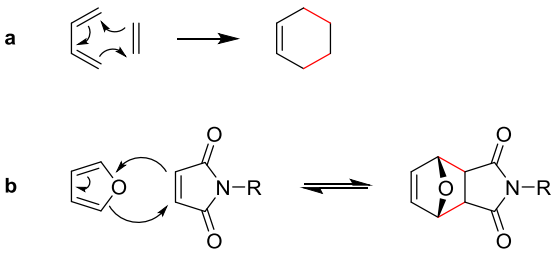

Figure 2.01. The Diels-Alder cycloaddition, with newly formed σ-bonds highlighted in red. a – the general reaction between a diene and dienophile (butadiene and ethene respectively) and b – the prototypical thermoreversible Diels-Alder reaction between furan and a maleimide.

The DA reaction is generally considered to proceed via a concerted mechanism with a cyclic transition state, with no intermediates. With respect to regioselectivity, relatively simple 'electronic demand' scenarios can be used to predict the regiochemical outcome from the relative contributions of different atoms to the frontier orbitals. Generally, the product structure follows the 'ortho-para' rule, borrowing the naming system of substituents generally reserved for arenes (i.e. two functional groups on adjacent atoms are ortho to each other). This rule dictates that with the usual case, an electron donating group (EDG) on the C1 (terminal) position of the diene results in the greatest orbital contribution to the HOMO (HOMO coefficient) at the C4 position, Figure 2.02. A dienophile with an adjacent electron withdrawing group (EWG) has greatest LUMO coefficient on the C2 position, and as a result the most well-matched HOMO-LUMO pair react with each other (C4 with C2), which gives an

ortho regiochemical configuration. Different types of functional group (EDG/EWG) on different positions on the diene/dienophile thus give different products which can be easily predicted.[2]

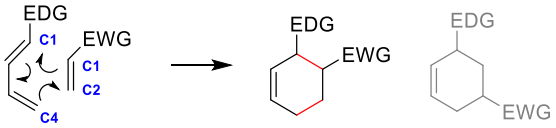

Figure 2.02. An example of the regioselectivity of the Diels-Alder reaction. The 'ortho' substituted product (black) is the exclusive product from this combination of reactants, the grey (meta) product is not formed.

The DA reaction is also highly stereospecific due the concerted nature of the reaction mechanism (all bonds making and breaking concomitantly); if a single isomer is present in the starting material, this stereochemistry will be preserved in the product (or adduct). In many cases the outcome is predictable, particularly in 'normal demand' situations (e.g. diene + a dienophile with an EWG). In such cases, a preference for the endo transition state is observed (*vs*. the exo transition state). This observation is generally explained by a secondary orbital effect—whichever transition state has more π-orbital overlap is preferred (usually endo).[3] This concept of endo/exo structures is returned to later (see Figure 2.06).

In synthetic chemistry, the DA reaction itself is a useful tool for introducing cyclic structures into complex target molecules.[4] Outside of synthesis, the DA reaction is also important; the microscopic reversibility of the DA reaction makes it a powerful tool in the fields of DCC and materials science.

2.1.2 The retro-DA reaction and DA polymers

The variety of DA substrates, both diene and dienophile, means that the associated reaction kinetics and thermodynamics vary substantially. By extension, the temperatures required to effect both the forward (DA) and reverse (rDA) reaction vary accordingly. Some DA reactions proceed rapidly at room temperature,[5] whereas others require temperatures of 200–300 °C or more.[6,7] Highly polar solvents, particularly water, are known to greatly accelerate DA reactions, as does sonication, the presence of acid catalysts and the use of high pressures (a substantial volumetric change is observed as diene and dienophile react to form an adduct).[8] The retro-DA reaction is similarly varied and tends to become significant at higher temperatures. It is this temperature dependence and the rate of dissociation which are of principal interest in the fields of DCC and dynamic materials.

The furan-maleimide system (Figure 2.01b) is undoubtedly the most studied DA reaction in polymer chemistry. It has seen such widespread attention partly due to its well-understood behaviour, but primarily because of its convenient reaction temperatures: the non-catalysed forward reaction typically proceeds rapidly at 60–80 °C and the retro reaction becomes significant at 110–120 °C.[9]

Aside from the furan-maleimide system, there are few examples of easily reversible, dynamic, DA reactions. The fulvene-(di/tri)cyanoolefin system is one such example, Figure 2.03. This system operates at significantly lower temperatures, generally between -10–50 °C and was pioneered by Lehn and co-workers to make the DA reaction relevant in DCC.[5]

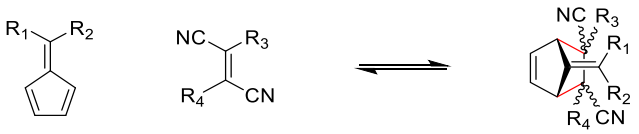

Figure 2.03. The DA/rDA reaction of a fulvene and a dicyanoolefin.

In 2011 Roy and Lehn reported another low-temperature reversible DA reaction, this time between anthracene derivatives and N-phenyltriazolinedione, which is particularly impressive given that anthracene DA adducts usually undergo retro reaction at particularly high temperatures (250–300 °C).[10,11] The key strategy for enhancing the rate of the retro reaction—and thus lowering the temperature at which it operates—is through using C–N bonds, which are approximately 40 kJ mol^{-1} weaker than their C–C analogues, Figure 2.04. In this system the forward reaction proceeds instantaneously, with almost complete conversion at room temperature within 2 min. By raising the temperature above 50 °C, the equilibrium constant (*K*) is reduced in favour of the starting materials (though the *K* values indicate that the adduct is still the major species at this temperature). As with the furan-based systems, by using anthracene as an aromatic diene, the restoration of aromaticity upon adduct reversion is a key driving force behind this reversibility. Despite the excellent dynamic properties of this system, the general instability of these compounds presents some problems. Critically, these reactions must be performed in the dark because anthracenes are known to photolytically dimerise. Moreover, the authors also reported that the triazoline diones also decompose photolytically.

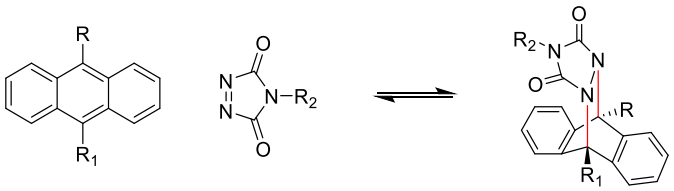

Figure 2.04. The DA/rDA reaction of an anthracene and an N-substituted triazoline dione.

The Diels-Alder reaction in materials science. Any robust reaction can theoretically be applied in polymer chemistry; what works for small molecules can generally also be used to construct macromolecules from monomer building blocks. However, due to the large number of bond forming steps in polymerisations, it is essential that the reactions be fast and reliable. The so-called 'click' reactions, of which the Diels-Alder reaction is an important example, find particular utility in polymer

chemistry.[12] 'Click chemistry' is a term coined by Sharpless to describe reactions which are 'modular, wide in scope, give very high yields, generate only inoffensive by-products that can be removed by non-chromotographic methods, and be stereospecific'.[13] By fulfilling these criteria a given chemical reaction can be used to generate high molecular weight polymers with a high degree of control (stereo-/regio-selectivity). It is therefore no surprise that the DA reaction has been widely used as a tool for building large macromolecules including homopolymers,[14,15] telechelic polymers,[16,17] star polymers/dendrimers,[18–20] block copolymers,[21,22] and graft/comb polymers.[23] More pertinent for this thesis are those materials which exploit reversible DA chemistry.

Wudl and co-workers' *Science* article from 2002 described the first network polymer in which all of the monomer connectivity was through reversible Diels-Alder reaction.[24] These authors exploited the furan-maleimide DA reaction by preparing and reacting a tetrafuran (**4F**) and a trismaleimide (**3M**) to form a densely crosslinked polymer, Figure 2.05.

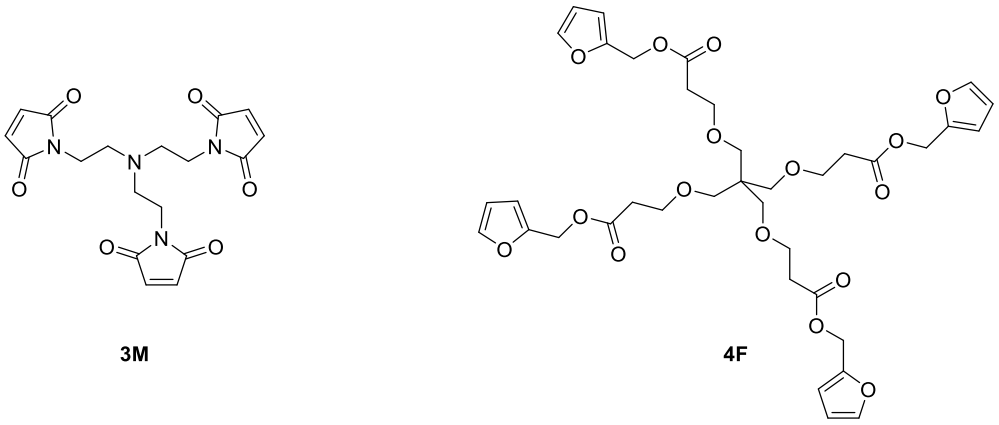

Figure 2.05. The trismaleimide and tetrafuran monomers Wudl *et al*. used to create a robust DA thermoset.[24]

After curing for 3 h at 75 °C, the resulting material had achieved a 95 ± 5% degree of polymerisation, as determined by UV-vis spectroscopy. Liquid nitrogen quenching allowed the authors to identify the level of connectivity after different thermal treatments via temperature-modulated DSC. Thermal treatments at 150 °C (15 min) resulted in approximately 25% de-crosslinking, though only 12% was observed in 25 min at 130 °C. Crosslinking was fully restored after thermal treatments at 80 °C. This reversible behaviour is particularly noteworthy since the samples were reportedly solid throughout these treatments—there is insufficient de-crosslinking to allow the material to melt. The healing of this material was investigated by compact tension tests; a thermal treatment of 150 °C (2 h) restored the material with approximately 50% efficiency (in terms of load recovery). Although Wudl *et al*.[24] did report an impressive Young's modulus of 4.72 GPa, this was determined through ultrasonic testing and not through conventional mechanical testing. Arguably more impressive are the high strengths reported for this material: 68 MPa (tension) and 143 MPa (flexure). Generally, one of the major

limitations of these systems derived entirely from small-molecule precursors is their tendency to be extremely brittle.[11] To overcome this brittleness, several researchers have employed a slightly different strategy, in which oligomers/short-chain polymers are functionalised and crosslinked together (via the DA reaction), though invariably this results in a polymer which is less efficient in self-healing. One example of this is the furan-maleimide functionalised polyamide reported by Liu and Chen.[25] Although these polymer films were both repairable and (qualitatively) tough, they had low tensile strength (~ 20 MPa).

In 2008, Adzima *et al*.[26] prepared a Diels-Alder network polymer exploiting the reversibility of the furan-maleimide reaction—which would later be described as a covalent adaptable network (CAN)—from 1,1'-(methylenedi-4,1-phenylene)bismaleimide and a trifunctional furan oligomer (prepared from the reaction of the respective triacrylate and furfuryl mercaptan. The authors went on to explore the rheological response of the material surrounding gelation (and reverse gelation), observing that the gel-point—the point at which a 'single molecule' percolates the entire reaction, as it transitions from sol to gel—of the furan-maleimide reaction agrees well with the Flory-Stockmayer equation

$$p_g = \frac{1}{\sqrt{r(1-f_M)(1-f_F)}} \qquad \text{Eq. 2.1}$$

where p_g is the fraction of gel-point conversion, r is the stoichiometric ratio, and f_M/f_F are the degrees of functionality for maleimide and furan respectively. From rheology measurements and FTIR s pectra, the kinetics of this DA system was explored while the extent of crosslinking was varied. Maximal conversion was observed from FTIR at 60 °C. Above 45 °C, the polymer melt enters thermodynamic control and the reaction is increasingly pushed back from adducts to reactants. Interestingly, the equilibrium conversion is reduced as low as 24% at 155 °C; however, at this temperature irreversible side reactions also operate. The authors noted that bismaleimide (BMI) homopolymerisation (HP) seems to operate gradually at temperatures as low as 120 °C, which was identified by a reduction in maleimide peak area and a concomitant increase in furan area (using FTIR spectroscopy).

Amongst several insights in his 2010 paper on trends in Diels-Alder material design, A. Sanyal discusses the use of the Diels-Alder reaction as a protecting group (or 'mask')–type strategy in the preparation of functional polymers.[27,28] By pre-reacting furan and maleic anhydride, and later converting this anhydride DA adduct into an imide, DA adducts can be built into polymer structures which would otherwise be impossible to prepare due to the reactivity of the maleimide, Scheme 2.1. The author highlighted the potential of such systems for creating novel scaffolds for drug delivery based on the latent reactivity revealed by subsequent retro Diels-Alder reactions.

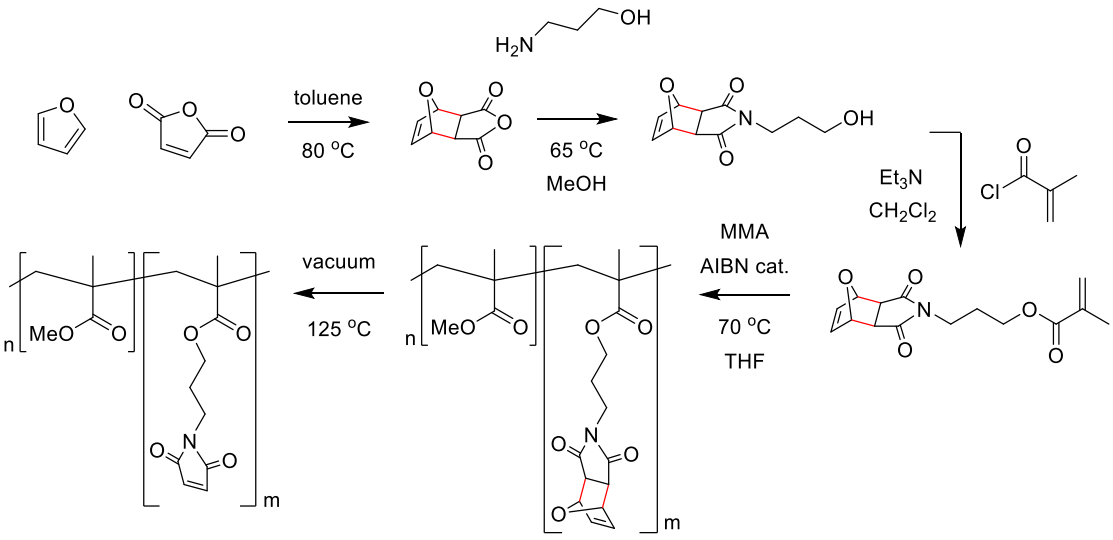

Scheme 2.1. The DA/rDA masking strategy employed by Sanyal and co-workers, wherein the DA adduct serves to mask an otherwise highly reactive maleimide group, at the end of the synthesis the furan is removed by heating to afford a highly reactive PMMA derivative.[28] The bonds formed by the DA reaction are highlighted in red.

In 2010, Canadell *et al*.[29] investigated the stereochemical aspects of thermally mendable DA polymers, finding that the two adduct stereoisomers (endo/exo) exhibited quite different thermal responses with most combinations of furan and maleimide, Figure 2.06. By using variable temperature ^{1}H NMR, the authors observed significant reversion to starting materials (after 3 h at 100 °C), though resonances corresponding to the exo adduct were still observable after this treatment. This led the authors to postulate that minor endothermic peaks observable at high temperatures represent the reverse reaction of these isomers. These endotherms were generally 30–40 °C higher than the primary endotherm, which is ascribed to the retro reaction of the endo isomer. The specific chemical structures of the maleimide and furan units only had a minor effect on the DA/rDA temperatures.

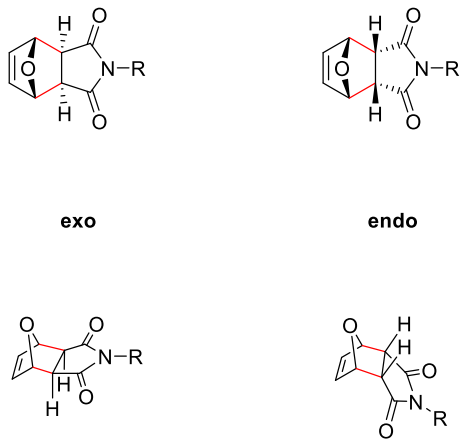

Figure 2.06. The endo and exo product geometries of the furan-maleimide DA reaction.

2.1.3 Diels-Alder composites

A few studies have previously investigated the use of DA polymers as composite matrices, two of which have previously been discussed in Chapter 1 (Section 1.3.3) under the topic of self-healing composites: the mendomer 401 CFRP of Park *et al*.[30] and the DA polyurethane (PU) of Heo and Sodano,[31] with impressive healing performance well-quantified in the latter. In addition, Zhang *et al*.[32] have investigated the use of DA/rDA chemistry at the fibre-matrix interface of CFRPs through micro-droplet debonding. This is a particularly interesting healing strategy since the fibre-matrix interface is a known weak-point and microcracking here can lead to extensive damage and material failure.[33] Good re-bonding (healing performance) was observed with carbon fibres pre-treated with a nitric acid oxidation step (up to 82%). However, it is unclear if this healing behaviour would function properly (provide significant healing) when embedded within an otherwise conventional composite—i.e. with only healable interfaces. Moreover, it remains to be tested whether the presence of healable interfaces alone is enough to add sufficient repairability value to FRP composites.

More recently, Park and co-workers investigated the recycling and repairability of cellulosic composites based on DA chemistry.[34] By preparing a furan-functionalised PU and crosslinking this via reaction with a bismaleimide, the authors achieved a good recycled performance (~60% strength recovery) after treatment in PGMEA (propylene glycol monomethyl ether acetate) at 120 °C. However, the composites (<7 wt% cellulose fibre) in this study are best described as soft materials (Young's modulus 10–25 MPa, tensile strength <5 MPa).

Another recent study has also investigated the potential of the furan-maleimide DA system to create recyclable composites. In their report, Fortunato *et al*.[35] look to address the recycling challenge in industrially relevant CFRP composites. These authors synthesised a bifunctional furan monomer and a trifunctional furan monomer from DGEBA and DGGO (N,N-diglycidyl-4-glycidyloxyaniline) respectively and reaction with furfurylamine in MeOH. The furans were then reacted with BMI1 in 20 wt% THF and the resultant gels were isolated, dried and milled prior to their incorporation in CFRPs, Figure 2.07. The resultant powder and reinforcement were combined via a compression moulding process in a PTFE-lined mould (120–140 °C, 200 bar, 1 h). Impressively, the authors showed that this material could be milled and reprocessed up to five times (still retaining a degree of reversibility). This is particularly noteworthy given the prevalence of secondary amine groups in both of their chosen monomers, which may be capable of participating in competitive Michael addition reactions, which in turn would be expected to reduce the efficiency of the rDA reaction. Indeed, the reduction in rDA endotherm area observed after subsequent heat treatments is attributed to this process and BMI homopolymerisation, as will be discussed in detail throughout this chapter. By employing solvolysis in either DMF, DMSO or propylene carbonate at 120 °C, Fortunato *et al.*[35] were able to recover the CF

(carbon fibre) reinforcement via hot filtration with a high yield (>96%) and only minor matrix contamination (~2 wt%). The authors also went on to demonstrate the utility of the recovered polymer gels as healable coatings. However, noteworthy limitations of this study are the low tensile strength (<6 MPa) of the neat resin, and the use of only a single layer of CF reinforcement. In addition, it is worth considering that solvent-assisted recycling can degrade the quality of fibres by removing the sizing (or surface treatment) so in that respect is disadvantageous compared to mechanical recycling methods. Nevertheless, the isolation of continuous fibres, which solvent- or supercritical fluid-based methods facilitate, could lead to higher value recyclates.

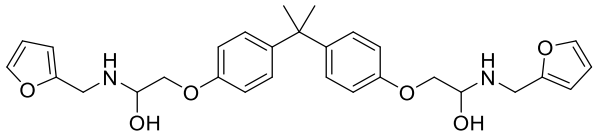

2F

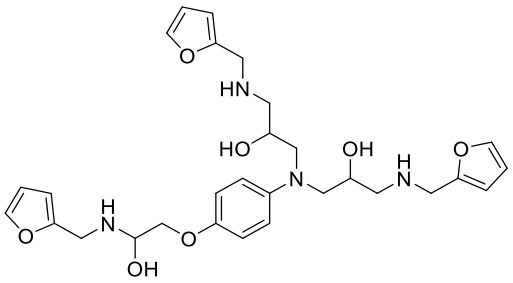

3F

Figure 2.07. The furan monomers prepared by Fortunato *et al.*[35]

In 2015, Turkenburg and Fischer reported a new DA resin based on furan-maleimide epoxies specifically for application in self-healing composites.[36] Considerable attention was given to potential side-reactions (Michael addition of nucleophiles with BMI, and BMI HP). Their strategy to minimise the risk of these side-reactions were to use melt reaction (*vs*. solution) and divide network formation into two steps: (1) prepolymerisation of furfurylamine and DGEBA and (2) BMI crosslinking in a screw extruder. The authors went on to prepare GFRP films and qualitatively confirm self-healing behaviour. The mechanical performance of this system was then explored in a subsequent study by Coope *et al*.[37] using tapered double cantilever beam experiments to quantify healing. Healing efficiencies (in terms of load recovery) in excess of 75% were consistently achievable even up to three repeat cycles. The authors conceded that the mechanical performance of this polymer was significantly lower than conventional epoxy resins but noted that in high fibre volume fraction composites this reduction in performance is likely to be quite small. The authors went on to demonstrate that the polymer could be used to create interleaves for conventional prepregs or as a composite matrix but did not quantify

any results concerning such composites. In a further follow-up study Lejeail and Fischer investigated the use of bisitaconimides as bio-derived alternatives to bismaleimides.[38] In this article, the authors use one of the prepolymers developed in the research presented in this chapter (PreDA0.5, *vide infra*), to reduce the level of crosslinking after reaction with their bisitaconimide (BII), in order to maximise resin processability. Interestingly, the BII resin seems to undergo retro DA reaction at lower temperature (endo 85 °C and exo 110 °C) than the similar BMI-based resin the authors compared it to (105 and 120 °C respectively) which is later introduced as DA0.5 in this chapter. Small GFRP specimens were later prepared from this BII resin system. Interestingly, the 3pb testing revealed that the BII composite suffered from much poorer recycled properties than the BMI composite, with flexural modulus decreasing from 5.32 GPa to 2.41 GPa (*vs*. 4.54 to 3.90 GPa) and flexural strength from 40.2 MPa to 29.6 MPa (*vs*. 56.2 MPa to 51.2 MPa). The reason for this behaviour is not explained; however, this will be discussed again in Chapter 3, Section 3.53—experiments from this thesis indicate that due to isomerisation of the crosslinker, the BII polymer may not be as crosslinked as Lejeail and Fischer expected. Nevertheless, despite this poor mechanical performance the reduction in rDA temperature is noteworthy and thus may be worth pursuing further.

2.1.4 Diels-Alder epoxies 1: aims and objectives

The primary objective of this sub-project is to build on existing DA technology to demonstrate the utility of DA CANs in FRP applications, principally in the form of repairability (self-healing, Section 2.6) and recyclability (Section 2.4.2). Due to the limited amount of research on CANs as composite matrices, secondary objectives include investigations into novel composite manufacturing techniques afforded by their unusual rheological profile (Section 2.5.1), as well as the drawbacks—mechanical or otherwise—surrounding these materials more generally. With this considered, the DA epoxies developed by Fischer and co-workers were the ideal starting point for this project.

2.2 Synthesis and chemical characterisation

2.2.1 Synthesis

Five polymers were synthesised at the beginning of this project based on the original Diels-Alder epoxy system reported Turkenburg and Fischer in 2015.[36] In their two-step process, DGEBA (Epikote 828 resin) was first oligomerised (chain-extended) by reaction with furfurylamine. The resultant prepolymer was then blended with bismaleimide—1,1‘-(methylenedi-4,1-phenylene)bismaleimide, trade name Homide 121 (HOS-Technik), reported hereafter as BMI1—in a screw extruder. The five polymers reported in this work were designed to probe the molecular origins of the thermomechanical behaviour. These include: a baseline system modelled on the most efficient ‘healing’ agent reported in the aforementioned article (DA1), an alternative with half the crosslink density (DA0.5) that should

be more easily recycled, and a second alternative with a more compact bismaleimide crosslinker (DA2). In addition, by testing the two prepolymers (PreDA1 and PreDA0.5) effects originating from the backbone structure of the polymer can be decoupled from the DA crosslinks, experimental details are provided in Section 2.8.

In this work, a one-pot method was used to produce two different prepolymers (PreDA1 and PreDA0.5) and from these, three different Diels-Alder crosslinked systems (DA1, DA2 and DA0.5), Figure 2.08.

Figure 2.08. Close-up of the reaction vessel (during prepolymerisation) prior to the addition of the end-capping reagent (dicyclohexylamine).

The cast product PreDA1 was a translucent off-white glassy solid, which became a white powder when milled (Figure 2.09).

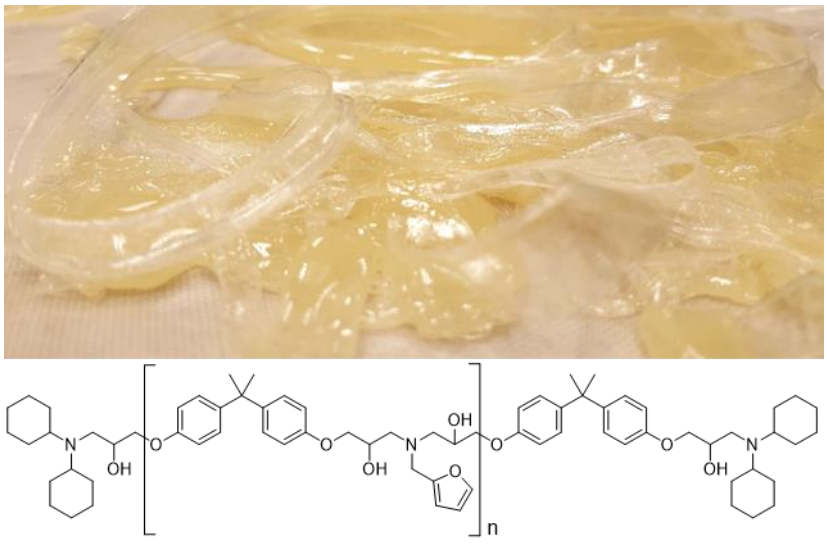

Figure 2.09. The chemical structure and appearance of PreDA1 as cast. On stoichiometric balance n = 4, though in reality a statistical distribution around 4 units exists.

The cast product PreDA0.5 was a translucent off-white glassy solid, which became a white powder when milled (Figure 2.10).

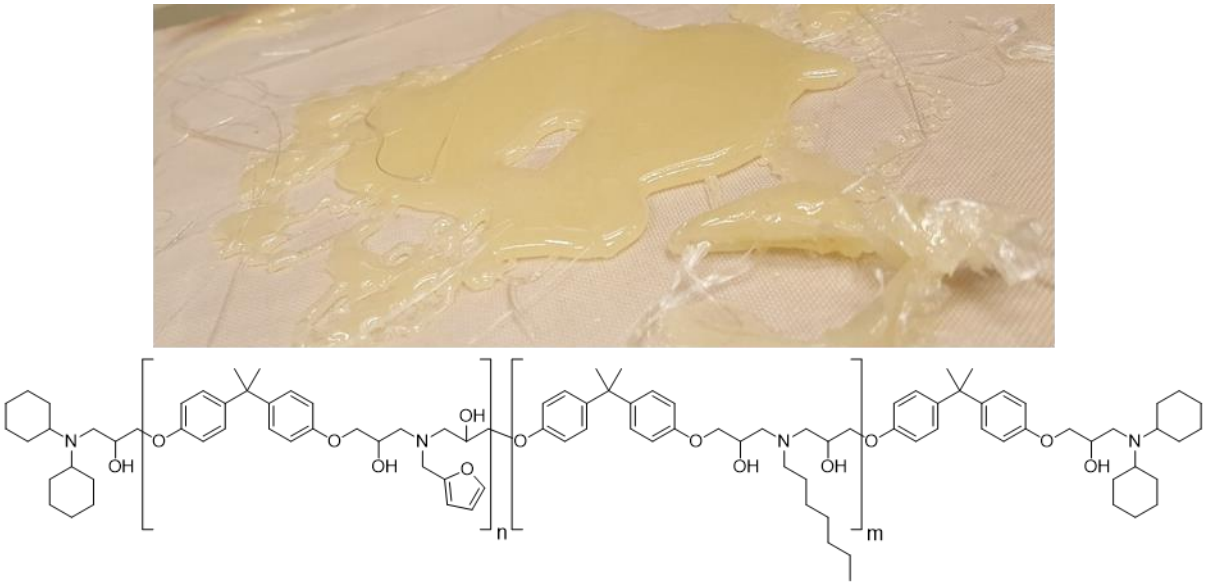

Figure 2.10. The chemical structure and appearance of PreDA0.5 as cast. In this example, the chain length corresponds to a statistical distribution around n = m = 2 (4 units in total).

As cast, DA1 is shown as a glassy solid in Figure 2.11, which was milled into powder prior to further use.

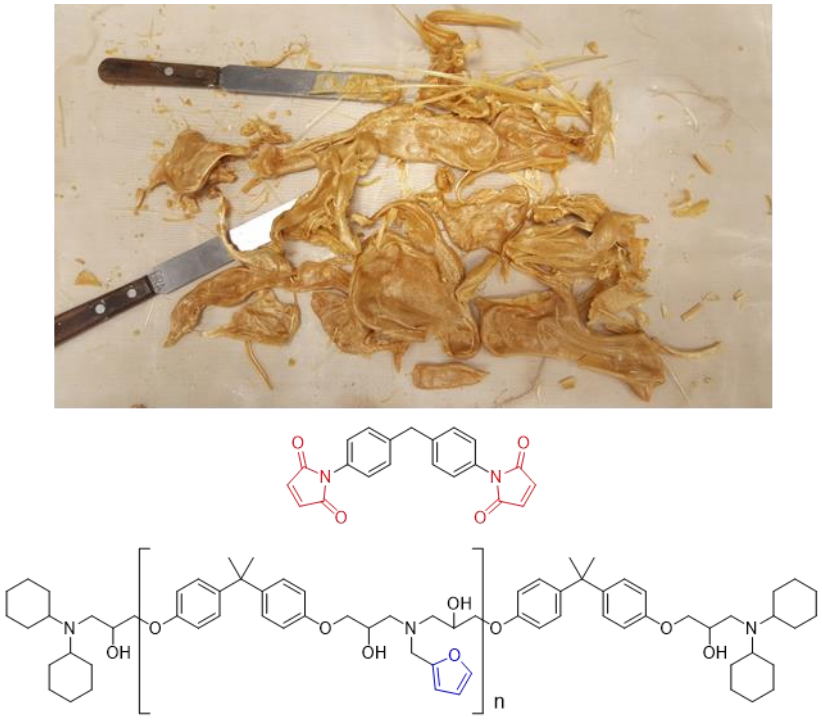

Figure 2.11. The chemical structure and appearance of DA1 as cast, where n is a statistical distribution around an average of 4. The active functional groups of the prepolymer (furan, blue) and crosslinker (maleimide, red) are highlighted. The actual crosslinks exist as the [4+2] cycloaddition adducts of these units (Figure 2.06).

Cast DA2, a brown glassy solid is shown in Figure 2.12.

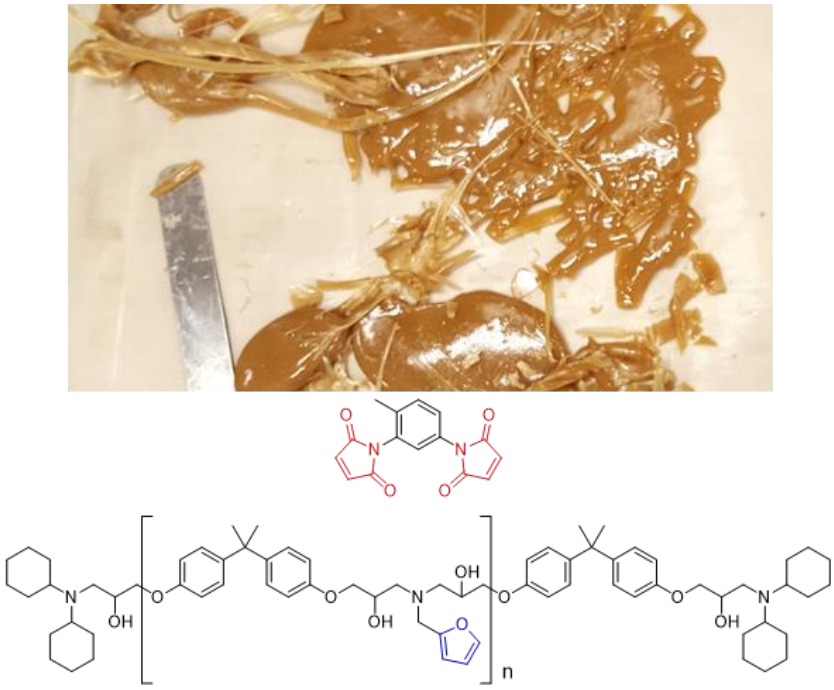

Figure 2.12. The structure and appearance of DA2 as cast, where n is a statistical distribution around an average of 4 monomer units. The active functional groups of the prepolymer (furan, blue) and crosslinker (maleimide, red) are highlighted. The actual crosslinks exist as the [4+2] cycloaddition adducts of these units, Figure 2.06.

Cast DA0.5 is shown as an orange glass in Figure 2.13.

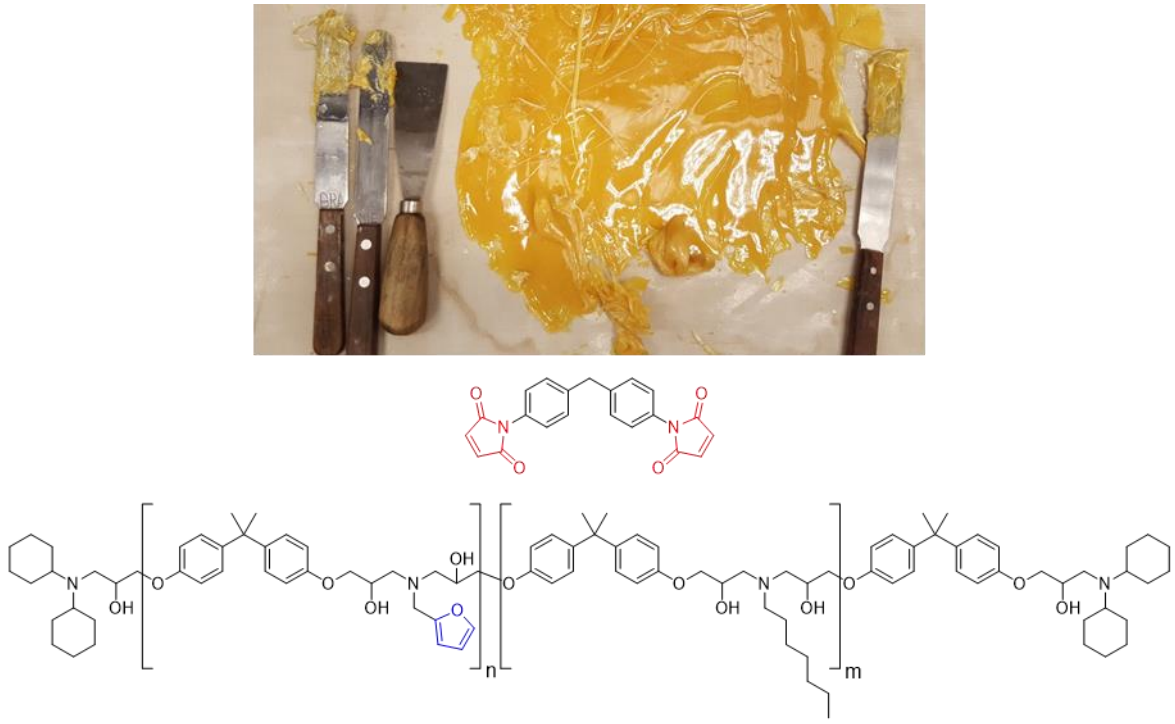

Figure 2.13. The structure and appearance of DA0.5 as cast, where n is a statistical distribution based on a stoichiometry of 2 for each monomer (total = 4). The active functional groups of the prepolymer (furan, blue) and crosslinker (maleimide, red) are highlighted. The actual crosslinks exist as the [4+2] cycloaddition adducts.

The principal differences from the originally published procedure[36] are as follows. First, in the original materials, the prepolymer had residual epoxide groups at each end due to the use of excess epoxide. The authors varied the amine:epoxide ratio and explored in detail how this affected the performance of the resultant polymer. In this work, this latent epoxide was consumed via reaction with a secondary amine. Dicyclohexylamine was chosen for this purpose due to its high boiling point (256 °C), which should allow it to react prior to boiling off. Although the latent epoxide groups facilitated easy incorporation into blends with conventional epoxies, these groups reduced the efficacy of healing—which is dependent on the rDA reaction—by creating irreversible crosslinks. Second, in the original process a screw extruder was used to combine the prepolymer and BMI. However, subsequent testing revealed that the Diels-Alder reaction could be performed in a simpler one-pot process, yielding polymer of similar quality. Accordingly, for the sake of simplicity and scalability the latter procedure was used in this work.

The formulations of each of these polymers are summarised in Table 2.1. The chosen stoichiometry through all five materials, prepolymers and crosslinked polymers, was consistent such that there were approximately 1.25 epoxides for every one primary amine (furfurylamine and *n*-heptylamine) and that there were the proportional number of secondary amines to compensate for this excess. The result of this is that there should be roughly five DGEBA units for every four linking amines and two end-capping amines. Ergo, the prepolymers should be a statistical distribution of oligomers around a modal species, the pentamer, where n = 4 (or n + m = 4) in Figures 2.09 and 2.10 respectively. However, this description is a slight simplification due to the distribution of DGEBA oligomers in the starting resin Epon 828. This resin is not pure DGEBA, but rather a blend of short oligomers. The purpose of this is to reduce the melting point, Epon 828 is a viscous liquid at room temperature whereas neat DGEBA is a solid. The epoxide equivalent weight (average molecular weight divided by the number of epoxide groups per molecule) given by the manufacturer suggests the majority of the resin is monomer. If it is assumed that the higher-order oligomers (3, 4, 5 etc.) are negligible, a crude calculation based on molecular weight suggests that approximately 85% of the resin is monomer and the rest dimer. Therefore, at a rough approximation one in five DGEBA units is a dimer, though since this should only have a limited effect on the thermomechanical behaviour of the polymers—and a negligible effect on the chemistry—these prepolymers can be fairly well approximated as distributions around the pentamer, with a slight bias to longer oligomers.

Table 2.1. The constituents of the DA polymers and prepolymers of this study.

Entry	Epoxy	Chain extender 1	Chain extender 2	End-cap	Crosslinker
PreDA1	DGEBA	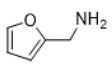	N/A	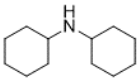	N/A
PreDA0.5	DGEBA	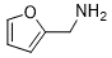		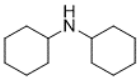	N/A
DA1	DGEBA	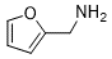	N/A	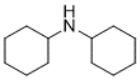	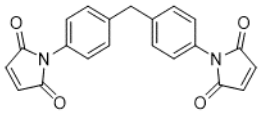
DA2	DGEBA	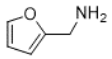	N/A	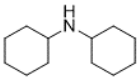	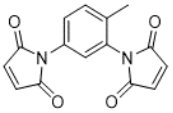
DA0.5	DGEBA	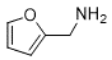		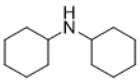	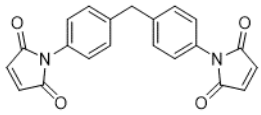
Ctrl1	DGEBA	N/A	N/A	N/A	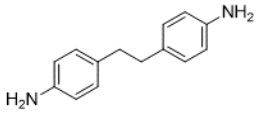
Ctrl2[a]	DGEBA	N/A	N/A	N/A	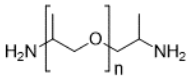

a – small quantities of tetraethylenepentamine, diethylenetriamine and bisphenol A are also used as crosslinkers

In the three crosslinked materials, DA1, DA2 and DA0.5, a ratio of 0.9 maleimide groups to one furan group was chosen. Overall, these stoichiometries were consistent with the best performing materials in the previous studies of Fischer and co-workers (in terms of thermal performance and solvent resistance). The presence of excess maleimide groups is observed to reduce crosslink density by consuming furan groups without bridging the oligomer chains. Although the pentamers are large molecules (MW ~2.5 kDa), on the scale of polymer chemistry, these chains are very short and thus there is unlikely to be any chain entanglement contribution to their mechanical performance. Ergo, the only major interaction holding the prepolymers together (and thus the only major contributor to their strengths) is intermolecular attraction: Van der Waals, π-stacking, dipole-dipole and hydrogen-bonding. The strength of the crosslinked CANs is thus intimately dependent on the DA crosslinks themselves.

There are two possible side reactions common to each of these syntheses. The first, Michael addition, is the 1,4-attack of a nucleophile (in this case an amine) to an electrophilic C=C bond, as found in maleimides (Figure 2.14a).[39] The second, BMI HP, is the self-polymerisation of BMI units which is observed above their melting temperature (Figure 2.14b).[40,41] In both cases the result of the side-

reaction is the formation of permanent crosslinks. Such crosslinks significantly erode the functionality of the polymer by both reducing chain mobility and the number of functional groups capable of participating in the desired DA/rDA reactions.

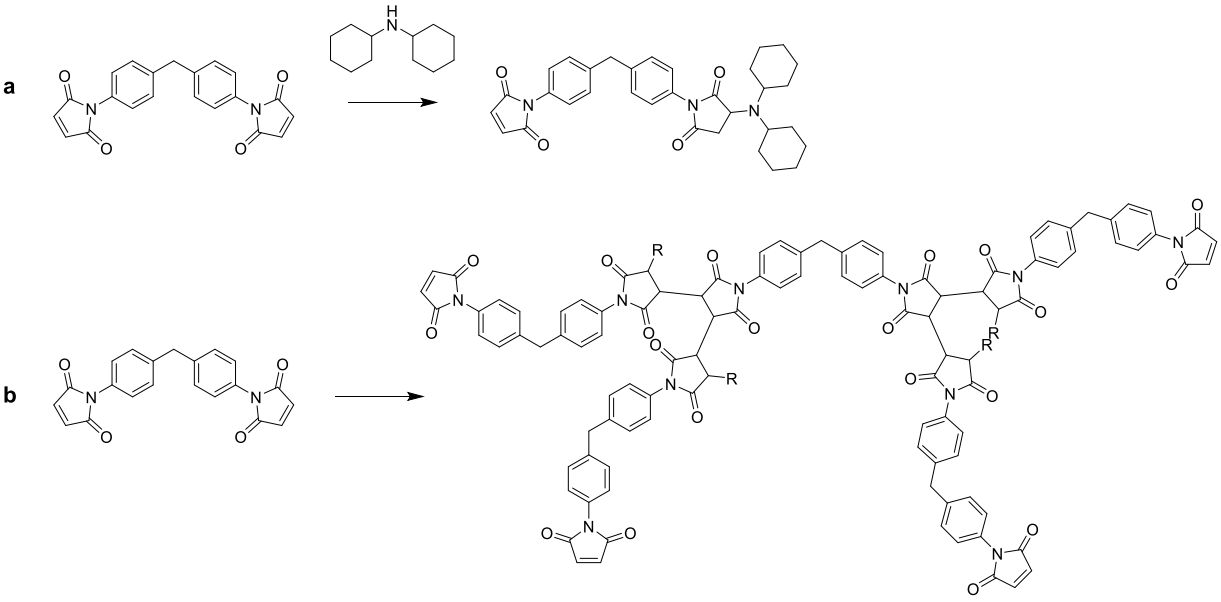

Figure 2.14. The side-reactions of Diels-Alder epoxy synthesis. (a) Michael addition (exemplified by the reaction of BMI1 and dicyclohexylamine). (b) BMI1 homopolymerisation.

Both side reactions result in a colour change from the original gold to a dark orange or red. This is potentially a useful visual indication as to when the DA-CAN has become unworkable, Figure 2.15.

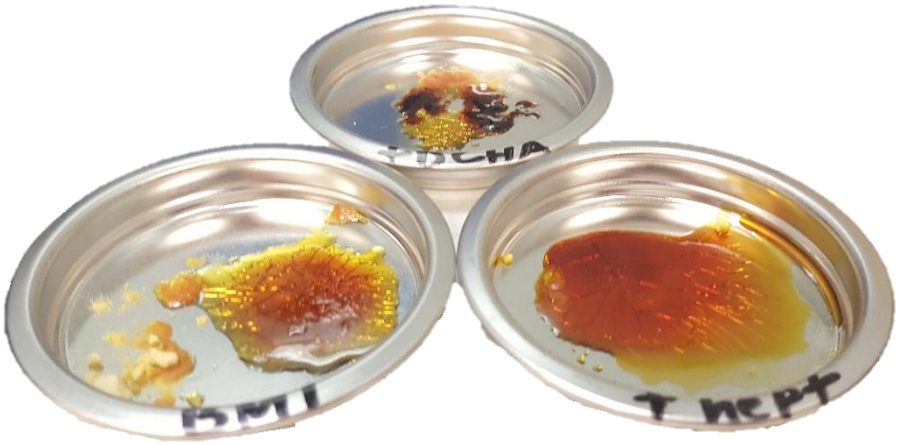

Figure 2.15. Visual indication of side-reaction in DA-epoxy synthesis. Left to right: BMI HP leads to a dark orange colour, the Michael addition of BMI1 and dicyclohexylamine results in a dark red colour and the analogous reaction of *n*-heptylamine and BMI1 results in a dark orange colouration.

The characterisation of these DA polymers and prepolymers is detailed in the following sections.

Two control epoxies were prepared (see experimental for details) as benchmarks for mechanical and thermomechanical comparison, Ctrl1, with an aromatic amine hardener and Ctrl2, with an aliphatic amine hardener. The components of which are also summarised in Table 2.1.

2.2.2 ^{1}H NMR spectroscopy

The ^{1}H NMR spectra of the DA prepolymers are shown in Figure 2.16, from these spectra we can deduce information concerning molecular structure and thus confirm the success of prepolymer synthesis. The two spectra are very similar with the only major differences the additional alkyl protons in the spectrum of PreDA0.5 (1–1.5 ppm, heptyl side groups) and the furyl protons, highlighted in cyan (~6.3 and ~7.4 ppm) which integrate to approximately twice the intensity in PreDA1 *vs*. PreDA0.5 as expected. The bisphenolic aromatics are visible as the two broad multiplets at 6.8 and 7.1 ppm (highlighted purple) and the backbone methyl groups at 3.9 ppm (highlighted orange). The water peak (highlighted grey-blue) is a solvent impurity (not representative of the polymers). Both spectra appear as expected with the ratio of furan integrals to backbone aromatic integrals consistent with the chosen stoichiometry.

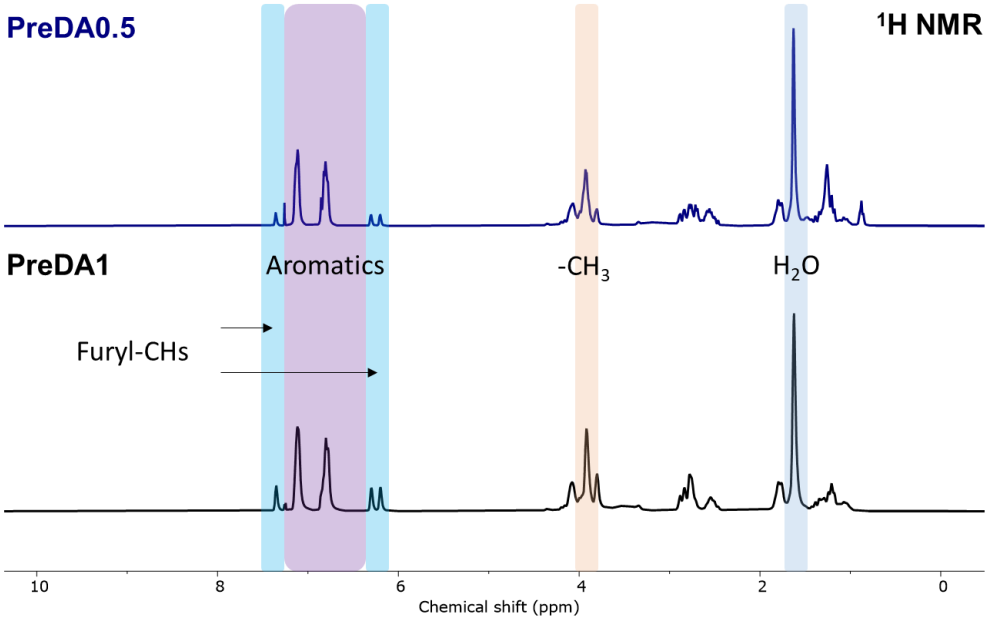

Figure 2.16. ^{1}H NMR spectra of the prepolymers (PreDA0.5 and PreDA1, navy and black respectively) in $CDCl_3$. Selected functional groups highlighted as labelled, non-highlighted peaks correspond to backbone and end-cap (cyclohexyl) CH_2s, hydroxyls and the alkyl side-chains in PreDA0.5.

Solution NMR is generally not appropriate for the analysis of crosslinked samples (such as DA0.5, DA1 and DA2), since this technique requires the sample to be solubilised.

2.2.3 FTIR spectroscopy

The FTIR spectra of each of the DA polymers and prepolymers (in powder form) is shown in Figure 2.17, recorded using a Perkin Elmer Spectrum Two and reported in transmission mode. As with NMR,

the principal purpose of infra-red spectroscopy in this study is to deduce information relating to molecular structure, providing additional evidence that the polymerisation reactions proceeded as anticipated.

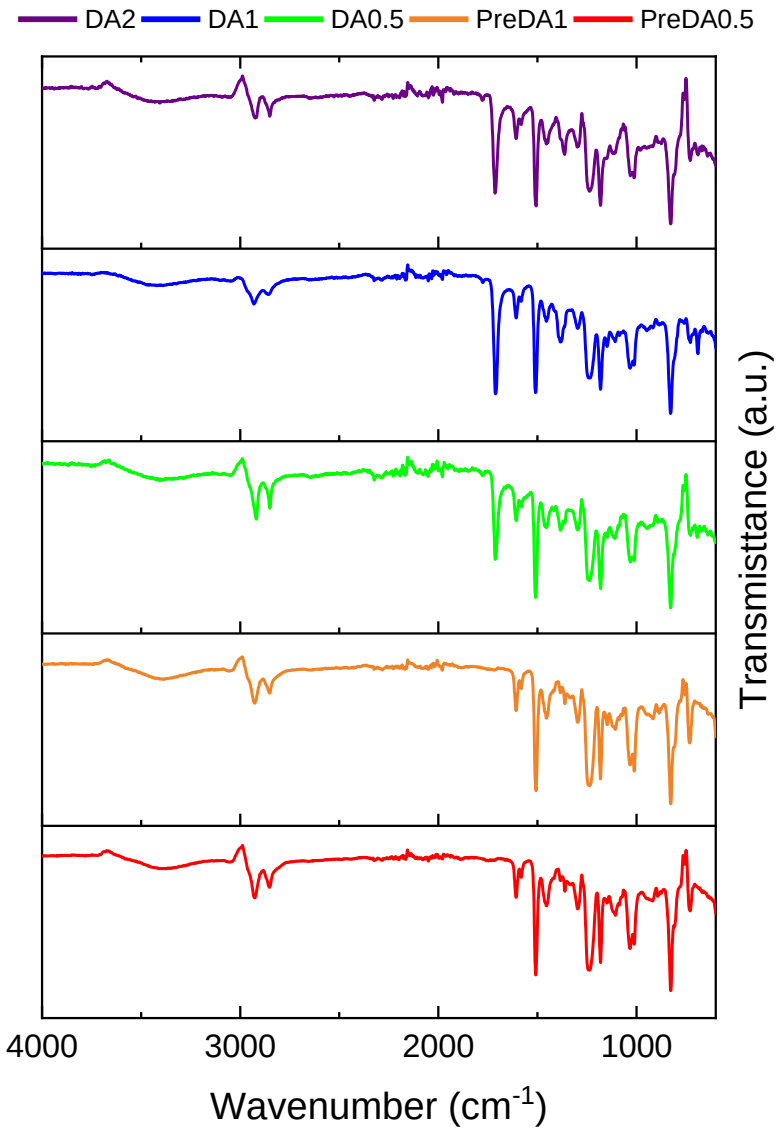

Figure 2.17. Bottom-to-top: FTIR (mid infra-red) spectra of PreDA0.5 (red), PreDA1 (orange), DA0.5 (green), DA1 (blue) and DA2 (purple) respectively (600–4000 cm^{-1}).

Each of the FTIR spectra look similar with several regions common to all five materials: (1) A very broad stretch in the region of 3700–3200 cm^{-1}, indicative of bound hydroxyl groups (participating in hydrogen bonding. (2) The peaks at 2931 and 2857 cm^{-1}, which correspond to alkyl C–H stretches and (3) the fingerprint region, 1500–600 cm^{-1}. This is as expected due their closely related structures. The only observable differences lie in the carbonyl stretching region (1600–1900 cm^{-1}), Figure 2.18.

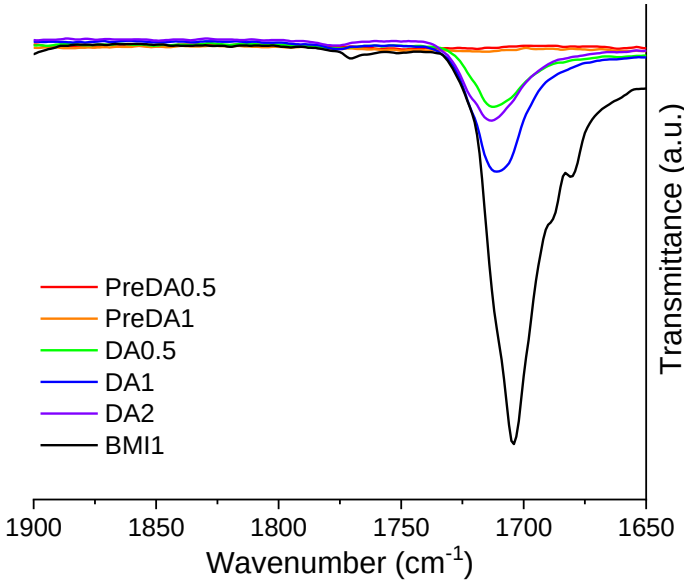

Figure 2.18. The carbonyl stretching region (1650–1900 cm^{-1}) of the DA polymers, prepolymers and BMI1, the bismaleimide crosslinker of DA0.5 and DA1.

As expected, no carbonyl stretches are visible for either prepolymer, but each of the crosslinked polymers exhibits a single broad C=O stretch which is comparable to the primary C=O stretching band of BMI1 (the bismaleimide crosslinker of DA0.5 and DA1), and is included for reference (black line). In each of the polymers the peak absorption (DA0.5: 1712 cm^{-1}; DA1: 1710 cm^{-1}; DA2: 1712 cm^{-1}) is shifted to a slightly higher frequency relative to the BMI reference (1704 cm^{-1}), which likely indicates the expected reaction—and the subtly different C=O environment in the crosslinked (adduct) state. However, these differences are very small; it seems doubtful that this can be used to infer the degree of crosslinking.

In no case is there evidence of significant primary or secondary amine (3200–3400 cm^{-1}) presence, although small quantities could be obfuscated by the broad hydroxyl stretching region. Similarly, there is no evidence of residual epoxide, which is typically observed at 915 cm^{-1} (C–O deformation).

The peaks at 1607 and 1582 cm^{-1} correspond to furyl C=C stretches, Figure 2.19. In this case, the prepolymers exhibit much stronger absorptions than the crosslinked polymers, as expected since these bonds are consumed in the Diels-Alder (crosslinking) reaction. Accordingly, these peaks could be useful for monitoring the extent of crosslinking with time-dependent FTIR, using a hot stage to heat the sample *in situ*. It is worth noting that caution must be exercised when comparing different samples because transmission% is sensitive to the sample size and the quality of contact with the probe.

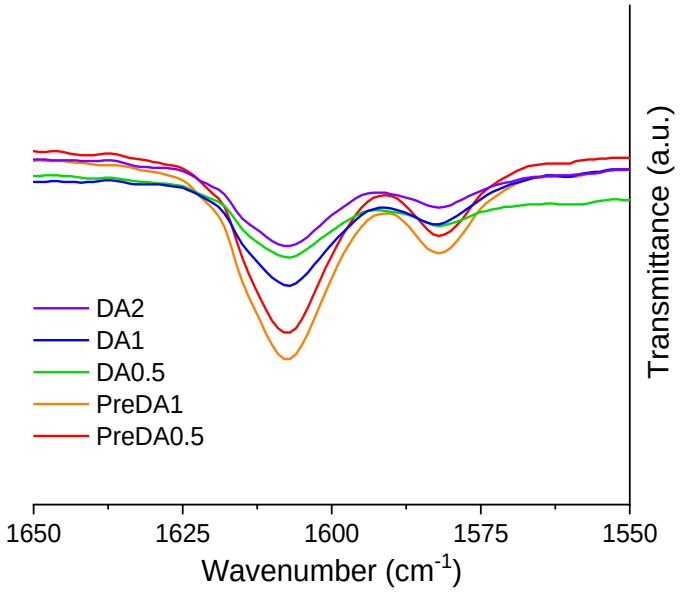

Figure 2.19. The furyl (C=C) stretching region of each of the DA polymers and prepolymers.

2.2.4 Molecular weight assessment: MALDI and GPC

The molecular weight is perhaps the single most important characteristic of linear polymers, since it has a fundamental role in defining all major thermal and mechanical properties. However, network polymers, including CANs, have an essentially infinitely large molecular weight, and thus this number has little significance. Nevertheless, the prepolymers/oligomers have measurable molecular weights, which are dependent upon the reactant stoichiometry. Critically, the molecular weight of these oligomers plays a significant role in terms of the thermal-mechanical behaviour of the CANs they are made into (as will be discussed in Sections 2.3 and 2.5, respectively), accordingly there is value in confirming the molecular weight of these species.

MALDI-TOF (matrix-assisted laser desorption/ionisation) mass spectrometry, behind GPC/SEC (gel permeation– or size exclusion–chromatography), is one of the most widely used methods of characterising polymers and determining their molecular weight. However, MALDI-TOF molecular weight analysis is not always straightforward and is widely reported to be ineffective when probing polymers of wide polydispersity.[42] This principal limitation of MALDI in this respect is that there is substantial discrimination against higher molecular weight oligomers, particularly due to detector saturation with low molecular weight oligomers. Since PreDA1 and PreDA0.5 consist of oligomers of molecular weights varying by over 1 kDa this effect is likely to be significant and thus this precludes accurate molecular weight assessment via this method. Nevertheless, while MALDI in this instance cannot provide average molecular weights, it can still be used to confirm the presence of specific oligomers and determine the repeating units in the polymers of this study.

In the spectrum of PreDA1 a regular pattern emerges from the dominant ion at 704.5 (and its shoulder at 703.5) m/z, of peaks of molecular weight increasing by 438 (1143.0, 1580.4, 2017.7, 2455.0, 2892.6 and 3331.1 m/z). A similar pattern of peaks is visible starting from 961.7 m/z, where peaks of m/z increasing by approximately 438 are again observed. 438.23 neatly corresponds to the molecular weight of the repeating unit shown in Figure 2.20a, thus we can state with confidence that the expected monomer, dimer, trimer and so on up to and inclusive of the heptamer are all present in the sample. Interestingly, the monomer produced (Figure 2.20c) from the reaction of DGEBA with two dicyclohexylamine units (703.54 m/z) appears to be the dominant ion at 704.5.

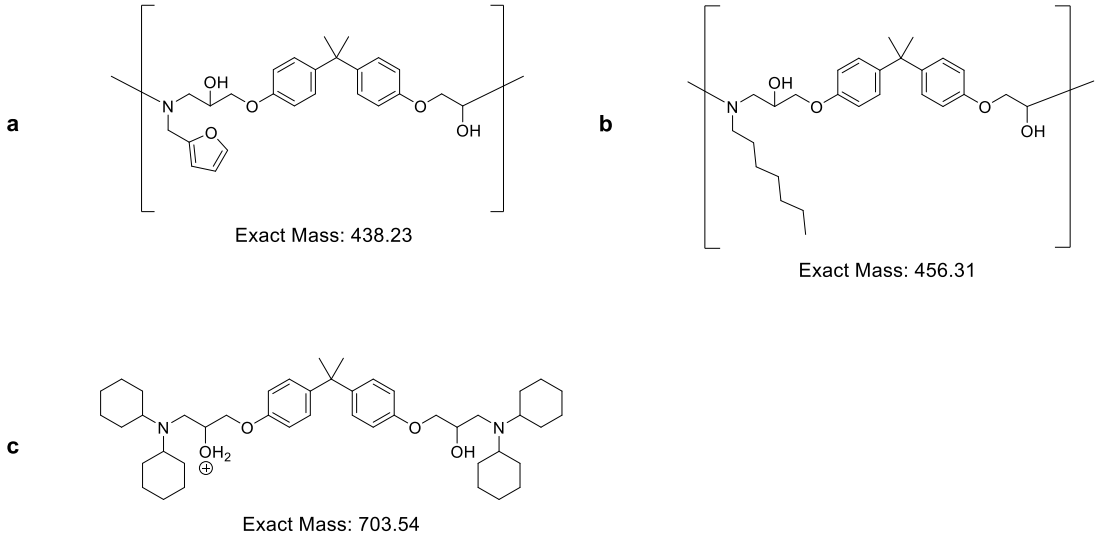

Figure 2.20. (a) the theoretical repeating unit of PreDA1 and its exact mass. (b) the second monomer in PreDA0.5. (c) the PreDA monomer.

The mass spectrum of PreDA0.5 was much the same as PreDA1, with the same dominant peak at 704.5 m/z and peaks consistent with dimers, trimer etc. also readily apparent. However, in this case the pattern is complicated by the presence of a second possible monomer (456.31 m/z, Figure 2.20b). As expected, a complicated pattern of peaks of m/z increasing by both 438 and 456 is observable.

It was conceivable that the process of milling the polymers, crosslinked or otherwise, may damage the material, eroding the chain length and with it the associated mechanical performance. Since all testing performed hereafter—except some rheology—concerns polymer that has been milled at least once, and the recycling process (*vide infra*, Section 2.4.2) requires an additional milling cycle, this is of fundamental importance to evaluate. To accurately determine molecular weight and assess the influence of milling upon molecular weight requires another technique, GPC.

Though GPC comes in a variety of guises, the principle is simple. A polymer solution is pumped through a column of porous particles, the polymer chains spend a certain amount of time residing within these

pores that is proportional to their coiled volume, which in turn is dependent on molecular weight: short polymer chains can most easily enter the pores of the packing material and hence reside on the column the longest. Conversely, the longer chains interact with the column to a much smaller degree and come through first. As the polymers leave the column they pass through a detector (often, but not exclusively a dynamic light scattering system) and from this, several molecular weights and associated metrics are calculated by the instrument. The most important are the number average molecular weight (M_n, the total weight of polymer divided by the total number of molecules), the weight average molecular weight (M_w, which uses the contribution of the molecular weight of individual chains to the overall average) and dispersity, Đ (formerly known as polydispersity index, the ratio of M_w to M_n).

PreDA1 and PreDA0.5 were analysed via GPC relative to a polystyrene (PS) standard in THF (through a polystyrene-divinylbenzene column). The lower molecular weight fractions of both polymers were approaching the calibration limit and were not completely resolved from the solvent peak; however, in all cases the majority of the peak was captured (Figure 2.21), which allows fairly reliable assessment of M_n, M_w and D (Table 2.2) relative to the standard. Each polymer was tested after 1, 2 or 3 milling cycles. Importantly, no significant difference (within experimental error) was observed between samples of different cycle. Thus the reduction of molecular weight due to milling is negligible compared to the molecular masses of the chains involved. Accordingly, this suggests that milling should not have a significant effect upon mechanical performance.

Table 2.2. GPC molecular weight assessment of PreDA1 and PreDA0.5 relative to a polystyrene standard.

	PreDA1			**PreDA0.5**		
	A	**B**	**C**	**A**	**B**	**C**
M_n / kDa	3.85	3.80	3.81	4.34	4.46	4.45
M_w / kDa	6.99	7.36	7.21	11.74	11.12	10.62
Đ	1.82	1.94	1.89	2.71	2.49	2.39

GPC separates polymers in terms of their column retention times dependent upon the apparent size of the polymers in solution. Different polymers of the same molecular weight may vary considerably in terms of their apparent size in a given solvent as a function of both intramolecular and intermolecular interactions. Accordingly, assessment of absolute molecular weights via GPC requires precise calibration. Such precise methods exist, such as by calibrating to the same material as is to be tested after determining molecular weight via other methods such as osmometry. Alternatively, universal calibration methods are widely used based on the seminal work of Benoit *et al*.[43] This method relies upon an viscosity analysis of several narrow standards. Time and equipment constraints

rendered these calibration methods impractical, thus for the sake of these simple analyses relative calibration was considered sufficient.

Although analysis of a wide range of polymers using a standard PS calibration is commonplace in the literature, it is well documented that the calculated molecular weights can deviate significantly from absolute values. The work of Noor *et al*.[44] in 2017 highlights this particular issue: the researchers found that a carefully designed calibration series that more closely resembled the polymers they were analysing, resulted in molecular weights (M_w and M_n) approximately 50% lower than analogous tests using a PS standard calibration. Importantly, these lower molecular weights were in close agreement with vapor pressure osmometry experiments.

Although the different samples may be reliably compared with each other, the results of this study should thus be used with caution—the absolute values are not likely to be accurate due to this non-optimised calibration.

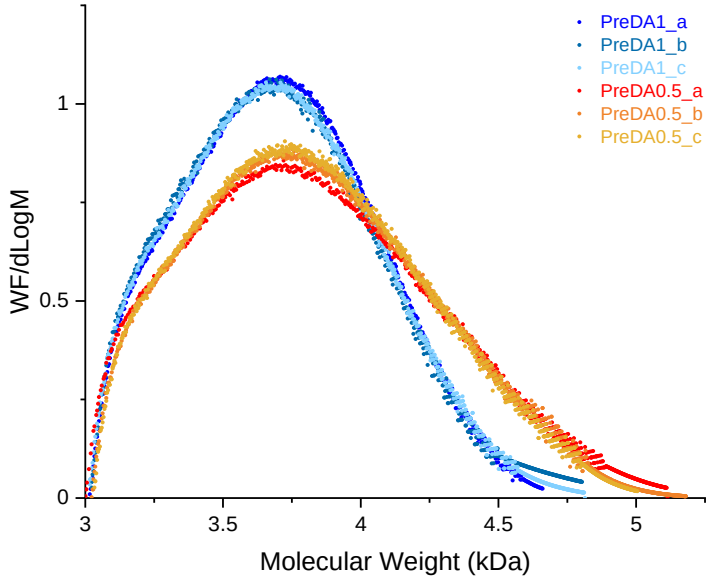

Figure 2.21. The raw molecular weight distributions observed from GPC. Where 'a', 'b' and 'c' refer to 1, 2 or 3 milling cycles respectively.

The theoretical modal species of both PreDA1 and PreDA0.5 based on their stoichiometries are the respective pentamers ~2.4 kDa or the analogous species where one of the five monomers is a DGEBA dimer, ~2.7 kDa. In either case the PS-calibrated GPC M_n values imply modal species of approximately 4.0 and 4.5 kDa respectively. Because these polymers are both bulkier and more polar than the PS standard, PreDA1 and PreDA0.5 will have a significantly shorter retention time than PS of equivalent molecular weight. This effect should be more pronounced for PreDA0.5, which due to the presence of the *n*-heptyl branches should have a significantly larger hydrodynamic volume (and apparent size in solution) than PreDA1. This is reflected in the results shown in Table 2.2. Though theoretically the two

prepolymers should be very similar in molecular weight (PreDA0.5 is 0.036 kDA heavier), the observed M_n of PreDA0.5 is significantly greater (~0.7 kDa heavier). The difference in M_w—which is biased by heavier components—is even more pronounced with PreDA0.5 ~4 kDa heavier. This is further reflected in the differences in Đ with PreDA0.5 showing a much broader molecular weight distribution, an expected product of the wider variety of components in PreDA0.5. In summary, these experiments show that both prepolymers are broadly in the region of molecular weights expected from theory, although there is significant disparity, this is to be expected from the calibration which was used. Importantly, both prepolymers show a broad molecular weight distribution, with PreDA0.5 significantly broader than PreDA1. There is negligible change in molecular weight observed after milling.

2.3 Thermal characterisation

2.3.1 Rheology

Rheometry is a highly versatile tool in polymer chemistry. The many variables determining the fluid behaviour of polymer melts (temperature, shear rate, geometry, molecular weight, thermal history etc.) mean that an infinite variety of experiments can be used probe the rheological behaviour of polymers. In thermoset (curable) systems, one of the most valuable insights from rheology is the processing window, i.e. how much time is available at a given temperature to formulate a polymer resin before the viscosity grows to such an extent it is unworkable. Or what temperature range the resin can be used in before the viscosity makes it unworkable. This 'working lifetime' concept will be explored later in this section with simple isothermal experiments. CANs, due to their reversible crosslinking, exhibit unusual rheological behaviour. In thermally activated (dissociative) CANs, as the polymer de-crosslinks it is associated with a large, sharp drop in viscosity, similar to a melt in some thermoplastics. As temperature decreases and the crosslinks reform, the polymer becomes a glassy solid again. Accordingly, experiments with a dynamic temperature profile (and constant shear rate) can be highly informative and are thus ideal for confirming CAN-type behaviour. Experimental details are provided in Section 2.8.

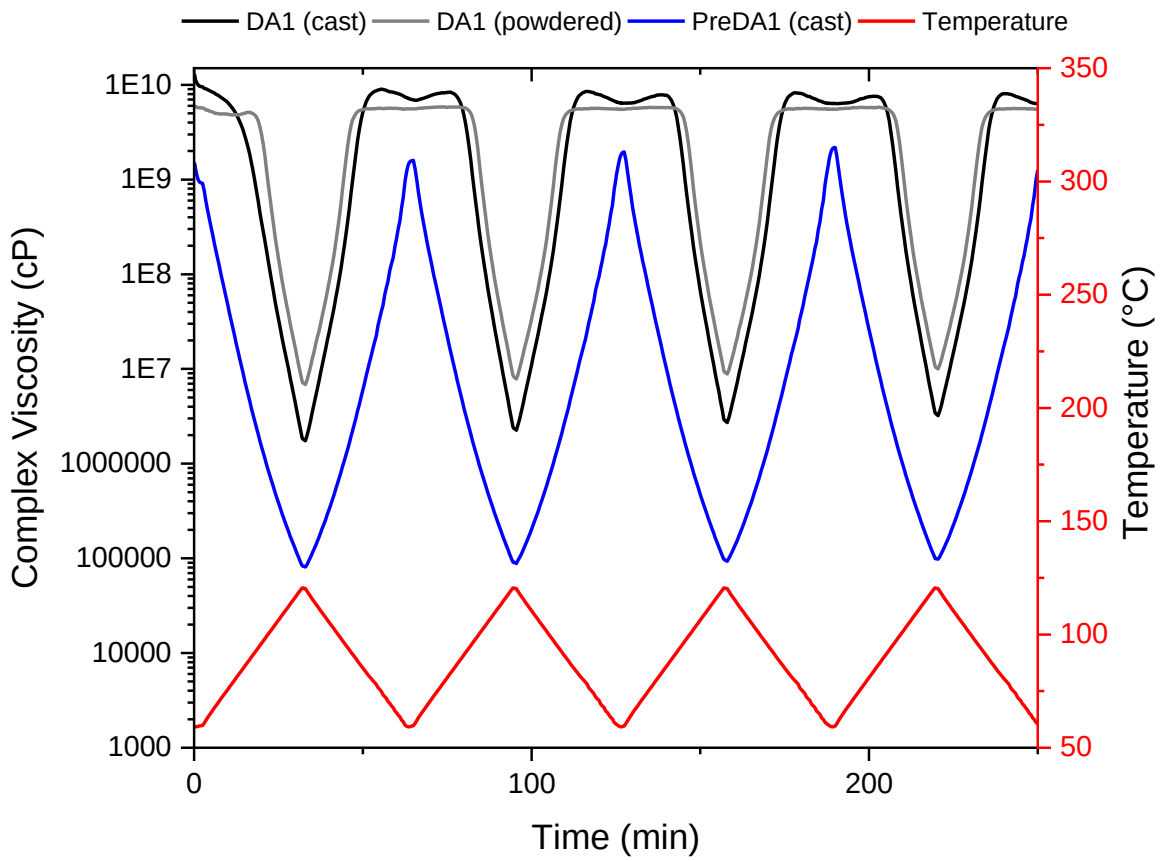

Figure 2.22. A viscosity-time-temperature plot comparing the behaviour of DA1 (both as cast and after milling) and its prepolymer (PreDA1, as cast) in cycles between 60 and 120 °C (parallel plate, 0.1% oscillatory strain, 1 Hz).

The prepolymer PreDA1 reversibly softens, with viscosity dropping from 10^9 cP to just under 10^5 cP at 120 °C, consistently for each cycle, Figure 2.22. Within this temperature range PreDA1 is above its glass transition temperature; a viscoelastic liquid throughout the experiment. In contrast, the two forms of the DA1 CAN show a more distinct transition from solid (10^{10} cP is approximately the upper limit of measurement) to viscoelastic liquid. Both forms show a slight increase in the minimum viscosity with each cycle, consistent with the material becoming increasingly crosslinked. This could be the product of either the material becoming more homogeneous, such that there are more Diels-Alder linkages, or indicative of permanent crosslinking due to side-reactions. In any case, this is a small effect at this temperature and clearly demonstrates the repeatable nature of the de-crosslinking process: this behaviour is not possible with conventional crosslinked materials (which remain solid up to the point of decomposition).

Interestingly, the two forms of DA1 show significantly different behaviour. The cast polymer shows a significantly lower minimum viscosity than the powdered material. Milling the polymer and re-melting it is certain to increase the homogeneity and this seems likely to be the dominant factor resulting in

this difference. The temperatures and durations in this experiment are unlikely to result in significant side-reaction.

In Figure 2.23, the three cast CANs, DA0.5, DA1 and DA2 are compared. There are several notable differences between these three CANs, the most obvious being the disparity in viscosity minima (at 120 °C). With half as many crosslinks to undergo the retro-DA reaction, DA0.5 has the lowest minimum of viscosity (~1E+6 cP). Presumably, this reflects the presence of a smaller number of residual crosslinks at 120 °C, in all cases the DA reaction is in equilibrium, and even at 120 °C, some intact crosslinks are expected. DA1 has only a slightly higher viscosity minimum (~2E+6 cP), which suggests that both DA1 and DA0.5 are almost entirely dissociated. However, when inspecting the profiles of the corresponding prepolymers, Figure 2.24, it becomes apparent that PreDA1 is significantly less viscous than PreDA0.5. Hence it is likely that DA0.5 has fewer residual crosslinks than DA1 and the similarity in viscosity minima is coincidental, a product of the differences in the prepolymer (which is essentially the fully de-crosslinked state). A much more substantial difference is observed when comparing DA2 to DA1 and DA0.5. With a viscosity minimum of ~1E+7 cP, DA2 has a significantly higher minimum viscosity. This observation can be readily explained by the difference in the Diels-Alder chemistry; the higher minimum suggests the presence of significantly more residual crosslinks. Indeed, the second notable difference between the curves—the onset of the viscosity drop (i.e. de-crosslinking onset)—seems to support this hypothesis. DA2 (~90 °C) has a later onset of de-crosslinking (relative to DA1: ~80 °C and DA0.5: ~65 °C), graphically shown by the widest plateaus at the top of the figure. Accordingly, it seems probable that the whole process of de-crosslinking is shifted to a higher temperature for DA2 relative to the other polymers, therefore a smaller fraction of its crosslinks are broken at 120 °C.

The final point to note from Figure 2.23 is that all of the DA polymers show that they can repeatedly crosslink and de-crosslink, with only a slight increase in the minimum of viscosity with each cycle. This trend of increasing viscosity is probably a product of both increasing homogeneity—resulting in a greater proportion of crosslinks formed after each cycle—and the side reactions discussed previously, Figure 2.14.

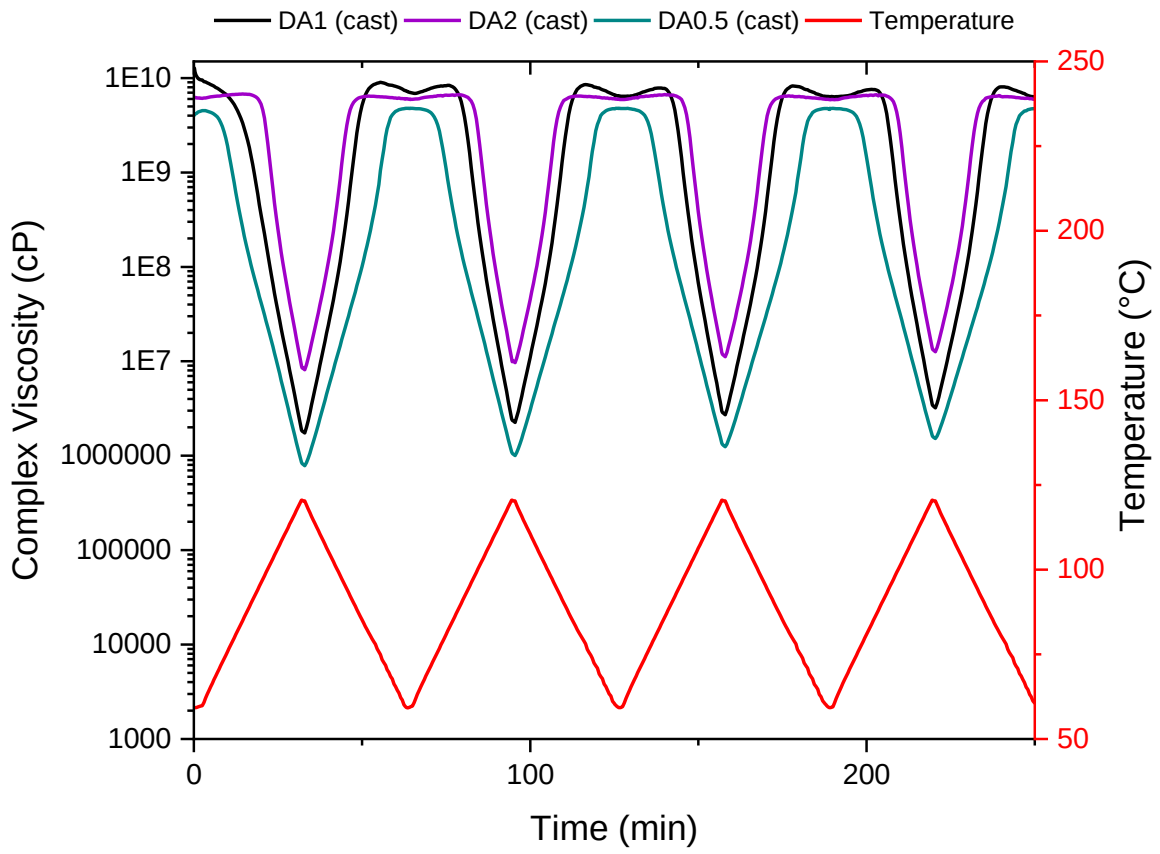

Figure 2.23. A viscosity-time-temperature plot comparing the behaviour of DA1, DA2 and DA0.5 between 60 and 120 °C (parallel plate, 0.1% oscillatory strain, 1 Hz).

The rheological behaviour of the two prepolymers, PreDA1 and PreDA0.5 is shown in Figure 2.24.

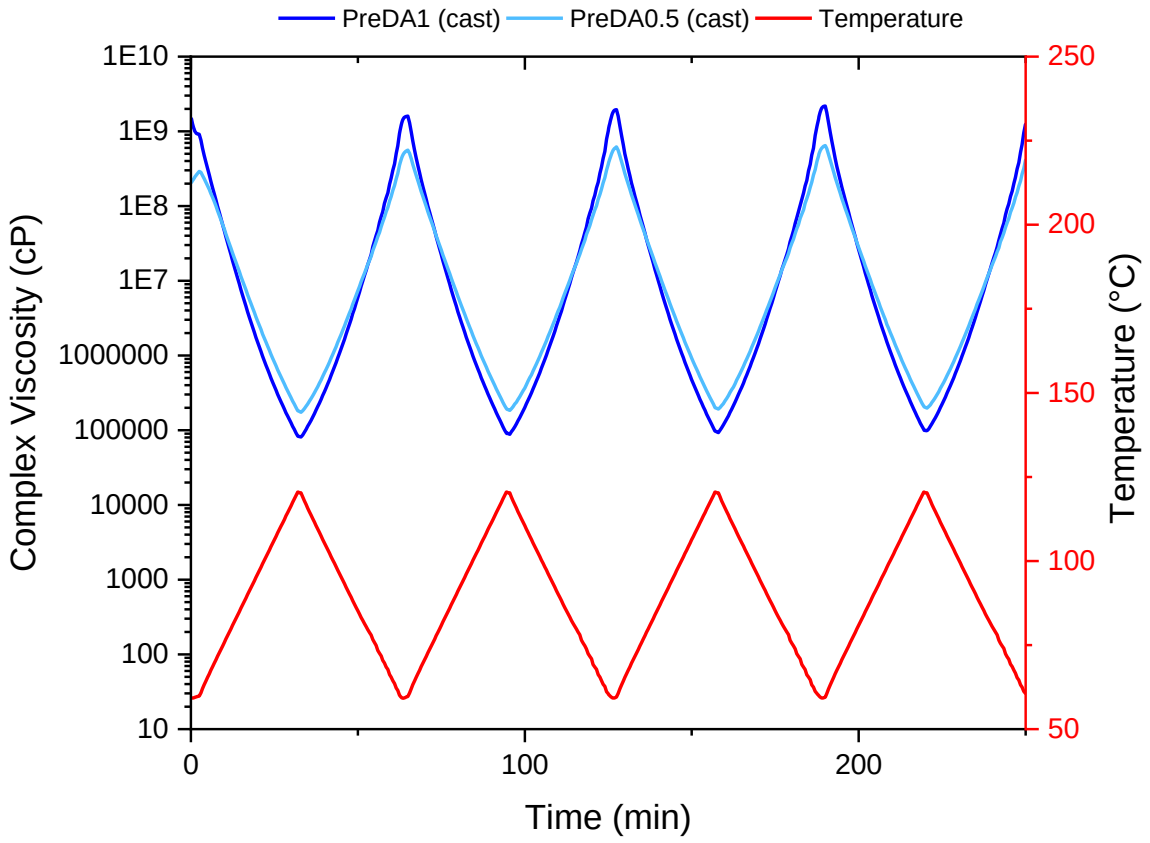

Figure 2.24. A viscosity-time-temperature plot comparing the behaviour of PreDA1 and PreDA0.5 in cycles between 60 and 120 °C (parallel plate, 0.1% oscillatory strain, 1 Hz).

A key feature of Figure 2.24 is the absence of an upwards trend in viscosity minima (observed of all the crosslinked polymers). In this case, the two prepolymers show no discernible difference in their viscosity minima with repeated thermal cycling, indicating that these materials are thermally stable within this temperature range and are not undergoing further chemical reactions (confirming the polymerisations as complete). Interestingly, the two profiles are quite different: PreDA1 has both a greater maximum viscosity (1.5E+9 cP) and lower minimum viscosity (8E+4 cP) than PreDA0.5 (5E+8 cP and 2E+5 cP respectively). On first inspection this might seem contradictory; however, both phenomena may be explained by the differences in chemical structure. At lower temperature, when the materials are best described as glassy solids, PreDA1 has a much more regular structure, with an aromatic backbone and aromatic side groups (furan), this material can stack much more efficiently and the net result of this is stronger intermolecular (inter-chain) interactions and a higher T_g (which will be explored later with DSC and DMA experiments). In contrast, the less regular structure of PreDA0.5, with two different side groups (one aromatic, one aliphatic) there is less efficient solid-state packing and this material has a lower T_g, softening earlier. At higher temperatures, beyond T_g, the prepolymers melt and are better described as viscoelastic liquids. As a melt, PreDA0.5 again is a a

much more complicated combination of molecular structures due to its two side groups, and importantly, the relatively long aliphatic (*n*-heptyl) side groups are likely to contribute to a larger radius of gyration and a less efficient flow of these chains over each other. On a macroscopic scale this would be expected to manifest as a relatively higher viscosity, as observed.

Each of the dynamic rheology experiments (with cast samples) are summarised in Figure 2.25.

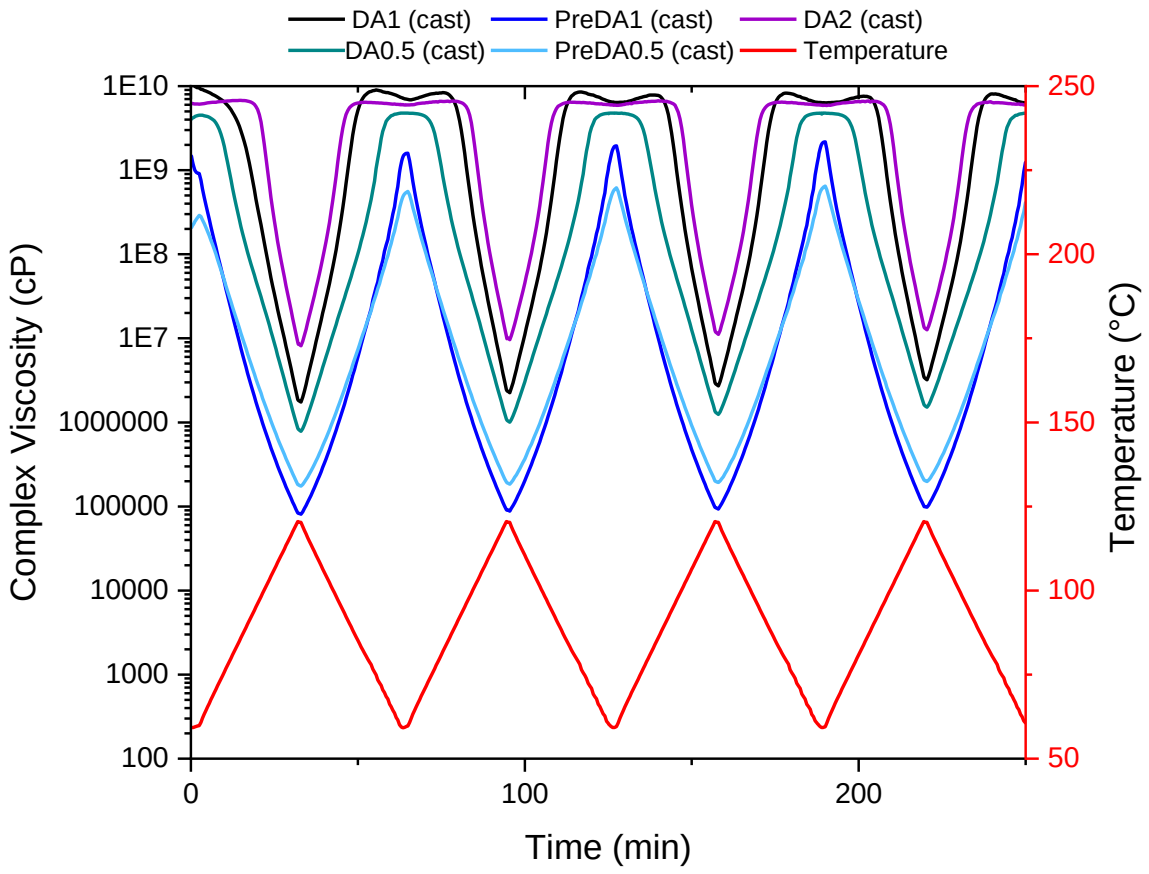

Figure 2.25. A viscosity-temperature-time plot demonstrating representative rheological behaviour of each of the polymers in this study, in cycles between 60 and 120 °C (parallel plate, 0.1% oscillatory strain, 1 Hz).

A second series of rheology experiments was performed to further examine the observed upwards trend of viscosity minima with the three crosslinked DA epoxies. In this series each of the polymers was held isothermally at 120 °C and the increase in viscosity was monitored over time. This provides information on 'working lifetime', Figure 2.26.

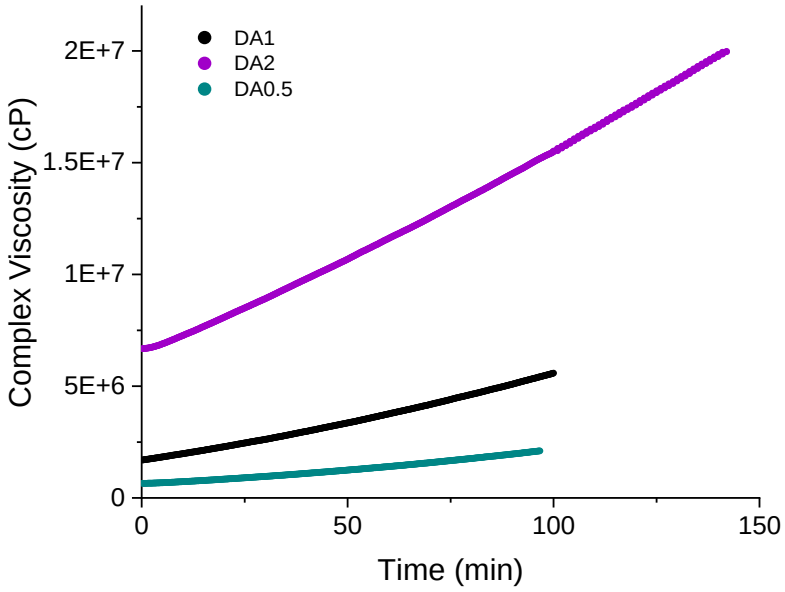

Figure 2.26. 120 °C isothermal rheology of the Diels-Alder epoxies (parallel plate, 1% oscillatory strain, 1 Hz).

With an initial viscosity of approximately 1.7E+06 cP, DA1 takes approximately 50 min to double in viscosity and 90 min to triple to 5.1E+06 cP. For comparison, DA2 with a much higher baseline viscosity of 6.7E+06 cP takes almost 80 min to double in viscosity and 140 min to triple in viscosity 2.0E+07 cP. In agreement with the dynamic experiments, DA0.5 is much more similar to DA1, with a lower baseline viscosity 6.6E+05 cP, a 54 min time to double in viscosity and 90 min to tripling in viscosity (to 2.0E+06 cP). As previously discussed, the mechanism behind the increasing viscosity is likely a product of both a gradual increase in homogeneity of the DA-linkages, and permanent crosslinking (side-reactions). This simple study indicates that DA1 and DA0.5 have a working lifetime in the region of >100 min at 120 °C; even a viscosity increase of three-fold leaves the CANs with some melt-like behaviour (viscosity around 5E+06 cP). DA2 is much higher in viscosity than DA1 despite the structural similarity. Although the increase in viscosity associated with DA2 is slow, its high baseline viscosity may make it unworkable within 1 h at 120 °C (viscosity above 1E+07 cP). This illustrates that the BMI has a significant influence on viscosity and therefore resin processability—a more flexible BMI crosslinker could be designed to optimise resin processability for specific manufacturing conditions.

With baseline viscosities of *ca*. 10^6 cP, which equates to 1000 Pa.s at 120 °C, the viscosities of these DA CANs are significantly above the processing viscosities of infusible thermoset resins (*ca*. 1 Pa.s) and even prepreg thermosets (*ca*. 10–100 Pa.s). This means that these polymers will require pressurisation during impregnation and thus may only be compatible with compression moulding techniques. However, unlike most CANs and vitrimers, these DA materials are pre-cured, which explains the high viscosity compared to conventional thermosets. This means these materials cannot compete with thermosets as was outlined as desirable at the end of Section 1.7. Instead, these CAN powders are

more akin to thermoplastics in terms of their processing conditions. Nevertheless, as unreactive powders these CANs have the advantages of easy storage/handling and an indefinite shelf-life.

2.3.2 Differential scanning calorimetry

The DSC profiles of each of the three DA CANs and their respective prepolymers are presented herein. These plots provide information concerning physical and chemical events (and their reversibility) and provide a first means of characterising glass transition temperature, T_g. For reference, the DSC profile of BMI1 is shown in Figure 2.27. Two large, sharp endotherms are evident in the first heating cycle at approximately 155 and 165 °C, representing the melt of crystalline phases. Almost immediately after the second endotherm (~170 °C), an exotherm indicative of BMI HP is evident.

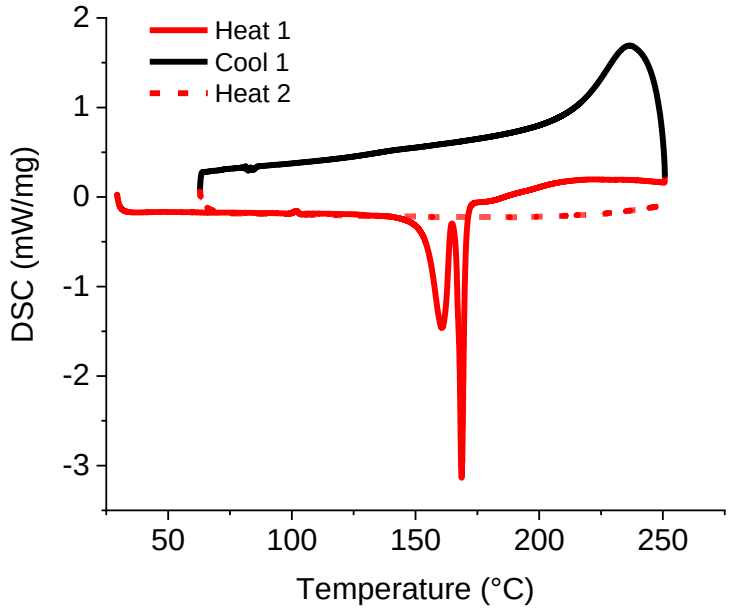

Figure 2.27. A representative heat-cool-heat of BMI1 between 30 and 250 °C (exo up, 10 °C min^{-1}, ~8 mg sample mass).

In Figure 2.28, a representative heat-cool-heat of DA1 is shown.

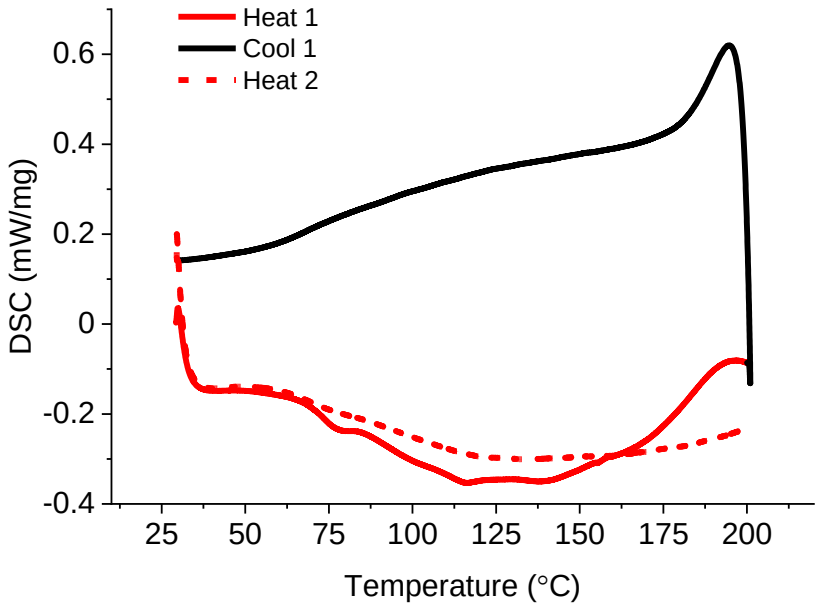

Figure 2.28. A representative heat-cool-heat of DA1 between 30 and 200 °C (exothermic up). Approximately 5 mg of polymer was used with a heating rate of 10 °C min^{-1}.

The glass transition of this polymer is clearly visible in both the first heating and cooling phases of the experiment as a second order event (or step in the curve) at approximately 75 °C. The key feature is the very broad endotherm between 70 and 180 °C which corresponds to the equilibrium of the DA/rDA reactions: as the temperature increases the equilibrium position shifts to increasingly favour the retro-DA reaction, becoming more endothermic as more bonds are broken. However, several other thermal events are superimposed over this, with the most important being an exotherm between 160 and 200 °C. It is likely that this corresponds to HP of free BMI1 (Figure 2.27): where rDA is favoured a significant proportion of the BMI crosslinker will be free in the polymer melt, and above their melting points (in this case 155 °C, which is detectable in the DSC trace) BMIs are known to homopolymerise. The result of homopolymerisation is the formation of a polyimide phase and an associated decrease in the number of DA crosslinks (that would otherwise reform on cooling). As expected, in the second heating phase the area of both the rDA endotherm and HP exotherm are significantly reduced. There are several other minor irreversible features superimposed on the rDA endotherm: at 70–85 °C, 115 °C, 140 °C and 155 °C. As previously alluded to, the small endotherm at 155 °C probably corresponds to a melt of BMI-rich regions. With regards to the other events, due to their size relative to the larger endotherm, it is unclear if these correspond to small exotherms/endotherms or second order transitions. One possibility is that these points reflect the maxima of the endo and exo rDA reactions. As discussed in Section 2.1.2, the *endo* DA adduct generally undergoes reversion at lower temperature.

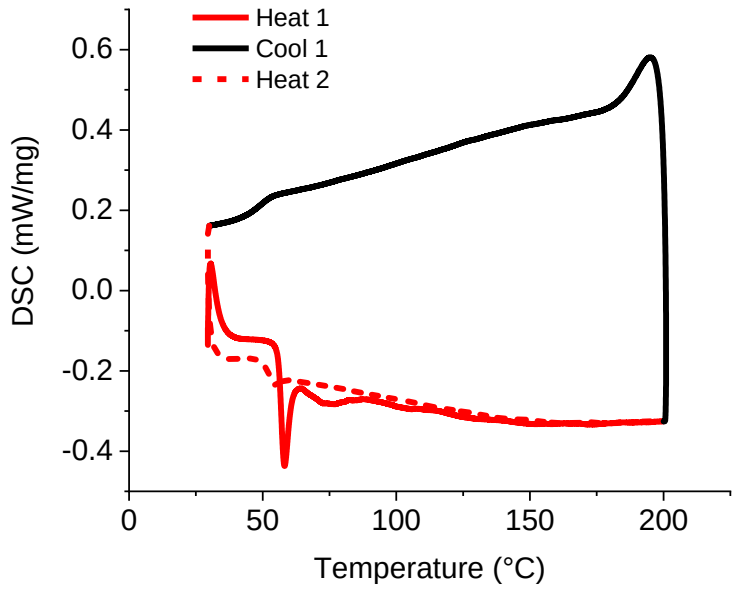

Figure 2.29. A representative heat-cool-heat of PreDA1 between 30 and 200 °C (exo up). Approximately 5 mg of polymer was used with a heating rate of 10 °C min^{-1}.

The glass transition of PreDA1 is obscured by a large melting event (sharp endotherm) in the first heating phase, though it is clearly visible in both the cooling and second heating phase as a step at approximately 52 °C. Secondary endotherms are visible at approximately 75, 100 and possibly 130 °C, which is likely a product of sample inhomogeneity.

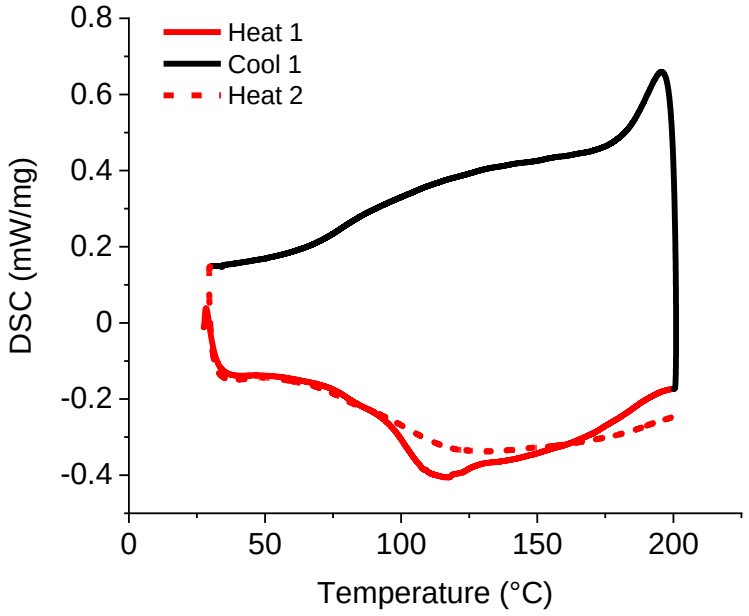

Figure 2.30. A representative heat-cool-heat of DA2 between 30 and 200 °C (exo up). Approximately 5 mg of polymer was used with a heating rate of 10 °C min^{-1}.

The DSC profile of DA2, the second polymer made from PreDA1 (with BMI2 as the crosslinker), is shown in Figure 2.30. The T_g is less pronounced than in DA1, but is just visible at approximately 80 °C.

This is slightly higher than the two other DA epoxies, which could be a product of the tighter interchain packing which would be expected from the shorter crosslinking unit (tolyl *vs*. bisphenyl). A larger DA endotherm is also observed at the slightly higher temperature range of 80–180 °C. This suggests a more abrupt change from the DA-dominated to rDA-dominated regimes. Beyond ~160 °C there is an exotherm indicative of BMI HP. Importantly, in this case there seems to be greater residual DA-activity (endotherm) in the *second* heating cycle of this material compared to the other two DA-epoxies. This supports the theory that BMI2 undergoes HP at a higher temperature than BMI1. This could be explained by the higher melting point of this compound (the manufacturer reports that its melting point is approximately 20 °C higher than BMI1).

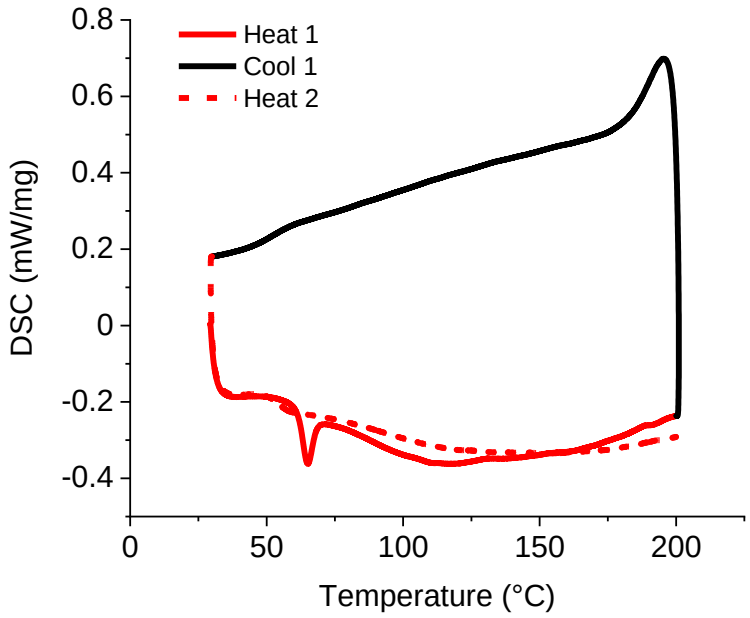

Figure 2.31. A representative heat-cool-heat of DA0.5 between 30 and 200 °C (exo up). Approximately 5 mg of polymer was used with a heating rate of 10 °C min^{-1}.

The glass transition temperature of DA0.5 (Figure 2.31) is approximately 55–60 °C and is considerably better defined than the more densely crosslinked materials (DA1 and DA2). In sharp contrast to DA1 there is a well-defined melting event at 65 °C, which likely corresponds to T_v, the topological freezing temperature, above which the dynamic chemistry become active. This may be more pronounced in the case of this polymer, due to the presence of short oligomers not bound into the polymer network, which would be expected of a material with much lower crosslink density. Otherwise, the same features are observed: a 70–180 °C endotherm corresponding to the DA/rDA equilibrium though this is less pronounced due to the reduced number of furan and maleimide groups. The exotherm corresponding to BMI HP is also less clearly defined for the same reason. Both of these major events are similarly diminished in the second heating process due to consumption of BMI by HP.

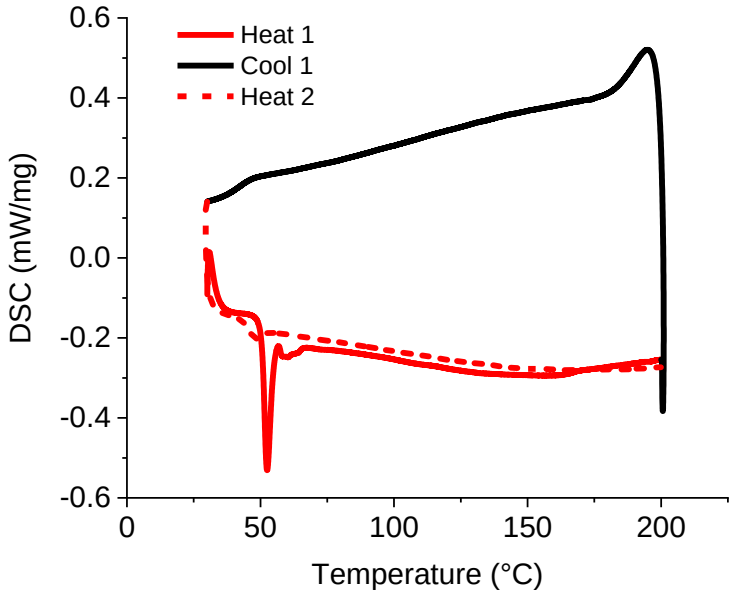

Figure 2.32. A representative heat-cool-heat of PreDA0.5 between 30 and 200 °C (exo up). Approximately 5 mg of polymer was used with a heating rate of 10 °C min^{-1}.

The glass transition of PreDA0.5 is at a slightly lower temperature (40–45 °C) than the more regular prepolymer PreDA1 (50 °C). As with the other prepolymer, PreDA0.5 shows a sharp endotherm corresponding to a primary melting event at approximately 53 °C (5 °C lower than PreDA1). A secondary irreversible endotherm is visible at around 60 °C, which likely corresponds to the melting event of a minor phase (perhaps a furfurylamine-rich phase as this is close to the melting event observed in PreDA1).

2.3.3 Dynamic mechanical analysis

In recent years, Dynamic Mechanical Analysis (DMA) has been established as one of the premier techniques for interrogating CANs, vitrimers and other functional polymers. This technique provides precise information concerning the thermal dependence of various measures of stiffness and is particularly valuable for determining T_g. Dynamic thermal sweeps remain the standard for characterising moduli temperature dependence, but static isothermal stress-relaxation experiments are now also widespread as they provide an excellent way of confirming vitrimer-type behaviour (Arrhenius-type stress relaxation). While vitrimers (associative CANs) soften at elevated temperatures as they pass through their T_g and T_v, they should remain solid, with significant residual stiffness (i.e. they exhibit a rubbery plateau) even when their dynamic chemistry is active. In contrast, with dissociative CANs such as the DA materials reported herein, de-crosslinking occurs at elevated temperature such that T_v is associated with an apparent melt.

The most important metrics produced by conventional dynamic mechanical analysis are storage modulus, loss modulus and tan(δ). Storage modulus (E') is simply the 'real' component of the material's stiffness, a measure of the storage of applied load as elastic energy. Loss modulus (E'') in contrast, is the imaginary component, a measure of energy dissipation through internal segmental motion. Below glass transition, internal segmental motion is small and oftentimes negligible as the polymer chains are rigidly fixed in place. As temperature increases above T_g these polymer segmental motions are slowly activated. However, these motions are initially greatly inhibited by molecular friction, which dissipates the applied force as heat, resulting in a sharp upturn in loss modulus. However, there is a concomitant drop in the storage modulus as less of the applied load is stored elastically. The two moduli are related by tan(δ), the loss factor, the other most widely quoted parameter in DMA. This is a measure of the phase angle between the real and imaginary components:

$$\tan(\delta) = \frac{E''}{E'} \qquad \text{Eq. 2.2}$$

Homogeneous crosslinked materials usually follow the same patterns outlined above: with storage modulus falling sharply from an initial plateau after passing through glass transition and then stabilising at an equilibrium low level as the polymer is fully relaxed, as illustrated by the two conventional epoxies Ctrl1 and Ctrl2 in Figure 2.33. Simultaneously, the loss modulus starts from an initial baseline, sharply rises to a maximum (after T_g) and then falls toward zero. As loss modulus tends to zero molecular frictions are reduced such that there is no dissipation of the applied load as heat, this is typical of polymeric materials after glass transition, with or without melting. As storage modulus tends to zero the material has no elasticity and becomes a liquid. Thermoset polymers, such as conventional epoxies, do not exhibit this behaviour. Instead, after T_g, thermosets usually exhibit a rubbery plateau which represents the residual elasticity of the relaxed polymer network. In contrast, all three DA CANs undergo both T_g and T_v at approximately the same temperature; the polymer network softens and then due to de-crosslinking, the polymer melts and storage modulus tends to zero. This behaviour is also reflected in the noise associated with each of the following tan(δ) curves around the melt (T_v)—as the storage modulus approaches zero measurement sensitivity is lost. If the oligomers were of significantly higher molecular weight (>10 kDa), chain entanglement would be expected to contribute to some residual network stiffness and so a rubbery plateau may be observed. The residual storage modulus (rubber plateau) is often used to calculate crosslink density, though even if these materials exhibited a rubber plateau, since the equilibrium position of the crosslinking reaction varies at elevated temperature, such calculations would be meaningless for these CANs.

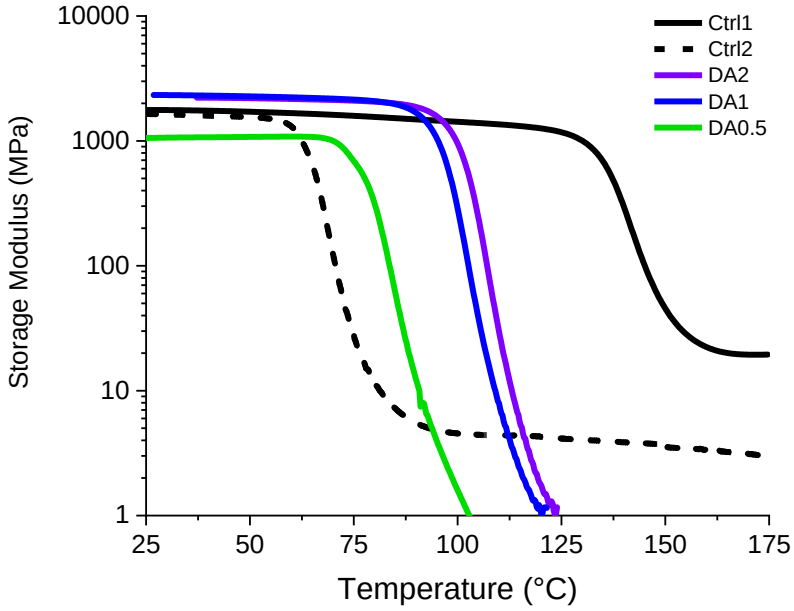

Figure 2.33. The storage moduli of each DA CAN and the control epoxies Ctrl1 and Ctrl2 (single cantilever beam geometry, 1 Hz, 15 µm amplitude, 5 °C min^{-1}). Ctrl1 is the simple copolymer of Epon 828 (DGEBA) and EDA (4,4'-ethylenedianiline). Ctrl2 is an in-house epoxy prepared from Epon 828 and a blend of alkylpolyamines.

The two primary differences between the three DA CANs are evident in Figure 2.33: initial stiffness and the onset of melting. The stiffnesses of both DA1 and DA2 are almost exactly identical with near perfect overlap, indicating that the structure of the crosslinker (the BMI)—which is the sole difference between the materials—has negligible influence upon the polymer stiffness at ambient temperature. In contrast, the half-crosslinked CAN (DA0.5), has approximately half the initial stiffness. This is likely in large part due to the poorer interchain packing between units as a result of *n*-heptyl side groups, though may also be a product of the reduced crosslink density. In agreement with DSC (Section 2.3.2) and rheology (Section 2.3.1) data, DA0.5 also undergoes melting (storage modulus tending to zero) at a much lower temperature than the other two CANs, with onset (T_{on}) at approximately 75 °C and completion (T_{end}) at just over 100 °C. DA1 has T_{on} = 90 °C and T_{end} = 120 °C, and the curve of DA2 is shifted by 5 °C to T_{on} = 95 °C and T_{end} = 125 °C, again in agreement with DSC results. Interestingly, in all cases the glass transitions and melting appear to occur simultaneously. This is to be expected of most de-crosslinkable systems, since each of the three most likely combinations of T_g and T_v favour this behaviour: (1) $T_g \approx T_v$, naturally, glass transition and de-crosslinking could occur at very similar temperatures independent of each other. (2) $T_g > T_v$, since de-crosslinking should result in the same effect of increased molecular mobility as glass transition does, if T_g would otherwise be higher, the melt would effectively induce it prematurely. (3) $T_g < T_v$, similarly, the increased molecular movement available to the polymer chains after passing through glass transition would be expected to enhance the rate of de-crosslinking by increasing the probability of the bond vibrations required to effect the

rDA reaction, hence this eventuality would also favour simultaneous (or near simultaneous) T_g and T_v. In all of these DA CANs, the DSC plots suggests that the T_g is well-defined and occurs just before the de-crosslinking endotherm. This suggests that these materials resemble scenario 3—the T_g helps to induce de-crosslinking (and thus melting).

The three major DMA profiles of a representative DA1 specimen are shown in Figure 2.34. The storage modulus has an initial value of approximately 2.3 GPa, whereas the loss modulus is initially 23 MPa. Each of the curves shows the expected profile, with E' sharply falling and both E'' and tan(δ) sharply rising after the T_g. There are several different points on DMA curves that researchers commonly use to define T_g: (1) The onset of the storage modulus (calculated from the intersection of the tangents to the horizontal and descending regions of the curve), (2) the peak of the loss modulus curve and (3) the peak of the tan(δ) curve. Each of these methods gives a different value of T_g, with (1) giving the lowest value, (2) a slightly higher value and (3) a significantly higher value. Though each measure has its merit, for simplicity only the intermediate T_g corresponding to the maximum of loss modulus (2) is reported herein.

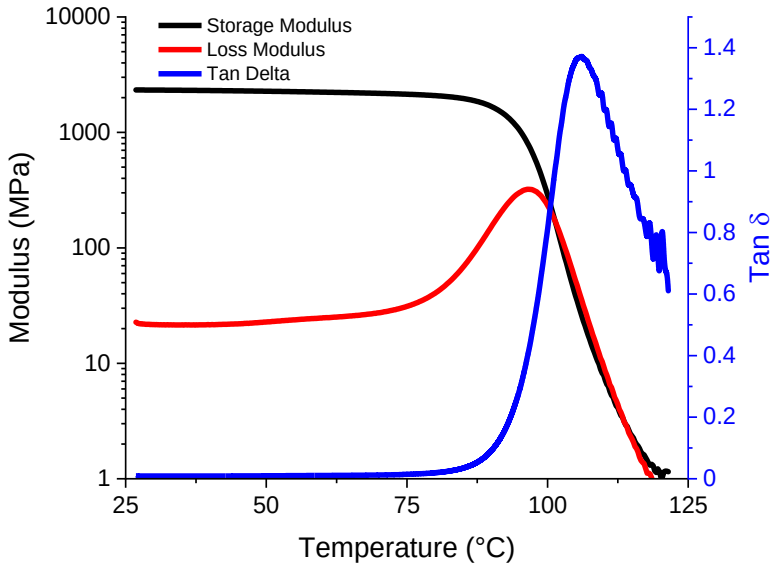

Figure 2.34. Representative single-cantilever DMA plots of DA1 (1 Hz, 15 µm amplitude, 5 °C min^{-1}). Left axis: storage (black) and loss (red) moduli. Right axis: tan(δ) (blue). E''_{max} = 97 °C.

The maximum of loss modulus corresponds to the point at which the maximum amount of the applied load is dissipated as heat. On the molecular level, this represents the point at which molecular motions are undergoing the most change, with a large amount of molecular motion and a large amount of molecular friction, in essence, the midpoint of the glass transition region. In the case of DA1, this maximum occurs at 97 °C. This is significantly higher than the value suggested from DSC (the step in heat capacity is around 70–85 °C). One key difference between the DSC and DMA experiments

discussed in this chapter is the heating rate, which is known to have a significant influence on T_g.[45] Generally, faster heating rates yield a higher T_g as a result of thermal lag and relaxation effects. However, in this case the DSC was performed at the higher heating rate (10 °C min^{-1}) than the DMA (5 °C min^{-1}). In these experiments the observed differences are instead attributed to the sensitivity differences between the techniques: DSC is a much less sensitive technique for determining T_g; the change in heat capacity at glass transition is considerably smaller than the change in moduli (which DMA measures). Accordingly, these values of T_g are much more reliable.

The DMA profiles of the prepolymer PreDA1 are shown in Figure 2.35. The baseline of storage modulus in this case is 1.15 GPa which is approximately the same as the baseline stiffness of DA0.5. Evidently, the prepolymer composition has an enormous effect on the material stiffness. As observed in the curves of DA1 and DA2, clearly a high crosslink density contributes to a marked increase in this stiffness. However, surprisingly, below a threshold concentration it appears the crosslinks do not have a significant influence upon stiffness. In contrast, the absence of crosslinks has a much more pronounced effect upon glass transition: the peak in loss modulus (T_g) for this prepolymer is much lower than the crosslinked CANs at 57 °C. One feature of this plot that is immediately apparent is its premature termination. Both storage and loss modulus curves would be expected to tend to zero as with the crosslinked polymers, but at a much lower temperature. As the polymers melt they can damage the DMA fixture jig, although the risk of this is mitigated by an automatic heater cut-off (when storage modulus approaches zero); however, fast-melting materials can overcome this cut-off. Accordingly, these experiments were terminated prematurely at 65 °C. With hindsight a maximum temperature of 70 °C may have been acceptable.

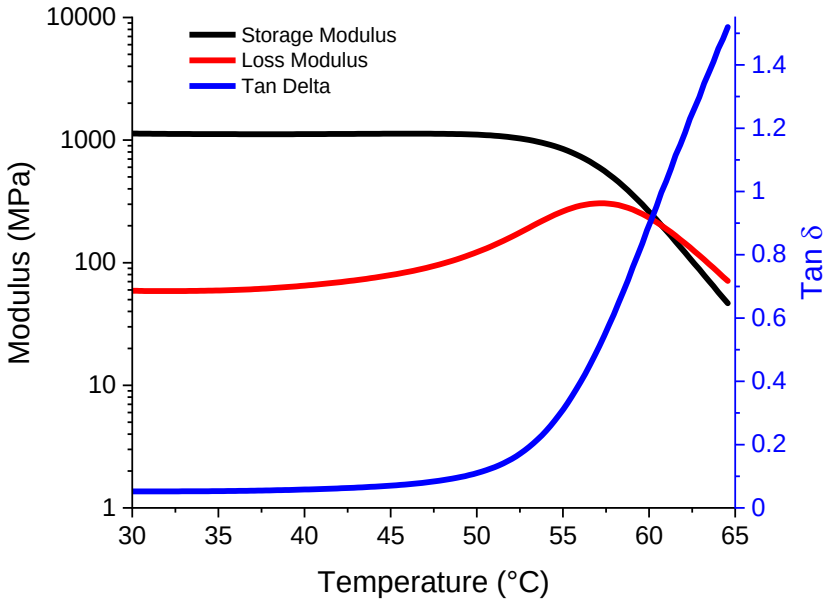

Figure 2.35. Representative single-cantilever DMA plots of PreDA1 (1 Hz, 15 µm amplitude, 5 °C min^{-1}). Left axis: storage (black) and loss (red) moduli. Right axis: tan(δ) (blue). E''_{max} = 57 °C.

The DMA results of a representative DA2 specimen are shown in Figure 2.37. As discussed previously, the baseline storage modulus of 2.2 GPa is almost identical to DA1 (2.3 GPa). The same is true of the baseline loss moduli (both 23 MPa). The only significant difference between the behaviour of the two materials is the difference in glass/melt transition. In this case the maximum of loss modulus is 101 °C, 4 °C higher than DA1, which implies that DA2 has more stable crosslinks, in good agreement with the differences observed in both rheology and DSC experiments. The two different crosslinkers are shown again in Figure 2.36.

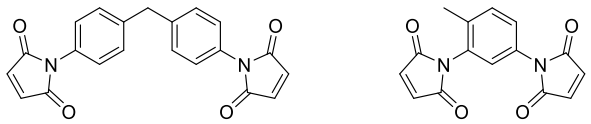

Figure 2.36. Left, BMI1 (1,1'-(Methylenedi-4,1-phenylene)bismaleimide), used in DA1/ DA0.5, and right, BMI2 (N,N'-(4-methyl-m-phenylene)-bismaleimide), used in DA2.

The primary differences between the two linkers are the length between the maleimide groups, which is significantly shorter in BMI2 and the presence of the methyl group on BMI2. The net influence of both features is that the maleimide moieties of BMI2 should be slightly more sterically encumbered. The result of this might be that the forward Diels-Alder reactions are slightly slower in DA2; however, this would not be expected to have a significant influence upon the rDA reactions. Instead, it is more likely that adducts are slightly thermodynamically stabilised in DA2, possibly a result of electron-induction moving electron-density toward the adducts from the methyl group (which is only present

in BMI2). As in DA1, the storage modulus of DA2 tends to zero after the glass/melt transition (~120 °C), as the polymer becomes a viscoelastic liquid.

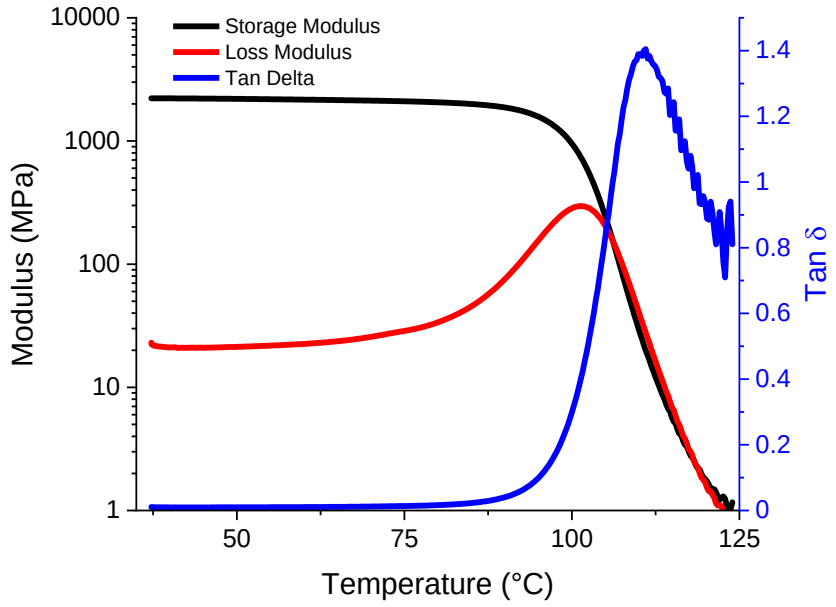

Figure 2.37. Representative single-cantilever DMA plots of DA2 (1 Hz, 15 µm amplitude, 5 °C min^{-1}). Left axis: storage (black) and loss (red) moduli. Right axis: tan(δ) (blue). E''_{max} = 101 °C.

In Figure 2.38 the three DMA results of a representative sample of DA0.5 are shown. As discussed previously, the baseline storage (1.03 GPa) and loss (56 MPa) moduli are approximately the same as the prepolymer PreDA1 (note however that this is *not* the prepolymer from which this CAN was made). With less crosslinks than DA1 and DA2, this CAN is much less stiff. This large disparity in stiffness could also be a product of the less regular backbone (with frequent *n*-heptyl branches) of the prepolymer PreDA0.5, which could disrupt the solid-state packing. The maximum of loss modulus in this case is 79 °C. This is again significantly higher than the value of T_g implied by DSC but follows the same trend as with DA1 and DA2. This confirms that DA0.5 melts at a significantly lower temperature than the other two CANs, though is still reasonably robust up to this point.

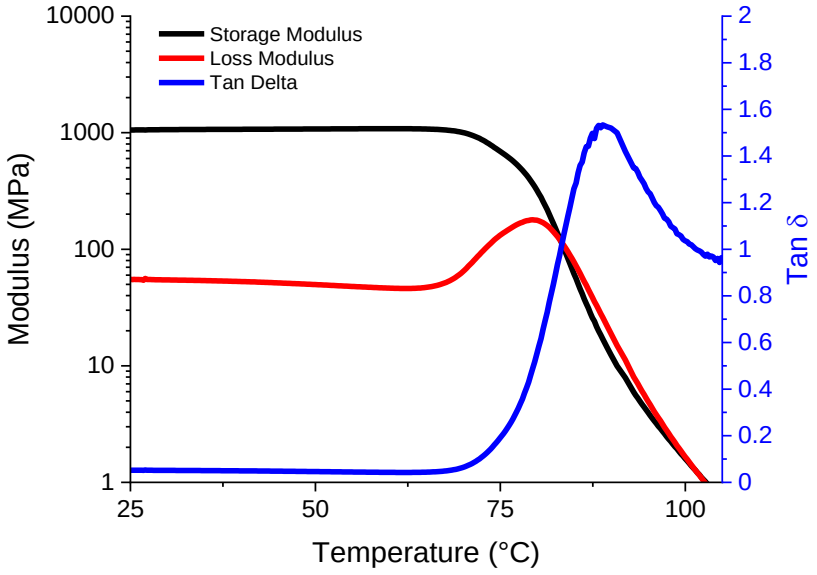

Figure 2.38. Representative single-cantilever DMA plots of DA0.5 (1 Hz, 15 µm amplitude, 5 °C min^{-1}). Left axis: storage (black) and loss (red) moduli. Right axis: tan(δ) (blue). An artefact—probably a jog to the machine—seen as a minor wobble in the moduli curves and a sharp spike in tan(δ) between 88–92 °C has been removed by smoothing. E''_{max} = 79 °C.

It is worth noting that attempts to prepare and test a specimen of PreDA0.5 were unsuccessful. This was principally a result of the polymer's brittleness, which is a feature common to both prepolymers and all three DA CANs—this will be discussed in some detail in later sections. Despite best efforts to minimise the risk (by lightly clamping the specimens and then pre-heating them to ~50 °C prior to tightening), approximately half of all specimens failed due to fracture on clamping to the test rig.

2.4 Solvent resistance and swelling

2.4.1 Solvent resistance study

The behaviour of polymers upon exposure to a solvent provides information concerning the extent of crosslinking. Conventional thermoset polymers are almost entirely insoluble in all solvents: the strong crosslinks between chains preclude their separation and dissolution. Instead, absorption of the solvent can occur to a greater or lesser extent, dependent upon the density of the polymer network and the relative polarities of both polymer and solvent. In contrast, thermoplastics can be partially or wholly soluble in certain solvents dependent upon polarity and molecular weight. High levels of solvent absorption or dissolution can preclude the use of materials in environments in which they are likely to encounter that solvent, because both effects can drastically alter the polymer's mechanical properties. This is often evident with absorption in terms of 'plasticisation' which reflects a substantial degradation of stiffness. This is most commonly a concern with water absorption due to the ubiquity of water in many environments. A simple experimental procedure was followed as outlined in Section 2.8 and the results are summarised below in Figure 2.39.

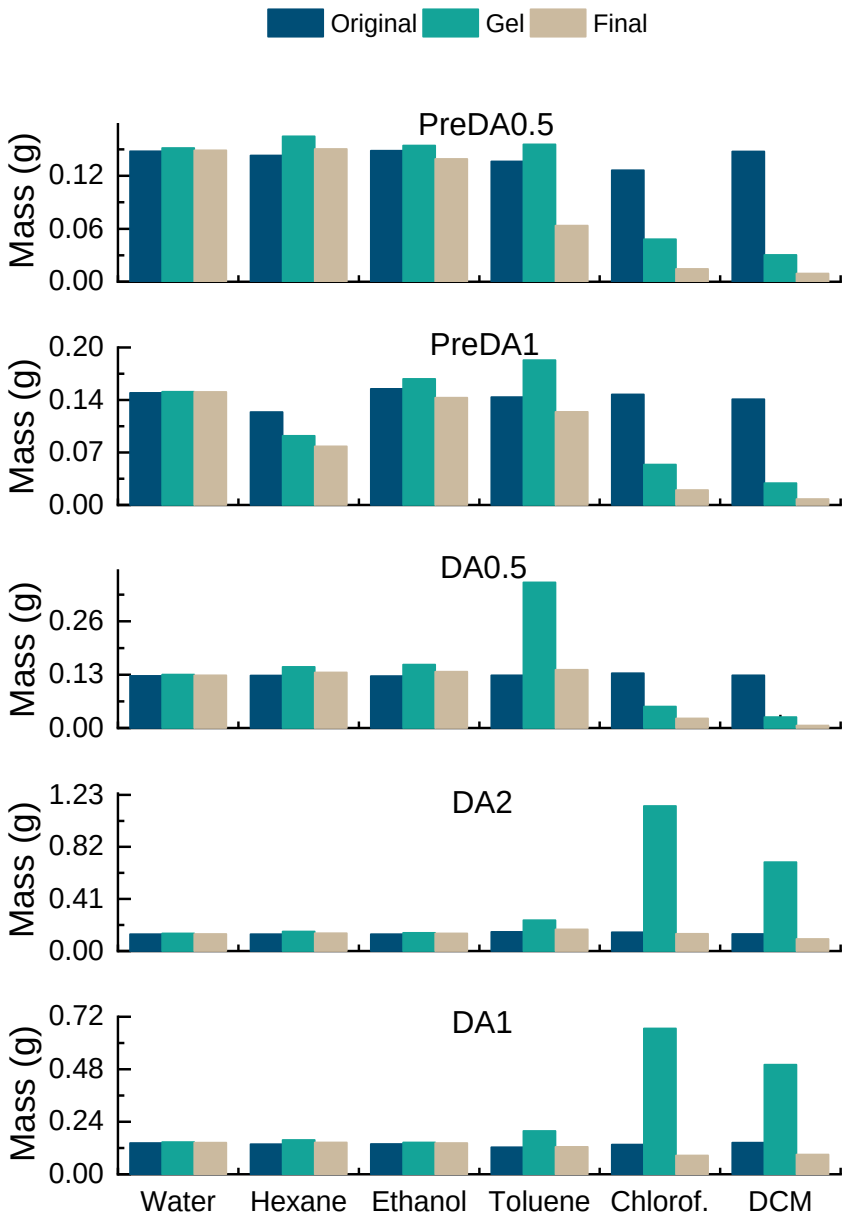

Figure 2.39. Summary of the mass changes of each of the five polymers after immersion in water, hexane, ethanol, toluene, chloroform and dichloromethane respectively.

Several trends emerge from Figure 2.39, as both the nature of the polymer and the nature of the solvent can have a large effect on the observed behaviour. In particular, it is clear that DA1 and DA2 follow a similar pattern to each other, as do PreDA1 and PreDA0.5, and DA0.5 is somewhat intermediate between the two extremes. In addition, the first three solvents (water, hexane and ethanol) induce a meagre change in mass when compared to the latter three (toluene, chloroform and DCM). These patterns are highlighted in Figures 2.40 and 2.41, which highlight the mass changes in terms of the solvent and polymer respectively.

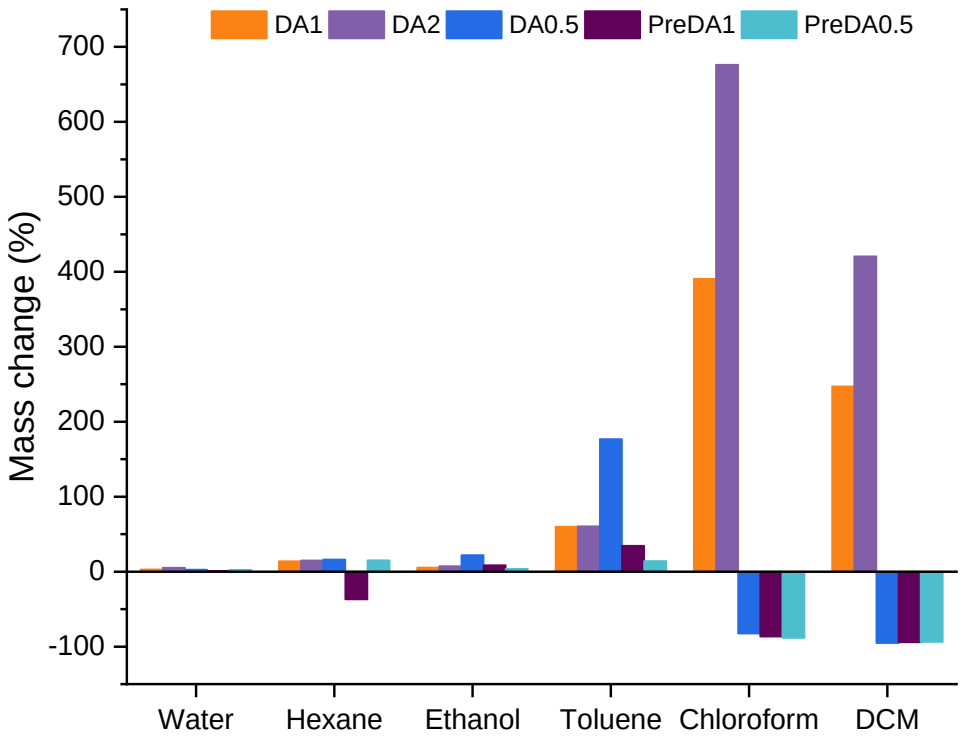

Figure 2.40. Percentage mass change of each polymer sorted by solvent. Positive values correspond to absorption dominated behaviour. Negative values correspond to dissolution dominated behaviour. The positive values are calculated from the gel mass, and the negative from the final dry masses.

The six solvents used in this study were chosen to reflect a range of polarities and structures, and are some of the most widely used. The first and most polar solvent, water, has only a minor effect on any of the polymers: after complete immersion in water for 6 days, DA2 absorbed the most, increasing in mass by only 5%. Ethanol, the next most polar, has a similarly small effect on all of the polymers but shows a slight increase in absorption levels. In this case the maximum absorption is with DA0.5, 22%. The least polar solvent, hexane, has a slightly more pronounced effect, with absorptions in the range of 15% for all of the polymers except PreDA1, which instead shows a decrease in mass associated with dissolution. Toluene is absorbed to a significant extent in all cases, reflecting its high compatibility with the regular aromatic structure of the polymer backbone.

The most pronounced changes resulted from immersion in the chlorinated solvents, chloroform and DCM, which both resulted in either complete dissolution or extreme levels of absorption (gel formation). The reason for this behaviour in these solvents rather than others is attributed to the combination of their modest polarity and small size, which could facilitate their penetration through the polymer network.

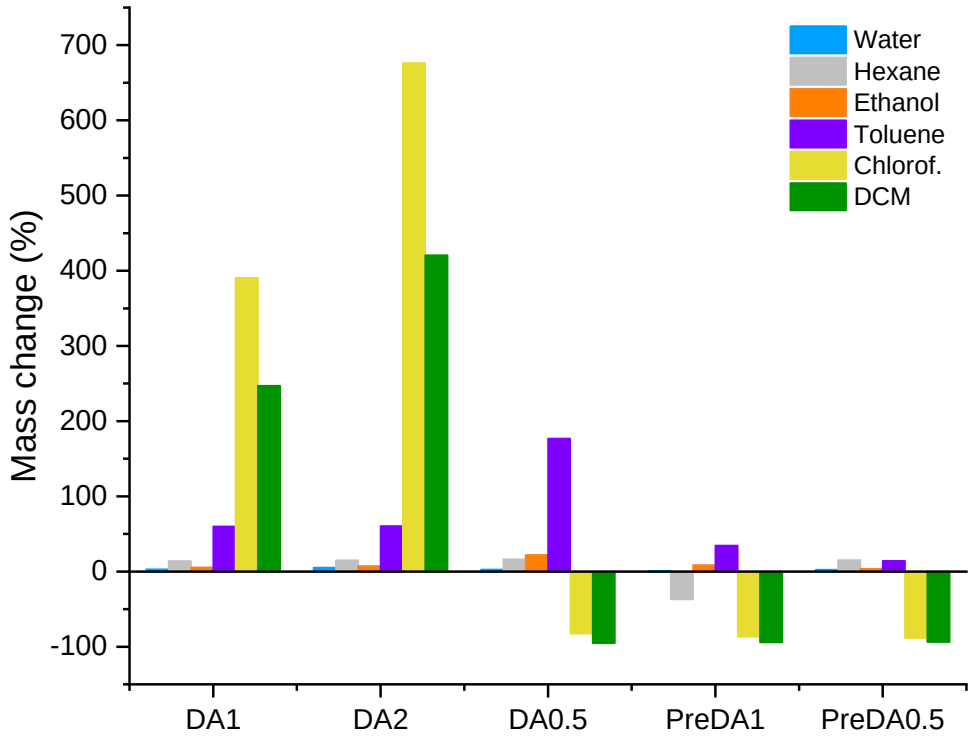

Figure 2.41. Percentage mass change sorted by polymer. Positive values correspond to absorption dominated behaviour. Negative values correspond to dissolution dominated behaviour. The positive values are calculated from the gel mass, and the negative from the final dry masses.

Although these experiments do not provide the subtlety required to decouple absorption and dissolution effects—it is likely that in some cases absorption and dissolution are in competition—these experiments clearly confirm that absorption is the dominant behaviour of both DA1 and DA2 in response to solvent exposure. This is strongly indicative of a crosslinked network. However, the levels of DCM/chloroform absorption are highly unusual: it is not generally possible for densely crosslinked polymers to swell into gels as seen here, Figure 2.42.

Figure 2.42. Photos of DA1 (cbe08) samples after 6 days of immersion in water, hexane, ethanol, toluene, chloroform and DCM respectively. The first three samples show no visible difference after exposure. Sample 4 (toluene) shows some surface bleaching. Samples 5 and 6 show gel formation.

This may indicate that the DA CANs are less densely crosslinked than expected. The fact that DA0.5 almost completely dissolves in both of these solvents provides further evidence of this; in this case, it appears that the level of connectivity between the prepolymer chains in DA0.5 is inadequate to form a complete network. Accordingly, in terms of solvent response, DA0.5 behaves more like the prepolymers PreDA1 and PreDA0.5 than DA1 or DA2. The extent of crosslinking in these materials is re-examined with respect to mechanical performance in Section 2.5.2.

De-crosslinking could provide an alternative explanation for the dissolution of DA0.5 and extensive swelling of DA1/DA2, which would allow for a greater number of initial crosslinks. A few studies concerning the retro Diels-Alder reaction have highlighted the possibility of stress-induced de-crosslinking.[46–48] Thus, it is conceivable that upon absorption of large volumes of chloroform/DCM the swollen network applies tensile stresses which are sufficient to induce the rDA reaction, and thus de-crosslink the material. Indeed, this concept of gelation induced retro-DA has been examined by Lyu *et al*.[48]

To investigate the possibility of solvent- (or gelation-) induced de-crosslinking, a simple experiment was devised whereby samples of polymer were immersed in $CDCl_3$ and then monitored with ^1H NMR at regular intervals. By monitoring over time the change in resonance integrals relative to a standard (the solvent residual peaks), it was hoped to distinguish different rates of dissolution between the prepolymer backbone and the BMI crosslinker. However, the results of this study were inconclusive. Although the integrals were increasing as the polymer dissolved, all peaks were doing so in a consistent manner. Accordingly, there was no evidence of de-crosslinking and in the interest of brevity this study is not reported here.

Gelation studies can be used to calculate the crosslink density of lightly crosslinked polymers (those that swell significantly). This is particularly significant with these DA CANs because the main alternative method of determining crosslinking density is through calculations relating to the rubbery plateau of storage modulus, which these materials do not exhibit. Futhermore, the crosslink density is temperature dependent so could not be calculated in this way. To determine crosslink density through swelling experiments, the number average molecular weight between crosslinks (M_c) needs to be determined through use of the Flory-Rehner equation and so material densities and solvent interaction parameters are required. The polymer density can be determined straightforwardly through application of Archimedes' principle, but extensive experimentation may be required to determine solvent interaction parameters of these (novel) polymers.

2.4.2 Scope for solvent-assisted recycling

Whether or not the vast absorption of DCM/chloroform into the DA CANs and subsequent gel formation is caused by less-than-expected crosslink density or de-crosslinking, the phenomenon makes these materials ideal candidates for solvent-assisted recycling. Colleagues from TNO Materials Solutions in Eindhoven, NL, have performed some recycling studies (currently unpublished) with these polymers with some success. By heating samples of DA epoxy in toluene to reflux, the DA polymers were thermally de-crosslinked, allowing the polymers to dissolve. Precipitation of the product solutions afforded recycled polymer in good yields. Furthermore, it was noted that the recycled material was much less brittle than the original polymer, which is probably indicative of plasticisation due to entrained toluene. Room temperature recycling with the much lower boiling solvent, DCM, thus could provide a low-energy alternative pathway with a reduced likelihood of entrained solvent.

With neat polymer a solvent-assisted method of recycling is unnecessary since these polymers can be milled and re-melted (moulded) multiple times. However, this melting-milling process would not be possible in continuous fibre reinforced polymer composites without prior separation of polymer and fibre, because the milling process would break the fibres. If the polymer could be freely melted away from the fibres a solvent-assisted method would also be unnecessary. However, achieving clean separation of fibre and polymer would require the de-crosslinked resin to be of very low viscosity, much lower than is achievable even with these systems. Accordingly, solvent-assisted methods are the most pragmatic way of recycling CAN-matrix FRPs, particularly with these DA resins. Scheme 2.2 illustrates the process of the recycling method proposed herein, which will be further discussed and applied in Chapter 3, Section 3.3.3.

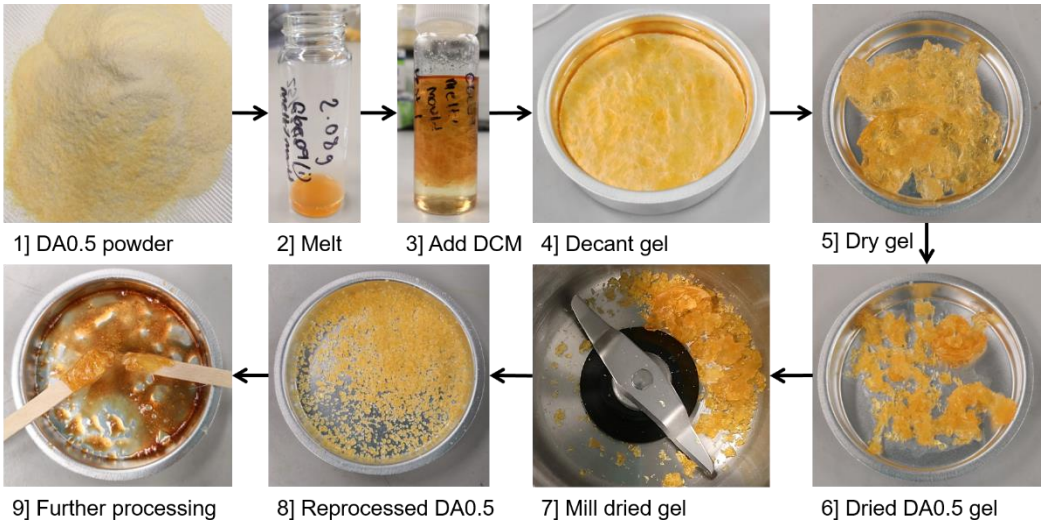

Scheme 2.2. DCM-assisted recycling of DA0.5, from powder to powder. The final image (9) demonstrates the continued thermal processability after recycling.

2.5 Moulding, processing, and mechanical characterisation

2.5.1 Moulding and processing

The moulding of good quality polymer plates is an essential first step towards the manufacture of composites and more complicated parts. Rheological and dynamic mechanical results indicate that all the DA CANs are melted at 120 °C (DA0.5 at 110 °C); ergo, this is a prudent starting point for a processing temperature. Viscosity does drop further with increased temperature, which could ease processing. However, this risks permanent crosslink formation, as determined by the thermal analysis (Section 2.3), which is deleterious to both processability during moulding and to the activity of the reversible chemistry (functionality).

Adding a further element of complexity to the moulding process is degassing. Degassing is a critical step in polymer processing, it serves to remove volatile, low molecular weight components (principally unreacted monomers) and trapped air. Volatile components in the case of these DA CANs should be negligible, though it is feasible that a very small fraction of residual amines could be present and that these could be removed by such a process. In contrast, a significant amount of inter- and intra-granular air is present in all of the polymers discussed in this chapter. Intergranular air is unavoidable when moulding powders and can be removed by using vacuum-assisted moulding techniques. The presence of intragranular air is a result of the synthesis—the high stirring rates and the addition of a powder (BMI) to a viscous liquid (prepolymer)—and is self-evident from the opacity of the cast materials (Figures 2.09–2.13). This trapped air is a problem principally because air bubbles are defects which can cause stress concentration, which in turn results in an apparent reduction in material strength.

Unfortunately, the high melting nature of both the prepolymer and crosslinking mixture prevents straightforward in situ degassing without the use of specialised equipment. Although degassing the starting materials might help reduce the quantity of trapped air, it is likely that the mixing process would re-introduce a large volume, negating the value of doing this. Accordingly, it was decided that degassing post-synthesis was the most pragmatic approach.

The conventional method of degassing reactive (thermoset) polymer systems is heating them in a net shape mould in a vacuum oven until bubble formation stops. This was attempted with and without the unreactive diluent toluene at 120 °C over the course of approximately 1 h, the results of which are shown in Figure 2.43.

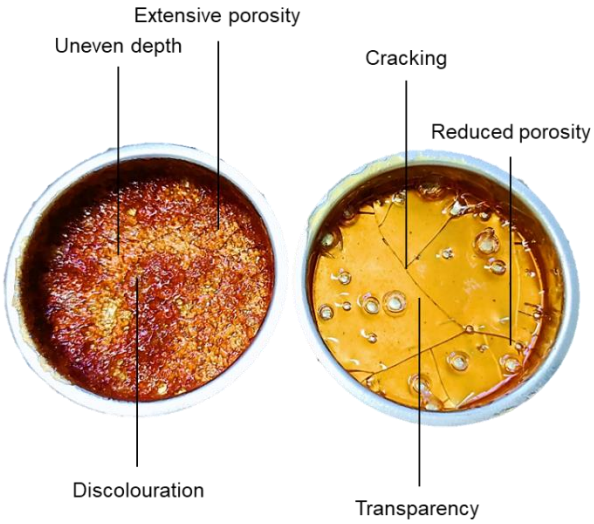

Figure 2.43. Left, neat DA1 after degassing at 120 °C in a vacuum oven for ~1 h and right, DA1 with 20 wt% toluene exposed to the same conditions.

The photograph shows that the neat DA1 material has changed to a deep red colour indicating the formation of permanent crosslinks through BMI HP. Evidently the viscosity at 120 °C is too high to allow vacuum degassing prior to material degradation. Unfortunately, attempts at higher temperature (150 °C), were similarly unsuccessful, although the initial viscosity is significantly lower—which accelerates degassing—rapid material degradation occurs resulting in permanent hardening of the material, which results in a similar porous red structure. Degassing in the presence of an unreactive diluent, toluene, as shown in the right of Figure 2.43 leads to a visibly much improved polymer. Although the polymer has still hardened significantly and likely no longer retains an appreciable amount of reversible activity, the majority of the material is transparent, with only some large bubbles remaining. Interestingly, the polymer in this case has not reddened as the neat DA1 did. This suggests that much less BMI HP (or other side reactions) has occurred. The mechanism behind this is unclear; however, one possible explanation is that the 20% dilution has helped homogenise the material, reducing the local BMI concentrations. Clearly diluents offer some potential to improve degassing of these DA CANs, though at the time of writing this has not been further explored.

Polymer melts can also be degassed in a similar fashion using a Schlenk line and appropriate glassware, if the subsequent polymer viscosity is sufficiently low to allow it to be poured into a mould. The advantage of this method is that it allows the use of higher performance vacuum pumps (giving faster

degassing). However, preliminary investigations suggested this was not feasible for these systems because they were too viscous.

One major alternative to degassing is widely used with thermoplastics: compression moulding. By applying enough pressure, it is possible to effectively 'degas' polymers through a combination of pushing gas out of the polymer and shrinking residual bubble size to the sub-micron scale. On the order of <1 µm, voids result in only minor stress concentration—if they are an appreciable distance from each other, *ca.* >1/2 void diameter. Indeed, in some cases such cavities may even serve to toughen the host material in much the same way that nanoparticular reinforcement can, by introducing yielding mechanisms and deflecting microcracks.[49]

As a first feasibility study of compression moulding these DA epoxy CANs, a primitive four-part 'picture frame' aluminium mould was used in attempt to prepare a thin film of DA1. This mould was coated with a release agent and tested with and without additional Teflon release film. In each experiment DA1 powder was added as centralised charge on a 40–50 g scale. Transparent homogenous films of DA1 were created using a simple moulding cycle with ramp up to 125 °C and then as little as 4 tons of compressive load for 2 min, Figure 2.44. The product films were found to be very brittle, fracturing to shards in all cases, precluding their use in film infusion processes, as was originally planned.

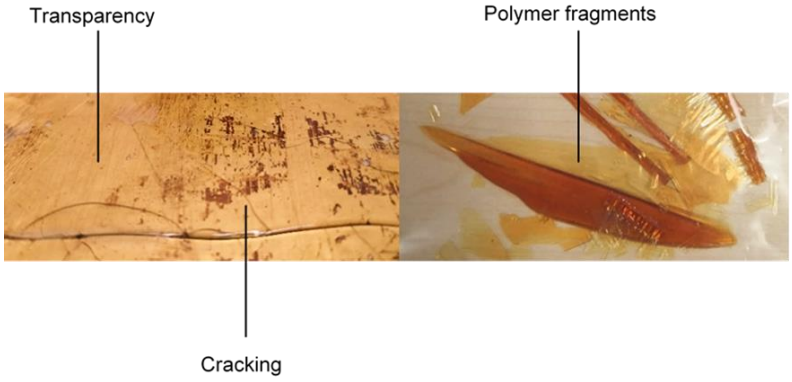

Figure 2.44. Compression moulding of DA1 films. Left, film attached to the mould insert with cracks visible. Right, flash (excess resin) from the edges of the mould.

A similar three-part steel mould (base plate, frame, insert and top plate) was designed to produce thicker sections of polymer appropriate for preparing specimens for 3-point-bend flexural testing (3pb). This was then used with a vacuum bag in a vacuum-assisted compression moulding (VACM) process, Figure 2.45. By ensuring adequate polymer loading (and thus sufficient polymer pressure) and enough dwell time (~5 min) to allow the polymer to reach the set temperature, the DA epoxy CANs could all be moulded with a high degree of homogeneity and transparency.

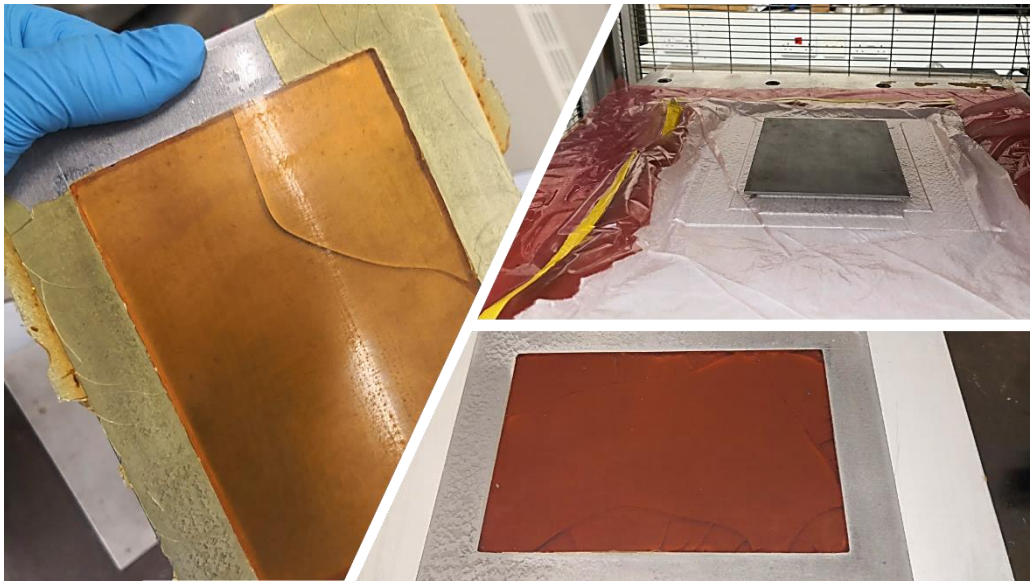

Figure 2.45. Vacuum-assisted compression moulding using a Hare mounting press (9 tons, 125–150 °C, top right) of DA0.5 (left) and DA1 (lower right).

Although high quality polymer was successfully moulded using this method, a significant amount of cracking was observed in all cases, which was often exacerbated during demoulding. This is a product of the polymer's brittleness and the CTE (coefficient of thermal expansion) difference between the steel and polymer: the mould will always expand more than the polymer when heated, and contract more when cooled. Unfortunately, this means an appreciable amount of compressive stress generated at the edges of the polymer when cooling and fracture as seen in Figure 2.45. One reliable method of mitigating the risk of such fracture is by simply using a mould of similar CTE to the substrate, i.e. using a polymeric mould. However, such moulds can be difficult to make and were considered unlikely to withstand the high loads required in this process. Instead, it was determined that this concept could be adapted such that the steel mould would still be used, by employing silicone inserts to line the mould cavity. In theory, the extreme elasticity of the silicone should allow it to absorb all of the thermal strain difference between the substrate and mould (through internal elastic deformation)—in effect cushioning the DA epoxy. This new method resulted in a much-improved success rate, Figure 2.46.

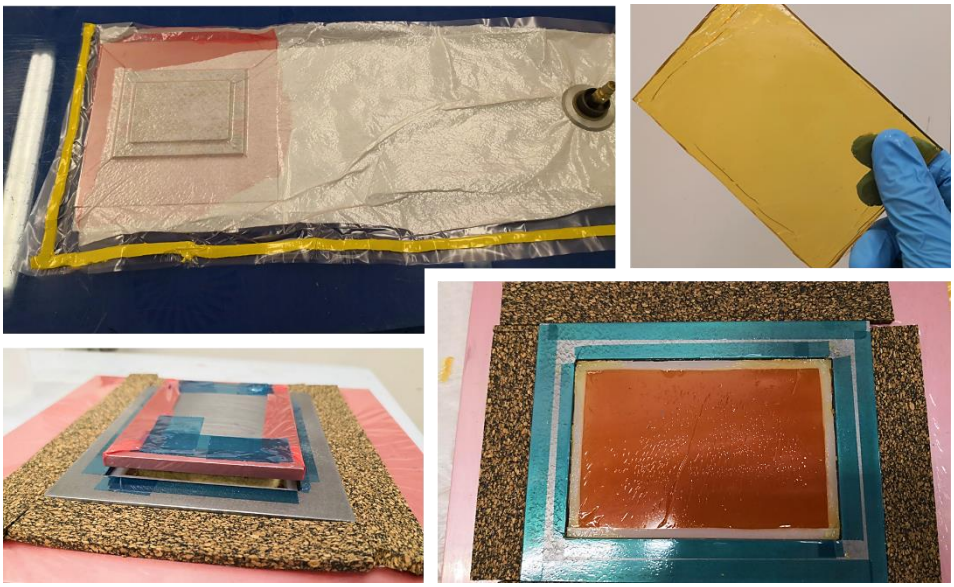

Figure 2.46. Clockwise from bottom left: DA1 powder in mould with silicone strips; the mould in vacuum bag; PreDA1 intact after moulding; DA1 intact in mould.

Each of PreDA1, DA1, DA2 and DA0.5 were successfully moulded at least twice during these compression moulding experiments, due to a limited supply PreDA0.5 was not successfully moulded. The moulded polymers were cut using a diamond saw into specimens for DMA (as discussed in Section 2.3.3) and 3pb testing. However, due to the extreme brittleness exhibited by all five polymers a lot of material was lost due to specimen fracture during machining, Figure 2.47.

Figure 2.47. Left, intact DA0.5 as moulded using silicone inserts. Right, extensive fracture of the same DA0.5 sample when cut with a diamond saw.

2.5.2 3-point-bend flexural characterisation

In principle a variety of common test methods could be used to determine the mechanical behaviour of the DA CANs. Tensile testing and any other procedure requiring grips was ruled out due to the brittle nature of the polymers; any means of gripping the specimens would be associated with a high risk of fracture prior to testing. Like 3pb, 4-point bending (4pb) was a viable alternative since the specimens do not require gripping prior to testing. The advantage of 4pb is that the applied stress is distributed over a significantly greater area (between the two loading noses) than in 3pb, where the stress is concentrated under the single loading nose. The result of this is that 4pb is less sensitive to defects and premature failure. However, 3pb tests are generally simpler to perform and interpret, and certainly provide adequate results for comparative studies such as required here. Accordingly, to quantify the mechanical performance of the DA CANs, they were tested in 3pb using a Shimadzu universal testing machine (10 kN load cell) and compared to the two control epoxies, Ctrl1 and Ctrl2, Figure 2.48. All specimens were tested using a gauge length close to 50 mm, with a loading rate calculated to induce a rate of outer fibre straining equal to 0.01 mm min^{-1}, this was varied (1.1–1.5 mm min^{-1}) with respect to the mean specimen depth of each sample series.

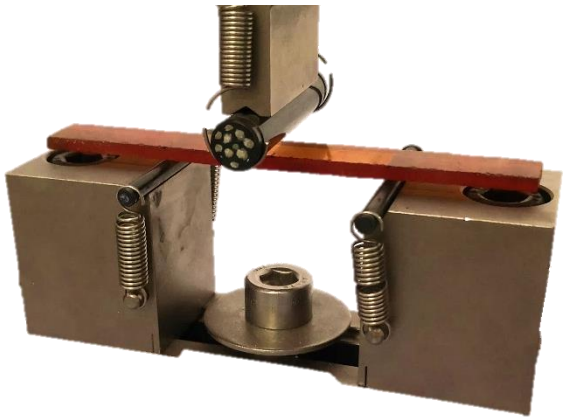

Figure 2.48. 3-point bend flexural testing of a DA2 specimen.

A plot of representative force-displacement curves is shown in Figure 2.49 and the data for all the tested polymers is summarised in the Figures 2.51–2.54.

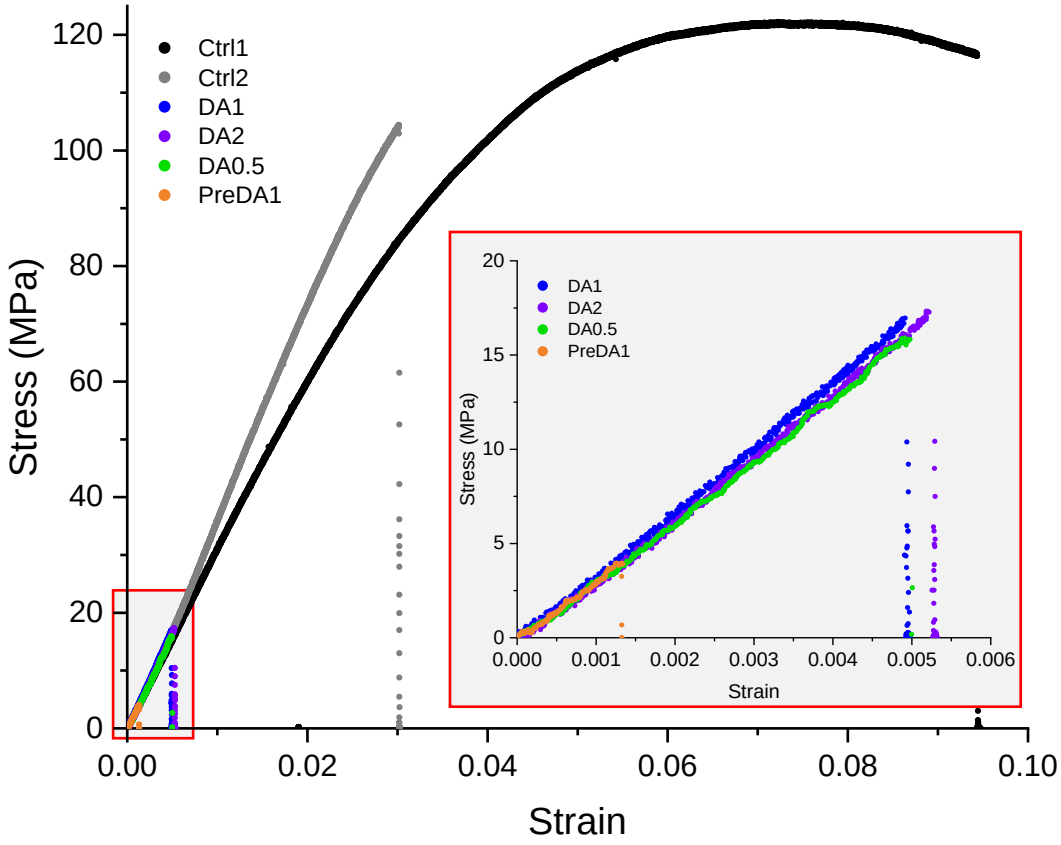

Figure 2.49. Representative stress-strain curves of the three DA epoxies, the prepolymer PreDA1 and the two control epoxies Ctrl1 and Ctrl2. Inset: magnification of low strain region in which the DA CANs failed.

It is immediately apparent from Figure 2.49, by comparing the mechanical response of the DA epoxies with the control epoxies, why moulding, machining and clamping has proved challenging. Although, the moduli of these materials are very similar to conventional DGEBA epoxies, the failure strength and failure strain are consistently on the order of 1/5th those of conventional systems, and much lower still for the prepolymer, PreDA1. In all cases, the new DA polymers were perfectly linear-elastic to failure, in contrast to both control systems which exhibited some (Ctrl2) and a lot of (Ctrl1) plasticity, respectively. Densely crosslinked epoxies are generally considered to be brittle polymers; nevertheless, the behaviour of DA0.5, DA1, DA2 and PreDA1 is uncharacteristically brittle.

The mean values of modulus, quoted as tangent modulus, are given in Figure 2.51. Ctrl1 has the lowest modulus (~3.0 GPa) and consistently exhibits a significant amount of plastic yielding. This plasticity is attributed to conformational changes accessible to the EDA under high loadings, Figure 2.50.

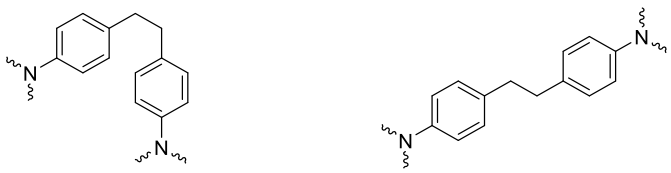

Figure 2.50. Conformations of the crosslinking EDA (4,4'-ethylenedianiline) units in Ctrl1.

Under ambient conditions ($T < T_g$, unstressed), the majority of EDA units will be fixed in place within the polymer network through a combination of the covalent bonds and intermolecular interactions, predominantly π-stacking interactions between adjacent aromatic rings. Many of these units will thus be locked in the more tightly constrained configuration (on the left of the figure). However, under stress (particularly tension), enough mechanical energy may be present to overcome the π-stacking interactions and induce the conformational change, thus absorbing energy (and deforming the epoxy) inelastically. In contrast, this behaviour is not possible in Ctrl2 without such crosslinks.

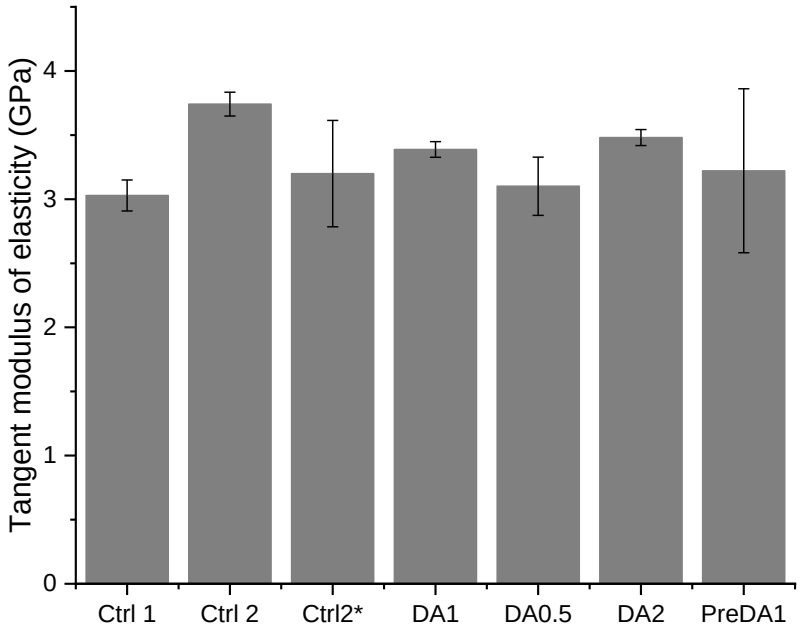

Figure 2.51. Mean (averages of 5, 5, 5, 5, 6, 5 and 8 tests respectively) tangent modulus of elasticity (flexure) ± 1 SD.

The three data series with the largest standard deviation, correspond to those associated with material defects (Ctrl2*) or experimental error (DA0.5 and PreDA1). Ctrl2* is a series of non-degassed Ctrl2 specimens (with lots of mm scale voidage). Although this was associated with some degradation of stiffness, the more pronounced effect was the increase in scatter, though this is unsurprising due to inhomogeneity of the defects—and sensitivity of 3pb flexure to the precise area of material under the loading nose. DA0.5 and PreDA1 were both subject to significant experimental noise. This is

attributed to a damaged data cable. The result of this was a loss of sensitivity and a large scatter in the data, which was considerably more pronounced with the very weak PreDA1 samples. These experiments were corrected with some success by smoothing with moving averages as shown in Figure 2.52. Attempts to repeat these measurements were unsuccessful due to specimen fracture during machining (Figure 2.47).

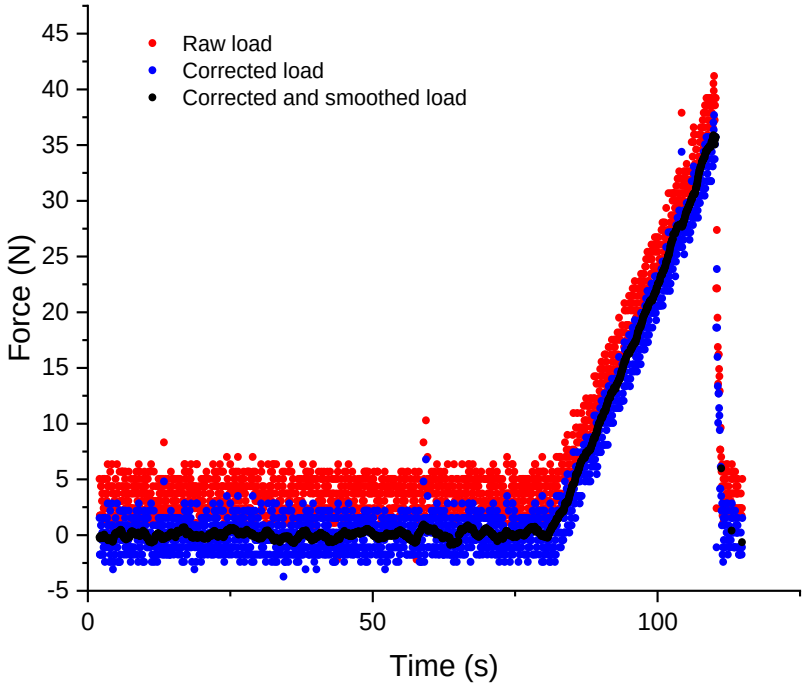

Figure 2.52. Data (force) smoothing of a representative DA0.5 specimen as performed for all flexure experiments of DA0.5 and PreDA1.

With the uncertainty of DA0.5 and PreDA1 considered, each of the tested polymers has a similar modulus, close to the conventional epoxies (Ctrl1 and Ctrl2), with DA0.5 and PreDA1 possibly having slightly lower stiffness, in good agreement with DMA (Section 2.3.3). This is in contrast to the mean strengths shown in Figure 2.53.

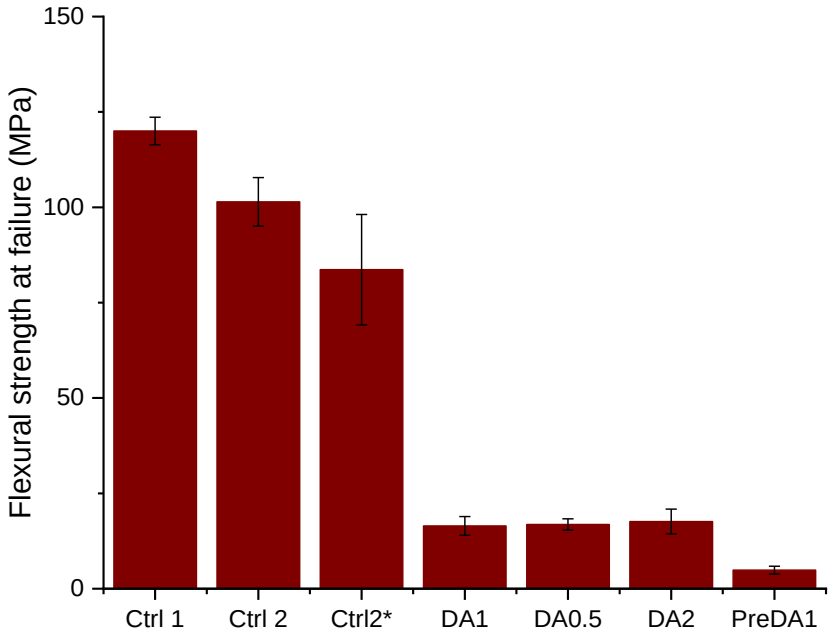

Figure 2.53. Mean (averages of 5, 5, 5, 5, 6, 5 and 8 tests respectively) flexural strength at failure ± 1 SD.

In terms of strength, Ctrl1 sets the upper benchmark at 120 MPa at failure. The second conventional epoxy, Ctrl2 has a significantly lower flexural strength at 101 MPa. Analogously to the modulus data, the high void content of Ctrl2* has a similarly deleterious influence on strength, with both a degradation of absolute values and an increase in scatter. However, the void-heavy series Ctrl2* still has strength (83.6 MPa) approximately five times higher than DA1 (16.5 MPa), DA2 (17.6 MPa) or DA0.5 (16.9 MPa) and 17 times higher than PreDA1 (4.9 MPa). Interestingly, the strengths of each of the DA CANs are within one standard deviation of each other. Clearly, the precise molecular architecture of neither the backbone (prepolymer type) nor the crosslinker is the dominant factor behind this low strength/brittleness. From these experiments alone it is hard to identify if these strength values are representative or if the extreme brittleness—lack of toughness—is inducing premature failure. This is always a feature of testing brittle materials (due to defect sensitivity) but is particularly acute in this study.

The failure strains (Figure 2.54) show much the same trends as the strength, with the DA CANs failing at much lower strain (~0.5%) than expected, *ca.* 6 times less than Ctrl2 (3%). PreDA1 has even lower failure strain (0.17%). The unusual plasticity of Ctrl1 is clearly illustrated by its much higher failure strain (9.3%).

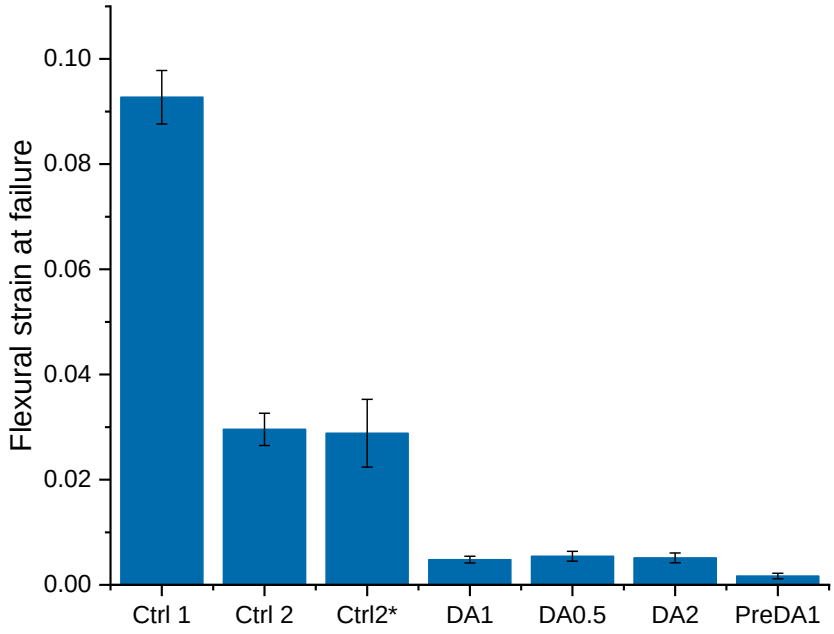

Figure 2.54. Mean (averages of 5, 5, 5, 5, 6, 5 and 8 tests respectively) flexural strain at failure ± 1 SD.

2.5.3 Brittleness

There are several conceivable reasons for the surprisingly high brittleness and low strength of these polymers:

(1) Defects (invisible, micro-nanoscale)

Given the inhomogeneity indicated by the presence of several secondary melting events in the DSC curves of each of these polymers, it is feasible that the moulded polymers are similarly not perfectly homogeneous. The boundaries of different domains, perhaps more or less crystalline, perhaps more or less crosslinker rich, could thus be present and might provide points of crack nucleation. However, none of these thermal events were observed in the second heating cycles of any of the DSC experiments. This suggests thermal homogenisation might occur during moulding, hence the test specimens are probably homogeneous. The smooth curves of each DMA experiment (with only one thermal event observed in each case) also implies a good degree of homogeneity. This is unlikely to have such a drastic embrittling effect.

Another possible source of defects is trapped air. Despite using vacuum-assisted compression moulding, there may be a significant amount of trapped air within these polymers. However, the excellent level of optical transparency after moulding suggests both that the polymer is highly amorphous, but also that if present, trapped air (voidage) is nanoscale or fully dissolved: larger voids would either be visible to the naked eye, or expected to scatter visible light, resulting in opacity. Moreover, if it is assumed that void size roughly correlates with the ideal gas equation:

$$pV = nRT \quad \text{Eq. 2.3}$$

Where p is pressure, V is void volume, n is moles, R is the gas constant (8.3145 J mol^{-1} K^{-1}) and T is the temperature (K). Void size is inversely proportional to pressure, thus if the pressure in the vacuum bag is approximately 1/1000th of atmospheric pressure (0.0001 MPa) and then the applied compressive load is 9 tonnes (cavity size = 0.0117 m^2, giving 7 MPa), the void size under load will shrink by a factor of 70000. Thus, the volume of trapped gases would be expected to be sufficiently small as to efficiently dissolve into the liquid resin. Furthermore, the difference (or lack thereof) between Ctrl2 and Ctrl2* in terms of failure strength, where a high level of voidage (up to the mm scale) resulted in only a 17.5% reduction in strength (which was not statistically significant) suggests that voidage alone is unlikely to explain such poor mechanical performance, though it could be a contributing factor.

(2) Incomplete DA reaction

Although the stoichiometry of maleimide to furan groups is such that there should be only a 10% excess of furan groups, it is feasible that a far smaller fraction of Diels-Alder adducts are actually present, even at room temperature. The DA reaction between a furan and maleimide is generally considered as 'click chemistry' due to its facile nature. However, it might be possible that crosslinking is incomplete if the resin is cooled rapidly; below glass transition, due to lack of chain flexibility, it is highly unlikely that further crosslinking could occur. Although this is a possibility, the cooling rates of the press used in all moulding experiments were rather slow—on the order of hours for the press to cool from moulding temperature to ambient. Accordingly, the polymers are likely to have gone through an effective 'tempering' process, maximising the amount of formed crosslinks. Moreover, the overall difference in thermal, mechanical and solvent resistance (Section 2.4) behaviour between the crosslinked CANs and their prepolymers is substantial. Thus, it seems unlikely that a significant amount of bismaleimide remains unreacted.

(3) Stress-induced de-crosslinking

The fracture of conventional thermoset materials requires the breaking of covalent bonds, either in the crosslinks, backbone or both. The covalent bonds through which conventional crosslinked polymers are held together are almost exclusively C–C, C–O and C–N single bonds. Although homolytic bond dissociation energies of covalent bonds vary considerably dependent upon precise chemical structure, these bonds are almost universally strong with BDEs (bond dissociation energies) on the order of 350, 360 and 300 kJ mol^{-1} respectively.[50] This means that their cleavage requires a very large amount of energy, and as a result this contributes to the high theoretical strength of crosslinked

polymers. In reality, defects can mean that applied loads are not distributed evenly (stress concentration) such that these high energy barriers can be overcome at lower-than-expected loads.

Though the bonds holding together the DA CANs are principally strong C–C bonds, the entropically favoured rDA provides a lower energy alternative to conventional C–C cleavage. Carneiro de Oliveira *et al*.[51] recently calculated the activation energy (E_a) from a kinetics study of the rDA reaction of a furan-maleimide system as 90 ± 10 kJ mol^{-1}, 3–4 times lower than the typical C–C bond strength. Moreover, as discussed in the solvent resistance and recycling section, there is literature precedent for mechanically induced rDA reactions. In a perfect, defect-free section of polymer, the inclusion of weak bonds or in this case 'kinetically unstable' (low activation energy) linkages would thus certainly reduce the strength. However, in real systems the strength is just as much a product of the bond strengths and their density as the 'quality' of the material (i.e. the nature, number and location of defects). Moreover, the high strength of the DA CAN prepared by Chen *et al*.[24] would seem to contradict this. Thus, although this could be a factor behind the lower-than-expected strength it is unlikely that this is the only contributing factor.

(4) Prepolymer length: non-network crosslinks

The average number of furan groups per prepolymer (oligomer) chain is approximately four (for DA1 and DA2). As discussed in Sections 2.1 and 2.2, this ratio was chosen based on the original studies of Fischer *et al*.,[36] which suggested that this gave the polymer which was most effective as a healing agent. This means that for the average chain, the maximum amount of other chains it can connect to (crosslink with) is four. However, the short length of these oligomers means that all of these furan groups are close to each other, thus there is a reasonable probability that any two oligomers may be connected to each other by two, three or even four crosslinks, resulting in 'crosslink redundancy' and a marked decrease in the network-forming capacity of the system. Although a statistical proportion of the oligomers will be longer and have a reduced propensity toward redundancy, others will be shorter and have an even lower likelihood of participating in network formation. Critically, for an individual oligomer to be truly crosslinked into the network it must be bound to at least three other oligomers. This concept is illustrated graphically in Figure 2.55, which compares the network forming capacity of Ctrl1 and DA1 based on the actual stoichiometry.

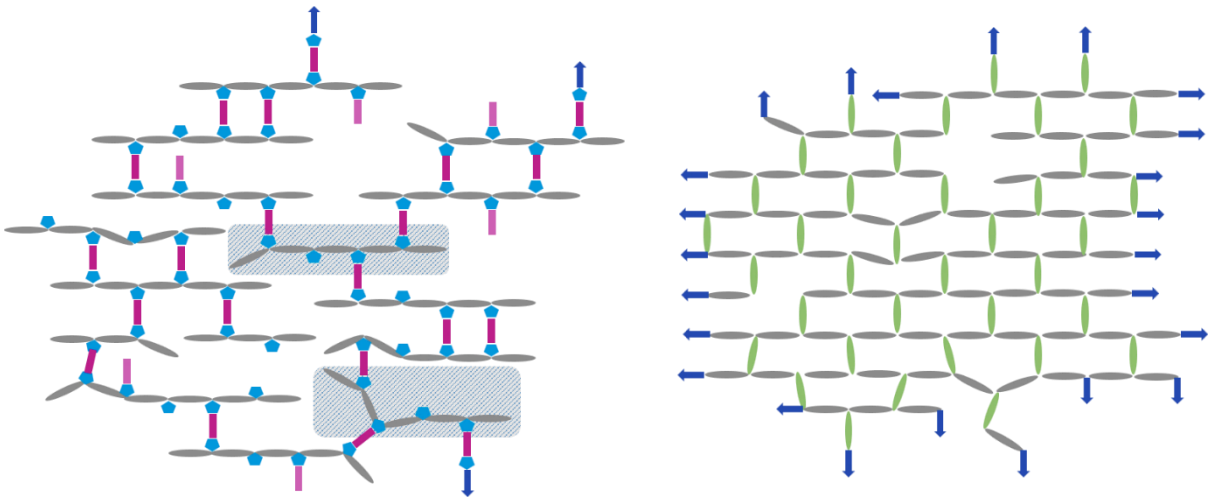

Figure 2.55. A graphical representation of DA1 (left) with 72 DGEBA molecules (grey ellipsoids), 60 furyl groups (blue pentagons) and 26 BMI units (pink rectangles), and Ctrl1 (right) with 72 DGEBA molecules and 36 EDA crosslinking units (green). The blue arrows illustrate connectivity into the wider polymer network.

The diagram of DA1 (Figure 2.55, left) shows high conversion with ~90% of the maleimide groups reacted and thus ~10% dangling. Despite this, only two (shaded blue-grey) of the 15 oligomers (the majority of which are pentamers) are linked to more than two other oligomers and thus can be termed 'network forming'. Ctrl1 shows a similar though slightly higher conversion (~95% N–H bonds consumed) but in sharp contrast, all of the crosslinks are network forming. Furthermore, from the number of arrows extending the networks beyond the figure, the potentially poor network forming ability of DA1 is immediately clear: despite high conversion there is potential for a deceptively low crosslink density. The presence of a soluble fraction in all cases (Section 2.4.2) provides some evidence of these non-network crosslinks.

It might be expected that the reduced number of crosslinks in DA0.5 would magnify this non-network effect, giving a much lower strength. However, the empirical results contradict this—each of the CANs has approximately equal strength. Instead, it is possible that this similarity in strength reflects a similar extent of network formation. Despite the fact that the oligomers of DA0.5 have only two furan groups on average (*vs*. four), these groups are statistically more likely to be further apart from each other. Thus, the furan groups of DA0.5 are proportionally less likely to give redundancy and more likely to be bound to different chains than in either DA1 or DA2. Accordingly, it is possible that a similar number of network-forming crosslinks exist in all three DA CANs, and that DA1 and DA2 have an excess of redundant crosslinks. Moreover, it is also important to consider here that the presence of more than two network-forming linkages is a requirement to forming an infinite network. In fact, if we consider the pentamer of PreDA0.5 as a difunctional monomer (on average it has two furan side groups), as it is in the case of the DA 'crosslinking' reaction, its reaction with bismaleimide (also difunctional) to

form DA0.5 might be better described as a chain extension reaction than crosslinking, since it is not strictly network-forming at all. The presence of a statistical proportion of oligomers means that there will be some components of higher functionality (tri-, tetra-, penta-functional etc.), but the end result is a very lightly crosslinked material. With this considered, the fact that DA0.5 has approximately the same strength as DA1 and DA2 suggests that the true crosslink density is much lower than was originally expected in all of these materials—even if the number of DA adducts is as high as expected, many of them may not be network forming.

(5) Prepolymer length: non-covalent interactions and chain entanglement

The fact that the prepolymers are both such brittle glasses provides good evidence for this hypothesis in itself. The oligomers are certainly far too short to afford any significant quantity of chain entanglement and thus without crosslinking are held to each other merely by a small number of weak intermolecular interactions. Conventional thermoplastics would be expected to be considerably more robust. By virtue of having much longer chains, applied loads are much more evenly distributed through the polymer via the much greater number of inter-chain interactions. Ergo, although the individual strengths of the interactions are much the same, polymers with longer chains have a much greater apparent strength even without including chain entanglement effects.

Each of the previous factors likely play some role in the poor toughness and strength of these CANs. However, there is reasonable evidence to suggest the first two, defect presence and incomplete crosslinking are minimal. Factor 3, ‘stress-induced de-crosslinking’ may contribute to some of the reduced strength. However, the latter two factors concerning prepolymer length, are very likely the dominant factors.

Methods of improving the toughness and strength are explored in Chapter 3.

2.6 Repair (self-healing)

The ability for thermally dissociative CANs to melt imbues them with a repairability which is not accessible to conventional thermoset materials. If the viscosity is sufficiently low (and the polymer chains are sufficiently mobile, i.e. above T_g and T_m), the polymer melt can flow into cracks and thus repair the damage. External pressurisation encourages polymer flow and can close the gap between fracture surfaces, which can enhance this process. As a result of their brittle fracture, there are two broad mechanisms of assessing healing efficiency from the flexural specimens tested in Section 2.5: (1) welding the broken pieces together prior to their re-testing and (2) milling the broken pieces back into powder and re-compression moulding specimens, prior to re-testing.

The first method allows specimen-by-specimen healing efficiency to be calculated and is both simpler and faster than the second. However, since it requires the manual application of heat and pressure, this introduces a significant chance of inconsistency between specimens. In contrast, the second method precludes specimen-by-specimen repair but ensures all samples would undergo the same treatment. Since method one seems more feasible with real structural parts (method 2 is more akin to recycling), this was used as shown in Figure 2.56, with a heat gun (120–150 °C) and aluminium tooling.

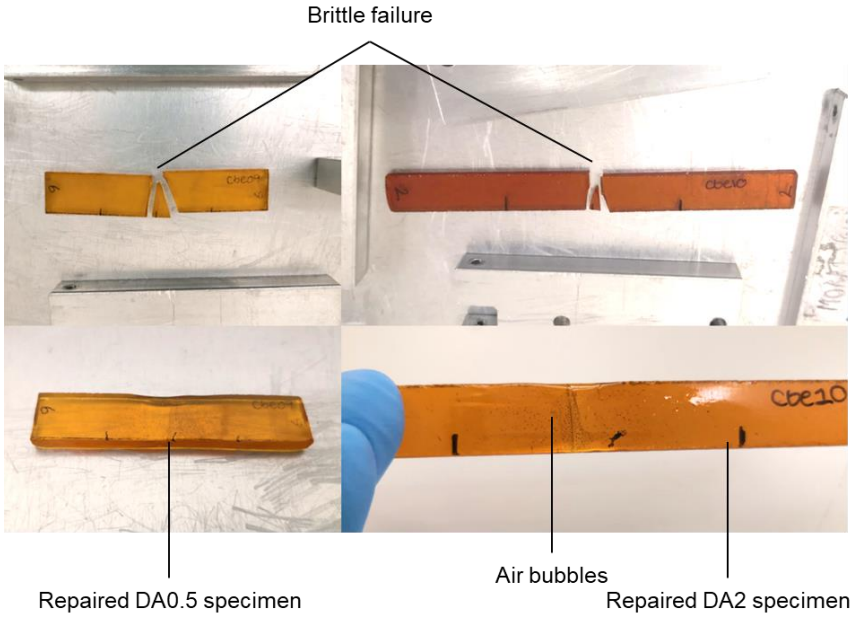

Figure 2.56. Flexural specimens of DA0.5 (left) and DA2 (right) before and after repair.

Considering the total failure of specimens prior to healing, visually this method of repair looks to be reasonably successful. In some cases, the interface between the two (or three) specimen pieces becomes almost completely invisible, though in others a fine line is visible afterward (Figure 2.56,

bottom right). However, in all cases significant specimen deformation occurred due to the imprecise distribution of heat from the heat gun—a more localised method of applying heat would be preferred. Moreover, the regions of the specimens which were heated produced many bubbles which were not present before, a close-up of this is shown in Figure 2.57.

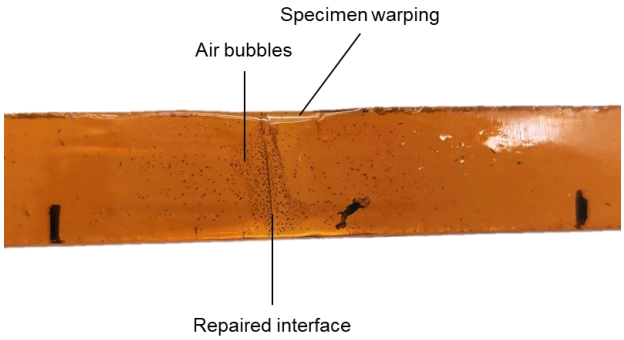

Figure 2.57. Close-up of a repaired DA2 specimen highlighting the appearance of voids (air bubbles) in the repaired region. The distance between the outer markings is 50 mm, and width of the specimen approximately 12 mm.

With hindsight, the formation of these voids is not unexpected; the compression moulding process does not truly degas the polymer melt, instead it uses high pressure to shrink the voids and aid their dissolution. By re-melting the polymer without pressurisation, the trapped air is allowed to re-equilibrate with atmospheric pressure and grow into microscale bubbles as seen in the photograph. As discussed extensively in Section 2.5.3, these voids could serve as defects which could induce premature failure.

The repaired specimens of each of DA1, DA2 and DA0.5 were remeasured and then retested following the same 3pb procedure from which they were originally characterised (gauge length, loading rate etc.), Figure 2.58. Percentage healing efficiency (η) in this case is calculated according to the following equation:

$$\eta = \frac{x_{healed} - x_{residual}}{x_{pristine} - x_{residual}} \times 100 \qquad \text{Eq. 2.4}$$

Where *x* is any material property which can be recovered, in this case the flexural strength at failure. The definition of healing efficiency has been broadly discussed and debated in the literature, though it is the belief of this author that this equation provides a much more useful metric compared to the simple healing efficiency (in which the residual/damaged performance is negated), as discussed in detail in our 2018 progress paper and Chapter 1, Section 1.3.4.[52] In this case since there is no residual strength because of complete specimen failure, the two principal methods of calculating healing efficiency give the same values.

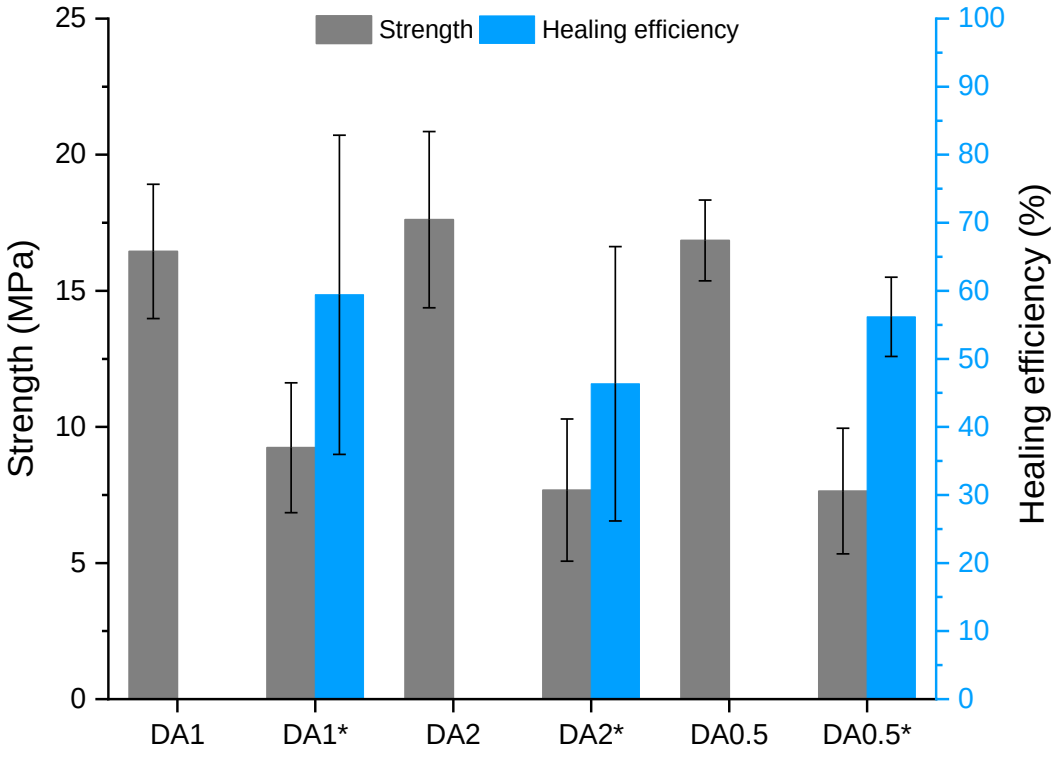

Figure 2.58. The mean strengths of neat and repaired (marked with asterisks) DA1, DA2 and DA0.5, and the calculated healing efficiencies (means of 5, 5 and 8 specimens respectively). In all cases the error bars represent ± 1 standard deviation.

The general trend in repaired strengths is approximately half the original value (mean healing efficiencies are 59%, 46% and 62% respectively). However, these mean values represent a very large scatter as alluded to by the standard deviations; the absolute values of these standard deviations are comparable to those of the pristine specimens but as a fraction of the mean they are much larger. This scatter reflects individual specimen recoveries of 20–110% (recoveries in excess of 100% indicate poor quality original specimens). This variation clearly reflects the hypothesised inconsistency associated with the repair method. Evidently, high quality repairs can be effected, thus it seems probable that the repair technique can be refined to increase these mean values towards 100%. A more localised heating method and compression jig (to precisely align the two fracture surfaces and force them together) would be a sensible place to start. It is worth noting that this system, as with almost all healing strategies (except foaming/expanding healing agents) requires some degree of pressurisation or compression to bring crack surfaces into contact, in much the same way that thermoplastics do. Nonetheless, engineering thermoplastics require higher temperatures and pressures to achieve this.

Importantly, neat polymer specimens which have undergone catastrophic brittle failure represent the worst-case scenario to attempt to repair. The brittle nature of these polymers in their current form precludes their use in structural parts without modification/reinforcement. If they were toughened,

reinforced or otherwise included in structures such that non-catastrophic failure occurs—i.e. cracking or deformation without failure—these parts would then be suitable candidates for healing. This will be discussed further in Chapter 3, Section 3.3.

2.7 Summary

In this chapter, three Diels-Alder–based Covalent Adaptable Networks were prepared from two furan-modified epoxies in conjunction with colleagues at TNO Materials Solutions Eindhoven. Two control epoxies were also prepared to provide points of comparison. The spectroscopic methods, FTIR and ^{1}H NMR were used to confirm their successful synthesis. MALDI-TOF mass spectrometry and GPC were used to further elucidate details on their structure.

Thermal techniques including rheology, DSC and DMA were used to confirm dissociative CAN–type behaviour (demonstrated as a sharp melting event above T_g) and investigate the (re-)processability of these materials. These techniques revealed some differences in thermal behaviour derived from the variation in molecular structure: significant differences were observed between the rheological profiles of DA1, DA2 and DA0.5. PreDA1 has both a later onset of T_g/T_m and a lower viscosity at processing temperature (120 °C) than PreDA0.5, which reflects the greater range of structures and bulkier side groups present on the latter. Among the CANs, DA0.5 has the lowest viscosity, reflecting the much lower quantity of BMI crosslinker, which acts a thickener when dissolved in the prepolymer melt (and lower T_g as shown in DMA/DSC). Importantly, DA0.5 melts at a much lower temperature, 105 °C, than the other two CANs (as shown by the tendency of storage modulus to zero) with DA1 melting at 120 °C and DA2 125 °C. DA1 has an intermediate viscosity and DA2 has a noticeably higher viscosity at processing temperature. This reflects the higher onset of both T_g and T_m (which are concomitant in all three CANs) in DA2. The higher melting temperature of both DA2 and its constituent crosslinker together serve to increase its stability at high temperature (*vs*. DA1), principally by increasing the onset temperature of BMI HP.

A vacuum-assisted compression moulding process has been developed, which combines a steel mould with silicone inserts to minimise cracking on cooldown. The pressure gradient created by the combination of a vacuum bag and mounting press helps to shrink (or dissolve) trapped air and create high quality, optically transparent, sheets of polymer. The behaviour of the polymers in the presence of a range of solvents was also explored, revealing a mixture of responses, some representative of conventional thermoset materials (small quantities of solvent absorption) and some not (large quantities of solvent absorption and dissolution). Mechanical characterisation in 3pb confirmed flexural stiffness was in all cases comparable to conventional epoxies. However, lower than expected strengths and failure strains were also observed. Together, unusual solvent and mechanical responses

suggest lower-than-expected crosslink density. Nevertheless, this unusual solvent-swelling behaviour could be exploited in a solvent-assisted recycling method, which shows potential as an FRP recycling strategy. However, it should be noted that by separating the fibres and matrix, the fibre-matrix interface is destroyed in solvent-assisted recycling methods. Moreover, unless the solvent is effectively recovered (in a closed-loop system), this could add a significant environmental burden to such recycling strategies. It is certainly debatable whether it is better to completely separate fibres and matrix through solvent-assisted methods (at the expense of the interface) or preserve the fibre-matrix interface by mechanical recycling methods (at the expense of fibre length and orientation control).

The three DA CANs were also investigated in terms of their potential for repair/self-healing. Specimens previously tested to failure in 3pb were manually repaired using a heat gun (120–150 °C). Though some strength recoveries around 100% were achieved, the mean values were closer to 50%; the intrinsic inconsistency of the chosen healing method, combined with the use of specimens which underwent complete failure, meant that these values were associated with a large specimen-to-specimen variability. Despite the inconsistency, these were excellent results given the ambitious nature of the repair (after brittle fracture) and the growth of voids upon heating.

The primary limitations of these materials are two-fold: (1) the low strength, low toughness of all the tested polymers, CANs and prepolymers alike. Although many methods exist in the literature to toughen brittle polymers, indeed it is an active field of research, these materials are much more brittle than expected. This likely reflects the short length of the polymer (oligomer) chains, which completely preclude chain entanglement and greatly reduce the efficacy of non-covalent interchain interactions and the covalent network-forming ability of the CANs. This means that even at very high conversions (high yields of DA adduct), there is a risk that relatively few of these adducts actually contribute to network forming (few oligomers are connected to >2 others). (2) High temperature side-reactions, particularly BMI HP, result in permanent crosslinking. This serves to decrease the efficacy of de-crosslinking and reduces the working lifetime of the polymer in question. However, isothermal rheology experiments suggest that a reasonable amount of de-crosslinking can occur even after 2 h at 120 °C. Future work and efforts to overcome both of these limitations are discussed in Chapter 3, Section 3.5 onwards.

To conclude, DA CANs with a range of thermal behaviours have been developed which can be readily repaired and recycled, courtesy of their propensity to de-crosslink at high temperatures.

2.8 Experimental

Polymer synthesis

PreDA1 was prepared as follows. DGEBA resin (212.38 g, *ca.* 0.559 mol) was added to an oil-jacketed steel vessel, heated to 125 °C and then stirred at approximately 400 rpm using an overhead stirrer equipped with a 6 cm diameter disc. Furfurylamine (42.47 g, 0.440 mol) was then added dropwise and left to react for 3.5 h. During this time, the stirring was temporarily stopped while the stirring disc was replaced with a smaller one (4 cm diameter) to reduce the load on the motor, and the stirring resumed. Thereafter, dicyclohexylamine (39.65 g, 0.219 mol) was added dropwise and then left to react for 1 h. At this stage the prepolymer was either isolated by casting onto a Teflon-coated mat or further reacted to prepare either DA1 or DA2.

PreDA0.5 was prepared as follows. DGEBA resin (210.00 g, 0.553 mol) was added to the reaction vessel, heated to 125 °C and then stirred at approximately 400 rpm. In a beaker, furfurylamine (21.37 g, 0.220 mol) and *n*-heptylamine (25.35 g, 0.220 mol) were blended prior to their dropwise addition to the heated steel vessel. After stirring at 125 °C for 3.5 h, the temperature was raised to 130 °C and dicyclohexylamine (39.89 g, 0.220 mol) was added dropwise and left to react for 1 h. At this stage the prepolymer was either isolated by casting onto a Teflon-coated mat or further reacted to form DA0.5.

DA1 was prepared by slow addition of BMI1 (Homide 121, 69.5 g, 0.194 mol) to PreDA1 over 20 min at 120 °C with a combination of motorised and manual stirring with a palette knife. After complete addition the resin was mixed until homogeneous and then cast onto a Teflon-coated mat as an opaque gold-coloured glassy solid. This material was then milled, yielding a fine pale-yellow powder (344.99 g).

DA2 analogously to DA1. To PreDA1 at 120 °C, BMI2 (N,N'-(4-methyl-m-phenylene)-bismaleimide, Homide 123, 54.76 g, 0.194 mol) was added slowly and progressively homogenised over 20 min. The polymer was cast as opaque brown glass and then milled into an orange-brown powder (332.83 g).

DA0.5 was prepared in a similar fashion. To PreDA0.5 at 120 °C, BMI1 (Homide 121, 34.76 g, 0.0970 mol) was added slowly and progressively blended using a combination of manual stirring and low speed overhead stirring over 15 min. The resultant polymer was cast as an opaque orange glass, which yielded a pale-yellow powder after milling (317 g).

Ctrl1 was prepared from a stoichiometrically balanced blend of Epon 828 (DGEBA) and EDA (4,4'-ethylenedianiline, 10.0 g). The Epon 828 (38.5 g) was heated and stirred at 60 °C, while being simultaneously degassed via attachment to a Schlenk line (vacuum). After 30 min degassing, the epoxy resin was returned to ambient pressure, prior to the slow addition of powdered EDA (10.0 g). After

the last of the EDA powder was manually pushed into the resin (with a spatula), the vessel was sealed and returned to vacuum to continue degassing at 60 °C. After 1.5 h, the resin was returned to ambient pressure and the temperature raised to 70 °C. After a further 1 h of stirring the resin darkened in colour and became homogeneous. Thereafter, the blend was poured out of the flask and into a steel mould. The resin was cured in an oven with a 1 h ramp to 120 °C and a 1.5 h dwell at this temperature. This was followed by a post-cure with a further 1 h ramp to 150 °C and 1.75 h dwell prior to cooling to room temperature.

Ctrl2 was prepared in an analogous fashion using Epon 828 (37.4 g) and the following in-house hardener blend (10.6 g) based on the commercial system Epikure 3072: 80 wt% poly(propylene glycol) bis(2-aminopropyl) (M_n = 230), 10 wt% tetraethylenepentamine, 5 wt% diethylenetriamine and 5 wt% bisphenol A.

Rheology

The rheology of each of the five polymers was tested using parallel plate rheology on an Anton Parr modular compact rheometer (MCR 302). In each experiment a 25 mm plate was used in oscillation mode (oscillations of 0.01 mrad, 1 Hz). A thin sample of approximately 1 g of material was placed on the plate and melted (120 °C, ~15 N compressive load applied) while a plate-plate separation of 1 mm was achieved, excess material was trimmed around the edges of the test geometry during this process. In this first series of experiments the polymers were tested in a dynamic cycle between 60 and 120 °C, where the heating/cooling rate was 6 °C min^{-1} and short dwells of 2 min were used (at 60 and 120 °C), for a total of four complete heating/cooling cycles.

Solvent-swelling

The following procedure was used to determine the solvent-swelling behaviour of the five polymers of this study. Approximately 130 mg of the given polymer powder was weighed into a vial and melted into a monolithic sample. 2 ml of solvent (either deionised water, hexane, ethanol, toluene, chloroform or dichloromethane) was then added and the vial capped. After 6 days, the excess solvent was decanted/filtered from the residual mass, which was then dried under a flow of nitrogen for roughly 10 s prior to weighing. This mass at this stage was recorded as the ‘gel mass’. The residual material was then left to dry in air for a further 72 h prior to re-weighing, giving the ‘final dry mass’. The combined data for all five polymers and all six solvents is shown in Figure 2.39.

All other experimental techniques were performed via standard techniques under the conditions described in the text and figure captions.

2.9 References

1 O. Diels and K. Alder, *Justus Liebigs Ann. Chem.*, 1928, **460**, 98–122.

2 B. M. Trost, J. Ippen and W. C. Vladuchick, *J. Am. Chem. Soc.*, 1977, **99**, 8116–8118.

3 R. Gleiter and M. C. Böhm, *Pure Appl. Chem.*, 1983, **55**, 237–244.

4 K. C. Nicolaou, S. A. Snyder, T. Montagnon and G. Vassilikogiannakis, *Angew. Chem. Int. Ed.*, 2002, **41**, 1668–1698.

5 P. J. Boul, P. Reutenauer and J. M. Lehn, *Org. Lett.*, 2005, **7**, 15–18.

6 J. K. Stille and T. Anyos, *J. Polym. Sci. Part A Polym. Chem.*, 1964, **2**, 1487–1491.

7 C. M. Wynn and P. S. Klein, *J. Org. Chem.*, 1966, **31**, 4251–4252.

8 U. Pindur, G. Lutz and C. Otto, *Chem. Rev.*, 1993, **93**, 741–761.

9 A. Gandini, D. Coelho and A. J. D. Silvestre, *Eur. Polym. J.*, 2008, **44**, 4029–4036.

10 N. Roy and J. M. Lehn, *Chem. - An Asian J.*, 2011, **6**, 2419–2425.

11 Y.-L. Liu and T.-W. Chuo, *Polym. Chem.*, 2013, **4**, 2194.

12 M. A. Tasdelen, *Polym. Chem.*, 2011, **2**, 2133.

13 H. C. Kolb, M. G. Finn and K. B. Sharpless, *Angew. Chem. Int. Ed.*, 2001, **40**, 2004–2021.

14 J. P. Kennedy and G. M. Carlson, *J. Polym. Sci. A1.*, 1983, **21**, 3551–3561.

15 J. A. Mikroyannidis, *J. Polym. Sci. Part A Polym. Chem.*, 1992, **30**, 125–132.

16 T. Brand and M. Klapper, *Des. Monomers Polym.*, 1999, **2**, 287–309.

17 H. Zhou and J. A. Johnson, *Angew. Chem.*, 2013, **125**, 2291–2294.

18 J. R. McElhanon and D. R. Wheeler, *Org. Lett.*, 2001, **3**, 2681–2683.

19 O. Gok, H. Durmaz, E. S. Ozdes, G. Hizal, U. Tunca and A. Sanyal, *J. Polym. Sci. Part A Polym. Chem.*, 2010, **48**, 2546–2556.

20 M. M. Kose, G. Yesilbag and A. Sanyal, *Org. Lett.*, 2008, **10**, 2353–2356.

21 A. J. Inglis, S. Sinnwell, M. H. Stenzel and C. Barner-Kowollik, *Angew. Chem. Int. Ed.*, 2009, **48**, 2411–2414.

22 K. Masutani, S. Kawabata, T. Aoki and Y. Kimura, *Polym. Int.*, 2010, **59**, 1526–1530.

23 A. Bousquet, C. Barner-Kowollik and M. H. Stenzel, *J. Polym. Sci. Part A Polym. Chem.*, 2010, **48**, 1773–1781.

24 X. Chen, M. A. Dam, K. Ono, A. Mal, H. Shen, S. R. Nutt, K. Sheran and F. Wudl, *Science*, 2002, **295**, 1698–1702.

25 Y. L. Liu and Y. W. Chen, *Macromol. Chem. Phys.*, 2007, **208**, 224–232.

26 B. J. Adzima, H. A. Aguirre, C. J. Kloxin, T. F. Scott and C. N. Bowman, *Macromolecules*, 2008, **41**, 9112–9117.

27 A. Sanyal, *Macromol. Chem. Phys.*, 2010, **211**, 1417–1425.

28 T. Dispinar, R. Sanyal and A. Sanyal, *J. Polym. Sci. Part A Polym. Chem.*, 2007, **45**, 4545.

29 J. Canadell, H. Fischer, G. De With and R. A. T. M. Van Benthem, *J. Polym. Sci. Part A Polym. Chem.*, 2010, **48**, 3456–3467.

30 J. S. Park, H. S. Kim and H. Thomas Hahn, *Compos. Sci. Technol.*, 2009, **69**, 1082–1087.

31 Y. Heo and H. A. Sodano, *Compos. Sci. Technol.*, 2015, **118**, 244–250.

32 W. Zhang, J. Duchet and J. F. F. Gérard, *J. Colloid Interface Sci.*, 2014, **430**, 61–68.

33 B. Chen, D. A. Dillard, J. G. Dillard and R. L. Clark, *Int. J. Fract.*, 2002, **114**, 167–190.

34 K. H. Park, C. Shin, Y. S. Song, H. J. Lee, C. Shin and Y. Kim, *Polymers (Basel).*, 2019, **11**, 1–10.

35 G. Fortunato, L. Anghileri, G. Griffini and S. Turri, *Polymers (Basel).*, 2019, **11**, 1007.

36 D. H. Turkenburg and H. R. Fischer, *Polymer*, 2015, **79**, 187–194.

37 T. S. Coope, D. H. Turkenburg, H. R. Fischer, R. Luterbacher, H. van Bracht and I. P. Bond, *Smart Mater. Struct.*, 2016, **25**, 084010.

38 M. Lejeail and H. R. Fischer, *Eur. Polym. J.*, 2020, **131**, 109699.

39 J. V. Crivello, *J Polym Sci Part A-1 Polym Chem*, 1973, **11**, 1185–1200.

40 U. S. Sahu and S. N. Bhadani, *Die Makromol. Chemie, Rapid Commun.*, 1982, **3**, 103–107.

41 M.-F. Grenier-Loustalot, F. Gouarderes, F. Joubert and P. Grenier, *Polymer*, 1993, **34**, 3848–3859.

42 H. Rashidzadeh and B. Guo, *Anal. Chem.*, 1998, **70**, 131–135.

43 Z. Grubisic, P. Rempp and H. Benoit, *Rubber Chem. Technol.*, 1969, **42**, 636–640.

44 M. A. Mohd Noor, T. N. M. Tuan Ismail, V. Sendijarevic, C. M. Schiffman, I. Sendijarevic, R. Ghazali and Z. Idris, *JAOCS, J. Am. Oil Chem. Soc.*, 2017, **94**, 387–395.

45 A. X. H. Yong, G. D. Sims, S. J. P. Gnaniah, S. L. Ogin and P. A. Smith, *Adv. Manuf. Polym. Compos. Sci.*, 2017, **3**, 43–51.

46 R. Göstl and R. P. Sijbesma, *Chem. Sci.*, 2016, **7**, 370–375.

47 H. Y. Duan, Y. X. Wang, L. J. Wang, Y. Q. Min, X. H. Zhang and B. Y. Du, *Macromolecules*, 2017, **50**, 1353–1361.

48 B. Lyu, W. Cha, T. Mao, Y. Wu, H. Qian, Y. Zhou, X. Chen, S. Zhang, L. Liu, G. Yang, Z. Lu, Q. Zhu and H. Ma, *ACS Appl. Mater. Interfaces*, 2015, **7**, 6254–6259.

49 G. H. Michler and H. H. K. B. Von Schmeling, *Polymer*, 2013, **54**, 3131–3144.

50 T. L. Cottrell, *The strengths of chemical bonds*, Butterworths, London, 2nd edn., 1958.

51 V. Roucoules, M.-P. Laborie and J. Carneiro de Oliveira, *Molecules*, 2020, **25**, 243.

52 A. Cohades, C. Branfoot, S. Rae, I. Bond and V. Michaud, *Adv. Mater. Interfaces*, 2018, **5**, 1800177.

Chapter 3: Diels-Alder epoxies 2

3.1 Introduction

3.1.1 Diels-Alder epoxies 2: aims and objectives

In this chapter, the three DA epoxy CANs prepared and characterised in Chapter 2 were tested for applications in fibre-reinforced polymer composites (FRPs). The main opportunities here surround the use of the CANs as both recyclable and repairable matrices—this could give CAN FRPs significant sustainability advantages compared to conventional composites. Accordingly, methods of composite manufacture using these CANs were investigated, and the resulting composites mechanically characterised (Section 3.2). These novel composites are then tested for self-healing (Section 3.3) and recyclability (Section 3.4). In Section 3.5, DA1 (Figure 2.11) was tested as a reversible adhesive using simple lap-shear experiments. Adhesives present several advantages over mechanical fasteners in composite structures, particularly in weight saving and in avoiding stress concentration (which is acute around fastener holes). However, one of the major drawbacks is their irreversibility. As such, reversible adhesives may present value in this area, and the dynamic behaviour of CANs make them ideal candidates. In Section 3.6, some of the limitations of these materials are discussed, and initial tests towards the preparation of a second (or third) generation of these materials are presented. Finally, the research in this chapter is summarised in Section 3.6. Future work will be discussed in the concluding chapter, Chapter 6.

3.2 Composite preparation and mechanical testing

3.2.1 Composite manufacture

The use of dissociative CANs such as DA-crosslinked materials as matrix resins for advanced composites provides several new opportunities and challenges for manufacture. On the one hand the low melting point, and moderate working viscosity provide an opportunity for reprocessing which is inaccessible to thermosets and often impractical (due to the prerequisite high temperatures and pressures) with engineering thermoplastics. Several unconventional moulding techniques become conceivably possible with such materials, including dry resin film infusion, powder compression moulding and the use of so-called ‘enduring prepreg’. However, the viscosity levels are too high to accommodate conventional infusion processes—even the viscosity of the prepolymer PreDA1 at 120 °C (*ca*. 100 000 cP) is 2–3 orders of magnitude too high.[1] Moreover, this viscosity also precludes conventional degassing processes as discussed in Chapter 2, Section 2.5.1.

An early concept tested in this project was dry film infusion, where films of solid polymer are compressed through woven reinforcement at elevated temperature (above their melting point). In contrast to conventional film infusion processes, which use partially cured resin films, a dry process might present advantages such as improved safety and increased resin lifetime. Experiments with small sections of film (i.e. shards) produced composite with some success, Figure 3.01. However, this method is not practical at scale due to challenges—namely brittle fracture—preparing intact sheets of resin.

Figure 3.01. A first feasibility study concerning dry resin film infusion of glass fabric (3 plies) with DA1. Cycle procedure: heat to 135 °C; 3 min dwell; 9 tons compression for 1.5 min. This fabric had previously been used to make another section of composite and was recycled prior to this test. The marking in the composite is an imprint from the press platen.

The concept of 'enduring prepreg', first coined by Odriozola *et al*.,[2] was also explored in preliminary experiments with DA1. In this concept individual plies of fibre reinforcement (woven or non-woven) are infused with resin. These infused plies can then be laid-up and 'cured' together in a similar fashion to conventional prepreg, in an autoclave or oven. The main advantage to such a process is alluded to in its name, courtesy of the polymer matrix in question being fully cured prior to use, these plies could be stored indefinitely at ambient temperature. This is in marked contrast with conventional prepreg rolls which are stored at low temperature (often -20 °C) and have a limited usable lifetime at room temperature because the resin is only partly cured—it continues to cure at ambient temperature and eventually becomes unworkable. Although there might be limitations with such a process, including a complete absence of 'tack', this could be overcome during lay-up with the use of heated tooling or heat guns. This could in fact be advantageous, allowing the manufacturer to choose when and where the material is tacky. Although the infusion of large individual plies of fabric with DA1 was successful, as was the combination of two of these 'enduring prepreg' plies; large fragments of resin readily flaked away from these plies due to the inherent brittleness (Figure 3.02). Accordingly, this process has not been further pursued with this generation of resins.

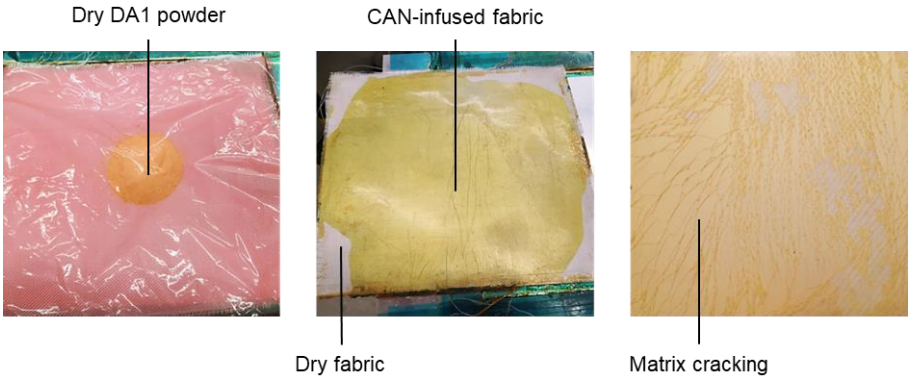

Figure 3.02. Preliminary studies using DA1 to make enduring prepreg (25 x 28 cm, full scale). Left to right: DA1 powder on a single ply of woven glass fabric under a sheet of release film; the infused ply as moulded; close-up after handling.

Vacuum-assisted compression moulding, using a procedure modified from that of the neat resin (Chapter 2, Section 2.5.1), was found to be highly successful. A 25 x 28 cm 8-ply cross-ply (0°/90°) woven glass laminate was prepared from DA1 powder (120 g) placed as a single charge on top of the dry fibres, Figure 3.03a. By heating this stack in an aluminium mould to 125 °C and applying a 9-ton load for 3 min, good infusion was observed with minimal flash and only small, isolated regions of dry fibre, Figure 3.03b. With the localised placement of additional DA1 powder (Figure 3.03c), the laminate was re-pressed under the same conditions (without a mould) to give an improved laminate. However, both of these moulding events were performed without a vacuum bag, which might explain the visible porosity in the product composite (in the form of microscale bubbles, Figure 3.03d).

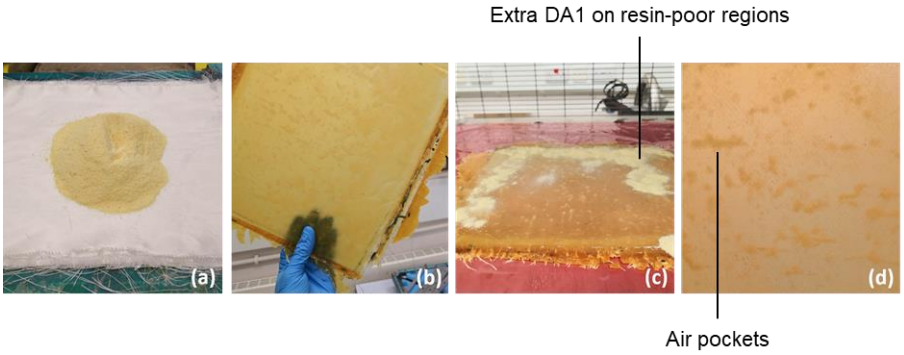

Figure 3.03. (a) DA1 charge placed on 8 plies of woven glass fibre; (b) 8plyDA1 after the first press; (c) the distribution of additional DA1 over resin-poor regions of the laminate; (d) 8plyDA1 after the second press with opacity indicative of resin-poor regions.

To overcome this porosity and demonstrate the importance of vacuum assistance, the laminate was pressed a third time at 125 °C under active vacuum, again in the absence of a mould. The final product '8plyDA1' (Figure 3.04a) was a well-consolidated GFRP laminate that was then trimmed and machined into specimens for flexural testing. To compensate for thermal lag, the compression mouldings reported in this chapter are consistently heated 5–10 °C higher than the target temperature of 120 °C.

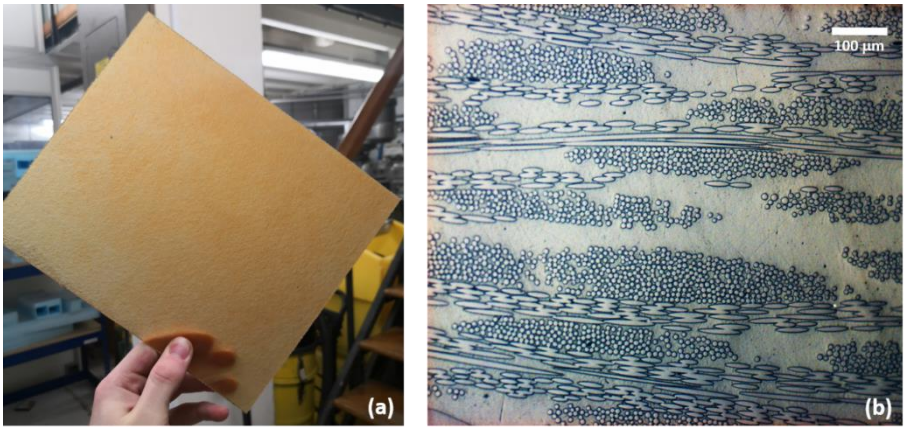

Figure 3.04. (a) 8plyDA1 after trimming; (b) an optical microscope image (10 x magnification) of 8plyDA1's cross-section.

Optical microscopy was used to probe the cross-section of an 8plyDA1 specimen, Figure 3.04b. The specimen was cut, mounted in fast-curing epoxy (cured at room temperature) and then finely polished with a Buehler automated polishing machine prior to analysis. Fibre volume fraction determination was initially attempted using an automated areal method: the software package ImageJ/fiji calculates the fractional coverage based on the contrast in the image. This type of methodology is reported to work well with carbon fibre composites,[3,4] in which there is intrinsically much greater contrast between fibre and matrix. Image processing techniques can be used to make this method possible with glass fibres. In general, the problem with image analysis of GFRP composites is that it is possible to resolve fibre interfaces well but there is otherwise poor contrast between fibre and matrix. Closed cells (such as circles) can be identified and automatically filled; however, highly consistent brightness and contrast levels are necessary to facilitate this. Ultimately, it was not possible to process the images to a sufficient standard to use this method. Instead, an alternative procedure: a combined areal/counting approach (modified from literature procedures) was used.[3,5]

The full cross-section of the 8plyDA1 specimen was sectioned into five cells, then by drawing around the perimeters of the tows (both 0° and 90°) the 'tow' and 'non-tow' areal fractions were calculated and averaged as 72 ± 2% tow and 28 ± 2% non-tow respectively. Void fraction on this scale was negligible. The fibre volume fraction of the tows was then independently calculated as follows. 9 x 2500 μm^2 cells were selected from 0° tows and the number of fibres (where more than 50% of the fibre was within the cell boundaries) counted, mean = 22.2 ± 3.03 (1 SD) fibres. The mean area of these fibres (approximated as a perfect circle from a mean of 24 diameters), calculated as 47.14 ± 0.81 (1 SD) μm^2, was then used to determine the average fibre volume fraction of a given 2500 mm^2 square of tow: 41.9%. A purely areal method was then used to determine the analogous fibre volume fraction in 90° tows after manually drawing around fibre perimeters in five further 2500 mm^2 cells (in 90° tows): 68.2%. As a cross-ply laminate there are an equal number of 0°/90° tows, thus the average V_f

of tow regions is 55.1%. Accordingly, the tow fraction (of the specimen cross section) multiplied by the tow fibre volume fraction gives an estimate of the overall fibre volume fraction of the laminate: 0.72 x 55% = 40%. Though this analysis was performed as carefully as possible, this number is only accurate to approximately ± 2%, due to the number of variables and the intrinsic inhomogeneity of the laminate. The overall void content of this laminate was negligible, << 1% (below the sensitivity of this analysis), confirming that the laminate was well consolidated.

A second DA-CAN laminate designed to give optimal recycling performance, was prepared using DA0.5 and 12 x 20 cm^2 plies of 0°/90° woven glass fabric (plain weave) and an analogous procedure to 8plyDA1. DA0.5 was chosen for this study because its low crosslink density facilitates enormous uptake of chlorinated solvents as reported in Chapter 2 Section 2.4. The product laminate, 12plyDA0.5, is shown in Figure 3.05.

Figure 3.05. 12plyDA0.5 before and after compression moulding.

3.2.2 Three-point bend flexural testing

Three-point-bending (3pb) was selected to quantify the mechanical performance of 8plyDA1 and 12plyDA0.5 for broadly the same reasons as with the neat polymers: matrix damage on clamping is probable with other tests and 3pb is very simple to perform and interpret. There is a further additional benefit to testing composites by 3pb, in that it may be possible to damage specimens only to the point of matrix cracking, without fibre damage. This presents an opportunity to investigate composite repair/self-healing when it can be most effective (with no fibre damage).

The first series of 8plyDA1 specimens were tested to failure using a Shimadzu universal testing machine, 40 mm span and 42 mm min^{-1} loading rate in compliance with ASTM D790 Procedure B (note that the higher loading rate procedure was chosen in attempt to induce failure prior to the outer surface strain limit of 0.05 mm min^{-1} imposed by the standard). Each specimen was loaded until a load drop criterion (to <25% of maximum) was detected to ensure each specimen had failed completely

(with a high level of fibre damage)—importantly, the composite specimens never split into multiple pieces. Inducing this high degree of damage would provide a reliable benchmark from which to consider 'less damaging' tests in subsequent experiments. The raw stress-strain data is presented in Figure 3.06. The calculated mean values (± 1 SD) of stress, strain and modulus are as follows: ultimate flexural strength, 474 ± 43 MPa; ultimate flexural strain, 5.40 ± 0.34%; tangent flexural modulus, 11.6 ± 1.1 GPa.

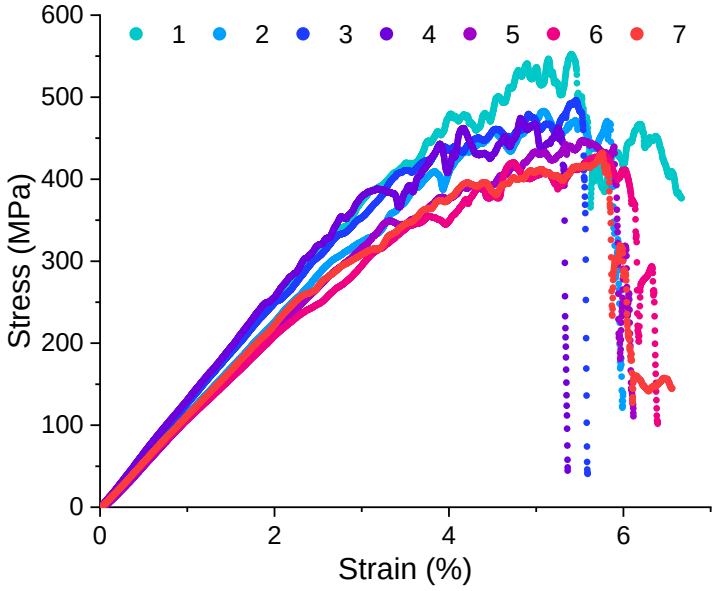

Figure 3.06. Stress-strain curves of the seven 8plyDA1 specimens tested to failure in 3pb. A span-to-depth ratio of 40:1 was used. Stress = the flexural stress at the midpoint of the outer fibres. Strain = the flexural elongation at the midpoint of the outer fibres. Note that stresses calculated herein are modified to account for the large span-to-thickness ratio in accordance with ASTM D790.

From Figure 3.06, three broad regions of the stress-strain curves can be defined: 0–2% strain, an approximate linear-elastic regime. 2–4% strain, intermittent damaging events (associated with drops in stress) and onset of non-linearity. >4% strain, frequent damaging events and substantial plastic deformation prior to ultimate failure. Note that the (unreinforced) DA CANs failed at approximately 0.5% strain (Chapter 2, Section 2.5.2); unsurprisingly, the 0°/90° glass fibres have resulted in a substantial improvement in mechanical performance.

The average ultimate flexural strain of 5.40% confirms that even with the use of procedure B of ASTM D790, failure was not consistently induced prior to 5% strain, the point at which the standard advises that tests should be terminated—in this case the standard advises reporting the 5% yield strength (456 ± 45 MPa). Nevertheless, in all cases the experiments were stopped close to this strain limit. One of the key reasons that such high levels of strain (for advanced composite) were reached is due to the thickness of the specimens. With an average (mean) central thickness of 0.93 mm these specimens

are very thin and are thus capable of large-scale deformation, as can be seen from their shape after testing, Figure 3.07. Naturally, under load these specimens were deformed even further.

Figure 3.07. 8plyDA1 specimens after 3pb testing to failure. Left, 'whitened' regions indicate delamination. Right, a profile highlighting the permanent deformation.

One hypothesis concerning 12plyDA0.5 was that the increased thickness (1.13 mm) of this laminate would result in less pronounced deformation and more reliable results. This is principally because of distributing load-carrying material further away from the neutral axis of bending. Improved repeatability could be particularly important for subsequent healing and recycling experiments since the additional processes those specimens would be subject to could introduce substantial variability. Accordingly, seven specimens of 12plyDA0.5 were cut and tested under 3pb in an analogous fashion to 8plyDA1, Figure 3.08.

Figure 3.08. 12plyDA0.5 3pb specimens.

In this experiment, a slightly wider span (gauge length) of 45 mm and slower strain rate of 30 mm min^{-1} were used, and the same failure criterion (load falling <25% of maximum) was used to automatically stop the test. The raw stress-strain data is plotted in Figure 3.09. Specimen 5 appears to be considerably more compliant than the other specimens, with approximately half the tangent flexural modulus. Accordingly, the data of specimen 5 was assumed to be defective and as such was excluded from mean and standard deviation calculations: ultimate flexural strength, 443 ± 36 MPa; ultimate flexural strain, 2.25 ± 0.23%; tangent flexural modulus, 18.5 ± 1.6 GPa.

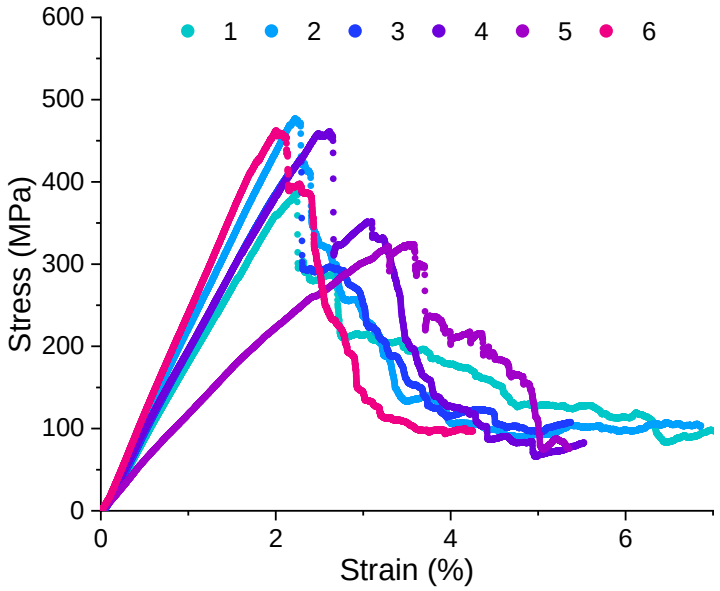

Figure 3.09. Stress-strain curves of the six 12plyDA0.5 specimens tested to failure in 3pb. A span-to-depth ratio of 40:1 was used. Stress = the flexural stress at the midpoint of the outer fibres. Strain = the flexural elongation at the midpoint of the outer fibres. Note that stresses calculated herein are modified to account for the large span-to-thickness ratio in accordance with ASTM D790.

The ultimate strength of 12plyDA0.5 is slightly lower than 8plyDA1; however, the values are within one standard deviation of each other, hence are best considered as approximately equal. This is as expected since the same glass fabric was used and there was no discernible difference in the strengths of the two matrices, DA1 and DA0.5. However, the moduli and strains of these two composites are considerably different, 12plyDA0.5 has approximately 1.5 times the modulus and half the ultimate strain. Overall, this second laminate is much less compliant. As previously stated, one reason for this is geometric, the distribution of load-bearing material further from the neutral axis of bending. However, a further potential explanation for this is fibre volume fraction. Since the mean thicknesses of 12plyDA0.5 and 8plyDA1 are 1.13 mm and 0.93 mm respectively (an increase of ~22%), but the number of plies is increased by 50%, it seems highly likely that the former has a considerably higher V_f. With a higher V_f the fibres account for an increased proportion of the composite mechanical performance, hence the increased stiffness.

3.3 Composite repair and re-testing

3.3.1 Composite repair/self-healing

One of the key applications of reversible crosslinks is in repair, also described as self-healing, as detailed in Chapter 1 Section 1.3. The lack of 'repairability' imbued by conventional composite matrices is a significant limitation. Unlike in conventional composites, the ability of CANs to de-crosslink can allow the polymer to flow, fill cracks and repair damage. As the stimulus (in this case heat) is removed, the polymer effectively 're-cures' restoring the mechanical performance. As reported in Chapter 2, with these resin systems a temperature of ~120 °C and moderate external pressure are required to give the greatest chance of effective crack filling (healing). One of the key limitations is that this method of healing—as with all others in the literature—cannot repair fibre damage.

On a real composite structure, one of the most effective ways to repair minor damage using these resin systems could be to 'iron' the affected region. Here, a combination of localised heating and pressure could be applied without affecting the wider structure. With flat flexural specimens, their small size would make such a repair challenging. However, a simple surrogate for this process is to use a hot press to effect the repair, in much the same way they were manufactured; though in this case the addition of extra powdered polymer should not be necessary. Accordingly, the failed 8plyDA1 specimens were repaired by pre-heating with a set temperature of 130 °C, with subsequent compression under 50 kN for 3 min, the specimens before and after repair are shown in Figure 3.10.

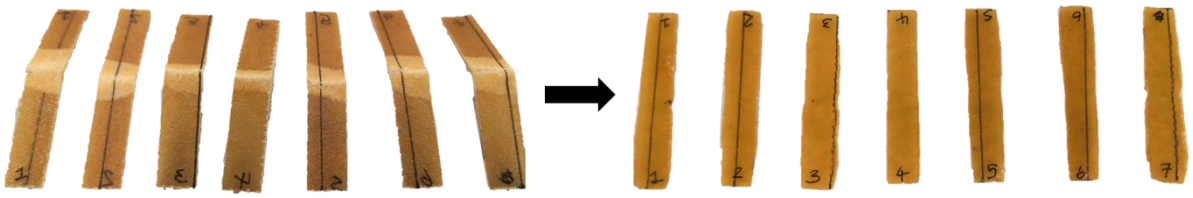

Figure 3.10. 8plyDA1 repair using a hot press.

It is immediately apparent from Figure 3.10 that the visible delamination (observed as whitening in the figure) has been repaired. Indeed, only close inspection of the recovered specimens revealed evidence of the prior failure—a faint line at the centre of the specimens was usually observable and likely indicates the points of fibre breaking. It is also evident from Figure 3.10 that the repair process has distorted the specimen shape, with a decrease in uniformity (non-parallel sides) associated with increased specimen width and decreased thickness. The specimen dimensions were re-measured prior to subsequent testing by 3pb. Raw stress-strain data for this series of experiments is shown in Figure 3.11.

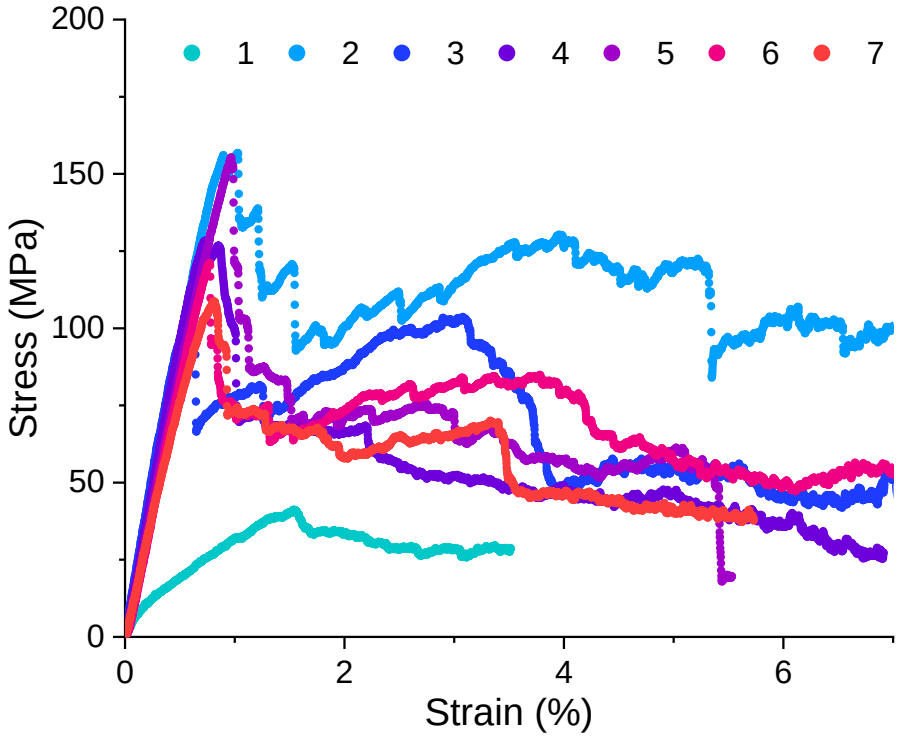

Figure 3.11. Stress-strain curves of 8plyDA1 (repaired) subject to 3pb. A span-to-depth ratio of 40:1 was used.

Specimen 1 was tested to failure twice prior to healing, hence the much-reduced performance. Accordingly, this data was excluded from the following mean and standard deviation calculations: ultimate flexural strength, 129 ± 23 MPa; ultimate flexural strain 0.79 ± 0.14%; tangent flexural modulus, 18.4 ± 1.6 GPa. Using ultimate flexural strength as the metric of recovery, this corresponds to a healing efficiency of 28 ± 5% (using Equation 1.2, Chapter 1, Section 1.3.4). Considering the substantial amount of fibre damage visible from the initial 3pb testing, this demonstrates excellent recovery and indicates some residual contribution from the fibres (neat DA1's ultimate strength was 16.5 MPa). The ultimate strain of the repaired specimen is also much reduced compared to the original value, this likely reflects the reduced contribution of the fibres to the composite performance and the relative increase in contribution from the resin which fails at *ca.* 0.5% strain.

In stark contrast to the stress/strain data, the modulus of the repaired specimens was consistently higher than the pristine specimens. This phenomenon is observed again in later tests and appears to be representative of a real change in material behaviour; the composite becomes more stiff. It seems most likely that this can be explained from the reduction in thickness associated with the pressurised healing treatment. At low strain, the matrix holds together broken fibres sufficiently well that they essentially contribute to stiffness as if there were no fibre damage. However, due to the reduction in cross-sectional area (the specimen width/thickness changes were not proportionate), the repaired specimens appear better consolidated. This difference in consolidation is also readily apparent by eye

as a significant proportion of excess resin has been pushed out to the sides of each specimen, leading to their deformed shape. One of these specimens was cut, potted in epoxy and subject to the same image analysis technique reported in Section 3.2.1; however, no significant change in fibre volume fraction was observed (within experimental error ~2%). Nevertheless, it is possible that specimen inhomogeneity post-healing is masking localised V_f changes, which are hard to detect via fibre counting methods (with microscopy).

Interestingly, the level of scatter (expressed as standard deviations) within this experiment is much lower than the self-healing experiments with the neat polymers (Chapter 2, Section 2.6). This almost certainly reflects the more consistent, reproducible method of repairing the composite specimens (which was not possible with the neat polymer).

These twice-broken specimens were then healed a further time using the same method as before (130 °C, 50 kN, 3 min). On this occasion, much greater specimen disfiguration was observed, resulting in visibly poorer composite, Figure 3.12. The central point of fibre fracture became much more obvious and was this time captured in the photograph as shown. These seven specimens were then tested again in analogous fashion to the previous two 3pb experiments.

Figure 3.12. 8plyDA1 specimens photographed on lined paper after twice being tested to failure and repaired. Note that the lined paper background can be seen through the higher quality specimens 1, 2, 5 and 7.

The extent of recovery with this series is limited due to the extensive fibre damage incurred during the previous two 3pb experiments and the increasingly unfavourable distribution of resin. This is particularly apparent with specimen 6, which exhibits a considerable amount of bare fibre at the surface and seems to have taken the shape of a semi-circular defect (from the press) at its midpoint. The raw stress-strain data is shown in Figure 3.13. In two cases (specimens 3 and 6) the strength was the same before and after 'failure' suggesting defective specimens, accordingly these results were excluded from the following mean and standard deviation calculations: ultimate flexural strength, 56 ± 18 MPa; ultimate flexural strain, 0.55 ± 0.30%; tangent flexural modulus, 14.4 ± 3.8 GPa.

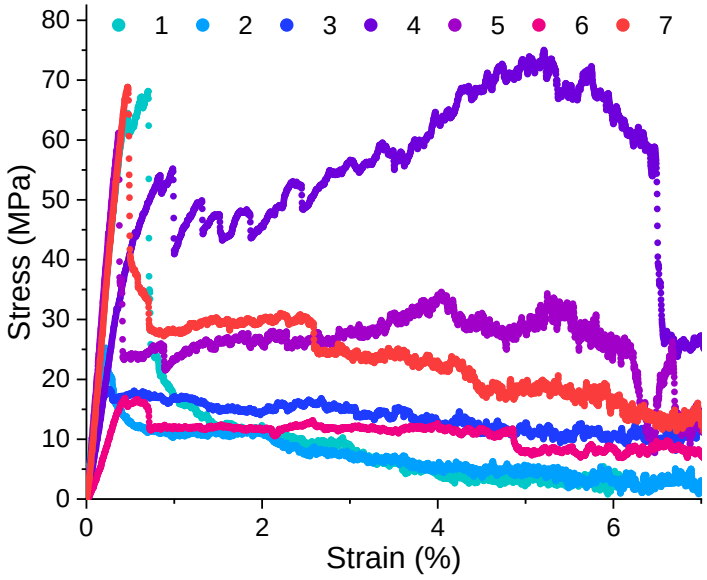

Figure 3.13. Stress-strain data (3pb) of the twice-repaired 8plyDA1 specimens. A span-to-depth ratio of 40:1 was used. Note that specimens 3 and 6 were excluded from calculations as there was no discernible difference between the peak strength and the residual strength after 'failure'.

Specimen 4 shows an anomalously high residual strength that goes on to surpass the initial peak stress at high strain (*ca*. 5%), for the sake of comparison with the other specimens the original peak was used for stress/strain averages. This indicates that in this specimen alone an appreciable number of unbroken fibres were present prior to testing, resulting in a progressive failure more reminiscent of the pristine specimens. A second more clearly defined drop in stress (indicative of a failure event) is apparent at approximately 6.5% strain.

The healing efficiency of these specimens relative to the strength of the original's averages is 12 ± 4% and with respect to the once-repaired specimens, 40 ± 19%. Although the mechanical performance of these twice-repaired specimens is very poor, it is impressive that they can be repaired to support a load at all. In all cases, the maximum recorded stress was greater than or equal to that of the unreinforced polymer (16.5 MPa), clearly demonstrating that the matrix was successfully repaired a second time and that the fibres were still contributing to load bearing (if only in a limited capacity).

3.3.2 Further composite repair/self-healing

A second series of specimens was cut from the 8plyDA1 laminate to explore the possibility of using 3pb testing to damage the composite to a lesser extent, where only the matrix and interfaces are damaged. It is crucial in the self-healing of composites to consider damage that can and cannot be repaired; by reducing the level of damage, healing efficiencies near 100% (i.e. full recovery) could be achievable. However, there are several major challenges associated with such experiments: (1) Damaging specimens such that there is consistently only matrix and interfacial damage—setting

experiments to terminate at a pre-determined displacement could ensure specimens are tested to a well-defined strain. Alternatively, setting experiments to terminate after a given reduction in strength could ensure consistent damage. (2) Identifying the damage—with GFRP specimens, delamination is easily visible; however, other forms of damage such as matrix microcracking are not always detectable with visual inspection alone. (3) Quantifying the damage—lesser forms of damage, such as matrix cracking may result in only minor degradation of the material stiffness and strength. Without testing specimens to failure, ultimate strength cannot be used to determine healing efficiency and determination of alternative stress metrics, such as yield strength may not be possible.

These are some of the major reasons that DCB testing has proved a popular method for quantifying composite healing in the past, since only the matrix and fibre-matrix interface is tested. However, specimen preparation, testing and analysis are often more complex than in other mechanical tests. In the following experiment, 8plyDA1 specimens were tested in 3pb to examine the prevalence of these challenges and explore simple methods of overcoming them.

From the original experiment, testing 8plyDA1 to failure using a high strain rate of ~40 mm min^{-1}, three broad regions of stress-strain relationship were identified. The second of these regions, 2–4% strain is where non-linearity is first observed and infrequent decreases in stress become apparent. Beyond 4% strain, significant fibre damage is evident from the frequent large drops in stress. Accordingly, ~4% strain is a logical starting point for inducing a measurable amount of matrix damage *without* significant fibre damage. One method of increasing the amount of damage while affording more control, is the use of slower strain rates, which would be expected to reduce the measured stiffnesses and strengths.[6] A strain rate of 3 mm min^{-1} was calculated in accordance with Procedure A of ASTM D790 and used in this study.

To ensure a measurable level of damage and explore its effectiveness, the Shimadzu Trapezium software's break detection system was employed throughout using percentage load mode. This mode terminates the given experiment when the load falls to a pre-determined percentage of its maximum. Specimens were either tested to 80%, 70%, 65% or 50%, with lower numbers inducing greater damage. After testing, each specimen was then retested with the same parameters. After the second series of tests the damaged specimens were repaired using a hot press set to 130 °C and then pressing under 2 tons for 3 min, Figure 3.14. All specimens were then tested under 3pb a third time to failure. The three stress-strain curves of a representative specimen are shown in Figure 3.15.

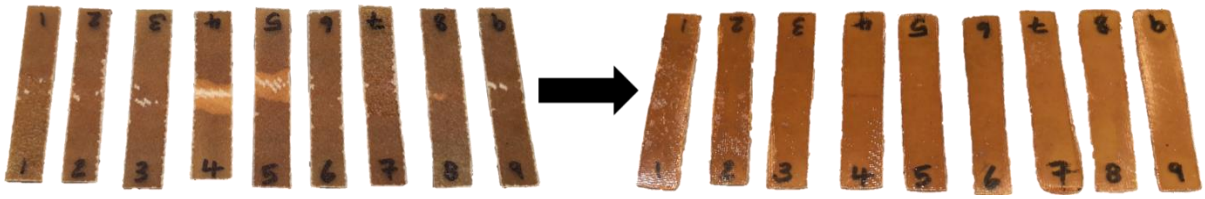

Figure 3.14. Left, partially damaged 8plyDA1 after the B series of tests. Note the more obvious damage (delamination) in specimens 4 and 5, with extensive fibre damage in the case of 4. Right, hot-press repaired specimens prior to the C series of tests.

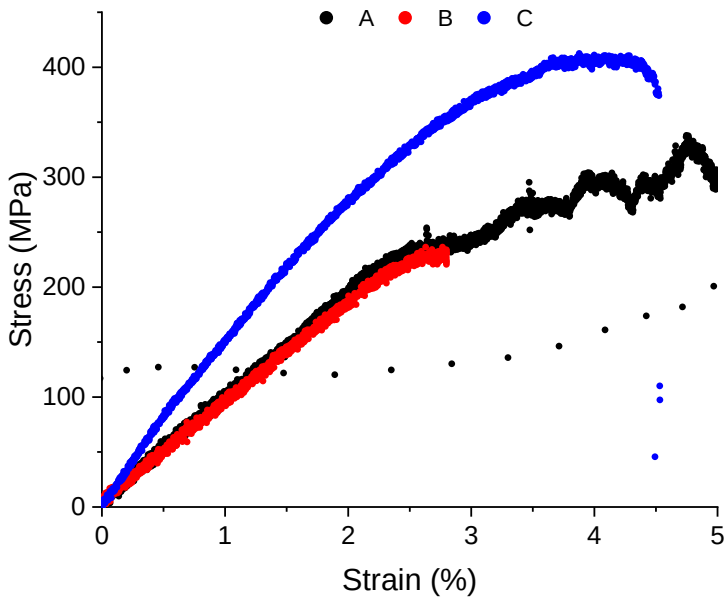

Figure 3.15. The 3pb stress-strain curves of a representative 8plyDA1 specimen (#6). A, initial testing with 65% load break detection. B, repeat testing to determine the influence of damage (manually terminated). C, repaired specimen testing to failure.

Since ultimate strength could not be used to determine healing efficiency, two alternative metrics were considered for use in this calculation: (1) modulus and (2) yield strength. Since tangent flexural modulus is calculated using the onset of the stress-strain curve, this can be reliably measured in all experiments without testing to failure. The tangent flexural moduli of each test series are shown in Figure 3.16. Where A represents the initial tests (mean = 10.05 ± 0.83 GPa), B the damaged specimens (mean = 8.38 ± 0.84 GPa) and C (mean = 15.37 ± 0.87 GPa) the repaired specimens. The specimen number is quoted alongside the break detection values (as a percentage of maximum load).

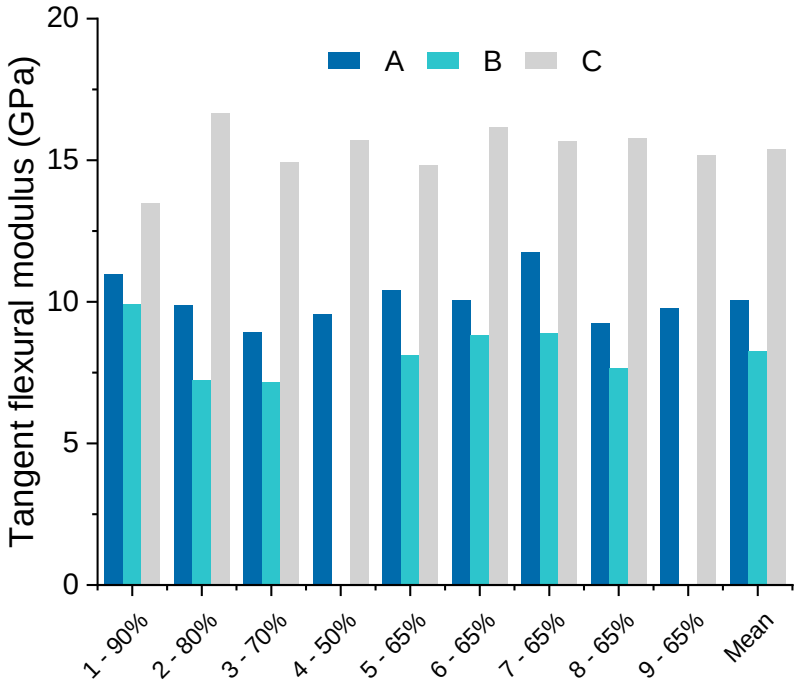

Figure 3.16. Tangent flexural moduli of all tests of the part-damaged 8plyDA1 experiment. In accordance with ASTM D790, tangent modulus is calculated from the steepest point of the stress-strain curve. Specimen 4 failed during its original testing, hence the absence of 4B. 9B is missing due to data corruption.

Modulus recovery. No experimental 'toe' or seating effects (from slack in the loading geometry) were observed in the raw data and consequently no compensation was required. However, deviations of up to ~20% in load-deflection gradient were observed when calculated over different strain ranges. Accordingly, to satisfy the requirements of ASTM D790, efforts were made to maximise the load-deflection gradient (determined with the LINEST function of Excel) and use this steepest point of the curve for the calculation of tangent modulus. This means that these moduli are not calculated over a consistent strain range, which could make comparisons between the different data sets (pristine, damaged and repaired) less reliable. To make sure of the trends in behaviour, a chord modulus calculated between 0–1% strain was also determined for each specimen. These calculations gave an average of A – 9.55 GPa, B – 8.69 GPa and C – 14.10 GPa. Although the A and C averages are lower than their respective tangent moduli and the B average higher, the overall trend is the same regardless of the method by which modulus is calculated.

There is a consistent degradation of modulus for all specimens (B *vs*. A), confirming that significant damage has occurred, and that—in principle—flexural modulus can be used as a damage metric.

The repaired specimens, denoted C, confirm that in all cases modulus is completely recovered and substantially increased compared to the original values. Though in cases of minor damage, such as this, 100% recovery is not unexpected, the substantial increase in performance is highly unusual. There

are two factors which are likely to be contributing to this phenomenon. The first factor is the chemistry. The sensitivity of the DA1 matrix to its thermal history courtesy of the combination of the Diels-Alder equilibria and BMI homopolymerisation (HP), mean that the resin chemistry may have changed substantially during the healing process. It is quite likely that the slow cooldown from the healing temperature led to a 'tempering' effect, where the Diels-Alder network is allowed to equilibrate into a more densely crosslinked material. Moreover, some permanent crosslinks may also develop from the side reactions discussed previously (i.e. BMI HP, Chapter 2, Section 2.1.4) Evidently, increased crosslinking would be expected to increase modulus, and the isothermal rheological experiments in Chapter 2, Section 2.3.1 seem to support this hypothesis. However, relatively small changes in matrix topology are unlikely to result in such substantial changes to the composite stiffness, in which the fibres have a much greater contribution. Accordingly, the second factor, fibre consolidation, is likely to be more significant. By subjecting the samples to a further compression moulding–type process, the fibres and matrix can be redistributed in such a way that apparent fibre volume fraction is increased. Although the quantity of the respective constituents will not change, it is possible that excess resin is pushed to the sides of the specimens, increasing the fibre volume fraction in the bulk. A mean reduction in specimen thickness of 18% is good evidence for this.

Fibre volume fraction analysis (using optical microscopy) was performed on a damaged specimen in an analogous fashion to the pristine specimen reported in Section 3.2.1. Figure 3.17 shows a representative microscope image of a repaired cross section. The same areal/counting method of determining the fibre volume fraction was used as previously described. The most striking difference between the cross sections of Figure 3.17 (repaired) and Figure 3.04b (pristine, Section 3.2.1) is the appearance of numerous voids. Indeed, this is representative across the width of the specimen and is observable with the naked eye too. This observation also appears to be consonant with the observations of bubble formation during the healing of neat resin specimens—a product of previously dissolved air evolving from the molten resin. This corresponds to a void content (volume fraction) of 2%. In contrast, the void content of the pristine sample was negligible at <0.1%.

Figure 3.17. An optical microscope image (10x magnification) of the cross section of an 8plyDA1 3pb specimen after repair. The black sections indicate resin porosity (air pockets).

In terms of fibre volume fraction, a value of approximately 40% was determined, the same value as with the pristine specimen. Since in theory no material (fibre or resin) should have been either added or removed during the healing process this seems logical. However, the distribution of fibre and resin does appear to have changed, which is most easily visualised at the specimen edges, Figure 3.18. In the pristine specimen, to the left of the figure, the edge is cleanly cut and the distribution of tows seems reasonably homogenous all the way to the edge. In contrast, the repaired specimen (to the right) shows a highly deformed edge, with significant outflow of resin (and some 0° fibres) beyond the original edge (demarcated by the termination of the 90° fibres). Importantly, this extra resin must have come from somewhere, meaning that there will be less resin and a higher fibre volume fraction toward the centre of the specimen. This effect is likely to be subtle, though even minor increases in fibre volume fraction (2–5%) could explain the observed stiffness increase after repair. Given this observation and the macroscopic changes to specimen dimensions, this seems the most likely explanation, though unfortunately this V_f determination methodology is not sensitive enough to confirm this proposed V_f gradient. A simple accountancy of errors, using the standard error of the mean (SEM) of average fibre diameter (and thus area) and average fibre number (0.0267 and 0.0455 respectively) gives a mean square error of 0.0528 for the 0° intra-tow V_f. The average of this error and the SEM of the 90° intra-tow V_f (calculated solely in terms of areas, 0.0327) gives an overall minimum error of 0.0428 for intra-tow V_f. The SEM of the average tow coverage is 0.0609, when combined with the intra-tow V_f as an overall mean square error, the error comes to 0.074, which in absolute terms is 3.0% V_f, which seems to be a reasonable estimation of the limits of accuracy with this methodology.

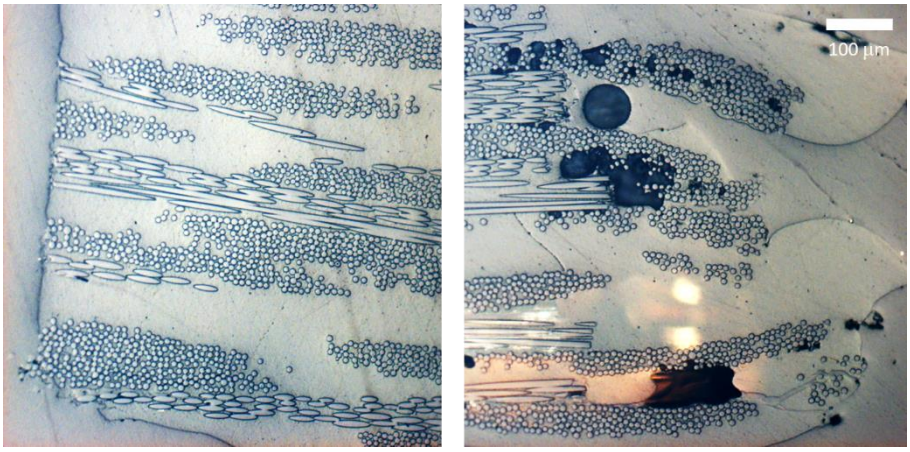

Figure 3.18. Left, an edge of the pristine specimen. Right, an edge of the repaired specimen. The discolouration visible on the repaired specimen is a reflection.

In theory, this methodology could be used to spatially resolve V_f in attempt to demonstrate the proposed redistribution of fibres and resin. However, the size and number of sample areas used for the calculation would be reduced to do this and consequently the uncertainty (error) would be expected to increase. This uncertainty could feasibly be reduced by repeating the measurements on multiple specimens, but it was determined that the chance of observing a statistically significant distribution of V_f across specimen width in a time-efficient manner would be low.

Yield strength recovery. If the composite yields prior to substantial fibre damage, yield strength could also be used as a damage metric if all tests exceed the quoted offset strain. This is true with 0.2% (offset strain) yield strength. By drawing plots such as Figure 3.19, where a stress-strain line at 0.2% strain offset is shown, the yield strength can be determined at the intersection. However, as is readily apparent from Figure 3.20, yield strength was not consistently degraded by the original tests, in many cases B > A. Accordingly, we can state that the composite was not sufficiently damaged in these experiments to use yield strength as a damage metric. If break detection (%MAX load) were to be used again to control the extent of specimen damage, these results would indicate that the tests should be terminated somewhere between 50% and 65% of the maximum load, since 65% did not produce enough damage and 50% produced too much (specimen failure). This highlights the challenge in ensuring an appropriate level of damage. One of the obvious alternative methods of terminating the experiments, using a pre-defined strain, is not necessarily a better candidate either: the mean yield strain of series A is 2.21% and is associated with a significant scatter (1 SD = 0.36%). Critically, many of the specimens exceeded 5% strain prior to break detection in these tests—beyond this threshold the stress calculations are not strictly valid. In other words, using strain limits of ≤5% strain would likely induce even less damage than is observed from the method used in this experiment. Terminating the tests at 5% strain *and* using a faster loading rate could together lead to a consistent, substantial

level of damage. Though this would require further experimentation into the strength–strain rate relationship. A potentially more robust methodology of testing self-healing of 3pb composite specimens was planned but not performed and will instead be discussed in future work (Chapter 6, Section 6.1.3).

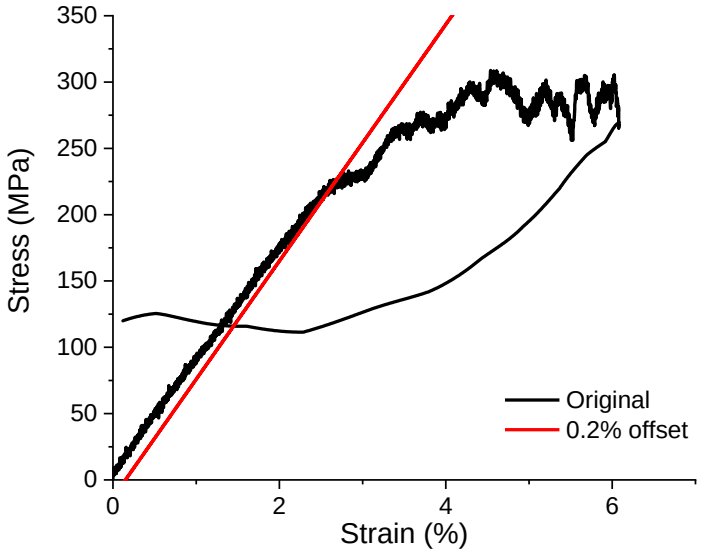

Figure 3.19. 0.2% yield strength determination of specimen 3A.

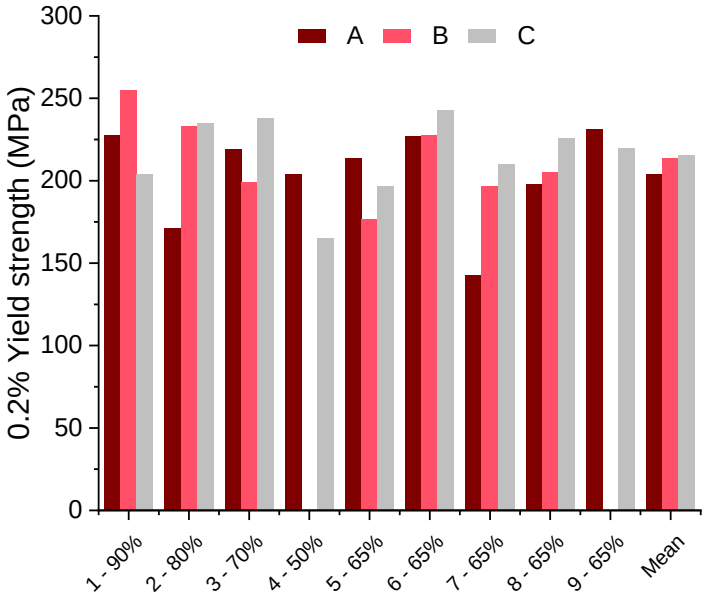

Figure 3.20. 0.2% flexural yield strengths of the part-damaged 8plyDA1 experiment. Specimen 4 failed during its original testing, hence the absence of 4B. 9B is missing due to data corruption.

3.4 Composite recycling and re-testing

As introduced in Chapter 2, Section 2.4, solvent-assisted methods appear to be the most pragmatic solution to recycling CAN-based composites. De-crosslinking can be exploited to break down the polymer into soluble oligomers, leaving the fibres largely unaffected. The fabric reinforcement can then be separated by hand from the solution and dried as individual plies ready for reuse. Separately, the polymer may then be precipitated from solution and dried. Since the reversible crosslink functionality (DA in this case) should remain unaffected by dissolution and drying, the polymer can be isolated and reused for further moulding. As discussed in Chapter 1, numerous researchers have achieved robust solvent-assisted recycling processes with CANs and related polymers by employing competition reactions, and in a few cases this has been extended to composites. The primary limitations with this methodology are that the solvents in question can be harmful and/or expensive, and these factors can be compounded if heating is required. If the solvent is not recycled in a closed-loop system itself, this may reduce the environmental justification for recycling the composite entirely. In addition, solvent treatments break the fibre-matrix interface and can remove fibre sizing and other surface treatments, which can significantly erode fibre performance. Furthermore, it can be challenging to completely remove the solvent from the polymer, particularly if it is high boiling—the inclusion of even a few wt% solvent can significantly influence mechanical properties. One of the major advantages of solvent methods over using superheated steam or related treatments, is that the polymer can be recycled if the solvent is chosen correctly, which is not the case with steam processing. Nevertheless, it may be that superheated steam recycling could be adapted to facilitate recycling of CANs, by inducing de-crosslinking reactions.

In contrast to other reversible systems, DA adducts, as purely dissociative dynamic units, are not appropriate candidates for the usual competition processes; the rDA reaction is always unimolecular—dissociation is not induced by any external species. Although a low molecular weight furan derivative could feasibly be used as a solvent or as an additive in solution, the DA polymer would still require substantial heating (120 °C) to induce dissociation. Consequently, this is unlikely to result in improved dissolution *vs*. simply dissolving the polymer at high temperature in a solvent such as DMSO (b.p. 189 °C), as has previously been reported in the literature.[7,8] Accordingly, any high-boiling solvent which can dissolve the oligomers (prepolymer) is a sensible candidate for recycling. Indeed, colleagues at TNO Materials Solutions in Eindhoven, NL, tested several such solvents with small GFRP samples of DA1 and DA0.5 (in unpublished work) and found that toluene (at reflux, 110 °C) was very effective for recycling DA0.5 composite. However, in our hands, a crude experiment with refluxing toluene did not cleanly dissolve DA1 from a section of 8plyDA1 composite even after 20 h, Figure 3.21.

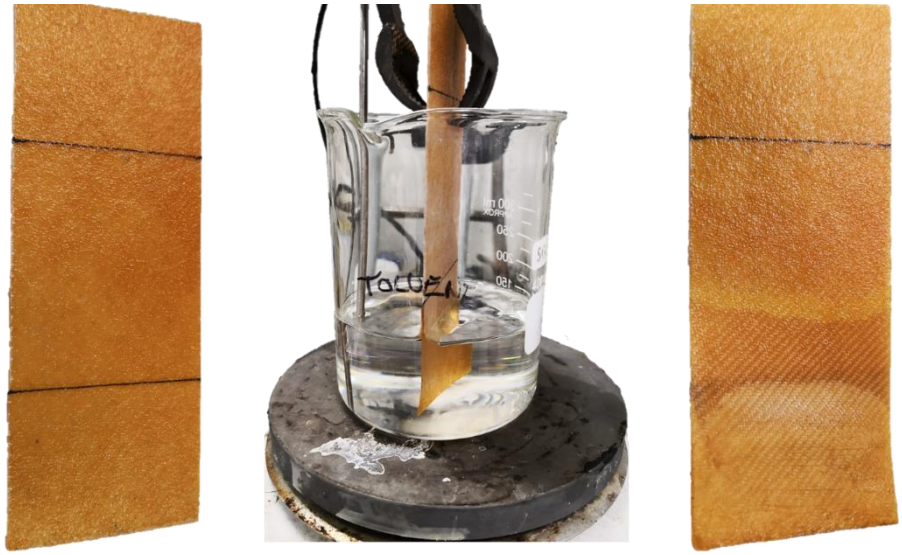

Figure 3.21. Left to right, 8plyDA1 prior to exposure, the composite dissolving in 110 °C toluene and the composite appearance after exposure.

As is evident from composite discolouration, some of the resin was successfully dissolved, but a significant quantity of DA1 remains on glass fabric (giving the orange colour). The contrast in observations between DA1 and DA0.5 are to be expected. As has been discussed in both this thesis and in the wider literature, generally the furan-maleimide rDA reaction requires temperatures in excess of 120 °C to operate effectively. However, with very few crosslinks, DA0.5 readily dissolves in refluxing toluene, despite the fact that the rDA reaction is relatively limited at this temperature. In contrast, higher boiling solvents such as DMSO and DMF should be quite effective at dissolving all of the DA polymers discussed in this work (when heated above 120 °C), particularly when the composite is fully immersed. As mentioned previously, it must be stressed that removing residual DMSO and other high boiling solvents would be challenging.

After discovering the potency of DCM as a solvent for cleaning surfaces and equipment contaminated with these DA CANs, the room temperature method of recycling presented in Chapter 2, Section 2.4, Scheme 2.2 was developed. This method exploits the unusual phenomenon of gelation which occurs when the DA CANs are immersed in chlorinated solvent (DCM or chloroform) as they absorb large volumes. Conveniently, the gelation process exerts a significant pressure between plies which facilitates their separation as shown in Figure 3.22. As previously described, the individual plies are simply dried and not further treated prior to reuse. The gel is then concentrated by evaporation of the residual solvent prior to drying (at RT overnight and then 60 °C for a further 24 h), milling and reuse. The section of 8plyDA1 shown in Figure 3.22, was then reconstituted (from recycled fabric and DA1) in an analogous VACM process to its original moulding (130 °C, 6 tons, for 3 min).

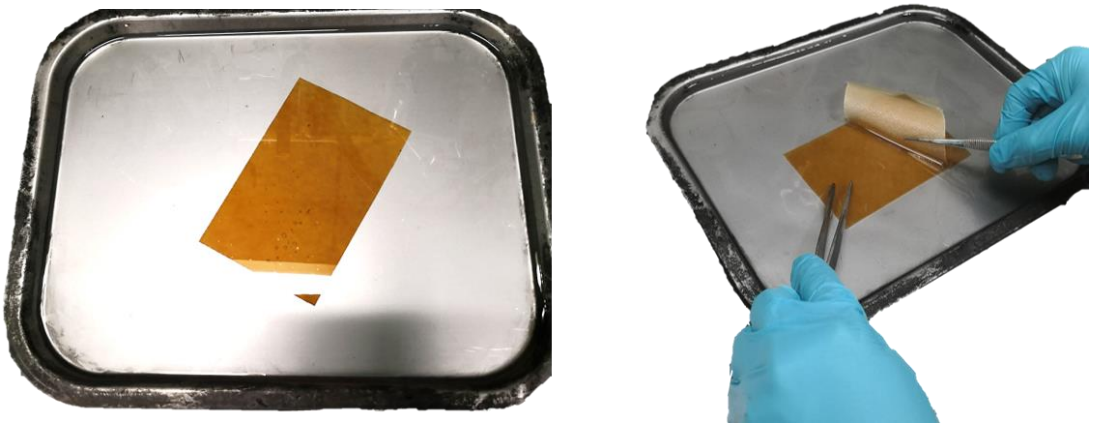

Figure 3.22. Recycling of 8plyDA1. Left, 8plyDA1 immersed in DCM for 2 h. Right, manual separation of the individual E-glass plies from the swollen composite.

The advantages of this process are two-fold: (1) the use of ambient temperature makes this method considerably less energy-intensive than heated processes. (2) the low-boiling point of DCM makes removal of residual solvent considerably more efficient than with higher boiling solvents such as toluene or DMSO. Accordingly, it is probable that there is much less residual solvent after processing with this method.

The significant drawbacks from this method are the hazards associated with DCM (and the alternative chloroform, which is even more hazardous): although it is non-flammable and an excellent solvent for a wide variety of materials—hence its ubiquity in chemistry laboratories the world over—it is a skin/eye irritant, suspect carcinogen and is associated with central nervous system targeted toxicity. However, it should be noted that the majority of widely used organic solvents are associated with similar hazards (and are typically highly flammable), and toluene is no exception to this.

To explore the efficiency of this process in terms of its influence on mechanical properties, recycled 8plyDA1, '8plyDA1R', was tested under 3pb and compared to the pristine composite (with a 39.96 mm span and 42 mm min^{-1} strain rate). The stress-strain curves are shown in Figure 3.23. The mean values (± 1 SD) of the seven specimens are as follows: ultimate flexural strength 331 ± 41 MPa, tangent flexural modulus 10.9 ± 2.4 GPa, and ultimate strain 3.74 ± 0.57%. In terms of strength, this equates to 69% of the original pristine strength (mean 474 ± 43 MPa), demonstrating unequivocally that DA CAN composites are efficiently recyclable. In much the same way as healing efficiency, this could be described as a 'recycling efficiency'. Nevertheless, a 31% degradation in strength, which is mirrored by a similar decrease in failure strain (3.74 *vs.* 5.40%) is clearly representative of some deleterious effects produce by the recycling process. Furthermore, each of the mechanical properties are associated with increased scatter, reflected in the increased values of standard deviation. One possible explanation for these observations is solvent (DCM) entrained within the polymer, even small

amounts could lead to matrix plasticisation, which in turn could manifest as a reduction in stiffness and strength. Even though DCM is particularly low boiling (39.6 °C), and the drying process is thorough, it is quite possible that there is a small amount trapped within the polymer. One way to confirm this would be to dissolve some of this composite in $CDCl_3$ and look for traces of DCM within the ^1H NMR spectrum. Indeed, a ^1H NMR spectrum of recycled and re-moulded DA1 did reveal an appreciable quantity (~2% of the total number of H atoms), which could have a significant plasticising effect. To overcome this, the polymer should be dried for longer prior to reuse. An alternative explanation for the reduced performance is through the loss of less soluble fractions during the process. Although none of the polymer or solution is actively discarded, some residues remained on the glassware and it is possible that these residues are enriched with a disproportionate amount of crosslinker (BMI) and/or longer oligomers, which would be expected to contribute significantly to the overall mechanical behaviour.

The fibres typically used in advanced polymer composites, be they carbon, aramid or glass, are relatively chemically inert by nature. Being completely inorganic, the E-glass fibres used throughout this research would be expected be almost completely inert to most organic chemicals, though research has shown that E-glass can be sensitive to acid corrosion.[9] It seems unlikely that the solvent treatment would have a significant effect on the individual fibres. Nonetheless, the performance is sufficiently reduced that it seems unlikely that the matrix alone can explain it. Perhaps the most likely explanation is weakened fibre-matrix interfaces. In this study, the recycled fibres were not additionally cleaned after separation (solvent treatment) and the result was a small but significant quantity of matrix residue was left on the fibres. It is conceivable that the residual layer of polymer resulted in poor fibre-matrix adhesion during the second (re-)moulding process. In contrast to the behaviour of the pristine composite (Figure 3.06), there are no minor breakage events (zig-zags in the stress-strain curves) visible in Figure 3.23. It is possible that those events represent energy release on debonding or matrix cracking, which is not occurring in the recycled specimens due to poorer quality interfaces.

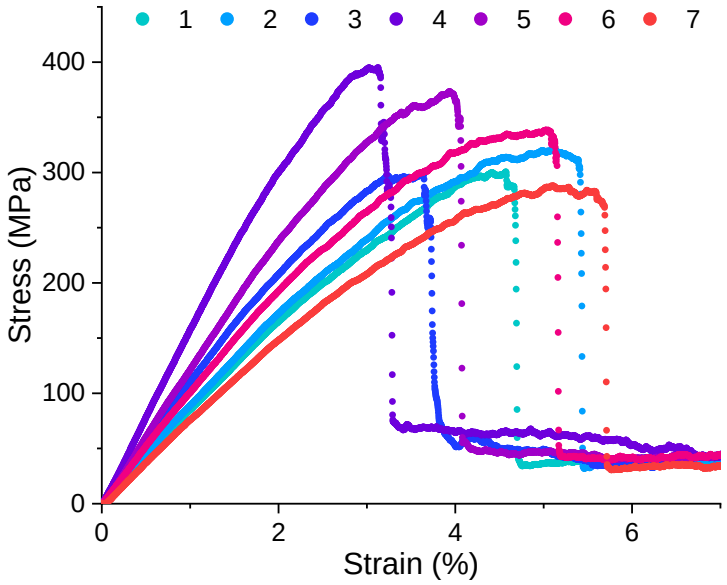

Figure 3.23. Stress-strain curves of 8plyDA1R. A span-to-depth ratio of 40:1 was used.

3.5 Reversible adhesion

With the increasing use of FRPs, the use of adhesives has also grown significantly. This growth is largely due to two factors: (1) the intrinsic brittleness of FRPs makes them highly susceptible to stress concentration effects—effects which are particularly acute around the holes drilled for rivets and similar joints. (2) Adhesives have a much lower density than metallic fasteners which combines well with the weight-saving potential of composites.[10–12] However, a major limitation of conventional adhesives is that they do not facilitate disassembly and thus present significant concerns for end-of-life. In recent years, there has been significant research into reversible adhesives,[13–16] and the Diels-Alder reaction is one of the key underpinning chemistries that has received considerable attention.[17,18] By introducing an element of controlled reversibility, the primary limitation of adhesives can be overcome, potentially enabling composites to reach their true weight-saving potential. Other techniques for joining certain composite parts exist, such as thermoplastic welding,[19–22] which have significant potential in their own right; however, these techniques are beyond the scope of this discussion.

Qualitatively, it can be easily demonstrated that these Diels-Alder CANs can be used as reversible adhesives, since they are sticky liquids at 120 °C and hard solids at room temperature. Quantifying this behaviour requires the use of a mechanical testing method, of which there are numerous examples in the literature. Two of the most prevalent are pull-off,[23–25] and lap-shear tests.[26,27] In theory, either of these tests could be used to test reversible adhesion, simply by performing the respective test at ambient and elevated temperature and comparing the results. However, single lap-shear testing was

chosen for this study due to its simplicity and compatibility with the available Shimadzu universal testing machine (that was equipped with a thermal chamber).

In an ideal scenario, the disassembly of a structure joined with a thermally reversible adhesive would use a heat delivery system that was sensitive and highly localised, such that heat could be applied to the bond-line without heating the surrounding material. This could potentially be implemented using resistive heating, lasers or possibly even a highly exothermic chemical reaction. Nevertheless, for the sake of a quick demonstration experiment, a thermal chamber—an oven that completely encases the test specimen—is ideal and should provide a more consistent heat delivery than a heat gun, another simple alternative. A series of 18 steel specimens were prepared in accordance with the specifications outlined in ASTM D1002, Figure 3.24, with a view to the preparation of analogous carbon fibre specimens at a later date.

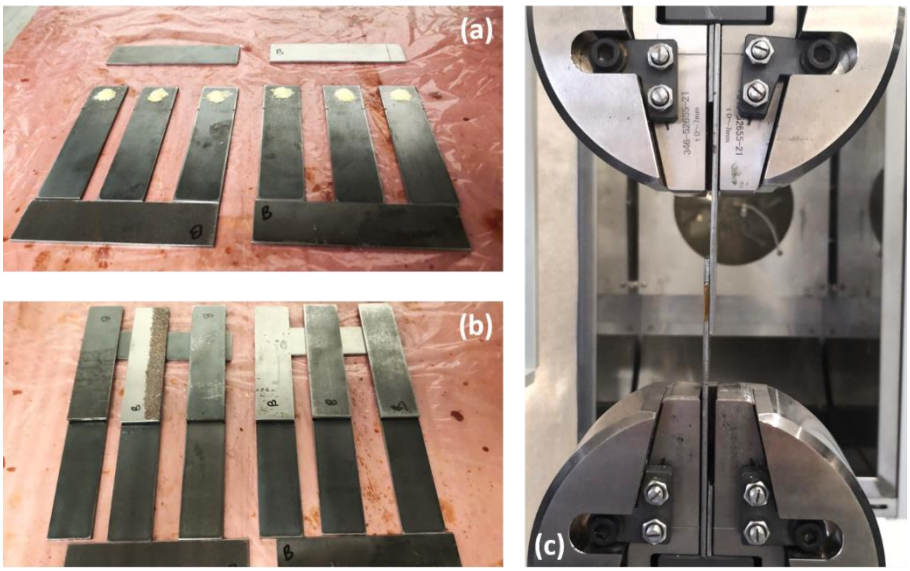

Figure 3.24. Single lap shear specimens. (a) DA1 powder on the lower of the two steel substrates (dimensions: 1.6 x 25.4 x 100 mm) of each specimen. (b) the upper substrate completing the six specimens shown (shear area of ~625 mm^2). (c) a specimen in the test machine, with thermal chamber in the background.

It is well documented that adhesive strength is highly dependent upon the quality of specimen surface preparation. As a result, adhesive manufacturers provide comprehensive instructions on how to produce such surfaces. These typically comprise steps such as ‘keying’, cleaning and primer application. Where keying is increasing the surface roughness in order to increase the true contact area of the bond-line. Cleaning is usually as simple as wiping the bonding surfaces with a specified solvent. Primers are typically dilute solutions of adhesive which can provide a more consistent surface for the primary adhesive layer to bond to. A simplified procedure was devised as a surrogate for these steps, grit-blasting the substrate surfaces to efficiently key them and then cleaning with DCM.

Unfortunately, the in-house grit blaster was not operational during the limited time available to prepare these specimens, hence each specimen was instead manually sanded with 240 grit Al_2O_3 sandpaper prior to DCM cleaning. As a result, the lap-shear strengths were expected to be lower than they could be. The two steel substrates were manually aligned and glued together using a hot mounting press (130 °C, 5 tons, 2 min) with 0.2 g of DA1, enough to form a thin continuous layer at the bond-line.

The tests were performed on a Shimadzu universal testing machine equipped with a 10 kN load cell and tensile grips. The room temperature samples were tightened by hand and then tested immediately. The high temperature specimens were first lightly gripped and then heated to 120 °C, allowing for a 5 min 'soak' before further tightening and subsequent testing. A 1.3 mm min^{-1} loading rate was used in all cases. At room temperature (ambient, ~20 °C), a mean shear strength ± standard deviation of 2.40 ± 0.85 MPa was calculated from the six successful tests, Figure 3.25. As expected, a much-reduced average strength of 0.43 ± 0.26 MPa was determined from the seven successful tests at 120 °C, which corresponds to 18% of the original (Figure 3.26). It is worth noting that two results were excluded because of specimen failure during gripping at elevated temperature, accordingly the mean strength is likely skewed to a higher value as the weakest bond lines are the most easily damaged and are thus not captured by the average.

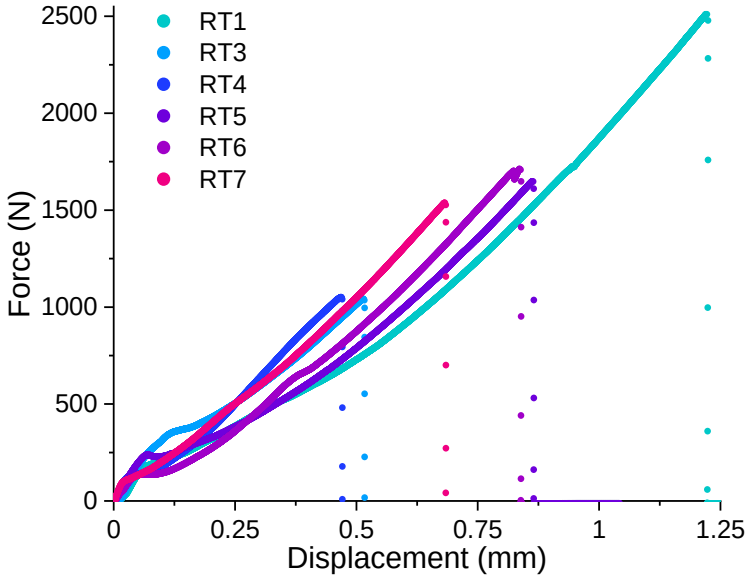

Figure 3.25. Force-displacement profiles of the room temperature series of lap-shear experiments. Specimen 2 failed prior to testing.

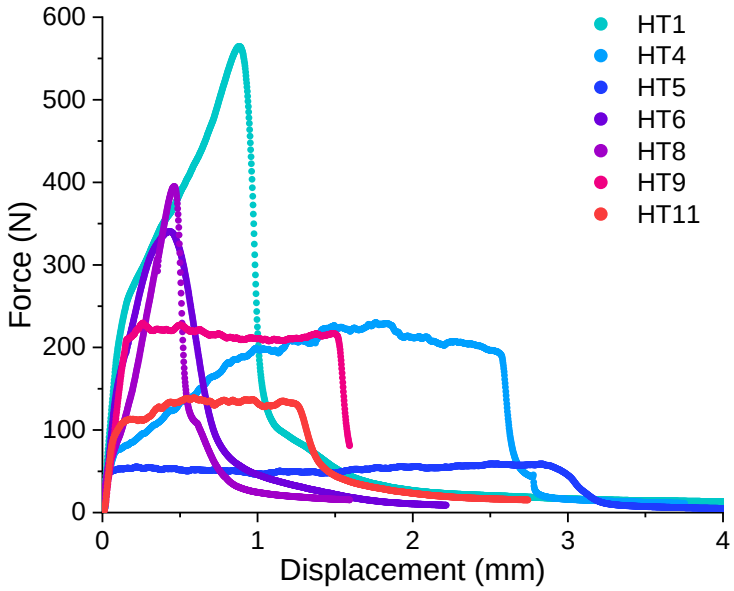

Figure 3.26. Force-displacement profiles of the high temperature (120 °C) series of lap-shear experiments. Specimens 2, 3, 7 and 10 failed during gripping and were thus omitted.

Each of the room temperature (RT) tests followed a similar load-displacement profile, with a toe region followed by an almost linear-elastic response to failure. In marked contrast, the high temperature (HT) experiments were inconsistent in profile, with those specimens that failed at higher strength exhibiting abrupt (brittle) failure and the low strength specimens exhibiting extensive plasticity—plateaus of substantially increasing displacement with little change in load. This latter behaviour appears to be representative of a stick-slip type phenomenon indicating that the bond is held together largely through friction. This is the expected response of an adhesive becoming a viscous liquid. The fact that a more conventional (abrupt) failure is observed in the three strongest specimens might suggest that the polymer had not melted. It would thus be prudent to explore the use of higher temperatures and longer soak times in any future experiments. A thermocouple at the bond-line could be used to ensure that the polymer reaches the desired temperature and melts as expected.

The failure strengths of both series are plotted together in Figure 3.27.

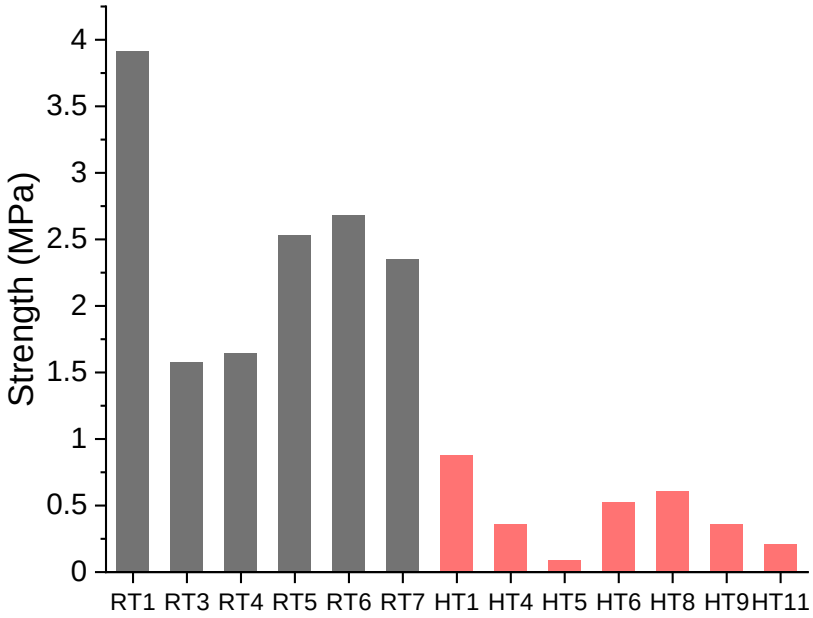

Figure 3.27. Single lap-shear strengths of room temperature specimens (RT#, grey) and high temperature specimens (HT#, red). Three specimens were excluded from the high temperature series due to failure during clamping. One specimen was excluded from the average of the room temperature series due to failure during clamping.

This study shows that shear strength is reduced by more than five-fold; however, improved surface preparation and a higher volume of adhesive could greatly improve the ambient performance. Since a very small amount of adhesive was used—the bonds in all cases were <1 mm thick—it is possible this led to an overestimation of the shear area, due to incomplete coverage. Furthermore, use of longer soak times or higher temperatures could make the de-crosslinking process more consistent and significantly reduce the strength at elevated temperature. Together, these modifications could greatly improve the ratio of ambient strength to elevated strength. Furthermore, it might also be expected that, due to chemical similarity, the DA CANs would better adhere to epoxy composites. In any case, it is evident that this polymer has potential as a reversible hot-melt adhesive.

3.6 Second generation DA CANs

From the conclusions of Chapter 2 there are two clear limitations concerning the DA CANs described thus far within these two DA chapters: (1) brittleness (and associated low strength), which is attributed to modest network-forming, and (2) a limited working lifetime at high temperature (due to side-reactions, principally BMI HP). Numerous methods have been reported in the literature for improving the toughness of polymers and polymer composites, including the addition of rubber particles,[28,29] the inclusion of thermoplastic phases,[30–32] Z-pinning,[33,34] tufting,[35] and nanofillers.[36] These methods can be very effective and are ideal for improving epoxies, which are infamous for their brittleness. However, as previously demonstrated (Chapter 2, Section 2.5.2) the DA CANs investigated herein are much more brittle and low strength than conventional epoxies, which is attributed to lower than anticipated network density—i.e. there are few DA adducts which contribute to network forming. In this case, the aforementioned toughening mechanisms would be expected to offer minimal improvement. Since these DA CANs excellent melt and healing behaviour, it seems probable there is scope to readdress the trade-off between mechanical performance and 'healing efficiency'. By increasing oligomer length, or otherwise increasing crosslink density mechanical performance should improve at the cost of decreased healing performance.

3.6.1 Prepolymer length

Increasing the prepolymer/oligomer length is simple to achieve in practice, since this length is determined by the ratio of the primary amine (furfurylamine) to diepoxide (DGEBA) in the first stage of polymer synthesis: the closer the ratio to unity, the longer the oligomers become. The caveat is that as the chain length increases the reaction may transition from a kinetic-limited to diffusion-limited regime, which may result in the reaction taking longer or the final chain length being shorter than expected. Any unreacted amine could be highly detrimental to the end performance of the polymer. Importantly, as the length of the chains increases, a higher proportion of the crosslinks (formed later in the synthesis) will be 'network forming', as any given chain will have an increased probability of connecting to more than two other chains. The trade-off with increasing the length is that the viscosity of the molten polymer will increase as there are more interchain interactions and chain entanglement becomes possible. Furthermore, it is also likely that with increasing interchain interactions, both the prepolymer, and to a lesser extent, the product CAN will progressively lose their well-defined melts in favour of broader melt transitions. It would be expected that such changes to the melt behaviour reduce the efficiency of healing and make composite manufacture more challenging (by inhibiting polymer flow). It is therefore important not to increase the prepolymer chain length too much. Accordingly, a sensible starting point to change the average oligomer length to would be 10

monomers, double the current number. Ideally, a wide range of lengths would be explored to find the best balance between mechanical performance and CAN activity (melt-ability), Figure 3.28.

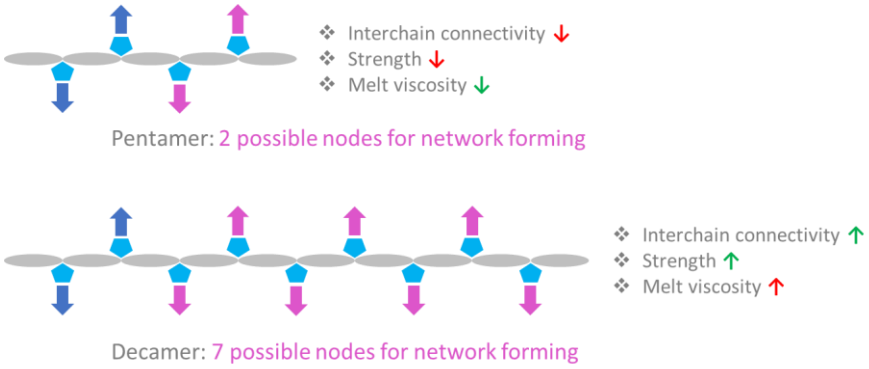

Figure 3.28. A graphic illustrating the theoretical performance trade-off of CANs determined by prepolymer length. The first two DA adducts formed are chain-extending, subsequent DA adducts are network forming.

As a preliminary experiment, a new prepolymer 'PreDAx' was prepared with a ratio of nine DGEBA units for every eight furyl groups (and two end caps), which should approximate a doubling of prepolymer length relative to PreDA1.

GPC analysis would arguably provide the most informative characterisation of this material, allowing a straightforward comparison of molecular weight relative to the original prepolymer, PreDA1. However, at the time of writing, analysis has been limited to ^{1}H NMR, FTIR, DSC and rheology. Where the former three techniques primarily provide information concerning the relative success of the synthesis, and rheology can be used to examine the melt behaviour of the polymer.

The ^{1}H NMR spectrum of PreDAx is compared with PreDA1 in Figure 3.29. The absence of a peak at ~2 ppm confirms that there is no residual primary amine remaining. However, the ratio of bisphenyl aromatics to furyl aromatics is increased approximately two-fold—compare the peaks highlighted in blue and yellow which represent the bisphenyl- and furyl-aromatics, respectively. This is opposite to what would be expected. By increasing the fraction of furfurylamine the prepolymer becomes longer as the ratio of N–H bonds to epoxide groups approaches unity. Accordingly, ignoring the higher order oligomers of DGEBA, the ratio of furyl protons to bisphenyl protons should approach 3:8 (or 0.375). Due to the higher order oligomers of DGEBA present in Epon 828 there will always be a further excess of (perhaps 20%) bisphenyl aromatics such that this ratio instead approaches 5:16 (or 0.3125). The ratio is 0.237 in PreDA1, but only 0.128 for PreDAx, less than half of the expected ratio from the chosen stoichiometry (~0.28).

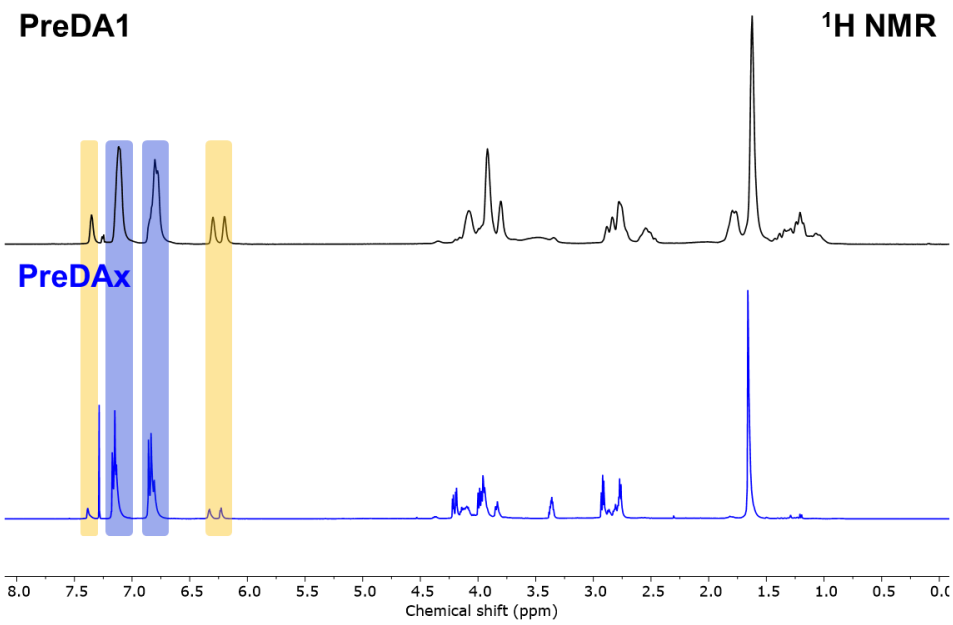

Figure 3.29. The proton NMR of PreDA1 (top) and PreDAx (bottom) in $CDCl_3$.

The FTIR spectrum of PreDAx is shown in Figure 3.30. At 3410 cm^{-1}, the broad (bound) hydroxyl stretch is clearly visible, though no other peaks are visible in this region which might otherwise correspond to residual primary or secondary amine functionality. At slightly below 3000 cm^{-1}, three distinct C–H stretches are also visible, though no other peaks are observed outside of the fingerprint region. One peak within the fingerprint region is highlighted at 915 cm^{-1}, this is not observed in the case of the original prepolymers PreDA1/PreDA0.5 (Chapter 2, Figure 2.17). This almost certainly corresponds to unreacted epoxy functionality, indicating that the chain extension/end-capping reactions were not complete.

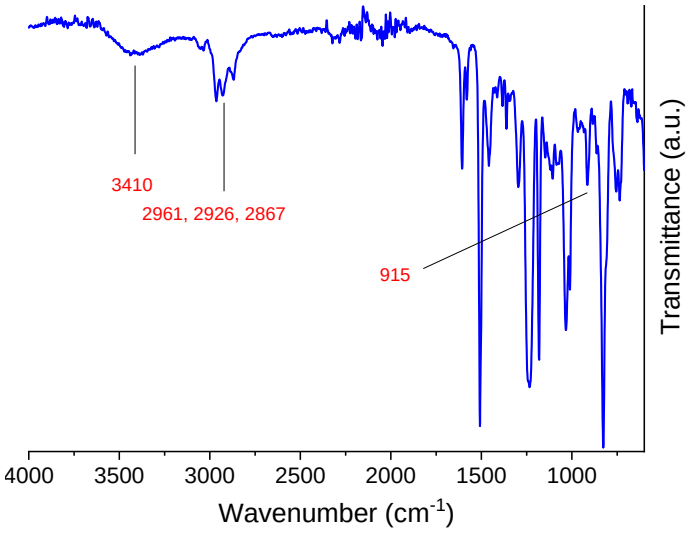

Figure 3.30. The FTIR spectrum of PreDAx, with selected peaks highlighted red.

In addition, no obvious thermal events were evident from the DSC (not shown) of PreDAx, though there may be a minor endotherm visible at approximately 40 °C, which could indicate a melting event. The absence of an exotherm indicates that no further epoxy-amine reaction takes place. Together, the results of the FTIR and NMR suggest that the polymerisation did not reach completion. It seems likely that a significant quantity of furfurylamine evaporated before it could react, suggesting that the scale (~5 g) and apparatus used (5 cm ϕ aluminium pan on a hot plate) are unfortunately not well-suited to this synthesis. An overhead stirrer with a jacketed reaction vessel would be more appropriate, as used in the original DA CAN synthesis in Chapter 2.

3.6.2 Alternative prepolymer end-capping

An alternative method of increasing the oligomer inter-chain connectivity, is to terminate each end of the chain with furan groups. This would serve to increase the network-forming ability of the CAN without increasing the oligomer length, potentially increasing mechanical performance without the trade-off of greatly increasing the melt viscosity. In practice this could be achieved by substituting the dicyclohexylamine (currently used as the capping agent) with bis[(furan-2-yl)methyl]amine (difurfurylamine); however, this is an extremely expensive reagent and is only available on ~1 g scales. There are potentially viable literature syntheses that could be tested to make difurfurylamine,[37–39] but a more straightforward alternative is the use of a thiol: furfuryl mercaptan. The structures of the proposed prepolymers which would be produced from these reagents are shown in Figure 3.31 alongside PreDA1.

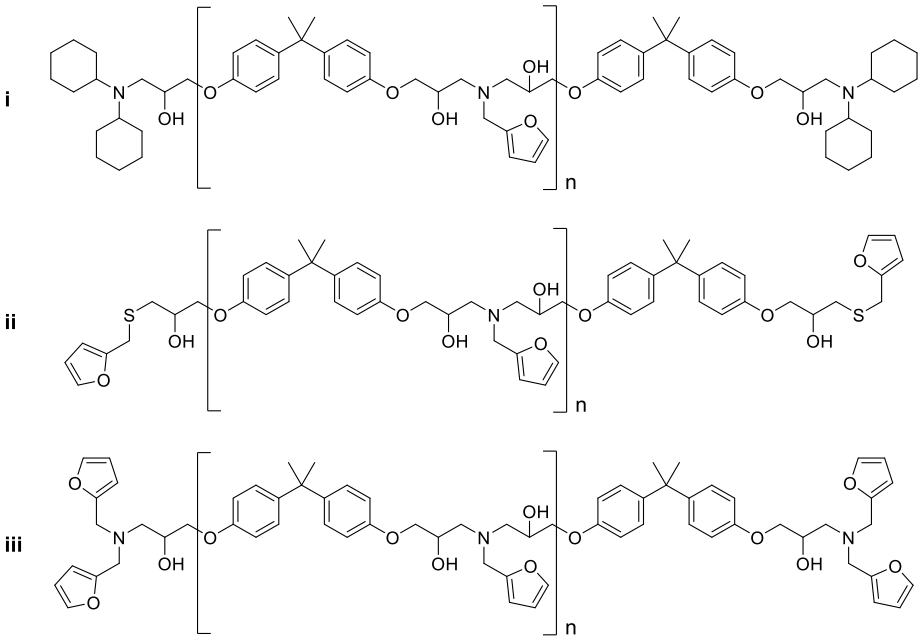

Figure 3.31. (i) PreDA1, (ii) PreDAy produced from furfurylmercaptan and (iii) PreDAz produced from difurfurylamine.

In principle, any monofunctional nucleophile capable of reacting with an epoxide could be used to cap the prepolymer chains. Due to the high reactivity of the strained epoxide ring, a wide variety of species could be used, including amines,[40–43] alcohols,[44–47] carboxylic acids (the reactive species in epoxy-anhydride reactions),[47–49] Grignards,[46,50] organolithiums[46,50] and thiols.[45,51–57] As long as the reaction is robust, any of these functional groups could be used. The reactions of amines and epoxides are rapid and well understood, hence the widespread usage of amines as epoxy crosslinkers. In contrast, the reactions of epoxides with acids/anhydrides, alcohols and thiols are slower and are thus often catalysed (typically with Lewis acids). The organometallic nucleophiles (Grignards, organolithiums) are the most reactive species, but this reactivity leads to an increased chance of undesired side reactions and necessitates the use of air-sensitive techniques, disfavouring their usage in bulk polymer synthesis. Secondary amines are thus the nucleophile of choice for capping the epoxide chains, but thiols are good alternatives.

The other important factor (in addition to reactivity) concerning the choice of end-capping reagent is the boiling point. Given that the prepolymer synthesis is performed at 120 °C, it is important that the capping reagent has limited volatility at this temperature, hence the choice of the original capping reagent dicyclohexylamine (b.p. 256 °C). As a relatively cheap, commercially available compound with a high degree of nucleophilicity and a high boiling point (155 °C), furfuryl mercaptan appears to be a sensible choice of end-capping reagent. It is possible that at 120 °C, the epoxide ring-opening by furfuryl mercaptan might occur at an appreciable rate without the need for a catalyst. However, a range of catalysts have been used in the literature and have been found to improve the efficiency of thiol-epoxide reactions including TBAF,[56] montmorillonite clay (K10),[58] phosphoric acids,[53] HBF_4-SiO_2,[51] Al_2O_3,[55] $Ga(OTf)_3$[59] and $LiClO_4.3H_2O$,[60] among many others. Of the cheap, commercially available Lewis acid catalysts, the catalyst with arguably the highest activity:cost ratio appears to be the $ZnClO_4.6H_2O$ system reported by Chakraborti in 2007,[57] in which the zinc complex was used (2.5 mol%) to effect epoxide thiolysis with a range of thiols and epoxides (RT, 30 min, solvent free). Amines including 1-methylimidazole (1MI) and 1,8-diaminonaphthalene (DAN) have also been demonstrated as effective catalysts for this reaction.[61]

Three methods of preparing PreDAy—by the stoichiometric (one thiol per free epoxide) reaction of furfuryl mercaptan with the uncapped prepolymer—were explored: uncatalysed, 1MI catalysed (0.5 mol%) and DAN catalysed (1 mol%). Due to time restrictions, the catalysts were purely chosen on what was available in the laboratory at the time. In each reaction the prepolymer was prepared (on a scale derived from 5 g of epoxy, ~6.5 g total) via a process analogous to that described in Chapter 2, Section 2.2.1, but using aluminium pans and magnetic stirrers. At the stage where dicyclohexylamine would normally be added, blends of furfuryl mercaptan and the respective catalyst were added instead. The

catalysed systems were reacted for 4 h at 80–100 °C to control the reactivity; higher temperatures led to a rapid increase of viscosity, indicative of crosslinking. Conversely, to promote reactivity, the uncatalysed system was heated at 120 °C for 2 h and then a further 1 h at 150 °C until no thiol smell remained—furfuryl mercaptan is benign but incredibly pungent.

The results of the oligomer-length study, Section 3.6.1, which was performed simultaneously with this enc-cap study, suggests that there is a risk of reactant evaporation, which could dramatically alter the stoichiometry. Indeed, the ^{1}H NMR spectra exhibit the following bisphenyl:furyl ratios. Uncatalysed, 1:0.168; DAN-catalysed 1:0.177; 1MI-catalysed, 1:0.187. Since the precursor (the oligomeric uncapped diepoxide) was prepared in an identical fashion to that used in the preparation of PreDAx, it is unsurprising that these values are also much lower than expected. However, the relative increase in ratio when comparing these PreDAy values with PreDAx is expected, and therefore does indicate successful end-capping from the furfuryl mercaptan. That the uncatalysed experiment shows the smallest amount of furyl groups is also unsurprising, since this was performed at much higher temperature; even if the high temperature overcame the reduced reactivity compared to the catalysed experiments, evaporation of the thiol is likely. No further differences are discernable from the different NMR spectra; furthermore, the FTIR spectra of the three PreDAy samples are indistinguishable from each other. As with PreDAx, each spectrum shows the presence of some residual epoxide with an absorbance at 915 cm^{-1}, though there is no evidence of residual thiol (which is typically observed in the 2550–2600 cm^{-1} region). From these observation we can deduce that each of the PreDAy end-cap reactions were partially successful, though it is hard to determine to what extent due to the incomplete chain extension reaction.

The additional experimental risk with each of these procedures is that the residual hydroxyls on the prepolymer backbone could also react with the remaining epoxides, resulting in permanent crosslinking. Although these hydroxyls are less acidic than the thiol and are substantially hindered due to being 3° alcohols, they are present in greater number. The bases used to catalyse the thiol-epoxy reaction may also be capable of catalysing this undesired side reaction. Even after 3 h, NMR samples of the uncatalysed and 1MI-catalysed (30 mg ml^{-1} $CDCl_3$) were far from completely dissolved, which may be evidence of this side reaction (crosslinking).

Despite the incomplete reaction, preliminary rheology experiments were performed using samples of the DAN-catalysed prepolymer. With the presence of the furan end-caps it would be expected that this polymer would have a decreased viscosity (at high temperature) when compared with the PreDA1 benchmark. The PreDAy sample was subject to a dynamic temperature sweep between 60 and 120 °C

at 1% oscillatory strain (1 Hz)—determined from a linear viscoelastic regime study—and is compared to PreDA1 in Figure 3.32.

Initially, both the viscosity minima (120 °C) and maxima (60 °C) are lower for PreDAy than PreDA1, though the minimum viscosity is in the same region ~10^5 cP. A slight increase in viscosity minima is observed with PreDAy that is not observed with PreDA1, this can be attributed to the latent functionality present in the system. The residual epoxides likely lead to some chain-extension and crosslinking reactions while at high temperature. Though this effect is small, it should not be apparent at all if the polymerisation reactions had proceeded to completion and could probably be avoided by using longer reaction times and lower reaction temperatures. It is also interesting that the maxima of PreDAy are significantly (>10-fold) less than PreDA1. Although the furyl end-caps would be expected to reduce steric congestion and the overall bulk of the oligomer chains (relative to the dicyclohexyl units), this is a big difference. Accordingly, part of this viscosity difference could be a side-effect of the incomplete reaction; it is likely that the average oligomer chain is shorter than in PreDA1, even though the polymer length was designed to be equal. Nevertheless, this reduction in viscosity is desirable for improving polymer processability. A lower viscosity prepolymer would be expected to form more processable CANs.

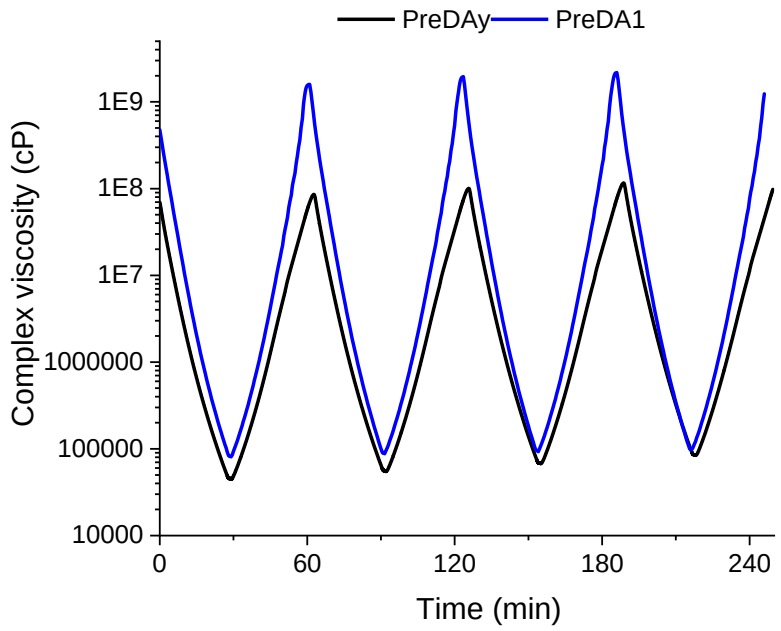

Figure 3.32. The dynamic complex viscosity of PreDAy and PreDA1 between 60 and 120 °C (parallel plate, 1% oscillatory strain, 1 Hz).

3.6.3 Bismaleimide alternatives: citraconimides and itaconimides

As discussed in Chapter 2, Section 2.1, a wide range of dienes and dienophiles can be used in Diels-Alder reactions, though the furan-maleimide reaction is the dominant pairing in materials chemistry.

There are two main mechanisms of undesired reactivity associated with maleimides that can compete with the desired DA reaction: Michael addition and homopolymerisation (HP). Michael additions can be efficiently prevented by ensuring complete consumption (using accurate stoichiometry and generous reaction times) of the amines—which would otherwise attack the maleimide moieties—prior to introducing the maleimide. Since the FTIR spectra of the original DA CANs (and prepolymers) indicate complete conversion of the N–H bonds during the polymerisation reactions, and given that the stoichiometry was carefully controlled, it seems unlikely that amine Michael additions significantly contribute to the degradation of thermoreversibility. It is conceivable that the free hydroxyls on the prepolymer backbone (produced from the epoxide ring-opening reactions) could contribute to a Michael-type reaction that could degrade the BMI. However, because these are all 3° hydroxyls there should be sufficient steric hindrance to minimise the rate of any such reaction.

Instead, it appears BMI HP is the dominant mechanism behind the loss of thermoreversibility (Chapter 2, Section 2.2.1, Figure 2.14). This is evidenced by the exotherms visible in the DSC traces of each of the DA CANs (Chapter 2, Section 2.3.2), with both an onset following the BMI melting point and a subsequent exotherm that correspond well with literature data.[62–64] Due to their utility as high-performance polyimides, BMI homopolymers have been the subject of extensive study for many decades.[63,65–70] Accordingly, numerous researchers have investigated the mechanism of polymerisation and though it is generally accepted to be a complicated, multi-mechanism process, the most widely accepted mechanism is one dominated by radical processes.[63,66] It is thus conceivable that the addition of a radical scavenger such as TEMPO [(2,2,6,6-tetramethylpiperidin-1-yl)oxyl] to the polymer blend might inhibit HP, such that it only becomes significant at higher temperatures. To mitigate the risk of such an additive leaching from the polymer, it might be preferable to cure the additive into the polymer, though there is a risk that doing so would reduce its efficacy as an inhibitor. Such a methodology may be feasible though would not be trivial.

An arguably more straightforward approach to increasing the high temperature stability of these DA CANs is to change the BMI crosslinker/s.

Replacing the maleimides with functional groups which are less susceptible to HP is one method of increasing the stability in DA CANs. Two possible options are itaconimides and citraconimides, which were developed as more- and less-reactive BMI alternatives respectively, Figure 3.33.

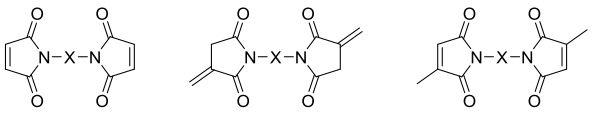

Figure 3.33. Left-to-right, a generic bismaleimide, bisitaconimide and biscitraconimide (X = backbone).

Itaconimides and their regioisomers citraconimides, first appeared in the literature in the 1960s and 1970s after several research groups explored the synthesis of polymers derived from itaconic acid and its derivatives.[68,71,72] Since then, several researchers have investigated bisitaconimides (BIIs) and biscitraconimides (BCIs) as reactive monomers.[65,73–75] Itaconimides have been shown to have both an increased propensity to homopolymerise,[68] and a decreased propensity to participate in Diels-Alder reactions (relative to BMIs),[74] making them a poor choice as a replacement for BMIs in DA CANs. Citraconimides are thermodynamically more stable than their itaconimide isomers, and are consequently often produced as side-products during itaconimide synthesis. Indeed, attempts to isolate pure BIIs in this work were unsuccessful due to isomerisation to the analogous BCIs. Importantly, citraconimides—though the subject of considerably less attention than their isomers—have been shown to (homo)polymerise at significantly higher temperatures than the analogous maleimides.[65] Furthermore, there is evidence that these species can still participate in DA reactions despite the extra steric constraint.[75] Accordingly, biscitraconimides are the primary focus of this study. Some proposed target compounds are shown in Figure 3.34. BCI1 and BCI3 were designed as stiff aromatic crosslinkers to closely mirror the original BMI1/BMI2 whereas BCI2 was designed as a more flexible alternative.

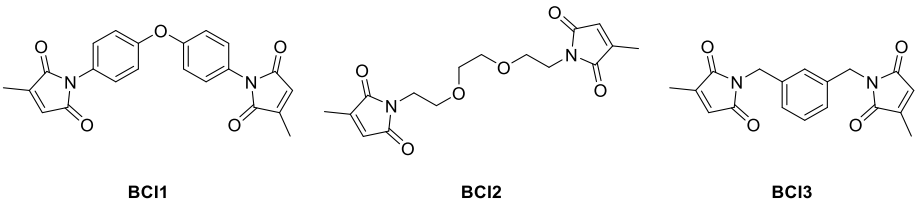

Figure 3.34. Target biscitraconimides, BCI1, BCI2 and BCI3.

BCI1 was initially prepared via an analogous method to BMI3 using 4,4'-oxydianiline and citraconic anhydride, Scheme 3.1.

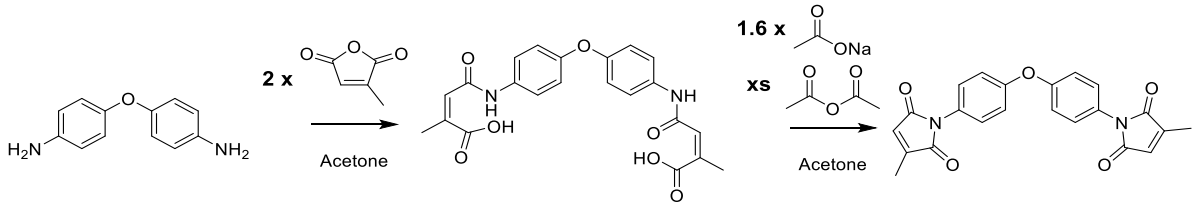

Scheme 3.1. The synthesis of BCI1 via the classical bismaleimide synthesis: amine-anhydride nucleophilic substitution to form a BCA, followed by sodium acetate induced cyclodehydration.

Although the first step of the reaction is relatively robust, several attempts to isolate the cyclodehydrated product were unsuccessful, producing the desired product and several impurities. This led to the exploration of the work of Galanti and Scola in 1981.[72] These authors reported a similar

lack of success in the synthesis of their citraconimides and postulated that the reaction conditions were leading to a partial reverse reaction. This led to their investigation of alternative methodologies and the subsequent discovery of an elegant alternative—simply melting and stirring the isolated biscitraconamic acids (e.g. BCA1–3), solvent-free. BCI1–3 were each prepared via this thermal process, Scheme 3.2 (see experimental for details).

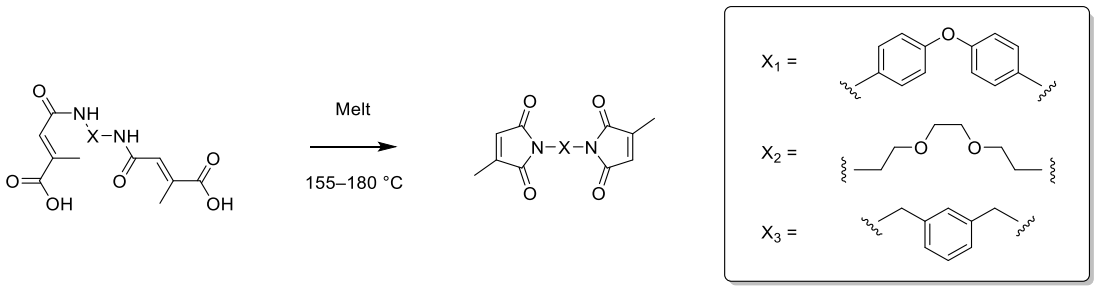

Scheme 3.2. Thermal (melt) cyclodehydration of biscitraconamic acids to biscitraconimides (BCI1–3).

A series of simple experiments were devised to test the reactivity of these citraconimides in Diels-Alder reactions relative to BMI1. As benchmark reactions, BMI1 (100 mg, 0.28 mmol) was dissolved in 10 ml of acetone and stirred with a 10-fold excess (2.8 mmol) of either furan or furylmethanethiol for 24 h at ambient temperature. After the reaction with the unsubstituted furan, the ^{1}H NMR spectrum revealed several minor resonances at 7.05, 6.56, 5.40, 4.02, 3.68 and 3.01 ppm (combined integral of 18%), not representative of either reactant, which are instead indicative of a small quantity of DA-adduct. It is worth noting that DA reactions with unsubstituted furan are precluded by its extreme volatility (b.p. = 31.3 °C). Substituted furans (with higher boiling points) are therefore more appropriate for DA reactions, particularly considering that some heating is often required. Due to its immediate availability, 2-furyl methanethiol was used as an alternative (b.p. = 155 °C), despite the presence of the thiol, which could lead to undesired Michael additions. However, without a catalyst or heating, the chance of a Michael reaction is low. After reaction with BMI1, extensive changes were observed by ^{1}H NMR. Amongst the emergence of a plethora of new resonances, the majority of the alkenyl resonance at 6.8 ppm has disappeared due to reaction. That the ratio of the CH_2 doublet to SH triplet remains 2:1 after reaction is good evidence that the majority of the observed reaction is a DA process (since the S–H resonance would be consumed by a Michael addition). In contrast, no evidence of reaction was observed between furan and BCI1 (in toluene), or 2-furyl methanethiol and BCI3 (in acetone), even with the latter process heated to reflux for 24 h. Subsequent VT ^{13}C{^{1}H} NMR experiments on the BCI1-furan reaction also revealed no reactivity even up to 120 °C. Despite literature reports suggesting that citraconimides are capable of DA reactions, it would appear that the small increase in steric bulk provided by the methyl groups is enough to completely preclude Diels-Alder reactivity in these citraconimides.

The DSC profiles of BCI1–3 confirm that HP is greatly supressed as expected. In Figure 3.35, melting endotherms are evident in both heating cycles of BCI1, but no HP (post-melt exotherm) is observed at all. An unusual feature of this profile is the presence of a large exotherm at 115 °C that is only present in the second heating cycle. Since this exists only in the second heating cycle it is unlikely representative of a reaction. Instead, this is tentatively assigned as a crystallisation process. The small exotherm visible at 100 °C in the heating cycles and 85 °C in the cooling cycle (which is more prominent in this case) is a calorimeter artefact. This is visible in most DSC profiles reported in this chapter (most prominent in Figure 3.41) and Chapter 4.

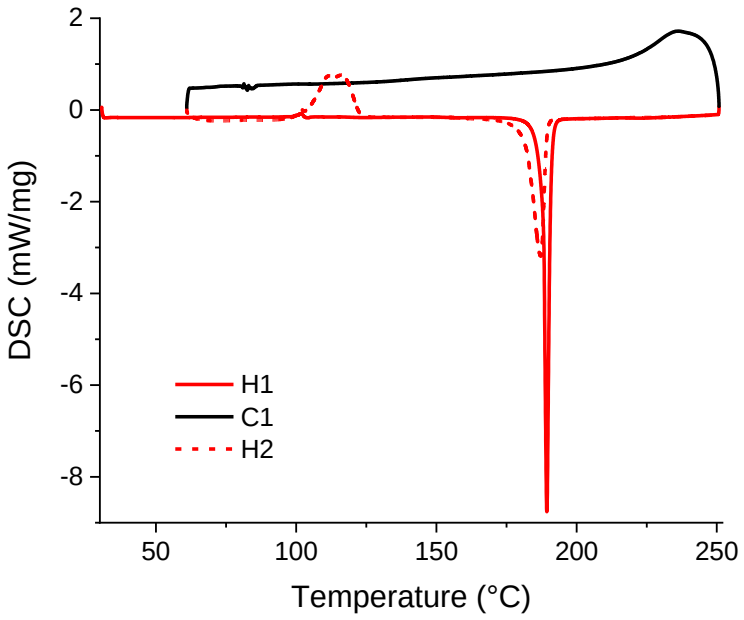

Figure 3.35. A representative heat-cool-heat of BCI1 up to 250 °C (10 °C min^{-1} heating, exothermic up).

The only thermal event discernible from the DSC trace of BCI2 (Figure 3.36) is its melt at 80 °C, which is much lower than either BCI1 or BCI3. In principle, this makes BCI2 a conveniently processible alternative; lower melting points generally make for easier resin blending. The absence of an exotherm means that no HP takes place.

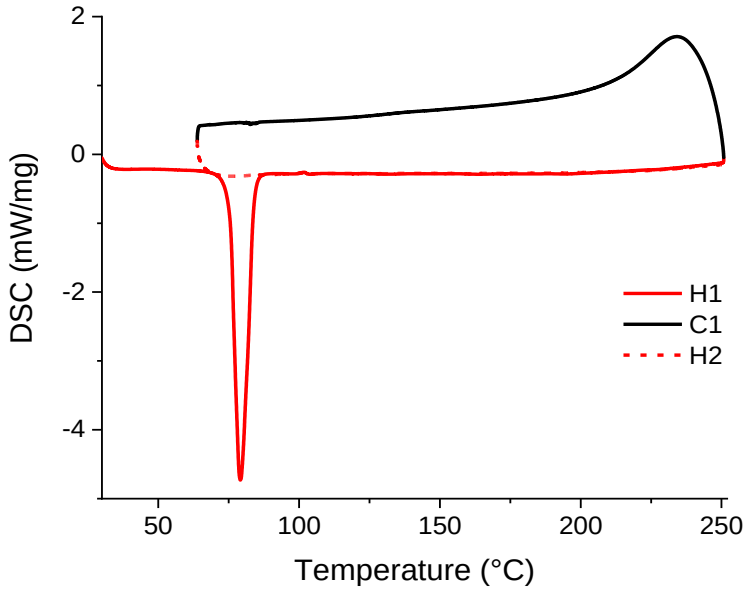

Figure 3.36. A representative heat-cool-heat of BCI2 up to 250 °C (10 °C min^{-1} heating, exothermic up).

In Figure 3.37 the DSC trace of BCI3 is shown. This trace is almost identical to BCI2, with no exothermic events (no HP) and a relatively low melting point, signified by the sharp endotherm at 94 °C.

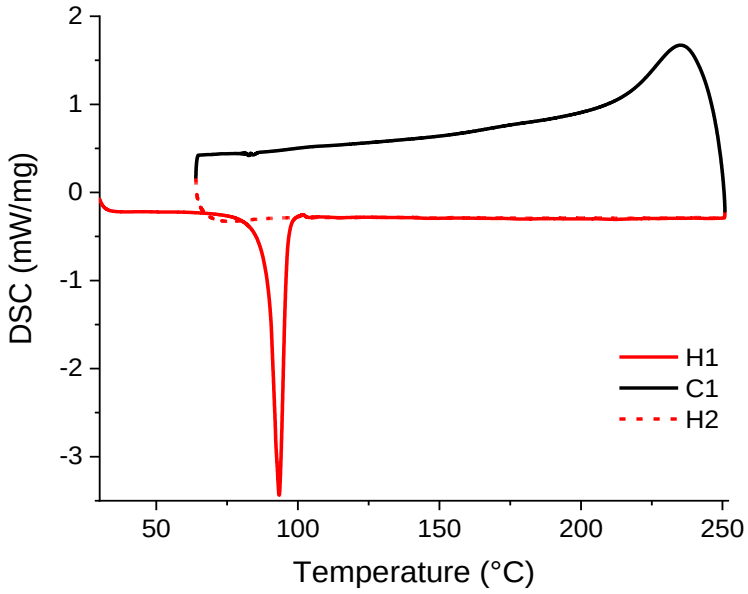

Figure 3.37. A representative heat-cool-heat of BCI3 up to 250 °C (10 °C min^{-1} heating, exothermic up).

In a further attempt to confirm the absence of any DA reactivity, each of the BCIs were also blended with PreDA1 (via melting and stirring by hand for 10 min at 120 °C). The resultant polymers were each subject to FTIR, DSC and rheology experiments. None of these techniques revealed any evidence of significant DA reaction and thus in the interest of brevity this data is not reported here.

3.6.5 High-melting bismaleimides

The BMI backbone can have a significant influence on the rate and onset of HP, mainly due to its influence on the melting point—it is believed that HP occurs only after melting. This is evidenced in Chapter 2 by the slightly higher de-crosslinking (activation) temperature of DA2 relative to DA1 (the only difference is the BMI backbone structure). Since BCIs do not seem like viable candidates as DA crosslinkers, higher melting BMIs might be the best means of increasing the thermal stability of these CANs.

Two examples from the BMI literature that melt (and thus polymerise) at higher temperatures than BMI1 (m.p. ~155 °C) or BMI2 (m.p. ~175 °C) are shown in Figure 3.38, BMI3 (m.p. ~212 °C) reported by Takeda *et al*. in 1988,[76] and BMI4 (m.p. ~222 °C) reported by Barton *et al*. in 1991.[65] With melting points and thus HP onsets significantly above 200 °C, both of these monomers are ideal candidates as alternative DA crosslinkers. Due to time constraints and its comparative simplicity, BMI3 was chosen for this study.

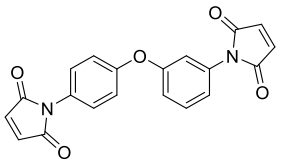

BMI3

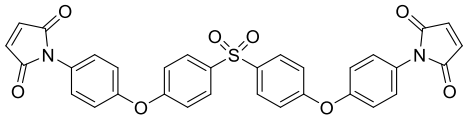

BMI4

Figure 3.38. BMI monomers BMI3, 3,4'-bismaleimidodiphenyl ether and BMI4, Bis-4-(4-maleimidophenoxy)phenylsulfone.

BMI3 was prepared via the original method tested for BCI synthesis, sodium acetate–induced cyclodehydration, Scheme 3.3.

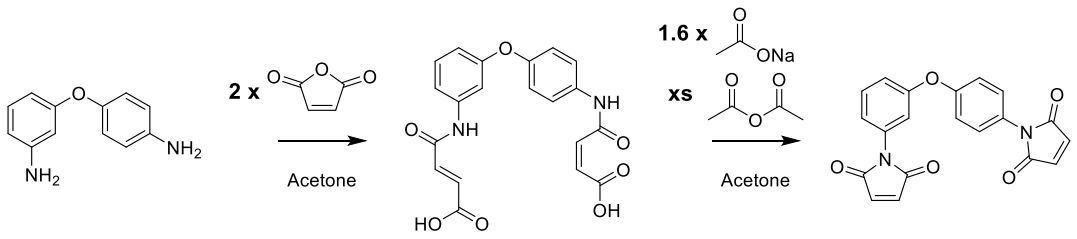

BMA3 BMI3

Scheme 3.3. The reaction of 3,4-oxydianiline to form a bismaleamic acid (BMA3), and subsequent cyclodehydration to form the bismaleimide, BMI3.

A representative DSC trace of BMI3 (10 °C min^{-1}) is compared with BMI1 in Figure 3.39, from this we can deduce the melting point at 208 °C and the onset of HP immediately thereafter. This is an increase of approximately 50 °C compared to BMI1, in close agreement with the literature, indicating BMI3 may be used to create DA CANs with a higher thermal stability than those reported in Chapter 2 and Chapter 3 thus far.

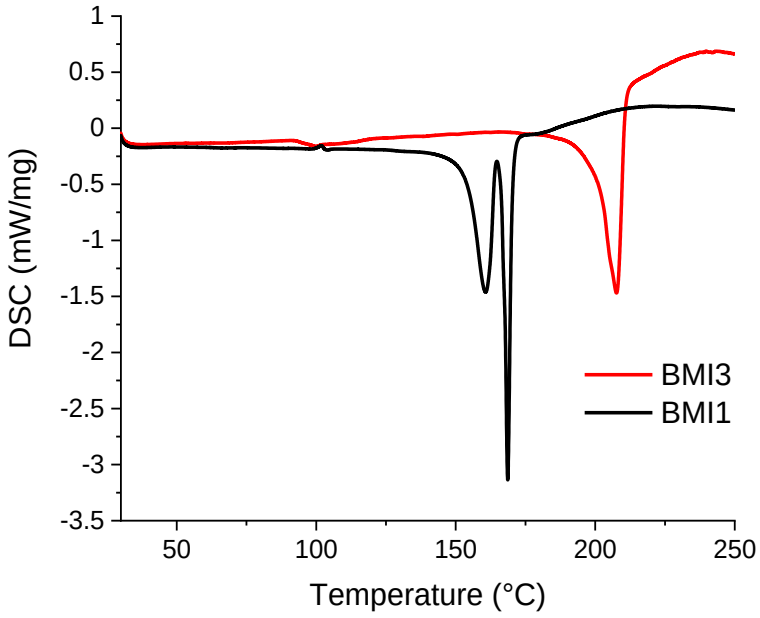

Figure 3.39. The DSC traces of BMI3 and BMI1 between 30–300 and 30–250 °C respectively (10 °C min^{-1}, exothermic up).

A new DA CAN (with stoichiometry consistent with DA1) was prepared by melting and blending together PreDA1 (2.00 g) with BMI3 (0.46 g) between 100 and 120 °C for approximately 10 min. The resultant polymer DA3 was characterised and tested as follows.

A section of the infrared spectrum of DA3 is shown in Figure 3.40 and compared with the precursor, BMI3. The selected wavenumber range shows the carbonyl region and the alkenyl region. As can be seen, the major carbonyl stretches at 1715/1705 cm^{-1} are slightly shifted from those in the neat BMI at 1713/1702 cm^{-1}. This shift, although subtle, is evidence of reaction, suggesting an appreciable degree of crosslinking (comparable to the original DA CANs). The maleimido C=C stretch is no longer visible in the product CAN, though any residual functionality may be obscured by the stronger absorption of residual furan units.

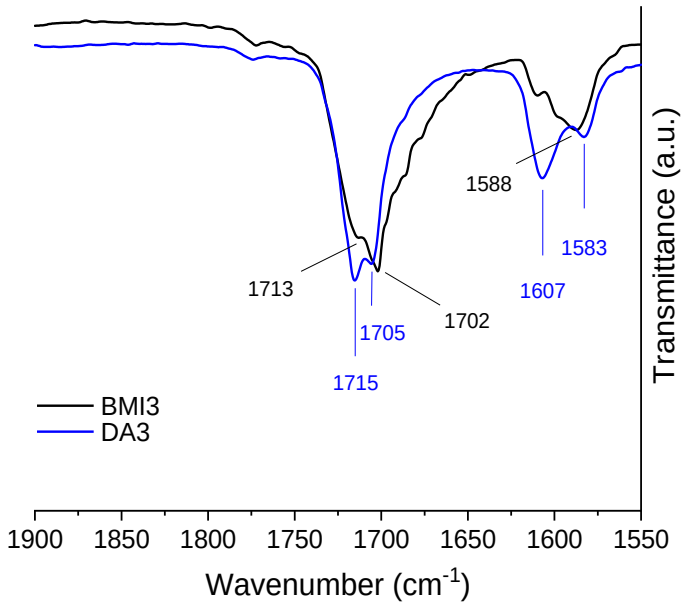

Figure 3.40. The solid-state FTIR spectra of DA3 and BMI3 between 1550 and 1900 cm^{-1}.

A representative heat-cool-heat DSC trace of DA3 is shown in Figure 3.41. In the first heating cycle a small endothermic event is observed at 62 °C, which likely corresponds to the melting a of a prepolymer-rich phase. Thereafter, at approximately 63 °C, a T_g is observed which is more apparent in the second heat cycle. Interestingly, there is no evidence of an endothermic event corresponding to an rDA process as is observed in the original DA CANs, this may be due to a relatively low crosslink density. Alternatively, it is also conceivable that the expected endotherm is too broad to be observable; the inequivalent maleimido groups of BMI3 would be expected to have subtly different reactivity. Moreover, it seems unlikely that BMI3 is incapable of the rDA reaction. At higher temperatures there are two broad exothermic events with peaks at ~200 and ~240 °C. At least one of these corresponds to the BMI3 HP reaction, from comparison with neat BMI3 it seems more likely that this is the higher temperature exotherm. It is possible that the inequivalent maleimides react at different temperatures, hence the two exotherms.

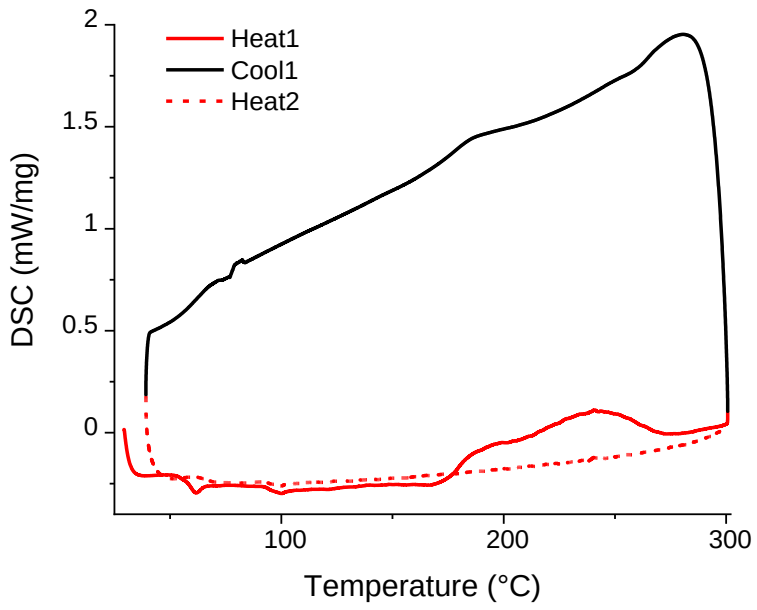

Figure 3.41. A representative heat-cool-heat DSC of DA3.

Dynamic rheology should be able to demonstrate whether DA3 exhibits CAN-type de-crosslinking as observed with the original DA CANs. Low temperature plateaus and subsequent sharp falls in viscosity are good evidence of this as shown in Chapter 2, Section 2.3.1. DA3 was treated in an analogous fashion to those experiments, and the results are shown in Figure 3.42. It is immediately apparent from the profile of the viscosity curve that DA3 exhibits dissociative CAN-type behaviour, with plateaus of viscosity at low temperature where the polymer exists as a solid, and subsequent sharp drops in viscosity as the polymer de-crosslinks. These plateaus are not observed in the prepolymers or conventional plastics. The shape of the curve is particularly similar to DA0.5 (Chapter 2, Figure 2.23), with relatively narrow plateaus of solid behaviour. This may represent a similarly low level of crosslinking, which is further evidenced by the low initial viscosity minimum of 4E+5 cP, even lower than DA0.5 (7E+5 cP). This limited degree of crosslinking explains the absence of an obvious rDA endotherm in the DA3 DSC trace; this is likely a product of insufficient reaction time during the initial blending of BMI3 and PreDA1. Interestingly, as with each of the original DA CANs, DA3 also demonstrates a steady increase in viscosity minimum. Since the maximum experimental temperature in this study is well below the onset of the exotherms shown in Figure 3.39, it is likely that this behaviour can be explained by a homogenisation or tempering-type effect. As the polymer is treated through progressive cycles, it has greater opportunity (through exposure to elevated temperature) to homogenise and reorganise into a more consistently crosslinked material.

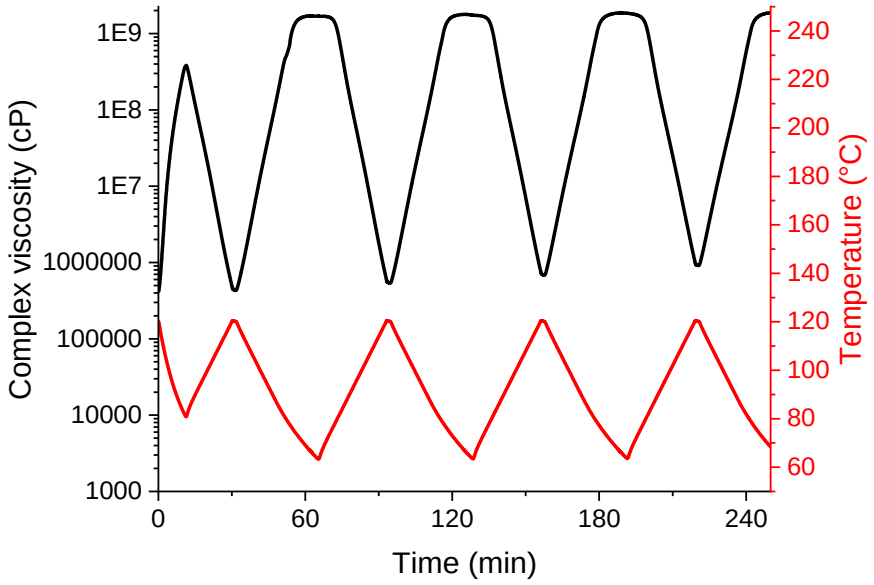

Figure 3.42. A viscosity-time-temperature plot of DA3 between 64 and 120 °C (parallel plate, 1% oscillatory strain, 1 Hz).

Further work is required, but these preliminary results indicate that BMI3 has potential as a more stable alternative to BMI1/2 in future DA CANs.

3.7 Summary

In this chapter, the three DA CANs developed in Chapter 2 were tested for their applications in composites. The primary utility of CANs in composites is as functional matrices. This led to the exploration of various composite manufacturing processes and the successful development of a vacuum-assisted compression moulding (VACM) process based on the one developed for use with the neat CAN resins. It was noted that the presence of fibres made moulding considerably easier and facilitated multiple re-moulding attempts—this could greatly reduce material waste compared to conventional composite manufacture. However, it was found that several composite manufacture techniques are not currently practical with these resin systems, notably the 'enduring prepreg' concept. This is due to resin brittleness, which is increasingly prevalent with thin samples, hence the difficulty in preparing individually infused prepreg plies.

Two crossply (0/90°) laminates, 8plyDA1 and 12plyDA0.5 were prepared from their respective polymers and woven E-glass fabric (plain weave) via VACM. 8plyDA1 was designed to have a good balance of mechanical performance and healing efficiency, whereas the choice of DA0.5 (and its reduced crosslink density) in 12plyDA0.5 was designed principally for ease of recycling. Due to the matrix brittleness identified previously, 3-point-bending was chosen as a suitable mechanical test for characterisation. With strengths, moduli and failure strains of 474 ± 43 MPa, 11.6 ± 1.1 GPa and 5.40 ± 0.34% for 8plyDA1, and 443 ± 36 MPa, 18.5 ± 1.6 GPa and 2.25 ± 0.23% for 12plyDA0.5, both GFRP

composites are robust, exhibiting good mechanical performance considering their additional functionality and fibre volume fraction. The V_f of 8plyDA1 was determined via optical microscopy as ~40%, which is reasonable, though could be improved with higher moulding pressures.

Repairability of the CAN laminates was tested in two studies, with healing performed after 3pb testing 8plyDA1 to failure, and once more with 8plyDA1 while attempting to damage only the matrix and fibre-matrix interface (i.e. without fibre damage)—which proved challenging with 3pb. The 8plyDA1 tested once to failure gave a (ultimate strength) healing efficiency of 28 ± 5%. After testing a second time to failure, the specimens could again be repaired but were then associated with a more modest healing efficiency of 12 ± 4%. This marked reduction in strength is associated with more extensive fibre damage after each series of 3pb. Although these are objectively modest values, these are excellent recoveries considering that the fibres contribute to the majority of composite strength (and cannot be repaired).

The second set of 8plyDA1 specimens were not tested to failure and were instead tested until a pre-determined drop in maximum-load was detected by the testing machine. This methodology was, unsurprisingly, associated with significant inconsistency, which was reflected in both the raw data and calculated metrics. Nonetheless, flexural modulus was consistently improved in the repaired samples relative to the pristine samples, indicating good recovery. This rather surprising behaviour was attributed to localised changes in fibre volume fraction. Unfortunately, the sensitivity of the optical microscopy method of V_f determination used herein was not sufficient to either support or discredit this hypothesis. A yield strength–based healing efficiency could not be determined for this study because the damaged specimens did not consistently exhibit a reduced yield strength, instead, both the damaged specimens and repaired specimens often exhibited increased strength relative to the original (pristine) values. This highlights the challenges associated with using 3pb to determine composite healing efficiency. As reported in our progress paper in 2018,[77] compression after impact would likely prove to be a better, though more practically challenging and labour intensive, experiment.

A section of 8plyDA1 was recycled using a room temperature, solvent-assisted, recycling process with DCM and compared with the pristine composite. The recycled composite, 8plyDA1R, was tested in 3pb which allowed assessment of ‘recycling efficiency’, which in terms of strength was 69%. This is an excellent result, highlighting that DA CAN composites can be recycled at room temperature without greatly compromising mechanical performance. Nevertheless, there is an appreciable degradation in strength which has not been conclusively explained. This could be due to removal of fibre sizing and associated damage to the glass fibre surfaces. Moreover, it is evidently debatable whether solvent-

assisted recycling methods such as these, are superior or inferior to mechanical processes that maintain the fibre-matrix interface but lose value in terms of fibre length and alignment: more extensive recycling analysis is required.

Critically, these experiments confirmed the potential of CAN matrices to extend the lifecycle of FRP composites in a three-pronged approach: (1) reprocessability at manufacture; reducing the amount of waste material, (2) self-healing; extending the operational lifetime and (3) recycling at end-of-life; allowing the composite to be repurposed. Crucially, the activation or de-crosslinking temperature of these DA CANs (at 120 °C, to enable the aforementioned processes) is much lower than is possible with thermoplastics. In this respect the DA CANs outperform thermoplastics (and thermosets, which cannot be healed or recycled). However, the pre-reacted, solid form of these CANs means that they do not have the usual low-viscosity, fibre-impregnation advantage that thermosets usually have over thermoplastics. Though it is important to note that this is *not typical* of CANs more generally, which are usually polymerised *in situ* like conventional thermosets.

In addition, a preliminary experiment investigating the potential of DA CANs as reversible adhesives via single-lap-shear tests has confirmed their utility in this area. Shear strength is reduced at least five-fold with a brief de-crosslinking treatment at ~120 °C.

Finally, the mechanical performance of the current generation of DA CANs is not adequate to compete with either thermosets or thermoplastics. For this reason, preliminary experiments concerning the development of a second generation of DA CANs were conducted. These included modifications to the prepolymer, which were designed to improve the mechanical performance of the CANs via a slight elongation of the prepolymer backbone, and modifications to the crosslinker (BMI) designed to improve the thermal stability (the working lifetime at elevated temperature). The citraconimides BCI1–3 were cleanly synthesised via a melt cyclodehydration method and fully characterised. As expected, they were found to be highly resistant to HP. However, their lack of reactivity in DA reactions precludes their use in DA CANs. BMI3 was also cleanly synthesised using a similar method and was also found to be less susceptible to HP than BMI1 and BMI2. Initial experiments blending BMI3 into DA CANs suggests this material successfully undergoes DA reactions and might be useful in creating high-stability DA CANs, though further work is required.

Due to pandemic restrictions associated with COVID-19, most of the experiments proposed for 12plyDA0.5 were not performed (i.e. healing, recycling and microscopy).

3.8 Experimental (synthesis)

General synthetic protocols and techniques are discussed in the experimental sections of Chapter 4 and Chapter 5.

PreDAx

5.00 g of Epon 828 (DGEBA, *ca*. 13.2 mmol) was heated in an aluminium pan to 100 °C, to which 1.04 ml furfurylamine (1.14 g, 11.7 mmol) was added dropwise and stirred by hand into a homogeneous mixture for 30 min. The reaction was heated to 120 °C and a magnetic stirrer added. The melt was left stirring for a further 1.5 h, changing from gold to bronze prior to the dropwise addition of 0.12 ml dicyclohexylamine (96 mg, 2.93 mmol). The reaction was left stirring for a further 1.5 h at 120 °C and then stopped with the removal of the stirrer and subsequent cooling to room temperature. The highly transparent bronze polymer was separated from the aluminium pan and milled into powder prior to further analysis.

BCA1 [4,4'-(biscitraconamic acid)diphenyl ether]

4,4'-dioxydianiline (4.00 g, 20 mmol) was added to a 2-neck round bottom flask equipped with a reflux condenser and dissolved in acetone (30 ml). The mixture was stirred and warmed to 50 °C, then after complete dissolution (15 min), a solution of citraconic anhydride (4.93 g, 3.96 ml, 44 mmol) in acetone (10 ml) was slowly added and the combined yellow solution set to reflux. The reaction was left to stir vigorously at reflux for 4.5 h. After this time, the mixture was allowed to cool to room temperature and the precipitate isolated via Hirsch filtration (with 5 x 5 ml cold acetone washes). The crude product, was air-dried overnight and then heated (60 °C) under vacuum for 2 h affording **BCA1** as an off-white powder (7.68, 90% yield). ^{1}H NMR (DMSO-D6, 400 MHz) (δ, ppm): 12.90 (bs, 2H, COO*H*), 10.20 (s, 2H, N*H*), 7.61 (m, 4H, Ar*H*), 6.96 (m, 4h, Ar*H*), 6.09 (q, 2H, J_{HH} = 1.63 Hz, C=C*H*), 1.99 (d, 6H, J_{HH} = 1.59 Hz, CH_3). FTIR ν(CO)/cm^{-1}: 1720, 1702. HR-MS (Nanospray-): *m/z* calculated for $C_{22}H_{20}N_2O_7$ [M-H]$^-$ = 423.1192, obs. = 423.1175.

BCA2 [bis(citraconamic acid)ethylamino ethylene glycol]

BCA2 was prepared using the same procedure, which yielded an off-white powder (41% yield). ^{1}H NMR (DMSO-D6, 400 MHz) (δ, ppm): 14.04 (bs, 2H, COO*H*), 8.61 (t, 2H, J_{HH} = 5.62 Hz, N*H*), 6.11 (m, 2H, C=C*H*), 3.52 (s, 4H, OCH_2CH_2O), 3.45 (t, 4H, J_{HH} = 5.71 Hz, CH_2OCH$_2$), 3.28 (t, 4H, J_{HH} = 5.71 Hz, CH_2N), 1.93 (d, 6H, J_{HH} = 1.55 Hz, CH_3). FTIR ν(CO)/cm^{-1}: 1700. HR-MS (Nanospray-): *m/z* calculated for $C_{16}H_{24}N_2O_8$ [M-H]$^-$ = 371.1454, obs. = 371.1452.

BCA3 [bis-m-xylyl citraconamic acid]

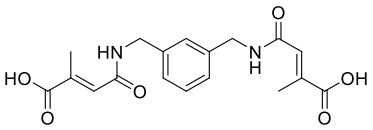

BCA3 was prepared using the same procedure, which yielded a pale-yellow solid (80% yield). ^{1}H NMR (DMSO-D6, 400 MHz) (δ, ppm): 13.77 (bs, 2H, COO*H*), 8.88 (t, 2H, J_{HH} = 5.96, N*H*), 7.25 (m, 1H, Ar*H*), 7.13 (s, 2H, Ar*H*), 7.12 (s, 1H, Ar*H*), 6.06 (m, 2H, C=C*H*), 4.28 (d, 4H, J_{HH} = 5.94 Hz, ArCH_2), 1.90 (d, 6H, J_{HH} = 1.58 Hz). FTIR ν(CO)/cm^{-1}: 1702. HR-MS (Nanospray-): *m/z* calculated for $C_{18}H_{20}N_2O_6$ $[M-H]^-$ = 359.1243, obs. = 359.1231.

BCI1 [4,4'-(biscitraconimido)diphenyl ether]

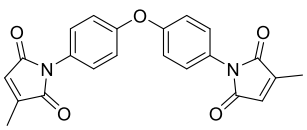

BCA1 (3.129 g, 7.37 mmol) was added to a round-bottom flask and heated to 180 °C. The melt was allowed to stir for 5 min prior to cooling to ambient temperature affording an orange-brown crude product (2.794 g, 97% yield). Traces of itaconimide and polymer were removed via liquid chromatography (60:40 EtOAc/hexane) to afford pure **BCI1** (864 mg, 30% yield). ^{1}H NMR ($CDCl_3$, 400 MHz) (δ, ppm): 7.31 (m, 4H, Ar*H*), 7.11 (m, 4H, Ar*H*), 6.48 (q, 2H, J_{HH} = 1.82 Hz), 2.18 (t, 6H, J_{HH} = 1.83 Hz, CH_3). ^{13}C{^{1}H} NMR ($CDCl_3$, 100.63) (δ, ppm): 170.8 (s, *C*=O) 169.8 (s, *C*=O), 156.3 (s, Ar*C*), 146.0 (s, Ar*C*), 127.7 (s, Ar*C*), 127.6 (*C*=C), 127.1 (s, *C*=C), 119.6 (s, Ar*C*), 11.3 (s, *C*H$_3$). FTIR ν(CO)/cm^{-1}: 1703. MS (APCI): *m/z* calculated for $C_{22}H_{16}N_2O_5$ $[M+H]^+$ = 389.1, obs. = 389.1.

BCI2 [bis(citraconimido)ethylamino ethylene glycol]

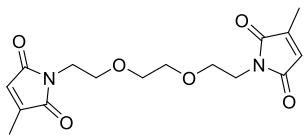

BCI2 was prepared in analogous fashion (at 160 °C) as a brown oil, purified by liquid chromatography (60:40 EtOAc/hexane) into a pale-yellow oil (40% yield). ^{1}H NMR ($CDCl_3$, 400 MHz) (δ, ppm): 6.32 (q, 2H, J_{HH} = 1.82 Hz, C=C*H*), 3.67 (m, 4H, NCH_2), 3.59 (m, 4H, NCH_2CH_2O), 3.55 (s, 4H, OCH_2CH_2O), 2.07 (d, 6H, J_{HH} = 1.88 Hz, CH_3). ^{13}C{^{1}H} NMR ($CDCl_3$, 100.63) (δ, ppm): 171.9 (s, C=O), 170.9 (s, C=O), 127.5 (s, *C*H=C), 70.1 (s, OCH_2CH_2O), 68.1 (s, NCH_2CH_2O), 37.3 (s, *C*H_2N), 11.1 (s, *C*H$_3$). FTIR ν(CO)/cm^{-1}: 1698. HR-MS (ESI): *m/z* calculated for $C_{16}H_{20}N_2O_6$ $[M+Na]^+$ = 359.1214, obs. = 359.1238.

BCI3 [bis-m-xylyl citraconimide]

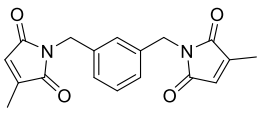

BCI3 was prepared in analogous fashion (at 156 °C) as a pale-yellow solid in 33% yield after chromatography (60:40 EtOAc/hexane). ^{1}H NMR ($CDCl_3$, 400 MHz) (δ, ppm): 7.29 (s, 1H, Ar*H*), 7.22 (m, 3H, Ar*H*), 6.33 (q, 2H, J_{HH} = 1.85 Hz, C*H*=C), 4.62 (s, 4H, ArCH_2), 2.08 (d, 6H, J_{HH} = 1.8 Hz, CH_3). ^{13}C{^{1}H} NMR ($CDCl_3$, 100.63) (δ, ppm): 171.5 (s, *C*=O), 170.5 (s, *C*=O), 145.9 (s, *C*=C), 136.9 (s, C=C), 129.1 (s, Ar*C*), 128.2 (s, Ar*C*), 127.7 (s, Ar*C*), 127.5

(s, Ar*C*), 41.4 (s, *C*H_2), 11.1 (s, C*H*$_3$). FTIR ν(CO)/cm^{-1}: 1699. HR-MS (ESI): *m/z* calculated for $C_{18}H_{16}N_2O_4$ $[M+Na]^+$ = 347.1002, obs. = 347.1014.

BMI3 [1-(3-(4-(2,5-dioxo-2,5-dihydro-1H-pyrrol-1-yl)phenoxy)phenyl)-1H-pyrrole-2,5-dione]

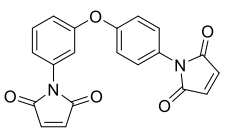

3,4-oxydianiline (4.00 g, 19.98 mmol) was added to a 2-neck round-bottom flask equipped with a reflux condenser and then dissolved in acetone (40 ml). This mixture was then warmed to 40 °C to encourage dissolution. After complete dissolution the deep brown solution was allowed to cool to RT. Maleic anhydride (3.96 g, 2.67 ml, 40.35 mmol) was added to a separate round bottom flask and dissolved in acetone (40 ml). The resultant colourless solution was added to the diamine solution in a slow stream and the combined solution heated to reflux under vigorous stirring for 3.5 h. The product mixture was then allowed to cool to ambient temperature prior to the removal of solvent under reduced pressure. The crude maleamic acid (BMA3) was dried further by heating to 60 °C under reduced pressure for 3 h prior to the following cyclodehydration reaction. The crude BMA3 (6.2 g, 15.6 mmol) was added against a flow of nitrogen to a 2-neck Schlenk flask equipped with reflux condenser. To the Schlenk flask, dry degassed acetone (50 ml, N_2-sparged and freshly distilled from B_2O_3) was added and the solution heated and stirred. After complete dissolution, anhydrous sodium acetate (2.02 g, 24.6 mmol) and acetic anhydride (10 g, 9.3 ml, 98 mmol) were added and washed into solution with a further 5 ml of acetone. The resultant dark brown solution was heated to reflux and stirred vigorously for 15.5 h. The reaction mixture was then poured into ice-cold DI water (60 ml) and the resultant precipitate purified via Büchner filtration. The isolated solid was washed with DI water (20 x 5 ml), 50:50 DI water/MeOH (3 x 10 ml) and finally pure MeOH (3 x 10 ml). The resultant product was dried at 65 °C for 3 h under reduced pressure, affording **BMI3** as a pale brown solid (5.128 g, 91% yield [71% overall]). ^{1}H NMR ($CDCl_3$, 400 MHz) (δ, ppm): 7.44 (td, 1H, J_{HH} = 8.06 Hz, J_{HH} = 0.63 Hz, Ar-*H*), 7.31 (m, 2H, Ar-*H*), 7.13 (m, 3H, Ar-*H*), 7.05 9m, 2H, Ar-*H*), 6.853 (s, 2H, C*H*=C*H*), 6.847 (s, 2H, C*H*=C*H*). ^{13}C{^{1}H} NMR ($CDCl_3$, 100.63 MHz) (δ, ppm): 169.6 (s, *C*=O), 169.3 (s, *C*=O), 157.3 (s, Ar-*C*), 156.3 (s, Ar-*C*), 134.4 (s, (O=C)*C*H), 134.3 (s, (O=C)*C*H), 132.6 (s, Ar-*C*), 130.3 (s, Ar-*C*), 127.8 (s, Ar-*C*), 126.6 (s, Ar-*C*), 121.2 (s, Ar-*C*), 119.6 (s, Ar-*C*), 118.5 (s, Ar-*C*), 117.0 (s, Ar-*C*). FTIR ν(CO)/cm^{-1}: 1713, 1702. HR-MS (APCI): *m/z* calculated for $C_{20}H_{12}N_2O_5$ $[M+Na]^+$ = 383.0638, obs. = 383.0632.

3.9 References

1 P. Spasojevic, in *Unsaturated Polyester Resins*, eds. S. Thomas, M. Hosur and C. J. Chirayil, Elsevier Inc., 2019, pp. 367–406.

2 A. Ruiz de Luzuriaga, R. Martin, N. Markaide, A. Rekondo, G. Cabañero, J. Rodríguez and I. Odriozola, *Mater. Horizons*, 2016, **3**, 241–247.

3 F. J. Guild and J. Summerscales, *Composites*, 1993, **24**, 383–393.

4 N. C. Davidson, A. R. Clarke and G. Archenhold, *J. Microsc.*, 1997, **185**, 233–242.

5 A. Todoroki, M. Tanaka and Y. Shimamura, *Compos. Sci. Technol.*, 2002, **62**, 619–628.

6 X. Li, Y. Yan, L. Guo and C. Xu, *Polym. Test.*, 2016, **52**, 254–264.

7 G. Fortunato, L. Anghileri, G. Griffini and S. Turri, *Polymers (Basel).*, 2019, **11**, 1007.

8 M. Fan, J. Liu, X. Li, J. Zhang and J. Cheng, *Ind. Eng. Chem. Res.*, 2014, **53**, 16156–16163.

9 P. Cousin, M. Hassan, P. V. Vijay, M. Robert and B. Benmokrane, *J. Compos. Mater.*, 2019, **53**, 3651–3670.

10 E. A. S. Marques, R. D. S. G. Campilho, M. Flaviani and L. F. M. Da Silva, in *Strength Prediction of Adhesively-Bonded Joints*, CRC Press, 2017.

11 D. Quan, J. L. Urdániz, C. Rouge and A. Ivanković, *Compos. Struct.*, 2018, **198**, 11–18.

12 G. Scarselli, C. Corcione, F. Nicassio and A. Maffezzoli, *Int. J. Adhes. Adhes.*, 2017, **75**, 174–180.

13 Y. Zhao, Y. Wu, L. Wang, M. Zhang, X. Chen, M. Liu, J. Fan, J. Liu, F. Zhou and Z. Wang, *Nat. Commun.*, 2017, **8**, 1–8.

14 W. Liu, C. Zhang and Y. Bai, *J. Adhes. Sci. Technol.*, 2020, **35**, 1–22.

15 C. Heinzmann, C. Weder and L. M. De Espinosa, *Chem. Soc. Rev.*, 2016, **45**, 342–358.

16 R. Ciardiello, G. Belingardi, F. Litterio and V. Brunella, *Compos. Struct.*, 2020, **244**, 112314.

17 L. M. Sridhar, M. O. Oster, D. E. Herr, J. B. D. Gregg, J. A. Wilson and A. T. Slark, *Green Chem.*, 2020, **22**, 8669–8679.

18 D. H. Turkenburg, H. van Bracht, B. Funke, M. Schmider, D. Janke and H. R. Fischer, *J. Appl. Polym. Sci.*, 2017, **134**, 1–11.

19 I. F. Villegas and R. van Moorleghem, *Compos. Part A Appl. Sci. Manuf.*, 2018, **109**, 75–83.

20 D. Stavrov and H. E. N. Bersee, *Compos. Part A Appl. Sci. Manuf.*, 2005, **36**, 39–54.

21 T. J. Ahmed, D. Stavrov, H. E. N. Bersee and A. Beukers, *Compos. Part A Appl. Sci. Manuf.*, 2006, **37**, 1638–1651.

22 A. Yousefpour, M. Hojjati and J. P. Immarigeon, *J. Thermoplast. Compos. Mater.*, 2004, **17**, 303–341.

23 M. P. K. Turunen, P. Marjamäki, M. Paajanen, J. Lahtinen and J. K. Kivilahti, *Microelectron. Reliab.*, 2004, **44**, 993–1007.

24 A. Dmitruk, P. Mayer and J. Pach, *J. Adhes. Sci. Technol.*, 2018, **32**, 997–1006.

25 G. Viana, M. Costa, M. D. Banea and L. F. M. Da Silva, *Proc. Inst. Mech. Eng. Part L J. Mater. Des. Appl.*, 2017, **231**, 488–501.

26 S. Liu, X. Cheng, Q. Zhang, J. Zhang, J. Bao and X. Guo, *Compos. Part B Eng.*, 2016, **91**, 431–440.

27 O. Chailee, T. Parnklang, P. Mora, T. Pothisiri, C. Jubsilp and S. Rimdusit, *J. Appl. Polym. Sci.*, 2020, **137**, 49371.

28 J. Wang, X. Zhang, L. Jiang and J. Qiao, *Prog. Polym. Sci.*, 2019, **98**, 101160.

29 A. Klingler, A. Bajpai and B. Wetzel, *Eng. Fract. Mech.*, 2018, **203**, 81–101.

30 A. Bahrami, F. Cordenier, P. Van Velthem, W. Ballout, T. Pardoen, B. Nysten and C. Bailly, *Compos. Part A Appl. Sci. Manuf.*, 2016, **91**, 398–405.

31 T. K. L. Nguyen, S. Livi, B. G. Soares, H. Benes, J. F. Gérard and J. Duchet-Rumeau, *ACS Sustain. Chem. Eng.*, 2017, **5**, 1153–1164.

32 A. Inamdar, J. Cherukattu, A. Anand and B. Kandasubramanian, *Ind. Eng. Chem. Res.*, 2018, **57**, 4479–4504.

33 A. P. Mouritz, *Compos. Part A Appl. Sci. Manuf.*, 2007, **38**, 2383–2397.

34 B. Zhang, G. Allegri and S. R. Hallett, *Mater. Des.*, 2016, **108**, 679–688.

35 G. Pappas, S. Joncas, V. Michaud and J. Botsis, *Compos. Struct.*, 2018, **184**, 924–934.

36 J. S. Jayan, A. Saritha and K. Joseph, *Polym. Compos.*, 2018, **39**, E1959–E1986.

37 P. T. K. Arachchige, H. Lee and C. S. Yi, *J. Org. Chem.*, 2018, **83**, 4932–4947.

38 M. Zolghadr, M. J. Zohuriaan-Mehr, A. Shakeri and A. Salimi, *Thermochim. Acta*, 2019, **673**,

147–157.

39 A. Blanpain, J. H. Clark, T. J. Farmer, Y. Guo, I. D. V. Ingram, J. E. Kendrick, S. B. Lawrenson, M. North, G. Rodgers and A. C. Whitwood, *ChemSusChem*, 2019, **12**, 2393–2401.

40 H. J. Flammersheim, *Thermochim. Acta*, 1998, **310**, 153–159.

41 C.-S. Chern and G. W. Poehlein, *Polym. Eng. Sci.*, 1987, **27**, 788–795.

42 K. Horie, H. Hiura, M. Sawada, I. Mita and H. Kambe, *J. Polym. Sci. Part A-1 Polym. Chem.*, 1970, **8**, 1357–1372.

43 F. A. Saddique, A. F. Zahoor, S. Faiz, S. A. R. Naqvi, M. Usman and M. Ahmad, *Synth. Commun.*, 2016, **46**, 831–868.

44 J. Barluenga, H. Vázquez-Villa, A. Ballesteros and J. M. González, *Org. Lett.*, 2002, **4**, 2817–2819.

45 H. Firouzabadi, N. Iranpoor, A. A. Jafari and S. Makarem, *J. Mol. Catal. A Chem.*, 2006, **250**, 237–242.

46 J. Gorzynski Smith, *Synthesis (Stuttg).*, 1984, 629–656.

47 L. Shechter and J. Wynstra, *Ind. Eng. Chem.*, 1956, **48**, 86–93.

48 S. Pappuru and D. Chakraborty, *Eur. Polym. J.*, 2019, **121**, 109276.

49 E. N. Jacobsen, F. Kakiuchi, R. G. Konsler, J. F. Larrow and M. Tokunaga, *Tetrahedron Lett.*, 1997, **38**, 773–776.

50 D. M. Hodgson, M. J. Fleming and S. J. Stanway, *J. Am. Chem. Soc.*, 2004, **126**, 12250–12251.

51 B. P. Bandgar, A. V. Patil, O. S. Chavan and V. T. Kamble, *Catal. Commun.*, 2007, **8**, 1065–1069.

52 M. H. Wu and E. N. Jacobsen, *J. Org. Chem.*, 1998, **63**, 5252–5254.

53 Z. Wang, W. K. Law and J. Sun, *Org. Lett.*, 2013, **15**, 5964–5966.

54 Z. Chen, S. M. Nasr, M. Kazemi and M. Mohammadi, *Mini. Rev. Org. Chem.*, 2020, **17**, 1–11.

55 G. H. Posner and D. Z. Rogers, *J. Am. Chem. Soc.*, 1977, **99**, 8208–8213.

56 D. Albanese, D. Landini and M. Penso, *Synthesis (Stuttg).*, 1994, **1994**, 34–36.

57 Shivani and A. K. Chakraborti, *J. Mol. Catal. A Chem.*, 2007, **263**, 137–142.

58 B. M. Choudary and Y. Sudha, *Synth. Commun.*, 1996, **26**, 2989–2992.

59 W. Su, J. Chen, H. Wu and C. Jin, *J. Org. Chem.*, 2007, **72**, 4524–4527.

60 N. Azizi and M. R. Saidi, *Catal. Commun.*, 2006, **7**, 224–227.

61 A. O. Konuray, X. Fernández-Francos and X. Ramis, *Polym. Chem.*, 2017, **8**, 5934–5947.

62 S. C. Lin, *High-Performance Thermosets: Chemistry, Properties, Applications*, Hanser Gardner Publications, Munich, 1994.

63 R. J. Iredale, C. Ward and I. Hamerton, *Prog. Polym. Sci.*, 2017, **69**, 1–21.

64 J. M. Barton, I. Hamerton, J. R. Jones and J. C. Stedman, *Polym. Bull.*, 1991, **27**, 163–170.

65 J. M. Barton, I. Hamerton, J. B. Rose and D. Warner, *Polymer (Guildf).*, 1991, **32**, 358–363.

66 J. L. Hopewell, D. J. . Hill and P. J. Pomery, *Polymer (Guildf).*, 1998, **39**, 5601–5607.

67 C. Börger, A. W. Schmidt and H. J. Knölker, *Synlett*, 2014, **25**, 1381–1384.

68 S. L. Hartford, S. Subramanian and J. A. Parker, *J. Polym. Sci. Polym. Chem. Ed.*, 1978, **16**, 137–153.

69 U. S. Sahu and S. N. Bhadani, *Die Makromol. Chemie, Rapid Commun.*, 1982, **3**, 103–107.

70 J. V. Crivello, *J Polym Sci Part A-1 Polym Chem*, 1973, **11**, 1185–1200.

71 S. Ishida and S. Saito, *J. Polym. Sci. Part A-1 Polym. Chem.*, 1967, **5**, 689–705.

72 A. V. Galanti and D. A. Scola, *J. Polym. Sci. Polym. Chem. Ed.*, 1981, **19**, 451–475.

73 A. Solanki, V. Choudhary and I. K. Varma, *J. Appl. Polym. Sci.*, 2002, **84**, 2277–2282.

74 M. Grigoras, G. Colotin and N. C. Antonoaia, *Polym. Int.*, 2004, **53**, 1321–1326.

75 A. Sultani, H. Dietrich, F. Richter and H.-H. Otto, *Monatshefte für Chemie - Chem. Mon.*, 2005, **136**, 1651–1669.

76 S. Takeda, H. Akiyama and H. Kakiuchi, *J. Appl. Polym. Sci.*, 1988, **35**, 1341–1350.

77 A. Cohades, C. Branfoot, S. Rae, I. Bond and V. Michaud, *Adv. Mater. Interfaces*, 2018, **5**, 1800177.

Chapter 4: Disulfides and diselenides

4.1 Introduction

4.1.1 Disulfides

The disulfide bond is one of the most heavily researched dynamic covalent bonds in materials science. In biology, the disulfide bridges of cystine units, Figure 4.01—formed from the thiol oxidation of two cysteine amino acid residues—are known to play a crucial role in determining protein structure and stability. Approximately one third of known eukaryotic proteins contain disulfides, and the sensitivity of these linkages to pH and different oxidative/reductive (redox) environments are key contributors to the dynamic nature of these macromolecules.[1–3]

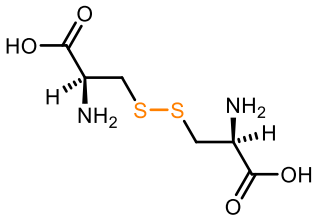

Figure 4.01. A cystine unit formed from the oxidative reaction of two cysteines.

The relative weakness of the S–S bond (*ca*. 260 kJ mol^{-1}) and its abundance in biological systems has led to significant research into its potential as a reversible bond in functional polymers. In recent years disulfides have been used to make covalent adaptable networks with thermally-reversible linkages (see Chapter 1), photoactive polymers,[4,5] and have even been applied in high performance composites.[6–9] One notable example of such a system is that reported by Odriozola *et al*.[6] in 2016 which uses dithiodianiline (DTDA) as an epoxy crosslinker (also known as di(*p*-aniline)disulfide or 4-aminophenyl disulfide), this will be referred to in more detail later.

The mechanism by which disulfides exchange with each other has been the subject of some debate over the last two decades.[4,10–16] There are three main mechanisms which have been suggested to operate dependent upon the specific system: thiol-disulfide substitution (where nucleophilic thiol groups effect the substitution), disulfide homolysis (with sulfanyl radicals as the active species) and direct disulfide metathesis, see mechanisms 1–3 respectively in Scheme 4.01.

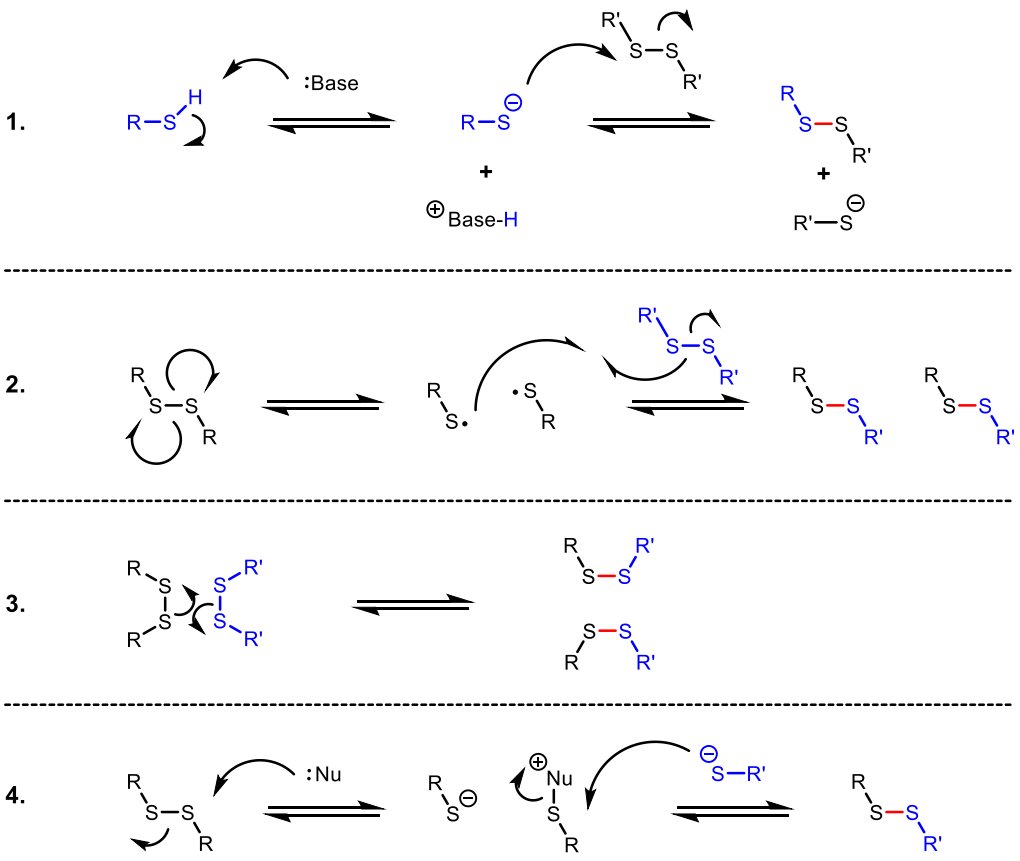

Scheme 4.01. The mechanisms of dynamic disulfide chemistry. 1 – thiol-disulfide substitution, 2 – disulfide homolysis, 3 – [2+2] disulfide metathesis, 4 – catalysed (NR_3, PR_3, NHC etc.) disulfide exchange.

In thiol-disulfide exchange, the thiol is first deprotonated to a thiolate to make it a potent nucleophile. For this reason, these processes generally operate at elevated pH, in the presence of basic catalysts.[17,18] The thiolate then readily attacks a disulfide, which produces a new disulfide and thiolate which can further propagate the reaction. It is this mechanism that has been established to dominate in biological systems with enzymatic catalysts.[19]

Disulfide exchange in the absence of thiols/thiolates has proved more contentious. The two simplest and most widely discussed mechanisms for this reaction are (2) and (3) Scheme 4.01. Although several authors have discussed the prospect of direct [2+2] metathesis (3),[10,20,21] the studies of Matxain *et al*.[12] and Nevejans *et al*.[14] present a strong case for the radical process (3) as the mechanism of uncatalysed disulfide exchange. In the Matxain article,[12] the authors used DFT to look for evidence of a [2+2] transition state but were unsuccessful. They then explored the radical pathway and found that the [2+1] radical transition state was viable (reaction enthalpies were typically on the order of 10–15 kcal mol^{-1}). An exploration of the relationship between substituents and bond dissociation energy (BDE), spin density on sulfur and other parameters, indicated that electron donating groups weaken the disulfide bond. Although weak compared to C–C bonds, the BDEs of disulfides (~50 kcal mol^{-1}) are not

so weak as to make thermolysis feasible at room temperature. However, an analysis of the excitation energies revealed that aromatic disulfides consistently absorbed in the near UV. Interestingly, electron withdrawing groups were observed to increase the absorption wavelength, shifting the first excitation wavelength closer to the visible spectrum. In the Nevejans study,[14] disulfide exchange was performed with and without the presence of 2,2,6,6-tetramethylpiperidinyloxy (TEMPO) as a radical inhibitor. The authors found that this additive slowed the reaction substantially. In contrast, when disulfide exchange was performed in the presence of UV the reaction rate was greatly increased. Both experiments strongly support the radical process. Interestingly, the authors went on to perform solid-state EPR experiments and found that the sulfanyl radical could be observed in some cases and not others. The authors attributed this to low sensitivity and a low concentration of the radicals in question. In further experiments an exploration of the amine/phosphine-catalysed process (4), *vide infra*, found no evidence of radical involvement.

In the presence of catalysts such as phosphines,[11] or N-heterocyclic carbenes (NHCs),[22] the disulfide-disulfide reaction can be performed in a manner more akin to the thiol-disulfide reaction. In these processes, the mechanism (4) appears to be slightly different from any of the previously mentioned mechanisms; the catalyst attacks the disulfide, cleaving it into a thiolate and a catalyst-sulfide addition product. As this reaction is generally reversible, another thiolate can then attack the addition product, to create a mixed disulfide.

Despite their weakness and widespread utility, in solution, disulfides do not generally exchange with each other without an external stimulus (e.g. catalyst, UV or pH change). Unusual behaviour of small-molecule disulfides was recently reported by Fritze and von Delius in which disulfide metathesis was induced in chlorinated solvents by ultrasonication.[16] These authors conclude that the reactions they observed also follow a radical process. In this case it appears that sonochemical solvolysis leads to the formation of the sulfanyl radicals that give disulfide exchange. It was this article which inspired our related research with diselenides (*vide infra*) and diphosphanes (see Chapter 5) which both undergo more facile metathesis.

4.1.2 Disulfides in CANs

The following section is a short, non-exhaustive review of the state-of-the-art concerning disulfide-containing covalent adaptable networks (CANs). An extensive volume of literature exists concerning the use of disulfides in polymers more generally and in the interest of brevity, those articles focusing on thermoplastics (non-crosslinked polymers) and elastomers (lightly crosslinked polymers) are not discussed here since the phenomena observed in soft materials are often not reproducible in hard, engineering materials.

In 2016, Odriozola and co-workers published two interesting articles relating to a catalyst-free DGEBA (bisphenol A diglycidyl ether) epoxy, crosslinked with dithiodianiline (DTDA, or 4-aminophenyl disulfide), Figure 4.02.[6,23] The aromatic disulfide linkages within this network polymer bestowed it with high temperature stress relaxation—indicative of dynamic crosslinks. DMA (stress relaxation experiments) revealed Arrhenius-type behaviour, consistent with the definition of a vitrimer (or associative CAN), with topological freezing temperature (T_v) at -13 °C. This is the temperature at which the material would transition from solid to liquid due to bond exchange reactions, defined by the point at which viscosity passes 1012 Pa s. A value of T_v that is much lower than their reported T_g (~130 °C) means the system is best described as a series of highly dynamic crosslinks frozen within a rigid polymer framework. The glass transition (both 130 °C) and general mechanical performance of the disulfide vitrimer compared well with their reference epoxy (DGEBA crosslinked with diethyltoluenediamine): tensile failure strength and failure strain were in the region of 80 MPa and 7% respectively, for both materials. Even the storage moduli of both the disulfide and control epoxy were almost identical at both low (RT) and high temperature (150 °C), 2.5/2.6 GPa and 20/20 MPa respectively. The only significant impact on physical performance was observed by decomposition temperature, where the vitrimer decomposed at 300 °C and the control at 350 °C. It is particularly interesting to note that the two polymers' properties were so similar given the substantial structural differences between the two crosslinkers, Figure 4.02.

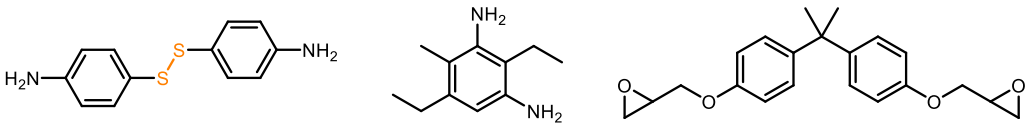

Figure 4.02. Left-to-right: dithiodianiline (DTDA, or 4-aminophenyl disulfide), diethyltoluenediamine and DGEBA.

Odriozola *et al*.[6] went on to demonstrate the reprocessability of this disulfide vitrimer at 200 °C and 100 bar, and how they could 'iron out' scratches with modest heat and pressure. Most impressively, the researchers went on to prepare carbon fibre using this disulfide as the matrix, using their so-called 'enduring prepreg' technique. Under mechanical testing, this material exhibited excellent performance, outperforming their conventional composite (prepared from manual lay-up) in terms of compressive strength, interlaminar shear strength, flexural strength and impact strength. However, the high-pressure manufacturing method used to prepare the disulfide composite was not used in the preparation of the conventional composite; it seems likely that this led to substantial differences in consolidation and probably fibre volume fraction (V_f). Nevertheless, these are impressive results, particularly given that the disulfide matrix could be readily dissolved from the composite (in solutions of 2-mercaptoethanol in DMF, 25 °C, 24 h) which is impossible with conventional polymer composites.

In a second article, the same material was examined in terms of its mechanochromism—upon grinding or impact, the polymer/composite changes colour, which could be useful for sensory applications.[23]

In 2017, Post *et al*.[7] prepared a glass-fibre reinforced polymer composite (GFRP) from another disulfide-containing polymer. In this example, the authors created a dual network polymer in which some of the crosslinks were irreversible and some were disulfides. In contrast to the Odriozola *et al*. polymer, this material contained thiol and a basic catalyst (triethylamine) as well as intact disulfides. Consequently, where the disulfide of Odriozola *et al*. operated through the radical mechanism, it seems the mechanism of bond exchange in the case of Post *et al*. is thiol-disulfide exchange. The authors prepared composite laminates with this resin using vacuum-assisted resin infusion moulding of V_f ~50%. The composite mechanical performance and self-healing were characterised by 3-point bending (3pb), double cantilever beam (DCB) and low-velocity impact testing. Self-healing of the composite was tested via these mechanical tests after treatment at several different temperatures, with reasonable strength recovery (45%) even after four cycles of bending (3pb) and repair at temperatures as low as 70 °C. However, it should be noted that each healing cycle was very long (16 h). The gradual loss of healing efficiency with each treatment cycle (through all of the different mechanical tests) is attributed to the consumption of the thiols by oxidation. This is one major limitation of the thiol-disulfide bond exchange mechanism, thiols gradually oxidise to disulfides in the presence of air. A further interesting feature of this article is the use of image analysis and 'damaged area' to quantify healing after impact testing.

In 2017 Ma *et al*.[24] extended the work of the Odriozola group, again using DTDA as an epoxy crosslinker. Though in this case the diepoxide used was synthesised from *biomass-derived* isosorbide in attempt to improve the green credentials of the system. The reported polymers were then characterised and found to be reprocessable, behaving similarly to the original DGEBA system.

Bangash *et al*.[25] published an article in 2018 concerning the synthesis of a bi-phasic composite system, in which layers of carbon fibre were infused with a soft (elastomeric) disulfide-containing poly(urea-urethane). These layers were combined with additional layers of carbon fibre infused with a hard disulfide-containing epoxy, into a single laminate. This 'double matrix' composite was designed in an attempt to increase the composite toughness in terms of impact resistance (relative to more conventional composite configurations). Both matrices again used the aromatic disulfide DTDA as the dynamic linker. The presence of this disulfide in both polymer types is what allows the previously discrete phases to be bonded together (at 200 °C and 100 bar). However, the double matrix composites were found to exhibit much poorer strength and stiffness compared to the single matrix control. This is attributed to a very high void content (>10% in some cases), particularly at the

interphases, which indicates that there is room for improvement. Nevertheless, the authors did report that in some cases the impact resistance (in terms of damage initiation energy) was significantly enhanced in the double matrix composites.

Fortman *et al*.[26] discussed the development of a polyhydroxyurethane which incorporated a disulfide moiety. Polyhydroxyurethanes—produced from the reaction of amines and cyclic carbonates—are particularly attractive alternatives to polyurethanes since they are intrinsically reprocessable via transcarbamoylation (Chapter 1, Section 1.5.4, Figure 1.7). However, to activate this reaction and the resultant reprocessability, high temperatures (>150 °C) and long reaction times (several hours) are typically required. By incorporating a diaminosulfide (cystamine) into the polymer backbone, a highly reprocessable material was prepared, Scheme 4.02. Stress relaxation (5% strain, DMA) experiments revealed that relaxation times as short as 30 s were achievable at 150 °C and the relaxation was still rapid at 120 °C. Unsurprisingly, the rate of relaxation was slower with decreasing disulfide concentration. The material could also survive repeated cycles of milling and compression moulding (150 °C) with negligible change in dynamic mechanical behaviour. The contribution from the disulfides to the dynamic behaviour seemed to be much greater than from transcarbamoylation. The authors speculated that the amines present in the polymer backbone may help to catalyse disulfide exchange.

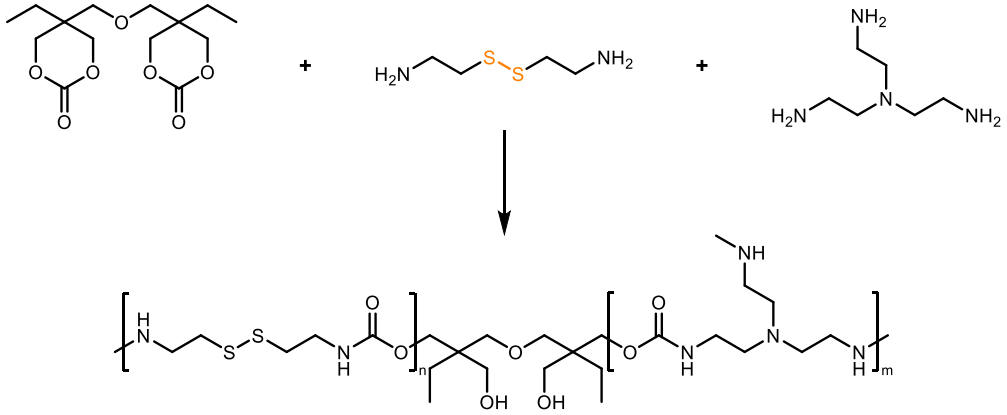

Scheme 4.02. The disulfide-containing polyhydroxyurethane reported by Fortman *et al*.[26]

Zhang *et al*.[27] reported a new disulfide-containing epoxy prepared via anhydride curing. In this article, the authors prepared a disulfide anhydride (Scheme 4.03) and went on to co-react this with a conventional anhydride curing agent (methylhexahydrophthalic anhydride) and DGEBA. Mechanical testing revealed that the prepared epoxies were robust materials, with flexural modulus consistently in the region of 2.5 GPa and flexural strength >70 MPa. The authors went on to note a slight toughening effect in those polymers containing disulfides relative to control polymers. This is a general feature of polymers containing 'weak' bonds, since their cleavage presents a mechanism of energy absorption/dissipation. Self-healing was tested via lap-shear adhesion testing (after fusing two lengths

of polymer together) and the reprocessability—or malleability—was explored through milling the cured polymer into powder prior to reconstituting it through compression moulding. The authors then tested the polymer as a matrix in an electronic device and demonstrated the recyclability of the device via use of a thiol-DMF solution, which effectively dissolved the polymer.

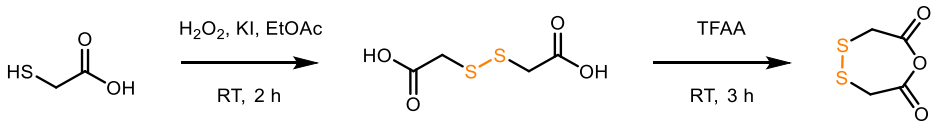

Scheme 4.03. The synthesis of the disulfide anhydride used by Zhang *et al*.[27] EtOAc = ethyl acetate and TFAA = trifluoroacetic anhydride.

Zhou *et al*.[9] modified DTDA by reacting it with para-formaldehyde to produce hemiaminal dynamic covalent networks (HDCNs, Figure 4.03). Carbon fibre prepregs were prepared by soaking dry fibre cloths in solutions of this HDCN material and DGEBA; the excess solvent was slowly allowed to evaporate as the resin partially cured (β-staged) onto the carbon cloth. The prepregs were further dried, layed-up into a single laminate and cured together in a hot press (150–200 °C, 5 MPa, 2 h). This is another example of a dual-dynamic network since the disulfides are thermally sensitive and the hexahydrotriazine rings are acid sensitive. The authors reported that the resulting composite had good mechanical performance and recycling/reprocessability and, as reported in other articles, this polymer was readily dissolved in DMF/thiol solutions.

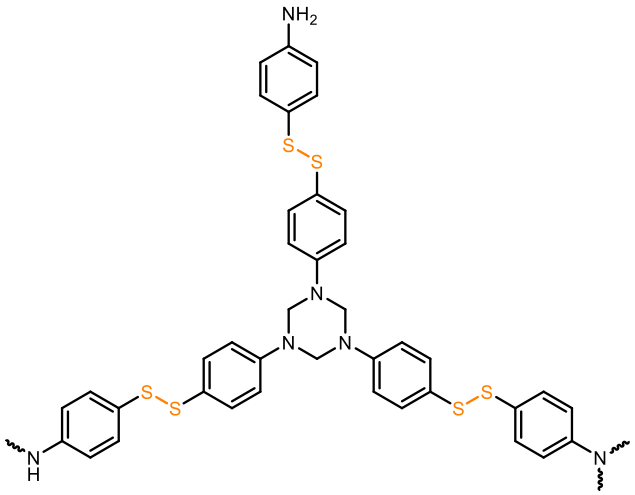

Figure 4.03. An example of the hemiaminal dynamic covalent network (HDCN) structure archetype employed by Zhou *et al*.[9] prepared via the reaction DTDA and paraformaldehyde.

Si *et al*.[28] again used DTDA as an epoxy crosslinker to prepare their disulfide CANs and their respective FRP composites, though in this study both the epoxide and crosslinker contained disulfides. This inclusion of essentially double the concentration of disulfides that was reported in earlier work (e.g.

Odriozola *et al*.[6]) resulted in significantly enhanced recyclability and high temperature stress relaxation.

In summary, several authors have demonstrated the healing, recycling and reprocessing performance of disulfide-containing polymers as composite matrices. As simple, well-understood systems, disulfide materials also compare favourably with Diels-Alder materials in terms of activation temperature, since the furan-maleimide retro reaction does not occur below 110 °C. In contrast, aromatic disulfides are capable of reaction below 100 °C, dependent on both the groups surrounding the disulfide and the rigidity of the surrounding polymer network. Indeed, several authors have taken dynamic disulfide chemistry and applied it in robust engineering polymers and FRPs that may be useful in primary or secondary structural applications. Though the thiol-disulfide mechanism has been employed, the thermal disulfide-disulfide exchange processes (catalysed or otherwise) are more common and preferred due to thiol instability. Arguably the next step with these systems is demonstrating their use in industrially relevant parts. However, it is equally desirable to look for ways of decreasing the processing/repair temperatures towards room temperature, which would prove highly valuable in certain applications. One such method may be through the use of diselenides.

4.1.3 Diselenides

Figure 4.04. Selenium and adjacent elements of the periodic table.

Sulfur and selenium express many chemical similarities originating from their Group 16 relationship, Figure 4.04. As a result, diselenides behave similarly to disulfides and are thus attractive targets for dynamic chemistry, not least because of the extreme weakness of their bonds (*ca*. 170 kJ mol^{-1}). As a consequence of their weaker bonds, diselenides compare favourably with disulfides in that they are capable of undergoing thermolysis at lower temperature and can even be photolysed by visible light.[29] At present, the amount of research in applying diselenides to materials chemistry is still small; however, there are now some examples of diselenide-derived materials which have shown self-healing behaviour (Section 4.1.4).[30,31]

Like phosphorus chemistry, selenium chemistry has an advantage over sulfur and other nuclei in that it has an isotope (^{77}Se) with I = ½. This makes ^{77}Se NMR a useful tool for both characterisation and reaction monitoring. Diselenides also present one particular synthetic advantage of their sulfur counterparts: a readily accessible dianion $[Se_2]^{2-}$ which is an ideal building block from which to prepare organodiselenides. This provides an alternative to the primary method of preparing disulfides, thiol oxidation,[32] Scheme 4.04—this is particularly valuable as a consequence of the foul smell of both thiols and selenols.

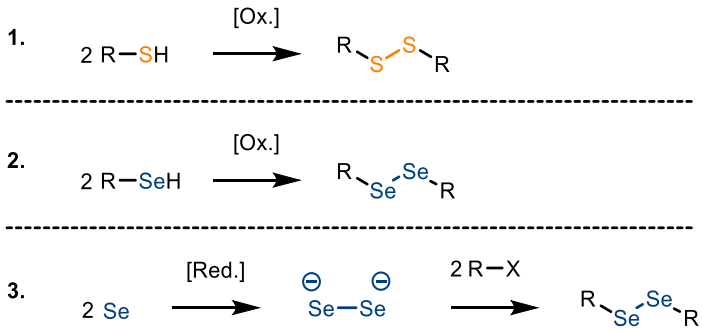

Scheme 4.04. Selected synthetic procedures in disulfide and diselenide chemistry: 1 – thiol oxidation, 2 – selenol oxidation and 3 – the reduction of elemental selenium to the dianion. Where [Ox.] is an oxidant such as oxygen, [Red.] is a reductant such as $NaBH_4$ and X is a leaving group such as a bromide or tosylate.

In a recent study, the use of ditellurides—the heavier Group 16 congener of diselenides—in dynamic bond exchange reactions has also been explored through the reaction of diselenides with ditellurides.[33]

4.1.4 Diselenides in dynamic materials

In this section, the state-of-the-art concerning diselenide-containing polymers is reviewed, with a focus on the use of diselenides in lightly-crosslinked (elastomeric) materials. Although several authors have discussed diselenide-containing thermosets (CANs), to date, there are no examples of diselenide CANs.

Much of the early materials research of diselenides concerned their use in biological soft materials. Diselenides have the capacity to be oxidised to selenic acids or reduced to selenols—both processes lead to Se–Se cleavage and both are reversible. By including diselenides in self-assembling block copolymers, researchers were able to design vesicular drug delivery vehicles which could be selectively opened in the correct redox environments.[34,35] Similar diselenide-containing vesicles were also prepared by Xia *et al.*,[36] who used osmotic pressure to induce diselenide cleavage (and thus vesicle rupture). Diselenide-containing block copolymer aggregates have also been used by Sun *et al.*[37] in a novel chemotherapeutic technique, where the cytotoxicity of the oxidised form of the diselenide

(selenic acid) was exploited. With an altogether different biological application in mind, Waliczek *et al*.[38] demonstrated the photometathesis of diselenides within peptides and argue that this process could be a valuable tool in this area.

Recently, several groups have made tentative first steps into the synthesis of diselenide-crosslinked materials. An *et al*.[30] explored the use of bis(4-aminophenyl)diselenide (Figure 4.05) in self-healing polyurethanes. In supporting DFT calculations, they reported that the transition states of the radical diselenide exchange mechanism were approximately 25 kJ mol^{-1} lower than in analogous disulfide reactions. This means that not only are the diselenides more susceptible to radical formation (less thermodynamically stable), they are also more kinetically reactive than disulfides, which was further supported by the DFT study of Irigoyen *et al*.[39] An *et al*.[30] converted commercially available propylene glycol into bis- and tris-functional isocyanates prior to crosslinking with bis(4-aminophenyl)diselenide, the resultant elastomer consistently outperformed an analogous disulfide in repair after tensile tests, with a superior healing efficiency and faster healing time.[30]

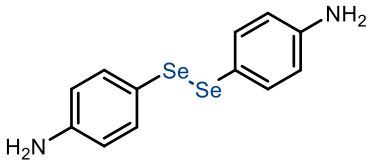

Figure 4.05. Bis(4-aminophenyl)diselenide, the analogous diselenide to dithiodianiline (DTDA).

Impressively, the method of healing in the An *et al*. study was simply contacting the cut surfaces (without external pressure or elevated temperature). This is possible because of the visible light–initiated mechanism of diselenide exchange, the flexibility of the surrounding polymer and the assistance of hydrogen bonding. The diselenide-containing polymer showed excellent reprocessability through several cycles of milling and compression moulding, again outperforming the analogous disulfide polymer.

The dynamic behaviour of diselenides was similarly exploited by Du Prez and co-workers in their preparation of healable elastomers and linear polymers.[40] Du *et al*.[31] also prepared healable diselenide-containing polyurethanes, in this case via the synthesis of bis(2-hydroxyethyl)diselenide, which was then incorporated into a polyurethane via a solution process. A similar healable urea-urethane, prepared from the reaction of an aminodiselenide and isocyanate-terminated poly(propylene glycol), was prepared by Qian *et al*.[41] in 2019.

4.1.5 Disulfides and diselenides: aims and objectives

From the aforementioned studies, it is clear that diselenide-containing polymers have great potential in healable/reprocessable materials. It is conspicuous that at present diselenide exchange has not

been used in hard materials such as CANs. Accordingly, the synthesis of diselenide CANs is the logical next step of this research area and this is as true at the time of writing (2021) as it was when this study began in 2017.

In this study the key objectives were as follows:

- Explore and confirm the mechanism of the diselenide exchange reaction (Section 4.2) and then synthesise new functional diselenides with a view to their use as polymer crosslinkers (Section 4.3).
- Reproduce the disulfide CAN of Odriozola *et al*. and compare it with the true carbon-based analogue. Use this material as a benchmark for comparison to new polymers (Section 4.4.1).
- Prepare and characterise the first examples of diselenide CANs (Sections 4.4.2 and 4.4.3).

4.2 Metathesis: dynamic chemistry

To explore the dynamic behaviour and stability of diselenides, the model reaction between diphenyl diselenide ($[PhSe]_2$) and di(*n*-butyl)diselenide ($[BuSe]_2$) was tested under a variety of conditions, Figure 4.06.

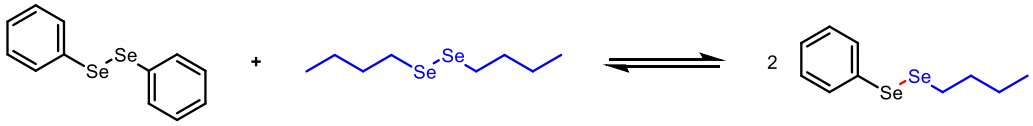

Figure 4.06. The metathesis of diphenyl diselenide and di(*n*-butyl)diselenide.

$[PhSe]_2$ was chosen as a widely-used commercially available reagent (purchased and used as received from Sigma-Aldrich) and $[BuSe]_2$ was chosen as a useful target to test the sodium diselenide (DMF) route of synthesis, Scheme 4.05.

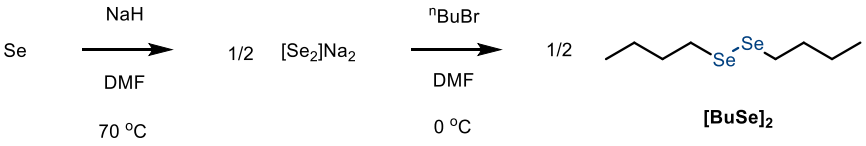

Scheme 4.05. The synthesis of di(*n*-butyl)diselenide via sodium diselenide.

The general procedure for this metathesis is as follows: $[BuSe]_2$ (10 mg, 0.035 mmol) and $[PhSe]_2$ (11.5 mg, 0.035 mmol) were added to an oven-dried NMR tube. Then, solvent (0.5 ml) was added and the tube shaken until dissolution and the reaction monitored by ^{1}H and $^{77}Se\{^{1}H\}$ NMR spectroscopy, Figure 4.07. The results under the various reaction conditions are summarised in Table 4.1.

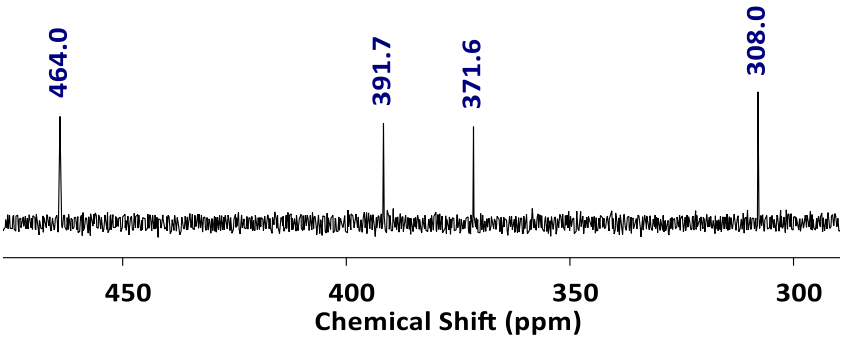

Figure 4.07. $^{77}Se\{^{1}H\}$ NMR spectrum of the metathesis reaction between di(*n*-butyl)diselenide (308.0 ppm) and diphenyl diselenide (464.0) in $CDCl_3$ after 24 h. The two resonances at 391.7 and 371.6 correspond to the mixed product ^{n}BuSeSePh.

Table 4.1. The results of diselenide metathesis.

Entry	Solvent	Conditions	Duration	Mixed SeSe[a]
1	$CDCl_3$	Ambient	25 min	20%
2	$CDCl_3$	Ambient	24 h	50%
3	$CDCl_3$	Dark[b]	24 h	33%
4	CD_2Cl_2	Ambient	36 min	36%
5	PhMe	Dark[b]	19 h	13%
6	$CHCl_3$	TTBP[c]	110 min	17%
7	$CDCl_3$	TTBP[c]	18 h	20%
8	$CDCl_3$	TTBP[d]	6 h	35%

[a] Determined from ^{77}Se integrals.

[b] Foil-wrapped in a dark cupboard.

[c] 2 eq. TTBP.

[d] 5 eq. TTBP.

From entries 1 and 2 it is evident that the time taken for the reaction to produce a statistical mixture (50% mixed product) was between 30 min and 24 h. As evidenced by entries 5–8, the metathesis is sensitive to light and the presence of the radical scavenger TTBP (2,4,6-tri-*tert*-butylphenol). This strongly suggests a photolytic radical mechanism. Since the reaction does appear to proceed in the dark, it is evident that only a small amount of light is required to initiate the reaction or there is an additional thermal process. It should be noted that the NMR spectra themselves were not measured in the dark—all samples were exposed to a small amount of ambient lighting. These findings are largely in agreement with those of Ji *et al*.,[29] but interestingly those authors found it necessary to use a non-ambient light source to initiate the metathesis.

The potential value of diselenides in CANs is thus immediately apparent. These bonds are capable of rapid exchange with only ambient light required as stimulus. Although the use of ambient lighting as a stimulus does pose questions concerning controllability, visible light-activated CANs could have great value in certain applications, particularly in dark environments.

A range of diselenides with different functionalities were selected as (crosslinker) targets for synthesis and integration into polymers, Figure 4.08.

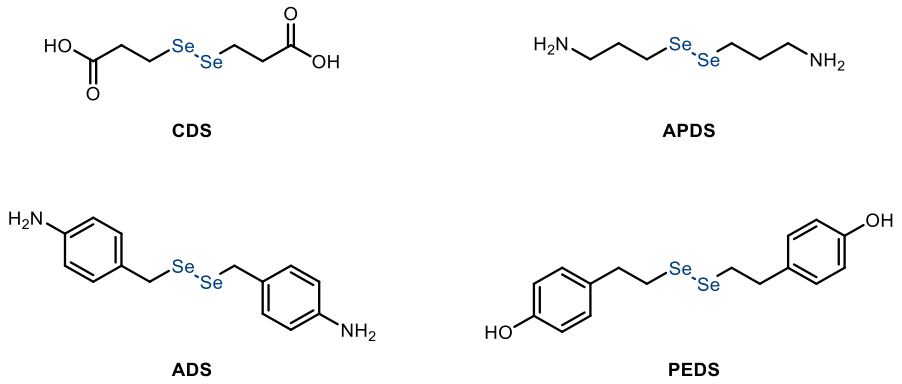

Figure 4.08. Target diselenides. **CDS** – carboxylic acid diselenide [3,3'-diselanediyldipropionic acid]. **APDS** – aminopropyl diselenide [3,3'-diselanediylbis(propan-1-amine)]. **ADS** – aniline diselenide [4,4'-(diselanediylbis(methylene))dianiline]. **PEDS** – phenolethyl diselenide [4,4'-(diselanediylbis(ethane-2,1-diyl))diphenol].

As diamines, A**PDS** and **ADS** are ideal candidates for epoxy crosslinking. The dicarboxylic acid **CDS** should also be capable of reaction with epoxides (carboxylic acids are believed to be the active functionality in epoxy-anhydride polymerisation) as demonstrated in the work of M. Chen *et al*.[8] and Y. Chen *et al*.[42] Carboxylic acids are also capable of reacting with isocyanates to form polyamides, as in the work of A. Chen *et al.*,[43] Blagbrough *et al*.[44] and Schotman.[45] The phenolic diselenide (**PEDS**), as a diol, should be an ideal candidate for polyurethane synthesis. The proposed polymerisation reactions to be used in this study are summarised in Scheme 4.06.

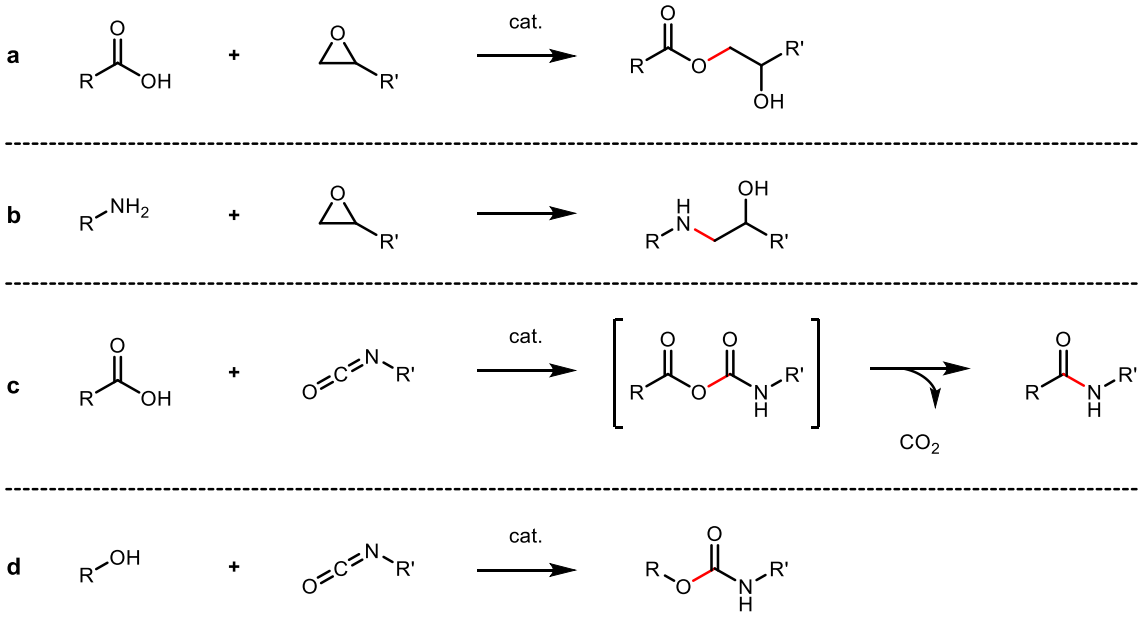

Scheme 4.06. The epoxy and polyurethane polymerisation reactions proposed for creating diselenide-containing polymer networks (diselenide CANs). **a** – epoxy carboxylic acid crosslinking. **b** – epoxy-amine crosslinking. **c** – polyamide formation from acid/isocyanate. **d** – polyurethane formation from alcohol/isocyanate.

4.3 Synthesis and characterisation of diselenide crosslinkers

4.3.1 3,3'-diselanediyldipropionic acid (CDS)

Of the four functionalised diselenide targets in Figure 4.08, the (di)carboxylic acid diselenide (**CDS**) is the only previously reported compound having been prepared by Nascimento *et al*.[46] and as such was the first target of this study, Scheme 4.07.

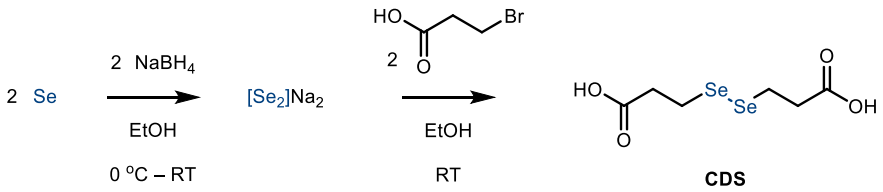

Scheme 4.07. Synthesis of carboxylic acid diselenide from sodium diselenide, **CDS**.

The literature procedure used a different solvent and reducing agent in the preparation of sodium diselenide than the method reported for $[BuSe]_2$ in Section 4.2. In this synthesis, the milder reducing agent ($NaBH_4$) and less harmful solvent (EtOH) make this a particularly attractive method. However, it should be noted that the reaction of $NaBH_4$ with EtOH releases H_2 gas and is exothermic, accordingly care should be taken to avoid dangerous pressurisation. The ^{1}H and $^{77}Se\{^{1}H\}$ NMR spectra are shown in Figure 4.09. With high yield (88%) and good purity (~94% by ^{1}H NMR) this is a robust reaction.

However, characterisation of **CDS** proved more challenging than expected, which would later prove to be representative of most of the diselenides prepared herein.

Of the conventional mass spectrometry techniques available (conventional EI/CI were not routinely available at the time of study), neither ESI nor nanospray ionisation techniques yielded spectra in which the molecular ion of **CDS** was visible. This is attributed to the extreme weakness of the Se–Se bond, which presumably undergoes rapid cleavage (fragmentation) when subject to the aforementioned techniques. APCI, atmospheric pressure chemical ionisation, was found to consistently produce spectra in which the molecular ion ($[M+H]^+$ or $[M-H]^-$ in this case) was observable for all of the weak-bond containing small molecules produced in the syntheses described in this chapter (Se–Se) and Chapter 5 (P–P, P–S and P–Se). Evidently this technique provides both a soft method of ionisation and high sensitivity. APCI is principally similar to conventional CI, but since ionisation occurs at higher pressure (atmospheric), the collision frequency between the analyte and corona discharge is much higher, which leads to improved sensitivity and ionisation efficiency—ideal for analytes which have a high chance of fragmentation.[47]

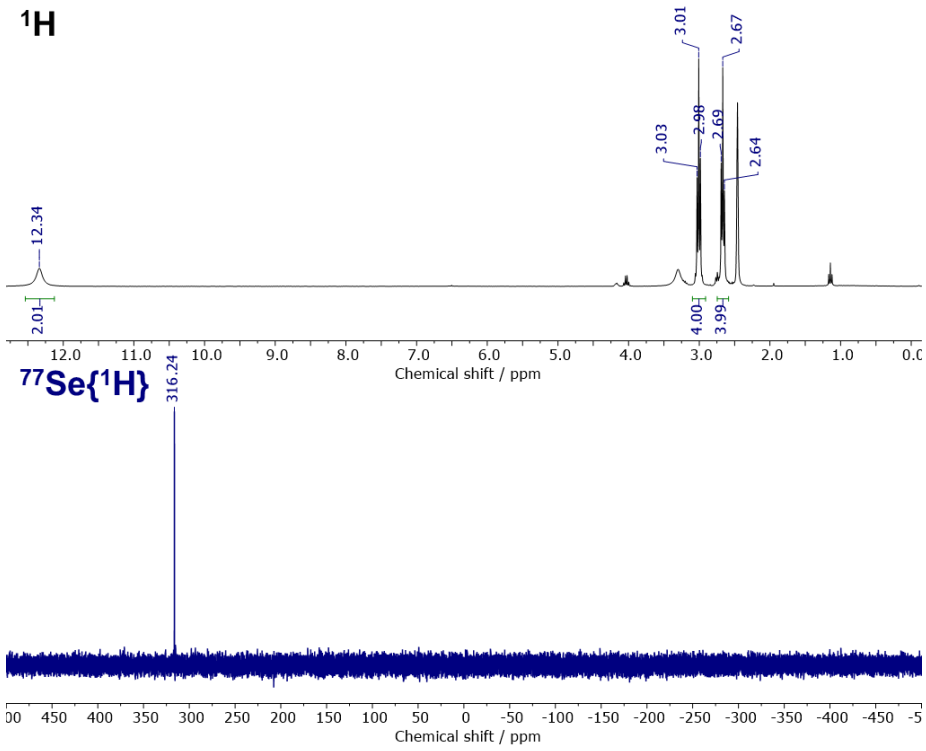

Figure 4.09. Top, ^{1}H NMR of **CDS** in DMSO-D6. Bottom, $^{77}Se\{^{1}H\}$ NMR of **CDS** in DMSO-D6.

Initially, numerous attempts were made to observe this compound by ^{77}Se NMR (and other target diselenides) with limited success. Despite the relatively low natural abundance of ^{77}Se (7.63%), ^{77}Se NMR has reasonable sensitivity—approximately three times that of ^{13}C. A spin ½ nucleus, it has no quadrupolar moment and is also broadly unaffected by NOE effects.[48,49] Moreover, although the

chemical shift range over which selenium nuclei resonate is large (-1000 to +3000 ppm), the diselenide region is well-known and covers a much narrower range: 200–500 ppm. Thus, it was initially surprising to discover that observing a diselenide ^{77}Se signal was so challenging. More detailed analysis of experimental parameters and the literature concerning ^{77}Se NMR led to the exploration of relaxation delay. Although the longitudinal relaxation times (T_1) of ^{77}Se are generally considered short, usually on the order of 'a few seconds', there are literature examples of selenium-containing species (including selenides and diselenides) with T_1 ~ 30 s.[50] Accordingly, adjustment of the default measurement settings from: 1 s relaxation delay, 30° pulse angle and 200 scans, to: 30 s, 60° and 1000 scans, led to consistently observable diselenide resonances. However, these parameters came at the cost of experiment duration (usually >10 h). In the particular case of **CDS** a relaxation delay of only 4 s was sufficient, suggesting that the relaxation mechanisms available to it are relatively efficient compared to the diselenides discussed hereafter.[50]

4.3.2 3,3'-diselanediylbis(propan-1-amine) (APDS)

A synthesis of diaminopropyl diselenide (**APDS**) has previously been claimed;[51] however, no characterisation or experimental detail was reported for this compound. Considering the success of the **CDS** synthesis and the lack of evidence to suggest the literature procedure is reproducible, an adapted protocol from the synthesis of **CDS** was used (sodium diselenide in EtOH), Scheme 4.08.

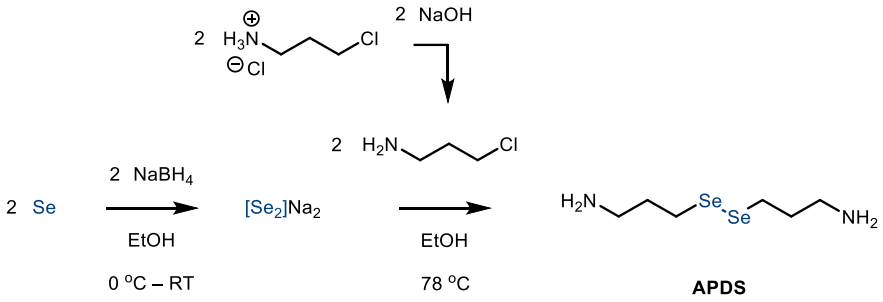

Scheme 4.08. The synthesis of **APDS** from sodium diselenide in EtOH.

Attempts to perform the reaction without prior deprotonation of the HCl salt were unsuccessful, but with the addition of sodium hydroxide the reaction proceeded successfully. Aside from this difference, the major distinction between this reaction and the **CDS** synthesis is the leaving group. Due to the use of a chloride, a significantly poorer leaving group (*vs*. bromide), we would expect the reaction to be slower. To compensate for the use of the chloride, the reaction mixture was heated to reflux and the reaction duration increased from 3 to 24 h. After extraction, the product **APDS** was isolated in modest yield (29%). Examination via ^{1}H NMR revealed a relatively pure sample (~90%), with no residual 3-chloropropylamine, indicating that the reaction had proceeded to completion. Accordingly, it is likely that part of the loss in yield can be attributed to the relative solubility of **APDS** in CH_2Cl_2 (DCM) *vs*.

water (brine). As a small di-primary amine, **APDS** is rather polar and thus likely has significant water solubility. With hindsight, this may make EtOAc extractions more appropriate. Previous diselenide syntheses suggest that the impurity is either the monoselenide, triselenide or both. This was confirmed by examination of the $^{77}Se\{^{1}H\}$ NMR spectrum (30 s relaxation delay, 60° pulse angle, 1000 scans), Figure 4.10.

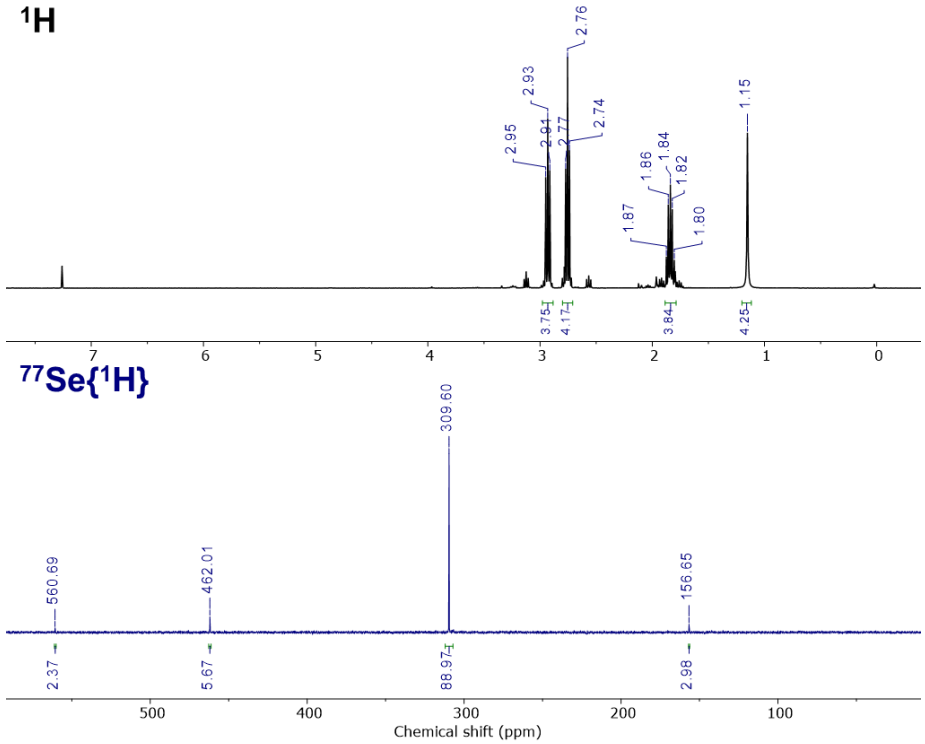

Figure 4.10. Top, ^{1}H NMR of **APDS** in $CDCl_3$. Bottom, $^{77}Se\{^{1}H\}$ NMR of **APDS** in $CDCl_3$.

The ^{77}Se spectrum indicates the presence of three minor selenium-containing impurities which—from their chemical shift—can be tentatively assigned as selenide/selanyl ether (RSeR, +157 ppm), triselenide (RSeSeSeR, +462 ppm) and tetraselenide (RSeSeSeSeR, +561 ppm). Although heteronuclear NMR integrals are often inaccurate, due to the lack of an NOE effect the integrals of these species are likely approximately representative and are thus labelled on the spectrum. In agreement with ^{1}H integration the diselenide appears to be ~90% pure. Since **APDS** is an oil it cannot be further purified by recrystallisation, a technique which has proved successful with several of the diselenides reported in this chapter. Distillation is also not feasible, in this case due to the thermal instability of diselenides. Accordingly, column chromatography is the most practical candidate for purification. However, chromatographic separation of such chemically similar (differing only in the number of Se atoms) species is not trivial. Given that the triselenide/tetraselenide species should have similar dynamic behaviour to the diselenide, it was decided that this crude product was good enough to proceed with polymer crosslinking, without chromatography.

As with **CDS**, the expected molecular ion of **APDS** was readily observed by APCI-MS.

4.3.3 4,4'-(diselanediylbis(ethane-2,1-diyl))diphenol (PEDS)

The phenol(ethyl) diselenide **PEDS** (Scheme 4.09) has not been previously reported, though with a combination of rigid aromatic rings at the nucleophilic sites and aliphatic flexibility around the diselenide moiety, it is ideal as a difunctional crosslinker. This compound was prepared using the same procedure for forming sodium diselenide in EtOH.

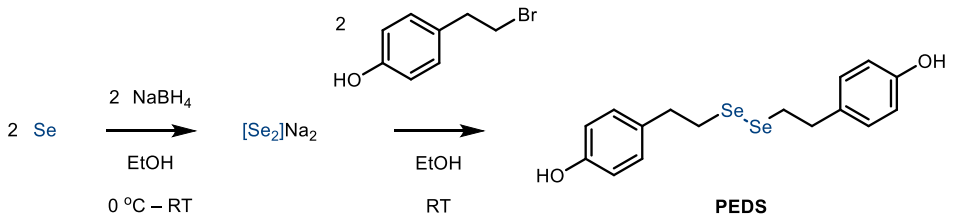

Scheme 4.09. The synthesis of **PEDS** from sodium diselenide in EtOH.

In contrast to the previous two syntheses, this reaction was stopped prematurely (after only 2.5 h). This shorter reaction time combined with the use of a slight excess (~10%) of sodium borohydride may explain why in addition to the target diselenide and the usual RSeR/RSeSeSeR impurities, a significant quantity of the foul-smelling selenol (RSeH) was also observed by ^{1}H NMR, Figure 4.11 (top). The selenol was removed by allowing it to oxidise to diselenide (by standing in air for *3 months*). Both column chromatography and recrystallisation from chloroform led to successful purification, though recrystallisation from EtOH was not successful. The highest purity product (Figure 4.11, panel 2) was treated via both chromatographic and recrystallisation processes. The ^{77}Se spectrum of **PEDS** was recorded with a 10 s relaxation delay, 60° pulse angle and 4000 scans. The molecular ion was readily apparent using APCI-MS (-ve ion mode).

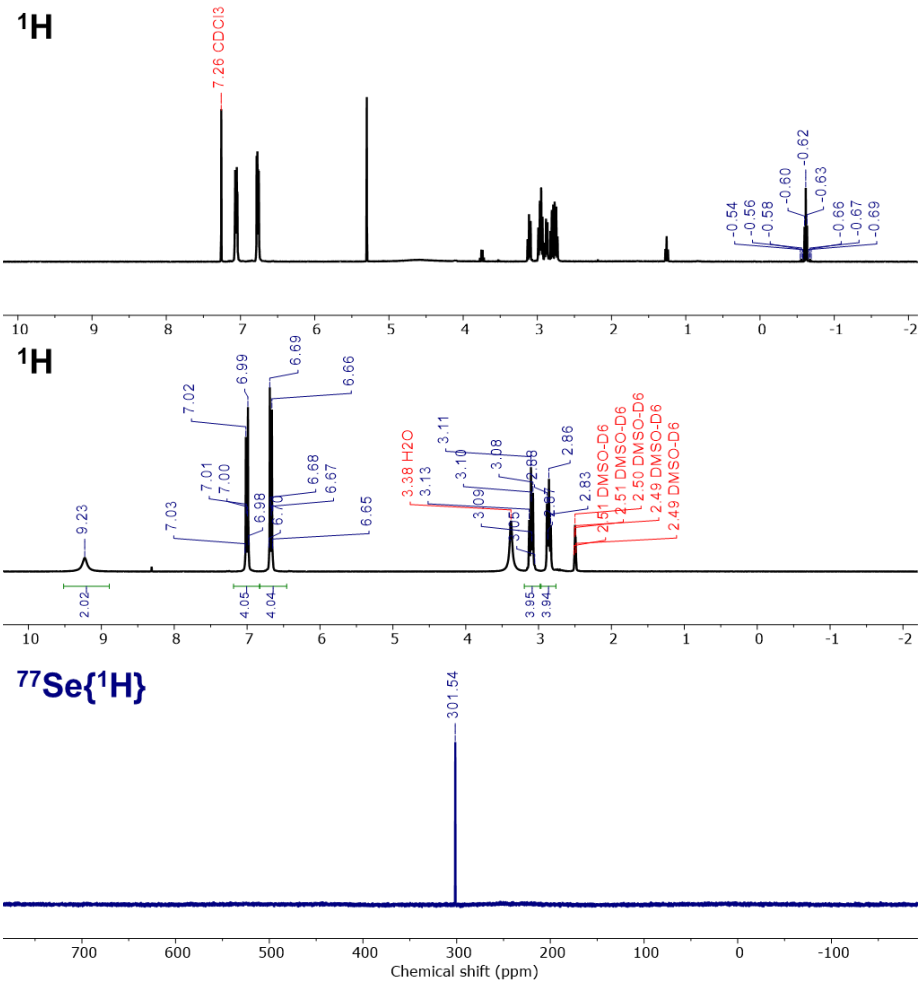

Figure 4.11. Top, ^{1}H NMR of crude **PEDS** in $CDCl_3$ with the Se–H (contaminant) resonance labelled at -0.5 ppm. Middle, ^{1}H NMR of pure **PEDS** in DMSO-D6. Bottom, $^{77}Se\{^{1}H\}$ NMR of **PEDS** in DMSO-D6.

4.3.4 4,4'-(diselanediylbis(methylene))dianiline (ADS)

As with **PEDS**, the aniline diselenide **ADS** has not previously been reported. It shares the same advantageous structural features (a flexible aliphatic linker between rigid aromatic units) and has the additional benefit of being a di-primary aromatic amine, ideal for controlled crosslinking of epoxies. A similar diselenide (bis(4-aminophenyl)diselenide) is commercially available but was deemed prohibitively expensive (in the region of thousands of pounds per gram), and impractical to make. Accordingly, **ADS** is an extremely valuable target for this research. The proposed synthesis is shown in Scheme 4.10.

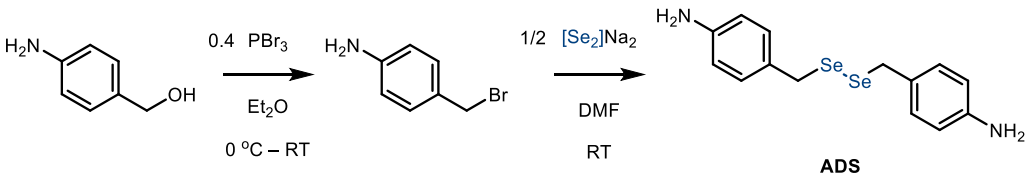

Scheme 4.10. Proposed synthesis of **ADS** from 4-aminobenzyl alcohol.

The preparation of the precursor, 4-aminobenzyl bromide proved challenging. The crude material was isolated as a yellow solid and attempts to separate the bromide from this were unsuccessful. The bulk of the solid product was insoluble in Et_2O, DCM, MeOH and water, strongly suggesting that the organic material had polymerised during the reaction. One way of circumventing this polymerisation problem is through a protecting group strategy.

A protecting group in this synthesis should selectively mask the reactive primary amine and ideally be stable to the brominating agent, PBr_3 and to one or more of the reducing agents used to prepare sodium diselenide (i.e. $NaBH_4$ or NaH). Critically, the chosen protecting group must be readily removed under mild conditions—conditions to which the product diselenide is stable. Some of the more widely used amine protection strategies are conversion to amides, imides, carbamates and the addition of trityl- or benzyl-groups.[52,53] Of all the protecting groups in common usage, *tert*-butyl carbamates (BOC) are arguably the most widely used. The ease of application (through reaction of amine with BOC anhydride) and the plethora of selective deprotection methods made this a good candidate for the synthesis of **ADS**. A revised synthesis with BOC-protection is shown in Scheme 4.11.

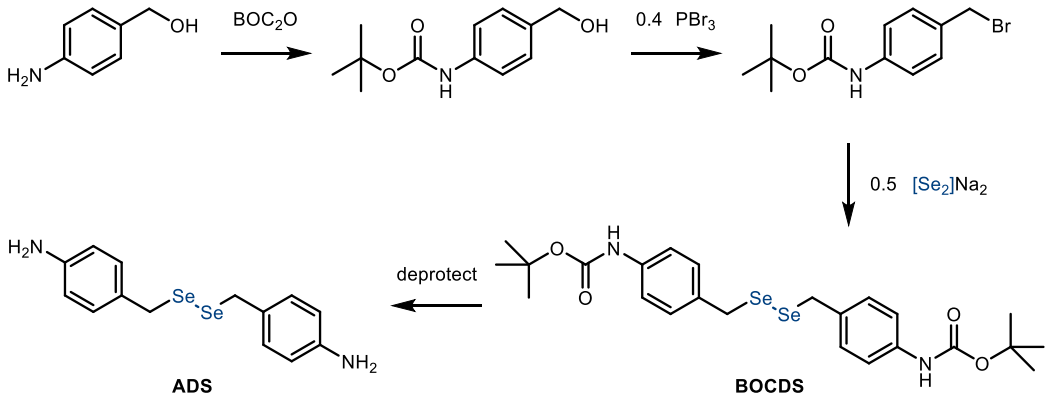

Scheme 4.11. The proposed synthesis of **ADS** using a BOC protection/deprotection strategy.

The proton NMR of each step is shown in Figure 4.12. The BOC protection method used in this study was that of Viswanadham *et al*.,[54] who reported a solvent- and catalyst-free method of BOC protection by performing a melt synthesis on a rotary evaporator. Conveniently, no work-up is required since the side-products, isobutene and CO_2, are continuously removed during the reaction. The BOC protection of 4-aminobenzyl alcohol proceeded in quantitative yield as reported in the literature. A *tert*-butyl resonance is apparent at 1.52 ppm (integral = 9H). In contrast to the bromination of the unprotected alcohol, the bromination of *p*-BOC benzyl alcohol produced a solid crude material which was soluble in organic solvents. *p*-BOC benzyl bromide was isolated cleanly, in good yield (67%), as evidenced by the disappearance of the hydroxyl resonance and (upfield) shift in benzylic proton resonance in the ^1H NMR spectrum.

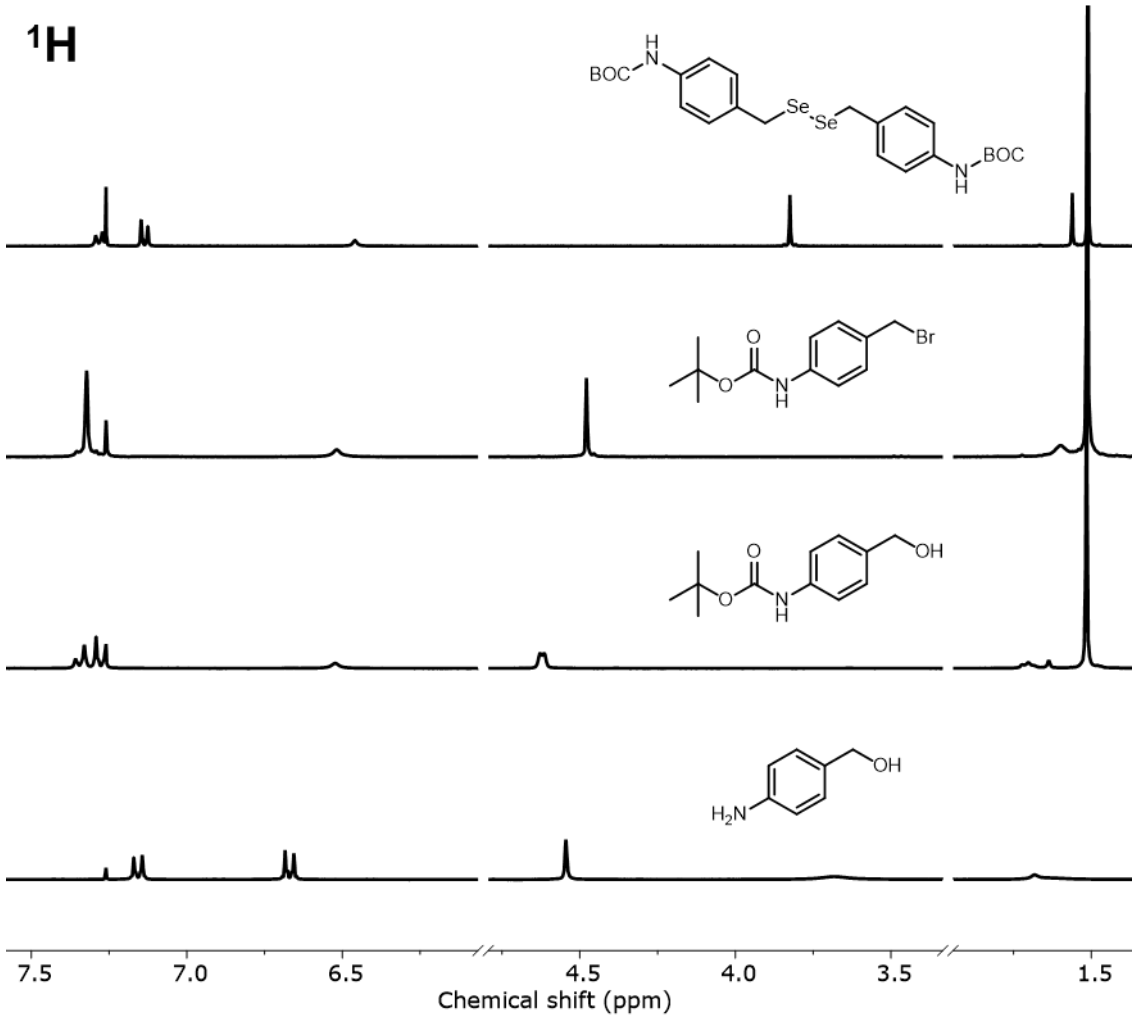

Figure 4.12. The ^{1}H NMR spectra of **BOCDS** synthesis ($CDCl_3$).

Thus far, two methods of sodium diselenide synthesis have been described (DMF/NaH and EtOH/$NaBH_4$), both of which have been employed with great success. A further two methods, 1:1 NaOH/$NaBH_4$ in THF and aqueous $NaBH_4$, were tested in different syntheses and were found to be much less reliable. The diselenide forming reaction of **BOCDS** was tested using the aqueous method, but some selenol and significant RSeR/RSeSeSeR contamination was observed. In this reaction and others, attempts to work-up the crude diselenide mixture were plagued by the disproportionation of the product, yielding large quantities of red selenium. Anecdotal evidence suggests that this could be due to the formation of greater amounts (>5%) of the higher (tri, tetra etc.) polyselenide species. The EtOH/$NaBH_4$ procedure was similarly unsuccessful in **BOCDS** synthesis, producing impure product which readily disproportionated. Fortunately, the NaH/DMF protocol—which includes a four separating funnel extraction train (see experimental)—proceeded smoothly, producing the diselenide in excellent yield (86%) and good purity (~90%). Both column chromatography and recrystallisation from EtOH proved useful purification techniques, allowing the isolation of analytically pure **BOCDS**,

which was characterised by ^{1}H NMR, ^{77}Se{^{1}H} NMR and HR-MS (APCI+). Satellites produced from $^{3}J_{SeH}$ coupling are visible either side of the main benzylic proton resonance at 3.83 ppm (14.6 Hz).

An extensive range of different methods of BOC-deprotection have been reported including trifluoroacetic acid (TFA),[55] phosphoric acid,[56] tetrabutylammonium fluoride (TBAF)[57] trimethylsilyl iodide (TMSI),[58] trimethylsilyl chloride (TMSCl),[59] iodine,[60] tin(IV) chloride,[61] sodium *tert*-butoxide,[62] and boiling water.[63] In an extensive testing campaign, seven of these methods were tested on **BOCDS**, though none were successful. Either negligible change was observed ($NaO^{t}Bu$, H_2O and phosphoric acid) or, if the BOC groups were successfully removed, disproportionation to red selenium/RSeR species dominated (TBAF, I_2, TMSI and TFA). The spectrum of **BOCDS** after TFA deprotection is shown in Figure 4.13. The *tert*-butyl protons at ~1.5 ppm were no longer observed, indicating the removal of the BOC groups. There are two major peaks (3.84 and 3.64 ppm) in the benzylic proton region, each with ^{77}Se satellites as labelled. This indicates the formation of two selenium-containing products. The larger of the two resonances at 3.64 ppm appears to be co-located with a broad singlet resonance which can be attributed to primary amine. The resonance at 3.84 ppm likely corresponds to the desired product (**ADS**) since it is very close to the 3.82 ppm resonance of the protected species. Unfortunately, it seems probable that the larger resonance at 3.64 ppm corresponds to the analogous RSeR species, which explains the appearance of large quantities of red selenium during the reaction.

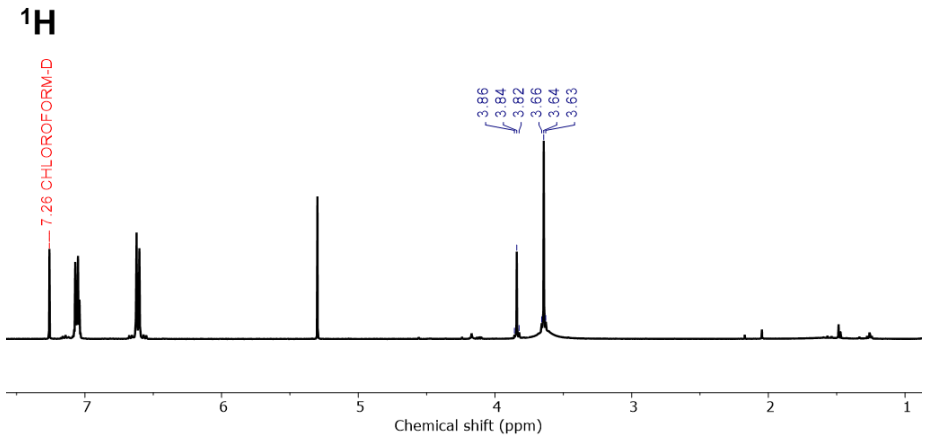

Figure 4.13. ^{1}H NMR of the deprotection of **BOCDS** with TFA. Benzylic resonances and their respective ^{77}Se satellites are labelled at 3.64 and 3.84 ppm. The large resonance at 5.30 ppm is residual CH_2Cl_2.

To further explore the stability of **BOCDS** under some of these deprotection conditions in a more economical fashion, dibenzyl diselenide ($[BnSe]_2$) was prepared and used as a surrogate, Scheme 4.12. This synthesis proceeded with similar success (86% yield) via the NaH/DMF sodium diselenide route. Analytically pure dibenzyl diselenide was isolated via recrystallisation from petroleum ether.

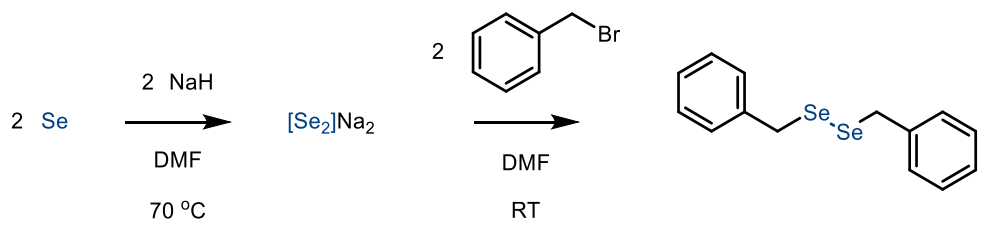

Scheme 4.12. The synthesis of dibenzyl diselenide from sodium diselenide in DMF.

When dissolved in 1:1 DCM/TFA, $[BnSe]_2$ remains intact. However, when 2 equivalents of aniline are added to this mixture, a red precipitate forms (red selenium). ^{1}H NMR revealed that this process also generated some dibenzyl selenide (BnSeBn), observable as a downfield-shifted benzylic resonance akin to that observed in Figure 4.13. This suggests that in contrast to $[BnSe]_2$, **ADS**, the amine-functionalised analogue, is not stable under acidic conditions, undergoing self-reaction to generate elemental selenium and the monoselenide. In the absence of acid, no reaction is observed between $[BnSe]_2$ and aniline—therefore, **ADS** may also be stable in non-acidic environments. Regardless, all attempts at deprotection with non-acidic conditions were unsuccessful.

An alternative protection strategy with FMOC was also tested, Scheme 4.13. In contrast to BOC, the major FMOC deprotection approaches use basic conditions, conditions under which diselenides should be stable. Although the protection and subsequent bromination were successful, the protecting group reacted with the sodium diselenide solution, generating a mixture of products during this reaction. This approach was not pursued further.

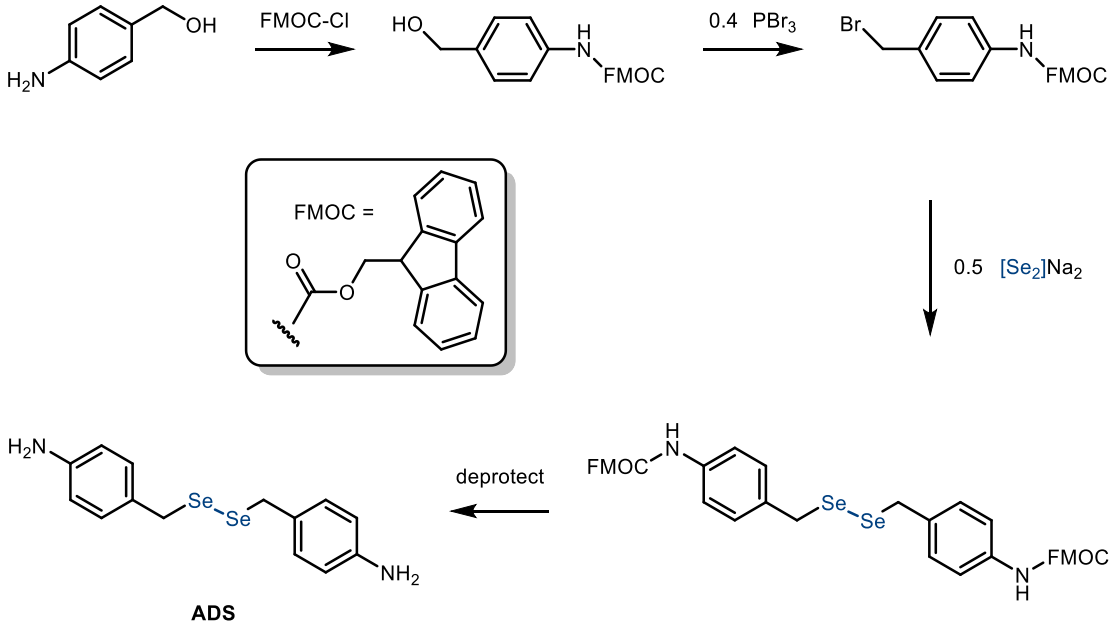

Scheme 4.13. Proposed synthesis of **ADS** via FMOC protection.

Despite the problems deprotecting **BOCDS** chemically, it is possible that the carbamates (as masked secondary amines) could still be used in reactions with epoxides; **BOCDS** may participate in polymerisation without deprotection. Furthermore, there is also a possibility of thermal deprotection—the BOC groups may cleave spontaneously with enough thermal energy, such as during polymer cure, see Section 4.4.

4.4 Polymer synthesis and characterisation

4.4.1 Benchmark study

In this section, the seminal work of Ruiz de Luzuriaga *et al*.[6] has been reproduced and assessed as a benchmark disulfide CAN. The thermal and mechanical performance of this material, denoted as EpxSS1 (epoxy disulfide 1), which is the epoxy produced from the reaction of DTDA and Epon 828 (DGEBA), is explored through DSC, DMA and 3pb testing. This has then been contrasted with an analogous disulfide-free epoxy (Ctrl1) and a more conventional poly(alkylamine)-cured epoxy (Ctrl2), Scheme 4.14.

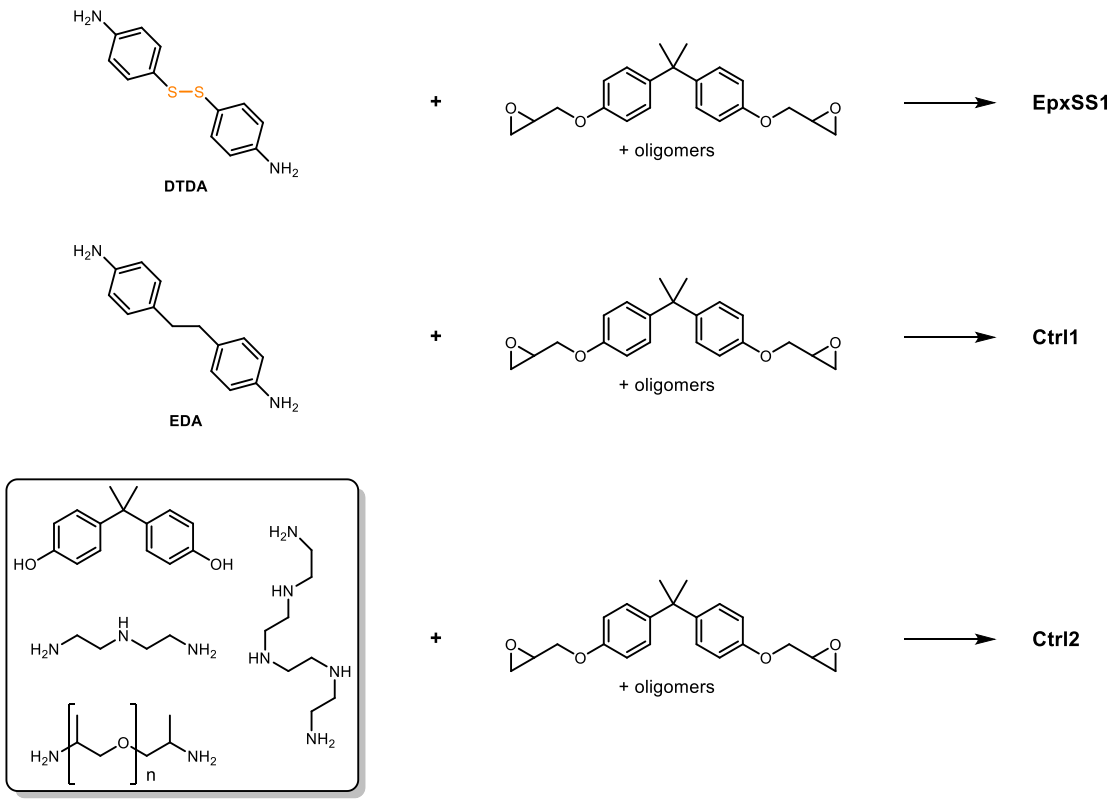

Scheme 4.14. The components of the epoxies used to benchmark this study. DTDA (4,4'-dithiodianiline), the crosslinker of EpxSS1, EDA (4,4'-ethylenedianline), the crosslinker of Ctrl1 and the polyamines (+ bisphenol A) used to crosslink Ctrl2.

The control epoxies, Ctrl1 and Ctrl2, were prepared in analogous fashion to Polydisulfide1 as reported in Chapter 2, Section 2.2.1. The molecular structures are described in terms of the starting monomers above in Scheme 4.14.

The first control polymer (Ctrl1) is identical to EpxSS1 in all but the presence of the sulfur atoms, this means that the influence of the disulfide bond can be directly investigated when comparing these polymers. However, the hardener used in Ctrl1 (EDA), although commercially available, is not widely used and so Ctrl2 was designed to be more similar to widely-used polyalkylamine hardening systems. For this reason, it is perhaps unsurprising that Ctrl2 was the most challenging system to work with—due to the presence of more reactive (aliphatic) amines—Ctrl2 cured rapidly and at the first two attempts, yielding polymer that cured during degassing. Interestingly, the disulfide was the least reactive curative and was thus the easiest to manage. Presumably, this reflects the decrease in nucleophilicity at the amines due to electron-withdrawal by the sulfur atoms.

Dynamic differential scanning calorimetry (DSC) was used to probe the cure and thermal behaviour of this disulfide polymer, analogously to Chapter 2, Section 2.3.2. A representative heat-cool-heat profile of cured EpxSS1 is shown in Figure 4.14.

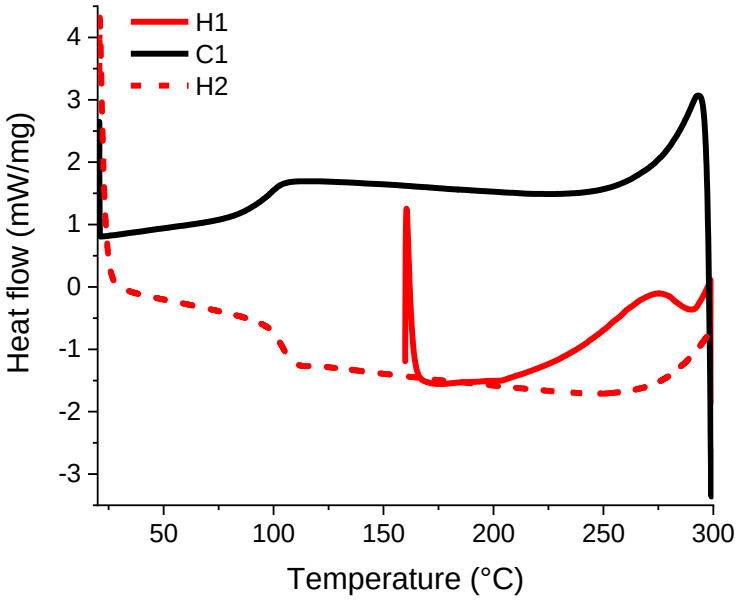

Figure 4.14. A temperature-heat flow (DSC) plot of EpxSS1 (10 °C min^{-1}).

Three major features are present in the heat flow curve: (1) T_g is evident at ~100 °C. (2) A non-reversing exotherm is evident in the first phase of heating, with onset at ~200 °C and peak at 280 °C. (3) A reversible exothermic event of onset ~250 °C is present up to the maximum temperature, 300 °C. The glass transition temperature at ~100 °C is in the region expected of properly cured DGEBA epoxies. The non-reversing exotherm indicates a chemical reaction; at such a high temperature, this could be

a decomposition event, or curing of some residual unreacted amine/epoxy groups. Since decomposition events should be irreversible (i.e. not visible on the cooling or second heating curves), the reversing exotherm is tentatively assigned as disulfide cleavage (and reformation).

The dynamic mechanical analysis (DMA, discussed in more detail in Chapter 2, Section 2.3.3) profiles of EpxSS1 are shown in Figure 4.15.

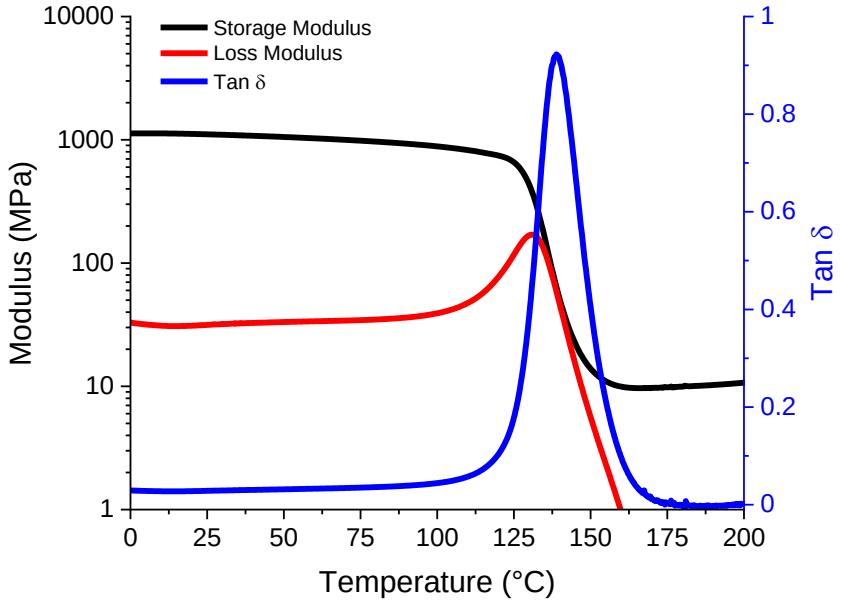

Figure 4.15. Representative single-cantilever DMA plots of EpxSS1 (1 Hz, 15 µm amplitude, 5 °C min^{-1}). Left axis: storage (black) and loss (red) moduli. Right axis: tan(δ) (blue). E''_{max} = 131 °C.

The onset of storage modulus is approximately 100 °C, in agreement with the T_g observed by DSC. The maximum of loss modulus is 131 °C, another measure of T_g as discussed in Chapter 2, which compares favourably with the DA CANs presented in that study (both DA1 and DA2 have loss maxima ~100 °C). This reflects a more densely crosslinked material, indicating that EpxSS1 is cured as expected. The storage modulus of EpxSS1 is presented again and compared with Ctrl1, Ctrl2 and DA1 in Figure 4.16.

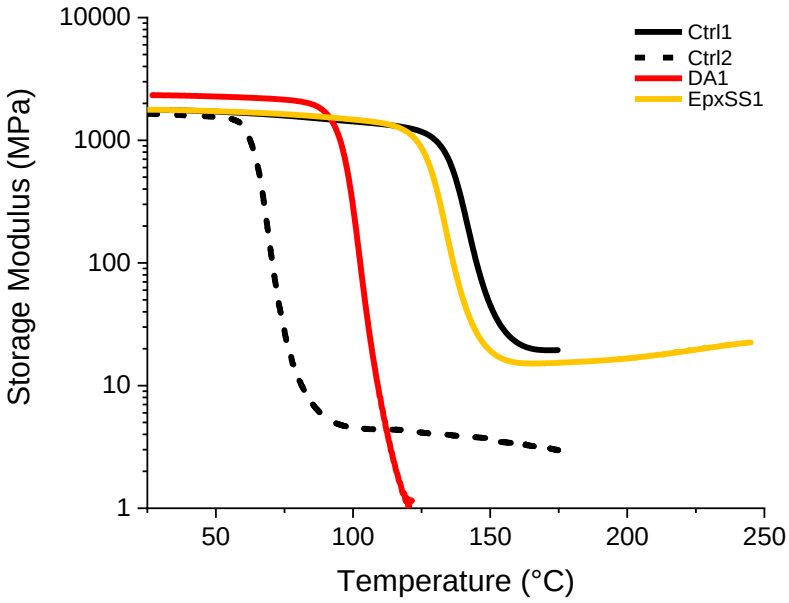

Figure 4.16. The storage moduli of EpxSS1, Ctrl1, Ctrl2 and DA1 (single-cantilever, 1 Hz, 15 μm amplitude, 5 °C min^{-1}).

From this figure, the similarity in behaviour between EpxSS1 and Ctrl1 is immediately apparent. The initial modulus at ~1750 MPa is essentially identical, indicating that the disulfides have no influence on stiffness at ambient temperatures. The onset of the rubbery transition is slightly decreased (~8 °C) by the presence of the disulfide moieties. This may simply reflect the increased rotational flexibility about the S–S bond relative to the $H_2C–CH_2$ unit, due to the absence of hydrogen atoms. However, this feature could also be a product of a disulfide exchange process—it has previously been reported that aromatic disulfides such as this are capable of dynamic processes even at room temperature, as long as the host polymer has sufficient flexibility (i.e. is in a rubbery state).[14] It may be that this exchange can happen at the early stages of the glass transition, but it is more likely that any exchange processes are restricted to higher temperatures (when the polymer is truly a rubber). Accordingly, the bond rotation argument seems more likely.

The residual (post-T_g) storage modulus of 15 MPa for EpxSS1 in the rubbery state is similar to the 20 MPa of Ctrl1, and notably larger than the 3 MPa of Ctrl2, which has much less residual stiffness due to the greatly reduced concentration of aromatic groups in its network structure. That there is any residual stiffness at all represents a marked difference from DA1, which melts after de-crosslinking. Indeed, this reflects highly contrasting behaviour between these two types of CAN. In contrast to the true de-crosslinking observed in DA CANs, as discussed in Section 4.1, it is widely accepted that the mechanism of disulfide exchange is *not* dissociative. Instead, the vast majority of disulfide units remain intact even at elevated temperature, only a few homolyse and lead to exchange via an associative, vitrimer-like process. Since this means these CANs are not capable of melting, their dynamic behaviour is not easily studied by rheology (as in Chapter 2). This makes DMA an even more valuable tool for the

characterisation of these materials. DMA-based stress-relaxation experiments are ideal for characterising the dynamic behaviour of associative CANs (vitrimers) such as EpxSS1. In these experiments, the specimens are deformed to a given strain at a given temperature and held isothermally for an extended period. This deformation induces a measurable stress. By comparing the relaxation time (the time required for the stress to be alleviated) at different temperatures, an Arrhenius plot can be made and an activation energy (E_A) corresponding to the exchange chemistry can be calculated—in polymers without dynamic chemistry, stress relaxation is greatly impeded. Indeed, this type of experiment was performed for this material by Ruiz de Luzuriaga *et al.*,[6] the results of which first led to the description of EpxSS1 as a vitrimer. In contrast, stress-relaxation isothermal DMA experiments are less appropriate for dissociative CANs because when these materials are activated, they melt and thus stress relaxation is near instantaneous.

To further explore the influence of disulfide bonds on the mechanical performance of epoxies, EpxSS1, Ctrl1 and Ctrl2 were subject to 3-point-bend (3pb) flexural testing (five specimens each). Representative stress-strain profiles are shown in Figure 4.17.

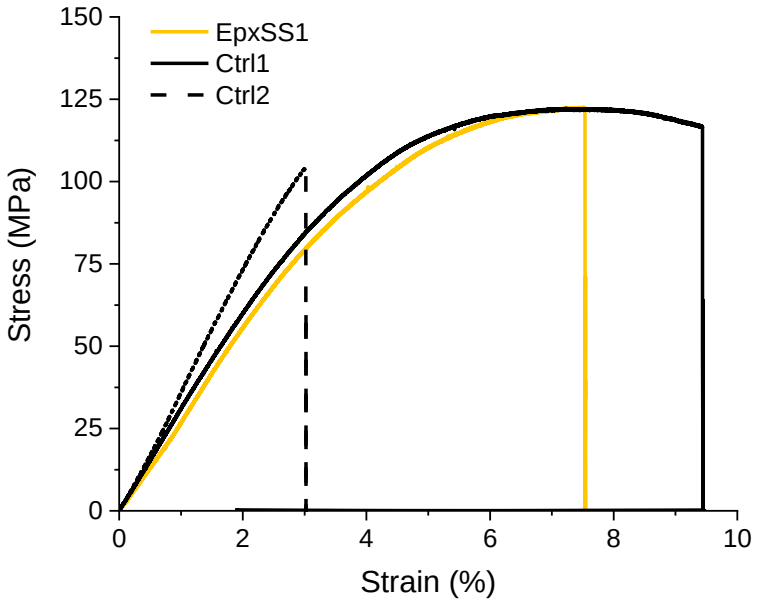

Figure 4.17. Representative stress-strain profiles of EpxSS1, Ctrl1 and Ctrl2.

The mean (± standard deviation) failure strength, tangent modulus and failure strain of EpxSS1, Ctrl1 and Ctrl2 are summarised as follows: ultimate flexural strength: 117.4 ± 3.0 MPa, 120.0 ± 3.6 MPa and 101.4 ± 6.4 MPa respectively; tangent flexural modulus: 2.78 ± 0.12 GPa, 3.03 ± 0.12 GPa and 3.74 ± 0.09 GPa respectively; flexural failure strain: 7.46 ± 1.17%, 9.27 ± 0.50% and 2.96 ± 0.30% respectively. From this data it is apparent that the disulfides themselves have a surprisingly limited effect upon mechanical performance as the tangent modulus and ultimate strengths of EpxSS1 and Ctrl1 are very

similar. It appears that EpxSS1 shares the same mechanism of plasticity as Ctrl1—shorter/longer conformations of the crosslinking unit—that was discussed in Chapter 2, Section 2.5.2 (Figure 2.50). This gives rise to the significant curvature of the stress-strain plots of these aromatic epoxies that is not observed from the aliphatic crosslinkers of Ctrl2. Seemingly the most significant difference between Ctrl1 and EpxSS1 is the ultimate failure strain. The average EpxSS1 specimen failed at >1% less strain than Ctrl1, this is likely a macroscopic product of the difference in bond strengths between S–S and C–C. At high strains, the polymer chains uncoil such that the individual crosslinking units are increasingly stretched into their most extended conformers. Eventually, at very high strains, all the crosslinking units are fully stretched (in their extended conformations) and at this point the load is increasingly channelled through those individual single bonds. At this stage, the difference in bond strength finally becomes significant and as a result the S–S bonds of EpxSS1 tolerate less extension than the C–C bonds of Ctrl1. Nevertheless, it is interesting that this does not translate into a significant decrease in strength. From this observation, we might expect that an analogous disulfide version of Ctrl2 would fail at both lower strength *and* strain, since it would not have the same plasticity mechanism to mitigate the bond strength difference.

From this study we can conclude that the inclusion of disulfides in thermoset polymers does not necessarily lead to a decrease in strength. If this observation translates to other weak linkages (e.g. Se–Se or DA crosslinks) this is of great significance; plasticity mechanisms may be designed into polymers to accommodate this.

4.4.2 Disulfide- and diselenide-crosslinked epoxies

The diselenides described in Section 4.3 have been used in small-scale polymerisation reactions to explore the viability of these materials in preparing CANs. The resultant polymers have then been characterised by FTIR, DSC and where possible, rheology. *Plans to characterise these polymers via DMA at the National Composites Centre (NCC) were curtailed due to the pandemic.*

EpxSeSe1 (epoxy diselenide 1) is the polymer formed by the reaction of the alkylamino diselenide, **APDS** with DGEBA, Scheme 4.15. As an alkyl amine, **APDS** should be highly reactive toward the epoxide groups of DGEBA and the resultant polymer should be more like Ctrl2 than any of the other epoxies discussed thus far.

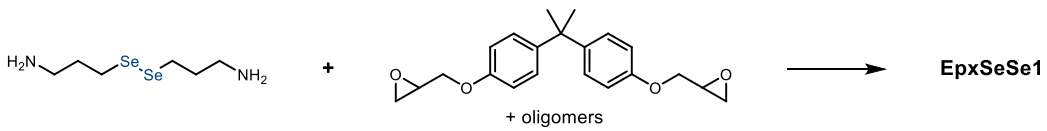

Scheme 4.15. EpxSeSe1.

Figure 4.18. EpxSeSe1, the epoxy produced from the reaction of **APDS** with DGEBA.

A sample of EpxSeSe1 (appearance shown in Figure 4.18) was milled into powder for further testing, though this proved challenging due to the high toughness of the material. This powder was then subject to DSC and FTIR analysis. Like EpxSS1, EpxSeSe1 was unable to melt and thus could not be analysed by rheometry. This indicates that the diselenides of this polymer bestow an associative-type CAN behaviour—this would be best characterised by DMA. Indeed, though the polymer did not melt, it is readily deformed out of shape when heated above T_g. The FTIR spectrum of EpxSeSe1, Figure 4.19, indicates a well-cured material. A small amount of residual epoxide remains, as evidenced by the weak absorbance at 916 cm^{-1}, but there is no evidence of amine bands overlaid with the broad hydroxyl peak at 3387 cm^{-1}. Nevertheless, it is possible that the weak absorbances at 1579 and 1606 cm^{-1} correspond to primary amine bending modes. Overall, this spectrum suggests that a longer cure would be advisable in future experiments.

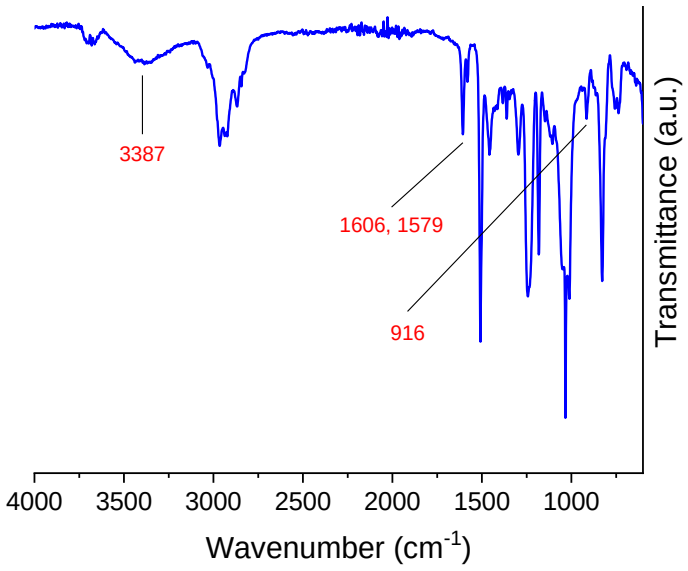

Figure 4.19. The FTIR spectrum of EpxSeSe1.

The DSC profile of the cured sample of EpxSeSe1 is broadly featureless, without even an obvious glass transition, hence its omission. Nonetheless, the absence of an exotherm agrees with the prior assessment of a relatively successful cure. The uncured profile is more informative: a representative heat-cool-heat is shown in Figure 4.20.

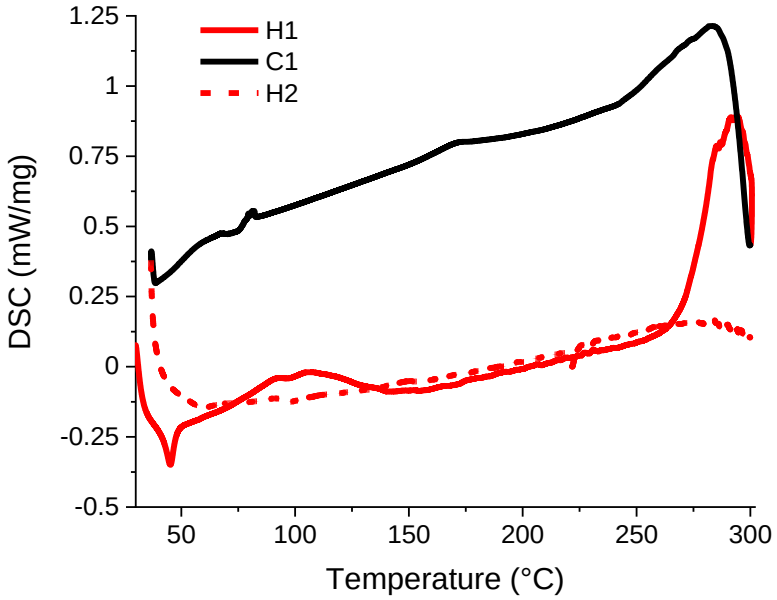

Figure 4.20. A heat-cool-heat of EpxSeSe1 between ambient and 300 °C (10 °C min^{-1}, exo up).

From this plot the amine-epoxy cure exotherm is readily observed as a broad peak centred around 100 °C. An endotherm is observed at lower temperature (45 °C), which likely represents a crystalline phase within **APDS** (which is broadly an oil at ambient temperature). It is possible that ultra-pure **APDS** is a low-melting solid, and that the impurities (principally the monoselenide) are otherwise preventing crystallisation. A large exotherm above 250 °C is likely indicative of thermal decomposition. As noted in Chapter 3, an artefact at ~100 °C during heating (and 80 °C during cooling) is observed of all DSC experiments performed on this machine at this time.

EpxSeSe2 (epoxy diselenide 2), the polymer formed by the reaction of the BOC-protected diselenide **BOCDS** with DGEBA, Scheme 4.16. Prior to attempting this synthesis, the thermal behaviour of the diselenide was investigated by DSC, Figure 4.21. Crucially, there are literature reports suggesting that BOC groups can be removed thermally.[64]

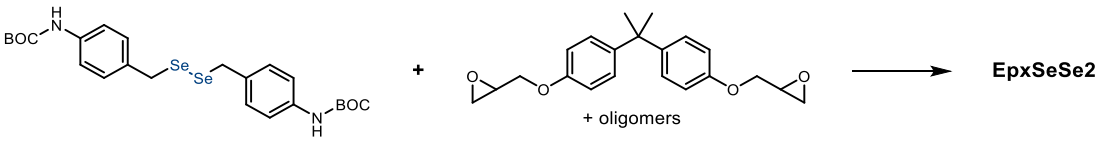

Scheme 4.16. The epoxy formed from reaction of BOC diselenide and DGEBA.

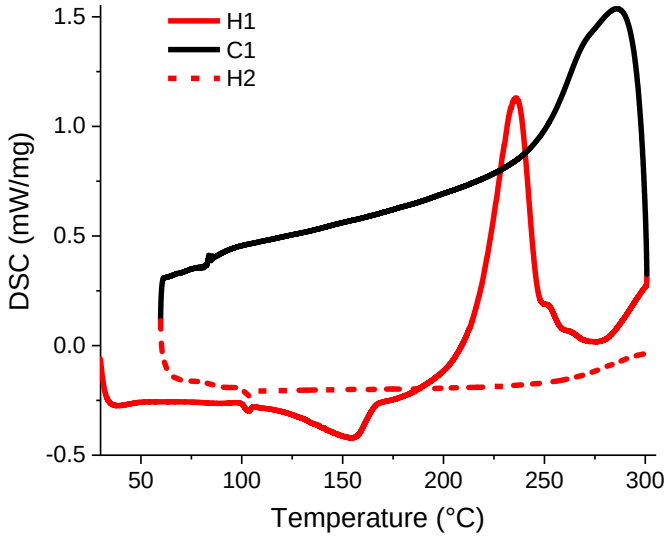

Figure 4.21. A representative heat-cool-heat of **BOCDS** between 30 and 300 °C (exo up, 10 °C min^{-1}).

A broad endothermic event representing the melt is visible between 110 and 160 °C, with peak (minimum) ~155 °C. At higher temperatures, a major exotherm dominates the plot, with onset around 175 °C and maximum at 230 °C. This certainly reflects a chemical reaction and the most likely process is the thermolysis of the BOC groups (loss of isobutene and CO_2). Towards 300 °C another change in heat capacity is evident, that appears to be exothermic and reversible, though at such a high temperature this may be decomposition. To confirm that the major exotherm is representative of BOC thermolysis, the ^{1}H NMR spectra of the material were compared before and after treatment at 210 °C (for 1 h). Unfortunately, after this treatment there was no ^{1}H NMR evidence of residual **BOCDS** or anything else that was soluble in $CDCl_3$ by ^{1}H NMR. This may be due to self-polymerisation; at such high temperatures, as the BOC groups are removed, the unprotected primary amine can presumably react with those carbamates which remain. However, it is also conceivable that this process is concomitant with thermal degradation. With this information considered, an initial cure temperature in the melting region is a sensible place to start the polymerisation. Despite these findings, a post-cure at high temperature (>220 °C) would still be required to form a *network* polymer; prior to the deprotection reaction, both DGEBA and **BOCDS** are difunctional and hence are only capable of forming linear chains. There is a chance that the desired epoxy-amine polymerisation may still occur, since the epoxides would be expected to be more electrophilic than the intact BOC carbamates.

Figure 4.22. EpxSeSe2, the epoxy produced from the reaction of **BOCDS** with DGEBA.

A sample of EpxSeSe2 (appearance shown in Figure 4.22) was milled into powder prior to FTIR and DSC analysis. As with EpxSeSe1, EpxSeSe2 also did not melt and so could not be tested with rheology. DMA stress relaxation experiments would be required to probe for CAN-type behaviour. The FTIR spectrum of EpxSeSe2 is shown in Figure 4.23.

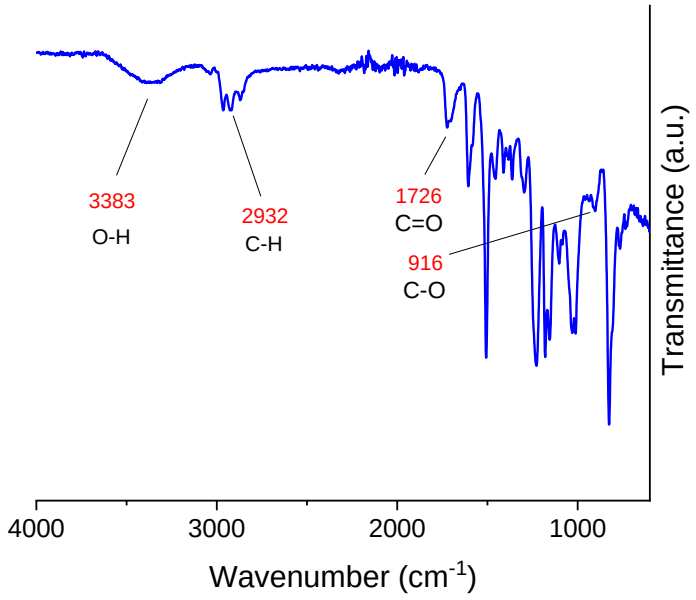

Figure 4.23. The FTIR spectrum of EpxSeSe2.

In contrast to EpxSeSe1, there is no evidence of residual epoxide in the FTIR spectrum of EpxSeSe2. There is similarly little evidence of residual secondary amine; however, arguably the most significant region is the carbonyl region which is contrasted with neat **BOCDS** in Figure 4.24.

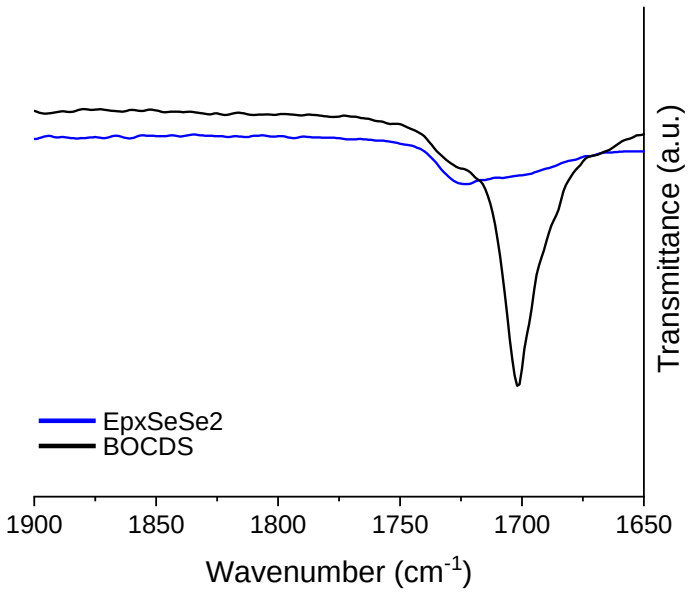

Figure 4.24. The FTIR carbonyl stretching region of EpxSeSe2 and **BOCDS**.

The absence of a significant carbonyl stretch indicates that the *in situ* deprotection of the diselenide (during cure) was successful. This is indicated visually by the porous nature of the product polymer, evidence of the evolution of CO_2 and isobutene. This suggests that boc-protected amines can function as epoxy crosslinkers. The DSC of uncured EpxSeSe2 is shown in Figure 4.25. This DSC profile is essentially the same as that of neat **BOCDS** (Figure 4.21)—like EpxSeSe1, the cured profile is essentially featureless, which indicates successful cure.

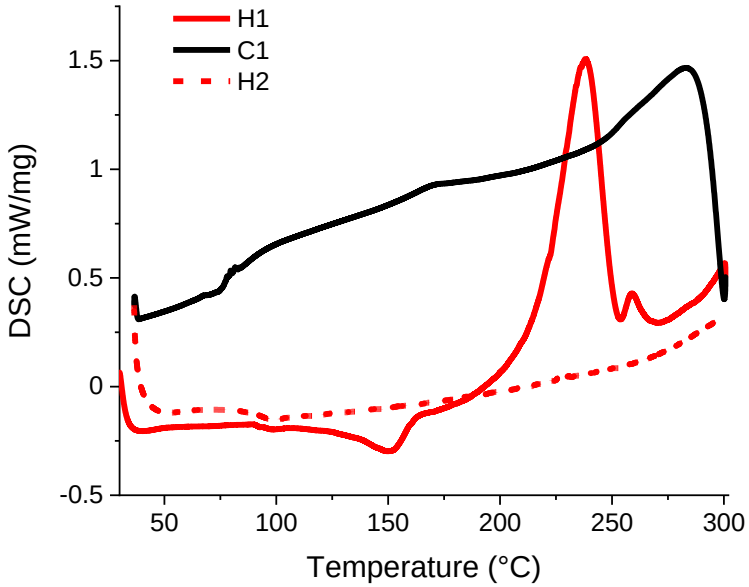

Figure 4.25. A representative DSC profile of uncured EpxSeSe2 between ambient and 300 °C (10 °C min^{-1}, exo up).

The fact that the DSC profile and more specifically, the size, shape and position of the major exotherm of EpxSeSe2 is almost identical to neat **BOCDS**, indicates one of two probable scenarios. (1) There is

little or no reaction between the diselenide and the epoxides, which would mean that the epoxy polymerised via self-reaction (since no residual epoxide is evident by FTIR spectroscopy). (2) There is no reaction between the secondary amine and epoxide but instead there is concomitant deprotection and primary amine-epoxide reaction (such that there is no distinction in DSC exotherm). Since, by FTIR, there is no evidence of residual secondary amine in the cured spectrum (Figure 4.26), the latter explanation seems more likely.

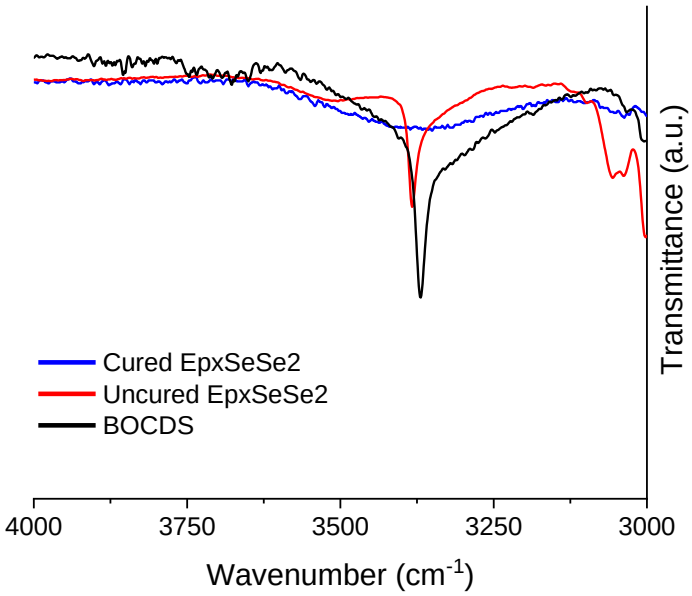

Figure 4.26. The FTIR spectrum (3000–4000 cm^{-1}) of uncured and cured EpxSeSe2 compared with neat **BOCDS**.

From this we can tentatively conclude that **BOCDS** has utility as a latent epoxy curative: the compound can successfully crosslink epoxies but only does so at greatly elevated temperature (220 °C) when the protecting groups are lost. Whether or not the diselenide bonds remain intact after these curing conditions is uncertain and not easily confirmed. Looking for dynamic behaviour (by DMA) would be one such method of confirmation.

EpxSeSe3 (epoxy diselenide 3), is the polymer formed by the reaction of the carboxylic acid diselenide **CDS** with DGEBA, Scheme 4.17. Inspired by the work of Chen *et al*.[8] and Altuna *et al*.,[65,66] this polymer uses carboxylic acids and an organic base catalyst to harden the epoxy in a similar fashion to epoxy-anhydride cure. Since the diselenide is difunctional, citric acid is added to ensure that a network is formed. TBD (triazabicyclodecene, 5 wt%) was chosen as a high-melting (>125 °C) catalyst with a known capacity for catalysing transesterification. By creating a network of ester linkages with many free hydroxyl groups and a reasonable catalyst loading, this polymer should be capable of undergoing two independent dynamic chemical processes: transesterification and diselenide exchange.

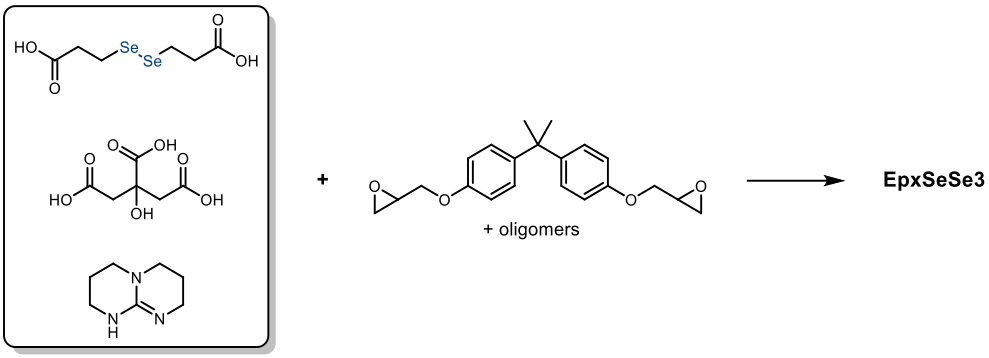

Scheme 4.17. The components of EpxSeSe3: 3,3'-diselanediyldipropionic acid (**CDS**, 0.85 eq.), citric acid (0.09 eq.), 1,5,7-triazabicyclo[4.4.0]dec-5-ene (TBD, 5 wt%) and DGEBA (1 eq.).

Figure 4.27. EpxSeSe3, the polymer produced from the reaction of DGEBA (10.5 epoxy equivalents), **CDS** (9.0 acid equivalents) and citric acid (1.5 acid equivalents) with 5 wt% TBD as catalyst.

A sample of EpxSeSe3 (a black, glassy solid, Figure 4.27) was milled into powder for subsequent testing by FTIR, DSC and rheology. In contrast to the other diselenide-containing epoxies described above, the polymer powder was capable of melting akin to the Diels-Alder CANs of Chapters 2 and 3. This may be a result of the relatively low crosslinking density. The molar ratio of citric acid to **CDS** is 1:4 and so on average, only every fifth unit has connectivity greater than two (i.e. network forming). Alternatively, the melt could be a result of the combination of the two different dynamic chemistries (Se–Se metathesis and transesterification) and a low T_g. Since there are no aromatic groups present in the linker structures, the polymer is likely to exhibit a relatively modest stiffness. Combined with a modest crosslink density, the low stiffness would be expected to yield a low T_g. Because glass transition is such a significant factor in determining the onset temperature of dynamic chemistry within polymers, the presence of a low T_g with these chemistries means that this polymer should have a highly dynamic topology.

The FTIR spectrum of EpxSeSe3 is shown in Figure 4.28 and compared with **CDS**. Importantly, there is no evidence of residual epoxide (no band at 915 cm^{-1}) in the cured polymer. Similarly, the major carbonyl stretch of **CDS** (1693 cm^{-1}) is also absent, with the only absorbances in this region at 1606 and 1590 cm^{-1}. It seems probable that these absorptions correspond to the esters formed by reaction of the acid groups with the epoxides, though these signals are weak and at the low end of the expected region.

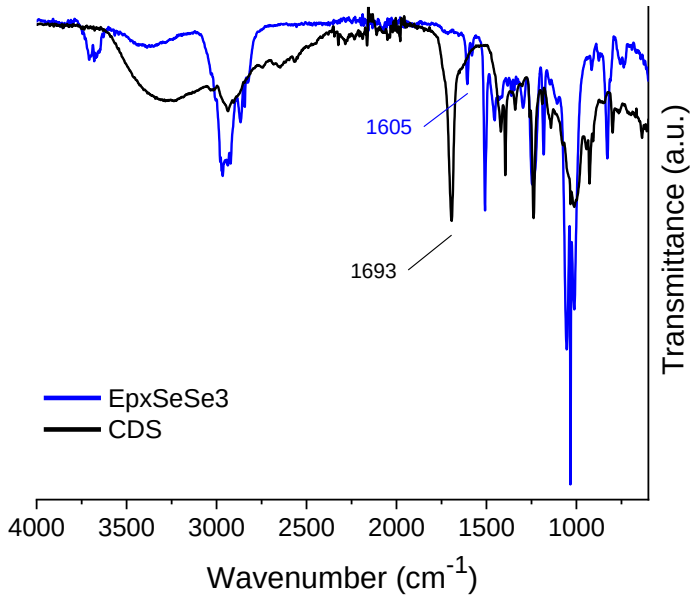

Figure 4.28. The FTIR spectra of EpxSeSe3 and **CDS**, with carbonyl stretches labelled.

A heat-cool-heat DSC curve of uncured EpxSeSe3 is shown in Figure 4.29. The analogous cured curve is featureless except for the endotherm at 223 °C which is also observed in the second heating curve of the 'uncured' sample. The first heating cycle is dominated by two distinct exotherms, one at 115 °C and the other at 255 °C. The former has an additional shoulder at around 150 °C, which could represent a separate process. The first exotherm likely corresponds to the desired epoxy-acid reaction. A plausible explanation for the shoulder is that this corresponds the citric acid–epoxy reaction, whereas the major peak corresponds to the reaction between epoxide and CDS.

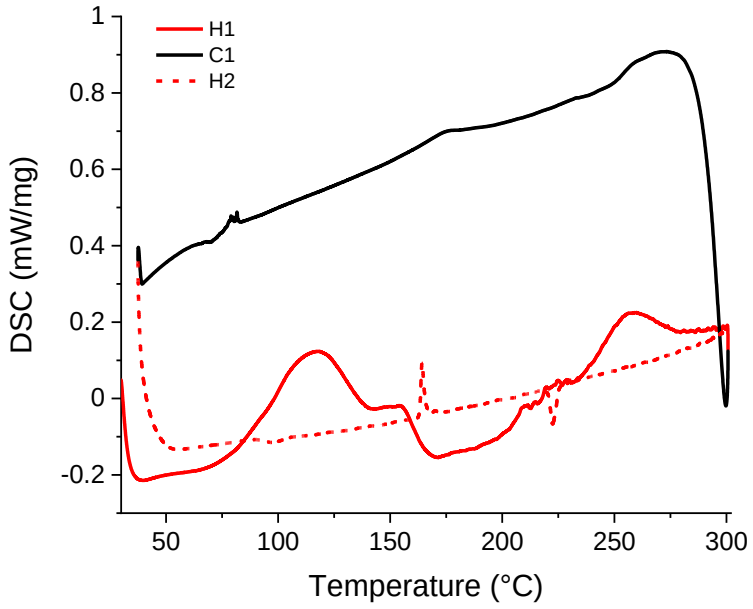

Figure 4.29. A representative heat-cool-heat of uncured EpxSeSe3 between 30 and 300 °C, exothermic up.

The significance of the latter exotherm is less obvious. Since it is such a high-temperature process, it is probable that this is a decomposition event. Since this second exotherm is not observed within the same temperature range of the analogous disulfide, *vide infra*, the most likely explanation is diselenide decomposition. This latter exotherm also has a possible shoulder peak at around 220 °C which is probably a related decomposition process. From this curve it is fair to conclude that a cure temperature of 150 °C would be sufficient (180 °C was used), and that the polymer is probably unstable above 200 °C—thermogravimetric analysis could be used to confirm this.

The second heating cycle (dashed curve) of EpxSeSe3 exhibits two features which were not present in the original cycle: a sharp exotherm at 164 °C and a sharp endotherm at 223 °C. The exotherm was not visible in any of the '180 °C cured' experiments (not shown), which indicates that this is a product of the high temperature exotherm of the initial heating cycle (and/or the subsequent cooling). The shape of this exotherm suggests that it could be a crystallisation process—citric acid has a melting point of 153 °C and since 3,3'-dithiopropionic acid has a melting point of 155 °C, it seems probable that **CDS** is similar. Ergo, this exotherm could be crystallisation of a small quantity of either compound (suggesting incomplete conversion). In contrast, the sharp endotherm observed at 225 °C is also visible in the first heating cycle of the cured material. This is most likely a melting event; due to the high temperature, this probably corresponds to the melt of a crystalline polymeric phase (and not either of the starting acids).

The dynamic viscosity of EpxSeSe3 was investigated by rheology, Figure 4.30. In contrast to the DA polymer of Chapters 2 and 3, there is no viscosity plateau at low temperatures (and subsequent steep

decline in viscosity) which is associated with the 'switching on/off' of the dynamic chemistry. However, this could also be due to the relatively high temperature minima, in this case ~75 °C, generally the DA polymers were tested down to 60 °C. The sharp increases in viscosity at the viscosity minima (temperature maxima) are probably experimental artefacts rather than representative of real phenomena. The most likely explanation is incomplete coverage/contact of the polymer with the geometry (i.e. the measuring plate).

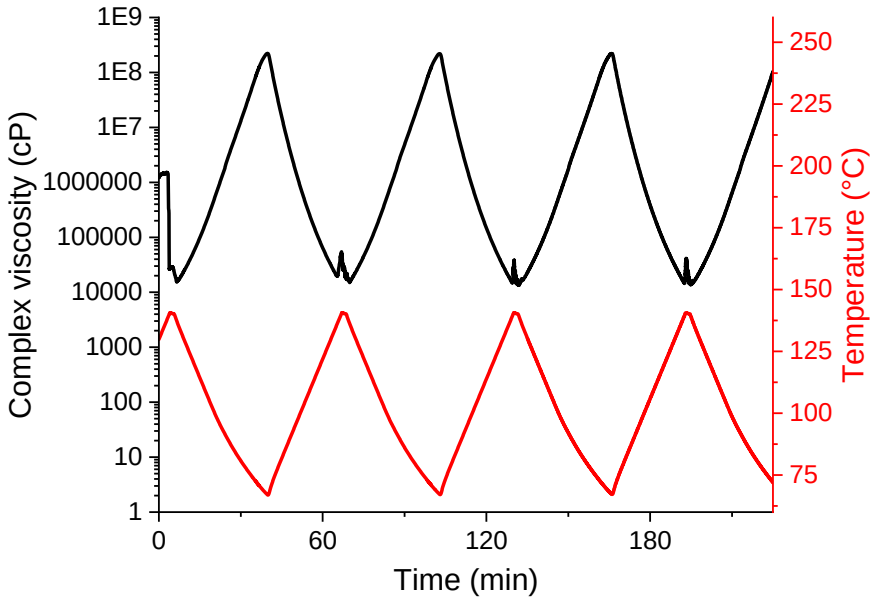

Figure 4.30. The dynamic viscosity behaviour of EpxSeSe3 between 70 and 140 °C (parallel plate, 1% oscillatory strain, 1 Hz).

EpxSS2 (epoxy disulfide 2, Scheme 4.18) is the analogous disulfide-containing polymer to EpxSeSe3. This polymer uses carboxylic acids and an organic base catalyst to harden the epoxy. Since the disulfide is difunctional, citric acid is added to ensure that a network is formed. In this case, both transesterification and disulfide exchange should be accessible as independent dynamic chemistries.

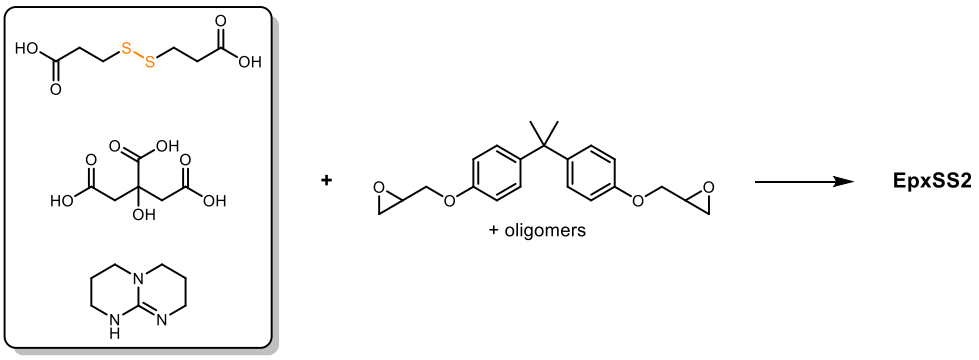

Scheme 4.18. The components of EpxSS2: 3,3'-dithiopropionic acid (0.85 eq.), citric acid (0.09 eq.), 1,5,7-triazabicyclo[4.4.0]dec-5-ene (TBD, 5 wt%) and DGEBA (1 eq.).

Figure 4.31. EpxSS2, the epoxy produced from the reaction of DGEBA (10.5 epoxy equivalents), 3,3'-dithiopropionic acid (9.0 acid equivalents), citric acid (1.5 acid equivalents) and 5 wt% TBD as catalyst.

A sample of EpxSS2 (appearance shown in Figure 4.31) was milled into powder prior to further testing. Unsurprisingly, like EpxSeSe3, this polymer was also capable of melting. Again, the ability to melt is likely a product of the combination of the two dynamic chemistries (transesterification and disulfide exchange) and the moderate crosslink density. The FTIR spectrum of EpxSS2 is essentially identical to EpxSeSe3, with only slight differences in intensity, for this reason the graph is not reproduced here. We can conclude that from the loss or shift of carbonyl absorbances, and the lack of a residual epoxide absorbance, that the polymer is well-cured, as confirmed by DSC. A representative heat-cool-heat of the 'uncured' resin is shown in Figure 4.32. The profile of the cured polymer (not shown) is featureless except for the presence of a glass transition superimposed on a small melting endotherm at 60 °C. This corroborates the FTIR data which suggested the curing regime was sufficient.

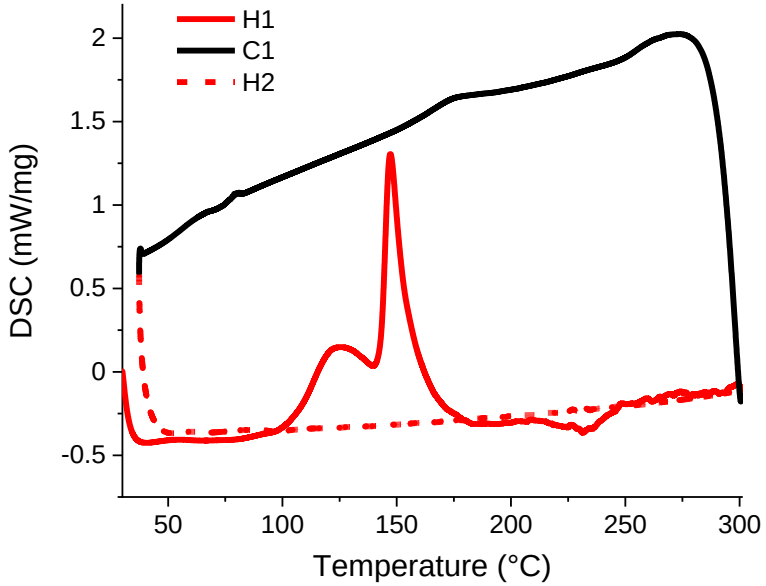

Figure 4.32. A representative heat-cool-heat of uncured EpxSS2 between 30 and 300 °C, exo up.

The DSC profile of EpxSS2 is substantially different to the analogous diselenide-containing polymer. In the first heating curve of the SS polymer there are two exotherms around 125 °C, though in the diselenide the second was a shoulder. This may suggest that the ~125 °C exotherm corresponds to the citric acid-epoxy reaction and that the ~150 °C exotherm corresponds to the SS/SeSe-epoxy reaction, since the size and shape of this exotherm is so different. At approximately 225 °C there is a suggestion of an endotherm—which may correspond to the dynamic chemistry. Beyond this, there are no further features and no evidence of decomposition. The second heating curve is completely featureless, in contrast to EpxSeSe3.

The dynamic viscosity of EpxSS2 was explored by rheology, Figure 4.33. As with EpxSeSe3, there is no evidence of a viscosity plateau at low temperatures, though again this could be due to the temperatures involved. Accordingly, it is not obvious if the melt is a product of dynamic chemistry. Stress-relaxation experiments could be used to help confirm this. In any case, both epoxies are highly fluid at 120 °C and so may be processible in a similar fashion to the DA CANs of Chapters 2 and 3.

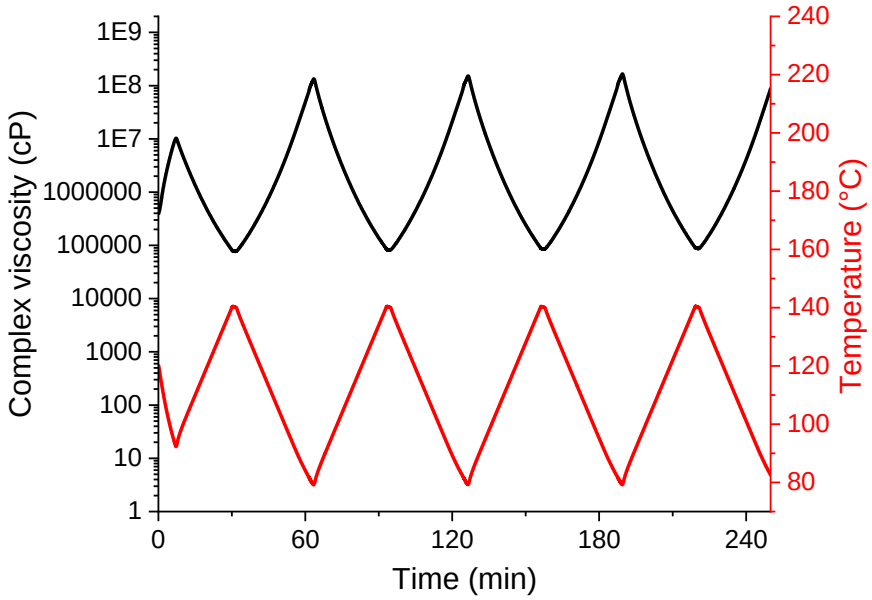

Figure 4.33. The dynamic viscosity behaviour of EpxSS2 between 70 and 140 °C (parallel plate, 1% oscillatory strain, 1 Hz).

4.5 Summary

In this chapter, the solution metathesis of diselenides was tested under ambient conditions. In contrast to literature reports, ambient lighting was found to be sufficient to induce exchange. As expected of a radical-mediated process, the exchange reaction was greatly inhibited by the presence of a radical scavenger (TTBP). Four new functional diselenide crosslinkers were prepared and characterised. One of these diselenides, the BOC-protected species showed potential as a latent curing agent; i.e. it is only reactive at high temperatures. Challenges in diselenide characterisation, both by

^{77}Se NMR and mass spectrometry were overcome by compensating for long (longitudinal) relaxation times (~30 s) and through the use of APCI, respectively. A variety of deprotection conditions were tested for the chemical removal of the BOC-protected diselenide, though no suitable process was identified which both removed the group and retained the integrity of the Se–Se bond.

For a benchmark study, the disulfide CAN reported by Odriozola and co-workers[6] (EpxSS1) was prepared. This polymer was then compared with control epoxies (Ctrl1 and Ctrl2) to examine the precise contribution of the S–S bond weakness to mechanical performance. Surprisingly, the disulfide had relatively little impact on modulus or strength at low strain (<5%). Only at higher strain values did the EpxSS1 and Ctrl1 differ significantly, with the disulfide-containing epoxy failing at lower strain (7.46 ± 1.17% *vs*. 9.27 ± 0.50%). However, the ultimate strengths of both materials were very similar (117.4 ± 3.0 MPa, 120.0 ± 3.6 MPa). Both materials were capable of significant plastic deformation due to the capacity of the aromatic crosslinkers to undergo conformational changes. This study indicates that such design features could prove useful in compensating for the inclusion of weak bonds in structural materials. In contrast to the dissociative DA CANs of Chapters 2 and 3, this disulfide CAN is associative and much more densely crosslinked. Accordingly, this polymer does not melt and is better characterised through DMA than rheology.

A series of preliminary experiments in preparing new disulfide and diselenide CANs via epoxy chemistry were then introduced. EpxSeSe1 may be one of the first examples of a diselenide CAN. DSC and FTIR data indicated its successful cure; however, DMA stress-relaxation experiments should be performed to confirm the expected CAN behaviour. A comparison of disulfide- and diselenide-containing polymers revealed that diselenide polymers appear to undergo thermal decomposition in the 200–250 °C region and are thus less thermally stable than their sulfur analogues. The next steps with these materials will be discussed in Chapter 6: Conclusions and future work.

Due to pandemic restrictions and limited access to laboratory equipment, associated with COVID-19, DMA experiments with the new disulfide/diselenide polymers have not been performed.

4.6 Experimental

General considerations

All diselenide-forming reactions were performed under an inert atmosphere of dry nitrogen using standard Schlenk technique. Dry Et_2O was collected from a Grubbs-type solvent purification system and deoxygenated using the freeze-pump-thaw method. Dry DMF was stored over 4 Å molecular sieves for at least 24 h prior to use and degassed by sparging with N_2. Ethanol was deoxygenated by sparging with N_2 for at least 30 min immediately prior to use. Deionised (DI) water was collected from a millipore dispenser system immediately prior to use. Selenium, di-*tert*-butyl dicarbonate, 4-aminobenzylalcohol, 3-bromopropionic acid, 3-chloropropylamine hydrochloride, ethyl acetate, hexane, petroleum ether, diethyl ether, magnesium sulfate, $NaHCO_3$, NaCl and NaOH were purchased from Alfa Aesar and used as received. Phosphorus tribromide was purchased from Alfa Aesar and stored in a Young's flask under a blanket of nitrogen. NaH powder was purchased from Sigma-Aldrich (Merck) and stored in an Argon dry box. Sodium borohydride, 1-bromobutane, ethanol, DMF, bromobenzene and 4-hydroxyphenylethyl bromide were purchased from Sigma-Aldrich and used as received unless stated otherwise.

NMR experiments were performed on either a Jeol ECS300, Jeol ECS400, Bruker Nano400, Varian ECZ400 or Varian 500 VNMRS spectrometers. $^{77}Se\{^1H\}$ spectra were referenced to an external standard of pure diphenyl diselenide, note that extensive experimentation was required to observe all of the diselenide resonances with this technique, as detailed in Section 4.3. MS experiments were performed by the University of Bristol Mass Spectrometry Service using either a Thermo Scientific Orbitrap Elite (APCI, LC-Orbitrap), Bruker micrOTof II (ESI, TOF) or Waters Synapt G2S (Nanospray, IMS-Q-TOF). FTIR experiments were performed using a Perkin Elmer Spectrum Two (solid state).

Note: 'ambient temperature', 'room temperature' or 'RT' corresponds to approximately 20 °C (293 K) throughout this chapter.

A description of the 'extraction train process' used to separate products from DMF is outlined under the 'extraction protocol for polar solvents' page of the 'Not Voodoo' website (Dr P. G. Hultin, University of Manitoba).[67] Last date of access: 19/03/21.

Dibutyl diselenide, $[BuSe]_2$

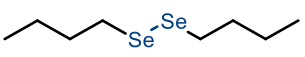

Selenium (1.00 g, 12.7 mmol) and NaH (334 mg, 13.9 mmol) powders were added to a Schlenk flask equipped with a magnetic stirrer while in an Argon dry box. Anhydrous DMF (10 ml) was then added, and the mixture stirred for 5 min, yielding a grey-black suspension. The reaction was heated to 70 °C for 2 h and then cooled to RT, resulting in a brown-black solution of

[Se_2]Na_2. The reaction vessel was then cooled to 0 °C and a solution of 1-bromobutane (1.37 ml, 12.7 mmol) in anhydrous DMF (10 ml) was added dropwise. The reaction was then allowed to warm to room temperature, having turned moss green and gradually becoming orange after stirring for a further 2 h. The crude product was isolated via Et_2O extraction (3 x 40 ml). The combined organic phases were dried over $MgSO_4$ and then filtered. The ether was removed under vacuum to yield [BuSe]$_2$ as a foul-smelling orange oil (1.45 g, 83% yield). ^{1}H and ^{77}Se spectroscopy revealed contamination with monoselenide, triselenide and tetraselenide (~18% combined). Attempts to separate these impurities via chromatography were unsuccessful. ^{1}H NMR ($CDCl_3$, 400 MHz) (δ, ppm): 2.91 (m, 4H, SeC*H*$_2$), 1.71 (m, 4H, SeCH$_2$C*H*$_2$), 1.42 (m, 4H, C*H*$_2$CH$_3$), 0.93 (m, 6h, C*H*$_3$). ^{77}Se{^{1}H} NMR ($CDCl_3$, 76 MHz) (δ, ppm): +308.0 (s).

Dipropionic acid diselenide, CDS

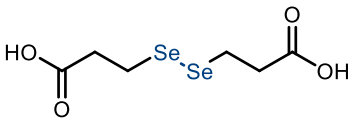

Selenium (2.50 g, 31.7 mmol) and sodium borohydride (2.40 g, 63.4 mmol) were added to a Schlenk flask. After cooling to 0 °C, freshly N_2-sparged EtOH (60 ml) was added carefully and, to prevent over-pressurisation, a vent needle was used. The reaction mixture was allowed to warm to RT, forming a pale grey solution of Na_2Se. After 5 min, a second batch of Selenium (2.50 g, 31.7 mmol) was added and washed into the mixture with additional EtOH (20 ml) resulting in a dark red-brown mixture, which indicated the presence of Na_2Se_2. The reaction was then brought to the boil and allowed to return to ambient temperature. To this Na_2Se_2 solution, 3-bromopropionic acid (9.17 g, 6.20 ml, 60 mmol) was added and the reaction left to stir for 3 h, forming a bright yellow suspension. The solvent was then removed in vacuo and the residue extracted from DI water (150 ml) using EtOAc (4 x 50 ml). The combined organic fractions were washed with brine (2 x 40 ml) and then dried over $MgSO_4$. The solvent was removed via heating (60 °C) *in vacuo*, yielding **CDS** as a pale-yellow powder (8.02 g, 88% yield). ^{1}H NMR (DMSO-D6, 300 MHz) (δ, ppm): 12.34 (bs, 2H, COO*H*), 3.01 (t, 4H, $^3J_{HH}$ = 7.05 Hz, (CO)C*H*$_2$), 2.67 (t, 4H, $^3J_{HH}$ = 6.98 Hz, SeC*H*$_2$). ^{77}Se{^{1}H} NMR (DMSO-D6, 57 MHz) (δ, ppm): +316.2 (s). FTIR ν(CO)/cm^{-1}: 1693. HR-MS (APCI-): *m/z* calculated for $C_6H_{10}O_4Se_2$ [M-H]$^-$ = 304.8826, obs. = 304.8832.

Diaminopropyl diselenide, APDS

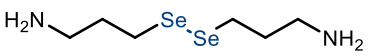

Selenium (10.00 g, 126 mmol) and sodium borohydride (4.80 g, 127 mmol) were added to a Schlenk flask. After cooling to 0 °C, freshly N_2-sparged EtOH (140 ml) was added carefully and, to prevent over-pressurisation, a vent needle was used. The reaction mixture was then allowed to warm to room temperature resulting in a deep dark red solution of Na_2Se_2. In a separate Schlenk flask equipped with a magnetic stirrer, 3-chloropropylamine hydrochloride (16.38 g,

126 mmol) and NaOH (5.04 g, 126 mmol) were partially dissolved in an EtOH (75 ml) and DI water (10 ml) mixture. After both reaction mixtures had stirred for 1 h, the 3-chloropropylamine suspension was added to the solution of sodium diselenide, and the residue washed in with a further 100 ml of EtOH (5 x 20 ml), affording a red-orange suspension. The reaction was then heated to reflux and left stirring for 24 h. After the mixture was allowed to cool to ambient temperature, the reaction solvent was removed under reduced pressure. The brown residue was then extracted from DI water (150 ml) using CH_2Cl_2 (3 x 80 ml). The combined organic fractions were washed with brine (2 x 50 ml), dried over $MgSO_4$ and then concentrated under reduced pressure affording **APDS** as a foul-smelling dark brown oil (4.76 g, 29% yield). ^{1}H and ^{77}Se spectroscopy revealed contamination with monoselenide, triselenide and tetraselenide (~8% combined). ^{1}H NMR ($CDCl_3$, 400 MHz) (δ, ppm): 2.93 (t, 4H, $^3J_{HH}$ = 7.32 Hz, H_2NCH_2), 2.76 (t, 4H, $^3J_{HH}$ = 6.79 Hz, $SeCH_2$), 1.84 (m, 4H, $CH_2CH_2CH_2$). ^{77}Se{^{1}H} NMR ($CDCl_3$, 57 MHz) (δ, ppm): +309.6 (s). HR-MS (APCI+): *m/z* calculated for $C_6H_{16}N_2Se_2$ $[M+H]^+$ = 276.9717, obs. = 276.9713.

Diethylphenol diselenide, PEDS

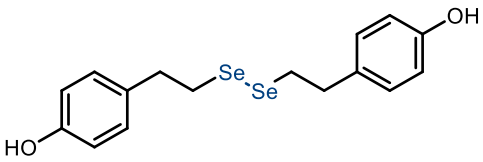

Selenium (3.95 g, 50 mmol) and sodium borohydride (2.05 g, 54 mmol) were added to a Schlenk flask. After cooling to 0 °C, freshly N_2-sparged EtOH (100 ml) was added carefully and, to prevent over-pressurisation, a vent needle was used. The reaction mixture was then allowed to warm to room temperature resulting in a deep dark red solution of Na_2Se_2. In a separate Schlenk flask equipped with a magnetic stirrer, 4-hydroxyphenylethyl bromide (10 g, 50 mmol) was dissolved in EtOH (80 ml). After the Na_2Se_2 solution had stirred for 2 h, the organobromide solution was added to it, resulting in a yellow-orange mixture. After 2.5 h the reaction was stopped, and the solvent removed under reduced pressure. The resultant pale-yellow residue was then extracted from brine (100 ml) with CH_2Cl_2 (2 x 80 ml). The combined organics were then washed with a further 80 ml brine prior to drying over $MgSO_4$. The CH_2Cl_2 was then removed *in vacuo* affording the crude product as a pale yellow solid (9.01 g, 45% yield). Contaminant selenol (identified by ^{1}H NMR) was allowed to oxidise to diselenide in air for 3 months. Pure **PEDS** (2.44 g, 12% yield) was isolated as yellow hedgehog-type crystals after a combination of column chromatography (60:40 hexane:EtOAc) and recrystallisation ($CHCl_3$). ^{1}H NMR (DMSO-D6, 300 MHz) (δ, ppm): 9.23 (bs, 2H, O*H*), 7.01 (m, 4H, (HO)CC*H*), 6.67 (m, 4H, Ar*H*), 3.10 (t, 4H, $^3J_{HH}$ = 7.66 Hz, $SeCH_2$), 2.86 (t, 4H, $^3J_{HH}$ = 7.69 Hz, $ArCH_2$). ^{77}Se{^{1}H} NMR (DMSO-D6, 95 MHz) (δ, ppm): +301.5 (s). HR-MS (APCI-): *m/z* calculated for $C_{16}H_{18}O_2Se_2$ $[M+Cl]^-$ = 436.9332, obs. = 436.9320.

_p_-BOC-benzyl alcohol

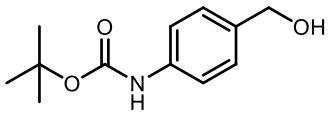

4-aminobenzyl alcohol (5.00 g, 40.6 mmol) and di-*tert*-butyl dicarbonate (8.86 g, 40.6 mmol) were added to a round-bottom flask. The flask was fitted to a rotary evaporator and heated under vacuum at 80 °C until the effervescence stopped (~45 min). The flask was allowed to cool to RT affording *p*-Boc-benzyl alcohol as a copper-brown oil (9.00 g, >99% yield). ^{1}H NMR ($CDCl_3$, 300 MHz) (δ, ppm): 7.29 (m, 4H, Ar*H*), 6.52 (bs, 1H, N*H*), 4.62 (d, 2H, $^{4}J_{HH}$ = 4.1 Hz, ArCH_2), 1.52 (s, 9H, CH_3). In agreement with literature data.[54]

_p_-BOC-benzyl bromide

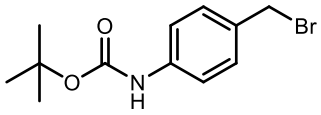

p-Boc-benzyl alcohol (9.00 g, 40.6 mmol) was added to a Schlenk flask and then dissolved in Et_2O (60 ml). The resultant brown solution was then cooled to 0 °C and the flask wrapped in aluminium foil. Phosphorus tribromide (1.54 ml, 4.39 g, 16 mmol) was then added dropwise, turning the solution pale yellow. The reaction mixture was left stirring in the dark for 2 h. Thereafter, the reaction mixture was poured into a combination of brine (50 ml) and saturated aqueous $NaHCO_3$ solution (50 ml). The layers were separated and then the aqueous phase was further washed with CH_2Cl_2 (2 x 60 ml). The combined organic phases were dried over $MgSO_4$ and then filtered to remove the solids. The solvents were removed under reduced pressure yielding *p*-Boc-benzyl bromide as an off-white powder (7.76 g, 67% yield). ^{1}H NMR ($CDCl_3$, 400 MHz) (δ, ppm): 7.32 (m, 4H, Ar*H*), 6.52 (bs, 1H, N*H*), 4.48 (s, 2H, ArCH_2), 1.52 (s, 9H, CH_3). In agreement with literature data.[68]

Diboc diselenide, BOCDS

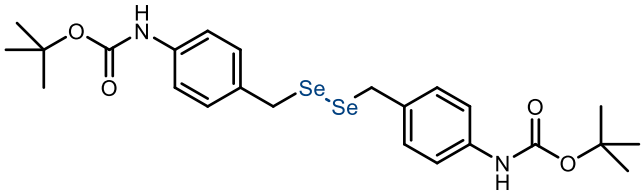

Selenium (1.72 g, 21.8 mmol) and sodium hydride (576 mg, 24.0 mmol) were added to a Schlenk flask while in an Argon dry box. The solids were dissolved in DMF (30 ml), yielding a grey-black suspension. The reaction mixture was heated to 70 °C and left to stir for 2 h. The resultant dark solution of Na_2Se_2 was allowed to cool to RT and then a solution of *p*-BOC benzyl bromide (6.24 g, 21.8 mmol) in DMF (50 ml) was added slowly. The orange-green-brown suspension was left to stir for 3 h, becoming a dark green suspension. The crude reaction mixture was poured into brine (150 ml) and the crude product isolated from DMF by use of an Et_2O-extraction-train in three separating funnels (1 x 160 ml, 2 x 80 ml Et_2O). An 80 ml brine wash was passed through each funnel consecutively and the process repeated four times (5 x 80 ml washes total). The combined organic phases were dried

over $MgSO_4$ and then filtered. The solvent was removed under reduced pressure yielding crude **BOCDS** as a yellow powder (5.32 g, 86% yield). Analytically pure **BOCDS** was successfully isolated as yellow crystals (1.3 g, 21% yield) after a combination of column chromatography (75:25 hexane:EtOAc) and recrystallisation from EtOH. ^{1}H NMR ($CDCl_3$, 400 MHz) (δ, ppm): 7.28 (m, 4H, Ar*H*), 7.14 (m, 4H, Ar*H*), 6.46 (bs, 2H, N*H*), 3.82 (s + sat., 4H, $^2J_{SeH}$ = 14.6 Hz, SeCH_2), 1.51 (s, 18H, CH_3). ^{77}Se{^{1}H} NMR ($CDCl_3$, 57 MHz) (δ, ppm): +453.9 (s). HR-MS (APCI+): *m/z* calculated for $C_{24}H_{32}N_2O_4Se_2$ $[M+H]^+$ = 573.0765, obs. = 573.0743.

Dibenzyl diselenide, $[BnSe]_2$

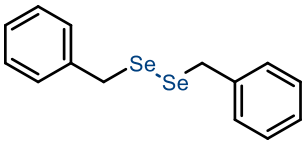

To a flame dried Schlenk flask equipped with magnetic stirrer, Selenium (2.00 g, 25.3 mmol) and sodium hydride (670 mg, 27.9 mmol) were added while in an Argon dry box. The solids were then dissolved in DMF (30 ml), yielding a grey-black suspension. The reaction mixture was heated to 70 °C and left to stir for 2.5 h. The resultant dark solution of sodium diselenide was allowed to cool to ambient prior to the addition of benzyl bromide (2.97 ml, 4.28 g, 25.0 mmol). Within 5 min the solution had become dark orange. The reaction was left to stir for a further 3 h. The crude reaction mixture was poured into brine (120 ml) and the crude product isolated from DMF by use of an Et_2O-extraction-train in four separating funnels (1 x 120 ml, 2 x 80 ml, 1 x 50 ml Et_2O). An 80 ml brine wash was passed through each funnel consecutively and the process repeated four times (5 x 80 ml washes total). The combined organic phases were dried over $MgSO_4$ and then filtered. The ether was removed under vacuum to yield crude e $[BnSe]_2$ as a yellow powder (3.67 g, 86% yield). Analytically pure $[BnSe]_2$ was isolated via recrystallisation from hot petroleum ether. ^{1}H NMR ($CDCl_3$, 400 MHz) (δ, ppm): 7.26 (m, 10H, Ar*H*), 3.84 (s + sat., 4H, $^2J_{SeH}$ = 14.5 Hz, SeCH_2). ^{77}Se{^{1}H} NMR ($CDCl_3$, 57 MHz) (δ, ppm): +403.2 (s).

Polymer synthesis

EpxSS1

EpxSS1 was prepared from a stoichiometrically balanced blend of Epon 828 (DGEBA) and DTDA (4,4'-dithiodianiline). Epon 828 (39.3 g) was added to a round-bottom flask equipped with magnetic stirrer and heated to 80 °C. While stirring the mixture, the epoxy was degassed via attachment to a vacuum pump/Schlenk line. When the effervescence stopped, the flask was returned to ambient pressure and DTDA (10 g) added. Once the DTDA powder was enveloped within the melt, the vessel was returned to vacuum to continue degassing the blend at 80 °C. After 2 h, the flask was returned to ambient pressure and the resin poured into a steel mould (pre-coated with Freekote release agent). The resin was then cured at 120 °C for 2 h (with a 3 °C min^{-1} heating rate from ambient) and post-cured at 150 °C for 2.5 h. The product, a translucent brown plate of polymer was then cut and machined prior to testing.

EpxSeSe1

To an aluminium pan equipped with magnetic stirrer, DGEBA (5.55 g) was added and then stirred at 50 °C. To this melt, 3,3'-diselanediylbis(propan-1-amine) (**APDS**, 2.00 g) was added and when the mixture became a homogeneous, gold-coloured oil, the stirrer was removed and the temperature increased to 70 °C. After 5 min, the temperature was further increased to 100 °C for 2 h. The pan was then heat treated at 120 °C for a further 1 h and then left to cool, yielding EpxSeSe1 as a dark brown polymer.

EpxSeSe2

To an aluminium pan equipped with magnetic stirrer, DGEBA (2.94 g) and **BOCDS** (2.23 g) were added at 70 °C and mixed to give an opaque, golden-brown liquid. The temperature was then raised to 120 °C and after 5 min, the melt became a translucent, orange liquid indicating homogeneity. While stirring the mixture, the pan was heated to 180 °C; from 150 °C upwards the melt became deep red and extensive effervescence was observed. After curing the material for 1 h at 180 °C, the temperature was raised to 220 °C and left to post-cure for a further 1.5 h prior to cooling it to ambient temperature, yielding EpxSeSe2 as a dark brown-black glass.

EpxSeSe3

To an aluminium pan equipped with magnetic stirrer, DGEBA (4.00 g) was added and stirred at 65 °C. To this melt, a blend of 3,3'-diselanediyldipropionic acid (**CDS**, 2.74 g), citric acid (0.19 g) and TBD (0.35 g) powders were added, with the melt becoming yellow and then golden-brown within 1 min of

addition. The stirrer was removed and instead the melt agitated by hand as the temperature was increased to 180 °C, to become dark brown. Above 165 °C, significant effervescence was observed, and the viscosity had dropped sufficiently to allow the resumption of mixing by magnetic stirrer. After 1.5 h at 180 °C the effervescence stopped and the stirrer was again removed. The polymer was allowed to cure for a further 2 h prior to cooling to ambient temperature, yielding EpxSeSe3 as a brown-black glass.

EpxSS2

In an aluminium pan equipped with magnetic stirrer, Epon 828 (DGEBA, 2.00 g) was heated to 50 °C. To the melt, a pre-mixed blend of 3,3'-dithiopropionic acid (946 mg), citric acid (96 mg) and TBD (150 mg) was added, which resulted in a colourless resin. This melt became golden yellow and then chocolate brown as the temperature was increased to 65 and then 100 °C. The melt continued to stir as it was further heated to 150 °C; after 30 min, the melt had darkened and thickened. The melt was then raised to 180 °C and stirred for a further 1.5 h before the magnetic stirrer was removed. The brown-black resin was then left to cure for an additional 2 h at 180 °C and then cooled, affording EpxSS2 as an opaque black glass.

4.7 References

1 G. Rajpal and P. Arvan, in *Handbook of Biologically Active Peptides*, ed. A. Kastin, Academic Press, 2nd edn., 2013, pp. 1721–1729.

2 H. Ishikawa, S. Kim, K. Kwak, K. Wakasugi and M. D. Fayer, *Proc. Natl. Acad. Sci. U. S. A.*, 2007, **104**, 19309–19314.

3 B. Wilkinson and H. F. Gilbert, *Biochim. Biophys. Acta - Proteins Proteomics*, 2004, **1699**, 35–44.

4 B. T. Michal, C. A. Jaye, E. J. Spencer and S. J. Rowan, *ACS Macro Lett.*, 2013, **2**, 694–699.

5 Y. Amamoto, H. Otsuka, A. Takahara and K. Matyjaszewski, *Adv. Mater.*, 2012, **24**, 3975–3980.

6 A. Ruiz de Luzuriaga, R. Martin, N. Markaide, A. Rekondo, G. Cabañero, J. Rodríguez and I. Odriozola, *Mater. Horizons*, 2016, **3**, 241–247.

7 W. Post, A. Cohades, V. Michaud, S. van der Zwaag and S. J. Garcia, *Compos. Sci. Technol.*, 2017, **152**, 85–93.

8 M. Chen, L. Zhou, Y. Wu, X. Zhao and Y. Zhang, *ACS Macro Lett.*, 2019, **8**, 255–260.

9 Q. Zhou, X. Zhu, W. Zhang, N. Song and L. Ni, *ACS Appl. Polym. Mater.*, 2020, **2**, 1865–1873.

10 R. Caraballo, PhD Thesis, Stockholm, 2010.

11 R. Caraballo, M. Rahm, P. Vongvilai, T. Brinck and O. Ramström, *Chem. Commun.*, 2008, 6603–6605.

12 J. M. Matxain, J. M. Asua and F. Ruipérez, *Phys. Chem. Chem. Phys.*, 2016, **18**, 1758–1770.

13 I. Azcune and I. Odriozola, *Eur. Polym. J.*, 2016, **84**, 147–160.

14 S. Nevejans, N. Ballard, J. I. Miranda, B. Reck and J. M. Asua, *Phys. Chem. Chem. Phys.*, 2016, **18**, 27577–27583.

15 J. Canadell, H. Goossens and B. Klumperman, *Macromolecules*, 2011, **44**, 2536–2541.

16 U. F. Fritze and M. von Delius, *Chem. Commun.*, 2016, **52**, 6363–6366.

17 M. Pepels, I. Filot, B. Klumperman and H. Goossens, *Polym. Chem.*, 2013, **4**, 4955–4965.

18 J. M. Wilson, R. J. Bayer and D. J. Hupe, *J. Am. Chem. Soc.*, 1977, **99**, 7922–7926.

19 P. A. Fernandes and M. J. Ramos, *Chem. Eur. J.*, 2004, **10**, 257–266.

20 A. Rekondo, R. Martin, A. Ruiz de Luzuriaga, G. Cabañero, H. J. Grande and I. Odriozola, *Mater. Horiz.*, 2014, **1**, 237–240.

21 Z. Q. Lei, H. P. Xiang, Y. J. Yuan, M. Z. Rong and M. Q. Zhang, *Chem. Mater.*, 2014, **26**, 2038–2046.

22 R. D. Crocker, M. A. Hussein, J. Ho and T. V. Nguyen, *Chem. Eur. J.*, 2017, **23**, 6259–6263.

23 A. Ruiz de Luzuriaga, J. M. Matxain, F. Ruipérez, R. Martin, J. M. Asua, G. Cabañero and I. Odriozola, *J. Mater. Chem. C*, 2016, **4**, 6220–6223.

24 Z. Ma, Y. Wang, J. Zhu, J. Yu and Z. Hu, *J. Polym. Sci. Part A Polym. Chem.*, 2017, **55**, 1790–1799.

25 M. Kashif Bangash, A. Ruiz De Luzuriaga, J. Aurrekoetxea, N. Markaide, H.-J. Grande and M. Ferraris, *Compos. Part B*, 2018, **155**, 122–131.

26 D. J. Fortman, R. L. Snyder, D. T. Sheppard and W. R. Dichtel, *ACS Macro Lett.*, 2018, **7**, 1226–1231.

27 Y. Zhang, L. Yuan, G. Liang and A. Gu, *Ind. Eng. Chem. Res.*, 2018, **57**, 12397–12406.

28 H. Si, L. Zhou, Y. Wu, L. Song, M. Kang, X. Zhao and M. Chen, *Compos. Part B Eng.*, 2020, **199**, 108278.

29 S. Ji, W. Cao, Y. Yu and H. Xu, *Angew. Chem. Int. Ed.*, 2014, **53**, 6781–6785.

30 X. An, R. H. Aguirresarobe, L. Irusta, F. Ruipérez, J. M. Matxain, X. Pan, N. Aramburu, D. Mecerreyes, H. Sardon and J. Zhu, *Polym. Chem.*, 2017, **8**, 3641–3646.

31 W. Du, Y. Jin, J. Pan, W. Fan, S. Lai and X. Sun, *J. Appl. Polym. Sci.*, 2018, **135**, 46326.

32 R. Leino and J. E. Lönnqvist, *Tetrahedron Lett.*, 2004, **45**, 8489–8491.

33 C. Liu, J. Xia, S. Ji, Z. Fan and H. Xu, *Chem. Commun.*, 2019, **55**, 2813–2816.

34 H. Xu, W. Cao and X. Zhang, *Acc. Chem. Res.*, 2013, **46**, 1647–1658.

35 L. Shi, Y. Jin, W. Du, S. Lai, Y. Shen and R. Zhou, *Polymer*, 2020, **198**, 122551.

36 J. Xia, P. Zhao, S. Pan and H. Xu, *ACS Macro Lett.*, 2019, **8**, 629–633.

37 C. Sun, S. Ji, F. Li and H. Xu, *ACS Appl. Mater. Interfaces*, 2017, **9**, 12924–12929.

38 M. Waliczek, Ö. Pehlivan and P. Stefanowicz, *ChemistryOpen*, 2019, **8**, 1199–1203.

39 M. Irigoyen, A. Fernández, A. Ruiz, F. Ruipérez and J. M. Matxain, *J. Org. Chem.*, 2019, **84**, 4200–

4210.

40 X. Pan, F. Driessen, X. Zhu and F. E. Du Prez, *ACS Macro Lett.*, 2017, **6**, 89–92.

41 Y. Qian, X. An, X. Huang, X. Pan, J. Zhu and X. Zhu, *Polymers (Basel).*, 2019, **11**, 773.

42 Y. Chen, S. Liu, J. Zhao, D. Pahovnik, E. Žagar and G. Zhang, *ACS Macro Lett.*, 2019, **8**, 1582–1587.

43 A. L. Chen, K. L. Wei, R. J. Jeng, J. J. Lin and S. A. Dai, *Macromolecules*, 2011, **44**, 46–59.

44 I. S. Blagbrough, N. E. Mackenzie, C. Ortiz and A. I. Scott, *Tetrahedron Lett.*, 1986, **27**, 1251–1254.

45 A. Schotman, PhD Thesis, Technische Universiteit Delft, 1993.

46 V. Nascimento, N. L. Ferreira, R. F. S. Canto, K. L. Schott, E. P. Waczuk, L. Sancineto, C. Santi, J. B. T. Rocha and A. L. Braga, *Eur. J. Med. Chem.*, 2014, **87**, 131–139.

47 R. Wang, L. Zhang, Z. Zhang and Y. Tian, *J. Pharm. Anal.*, 2016, **6**, 356–362.

48 H. Duddeck, *Annu. Reports NMR Spectrosc.*, 2004, **52**, 105–166.

49 V. K. Jain, in *Organoselenium Compounds in Biology and Medicine*, 2017, pp. 1–33.

50 J. D. Odom, W. H. Dawson and P. D. Ellis, *J. Am. Chem. Soc.*, 1978, **101**, 5815–5822.

51 M. D. Milton, S. Khan, J. D. Singh, V. Mishra and B. L. Khandelwal, *Tetrahedron Lett.*, 2005, **46**, 755–758.

52 M. Schelhass and H. Waldmann, *Angew. Chem. Int. Ed*, 1996, **35**, 2056–2083.

53 P. G. M. Wuts, *Greene's Protective Groups in Organic Synthesis*, Wiley, 5th edn., 2014.

54 B. Viswanadham, A. S. Mahomed, H. B. Friedrich and S. Singh, *Res. Chem. Intermed.*, 2017, **43**, 1355–1363.

55 N. Srinivasan, A. Yurek-George and A. Ganesan, *Mol. Divers.*, 2005, **9**, 291–293.

56 B. Li, M. Berliner, R. Buzon, C. K. F. Chiu, S. T. Colgan, T. Kaneko, N. Keene, W. Kissel, T. Le, K. R. Leeman, B. Marquez, R. Morris, L. Newell, S. Wunderwald, M. Witt, J. Weaver, Z. Zhang and Z. Zhang, *J. Org. Chem.*, 2006, **71**, 9045–9050.

57 U. Jacquemard, V. Bénéteau, M. Lefoix, S. Routier, J. Y. Mérour and G. Coudert, *Tetrahedron*, 2004, **60**, 10039–10047.

58 B. S. Richard Lott, V. S. Chauhan and C. H. Stammer, *J. Chem. Soc. Chem. Commun.*, 1979, 495–496.

59 R. K. Dieter, N. Chen and V. K. Gore, *J. Org. Chem.*, 2006, **71**, 8755–8760.

60 G. Pavan Kumar, D. Rambabu, M. V. Basaveswara Rao and M. Pal, *J. Chem.*, 2013, **2013**, 916960.

61 R. Frank and M. Schutkowski, *Chem. Commun.*, 1996, 2509–2510.

62 N. J. Tom, W. M. Simon, H. N. Frost and M. Ewing, *Tetrahedron Lett.*, 2004, **45**, 905–906.

63 C. Zinelaabidine, O. Souad, J. Zoubir, B. Malika and A. Nour-Eddine, *Int. J. Chem.*, 2012, **4**, 73–79.

64 B. Li, R. Li, P. Dorff, J. C. McWilliams, R. M. Guinn, S. M. Guinness, L. Han, K. Wang and S. Yu, *J. Org. Chem.*, 2019, **84**, 4846–4855.

65 F. I. Altuna, C. E. Hoppe and R. J. J. Williams, *Eur. Polym. J.*, 2019, **113**, 297–304.

66 F. I. Altuna, C. E. Hoppe and R. J. J. Williams, *RSC Adv.*, 2016, **6**, 88647–88655.

67 P. G. Hultin, Extraction Protocol for Polar Solvents, http://www.chem.rochester.edu/notvoodoo/pages/reagents.php?page=extraction, (accessed 19 March 2021).

68 S. Davies, B. L. Oliveira and G. J. L. Bernardes, *Org. Biomol. Chem.*, 2019, **17**, 5725–5730.

Chapter 5: Diphosphanes

5.1 Introduction

Sections of this chapter (5.1 and 5.4) are based on the article *'Radical-initiated P,P-metathesis reactions of diphosphanes: evidence from experimental and computational studies',* published in *Dalton Transactions.*[1] Some DFT (Density Functional Theory) calculations performed by T. Young from this article are reported and discussed herein.

5.1.1 Background

In 1972, McFarlane and McFarlane[2] first reported the exchange of diphosphanes in chlorinated solvents. After several days in CH_2Cl_2, mixtures of tetraphenyldiphosphane and tetramethyldiphosphane produced a doublet of doublets in the $^{31}P\{^1H\}$ NMR spectrum of the reaction mixture that was consistent with the formation of $Ph_2P–PMe_2$. Harris *et al*.[3] took this further, exploiting this exchange process in the synthesis of several unsymmetrical diphosphanes by mixing the symmetrical parent compounds in CH_2Cl_2, though these were usually observed in equilibria with the parent compounds. Curiously, solutions of diphosphanes, mixtures or otherwise, were inert to exchange in both benzene and toluene—and in some cases (e.g. $Ph_2P–PPh_2$ + $^tBu_2P–P^tBu_2$) no exchange was observed. In neither report was an underlying mechanism for the exchange offered. More recently, in a DFT study, Gilheany *et al*.[4] have shown that the calculated barrier to one of the simplest possible mechanisms, concerted [2+2] metathesis, is not consistent with the rapid kinetics observed in many cases. Indeed, this led the authors to postulate that diphosphane metathesis may be facilitated by an unidentified impurity originating from the diphosphane synthesis. This conclusion was shared by Grubba *et al*.,[5] who reported that both R_2PCl and R_2PLi can catalyse diphosphane metathesis.

Beyond this metathesis process, diphosphane chemistry may be broadly divided into two categories: those reactions where the P–P bond remains intact (e.g. metal coordination) and those where the bond is cleaved. The latter category is particularly relevant here and includes additions of X_2 across the P–P bond to give R_2PX species (e.g. X = H, Cl), and additions of $R_2P–PR_2$ across the unsaturated bonds of alkenes or alkynes,[6] or CO_2,[7] Scheme 5.01. In some cases, radical mechanisms have been proposed to explain the observed reactivity.[6,8,9]

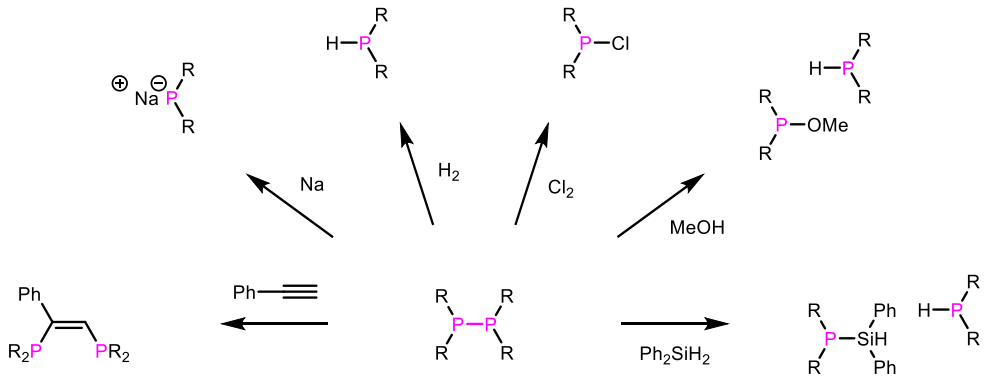

Scheme 5.01. Some reactions involving diphosphane cleavage, clockwise from the left: addition of diphosphanes across alkynes,[6] the cleavage of diphosphanes with sodium,[10] hydrogenation,[11] chlorination, methanolysis,[12] and the addition of phenylsilanes.[11]

5.1.2 Synthesis

A wide variety of methods have been used to prepare diphosphanes, including phosphide-chlorophosphine (R_2PCl) coupling,[5] R_2PCl-silylphosphine exchange (chlorosilane elimination),[12,13] secondary phosphine (R_2PH) dehydrocoupling,[14–19] iodophosphine coupling with mercury,[20] and R_2PCl coupling with reducing metals including lithium,[21] sodium,[22,23] potassium,[22] and magnesium,[24] Scheme 5.02.

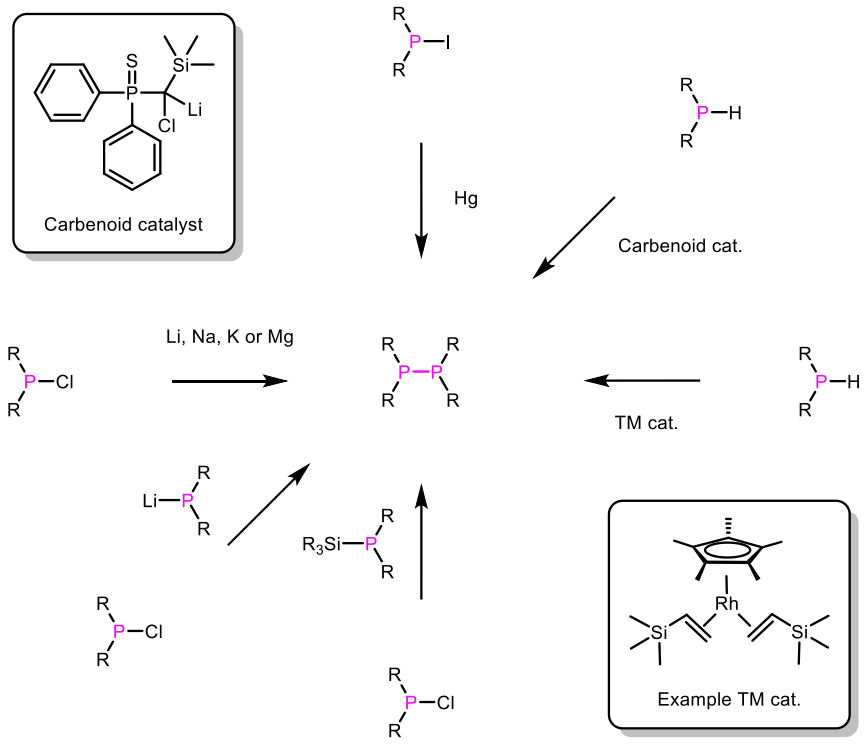

Scheme 5.02. Methods of diphosphane synthesis, clockwise from the top: Hg/iodophosphine reduction,[20] carbenoid-catalysed dehydrocoupling,[18] transition metal (TM)-catalysed dehydrocoupling,[16] chlorosilane elimination,[25] lithium phosphide-chlorophosphine coupling,[5] and chlorophosphine reduction with alkali/alkaline earth metals.[26]

Diphosphane, $H_2P–PH_2$, can be prepared in several ways including reacting white phosphorus with strong bases. However, these reactions tend to produce phosphine gas as a by-product. Moreover, there is little evidence that diphosphane can itself be further functionalised (selectively).[26]

Unsymmetrical diphosphanes have proved considerably more challenging to synthesise than their symmetrical analogues, since their attempted synthesis often results in equilibria with the related symmetrical diphosphanes. It was this observation that led Pringle *et al*.[27,28] to develop a borane-protection/deprotection strategy, Scheme 5.03.

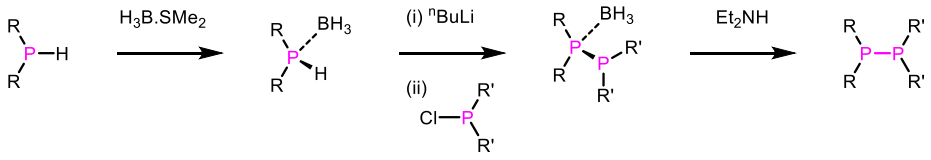

Scheme 5.03. The Pringle method of unsymmetrical diphosphane synthesis.

More recently, Grubba and co-workers prepared a large series of diphosphanes (often with alkylamino substituents), many of which were unsymmetrical.[5] Interestingly, these authors found that the classical lithium phosphide–chlorophosphine method was successful in many of these cases. The lack of diphosphane scrambling/metathesis in these cases may suggest that these compounds are thermodynamically stable relative to the symmetrical diphosphanes.

5.1.3 Functionalised diphosphanes

To enable their incorporation within polymers, diphosphanes with pendent reactive groups are essential. Such groups may include unsaturated moieties such as alkenes, nucleophiles such as primary amines or hydroxyls, and electrophiles such as halogens, epoxides or carbonyl functionalities. These compounds should ideally be P(III)–P(III) diphosphanes given their previously discussed reactivity; although the P–P bond strength is very similar in P(V)–P(V) species,[29] there are no reports of metathesis behaviour in these compounds. This may indicate that the phosphorus lone pairs are significant in the exchange mechanism.

The inconsistent nomenclature surrounding diphosphanes, which have also been referred to as diphosphines, biphosphines and bisphosphines, results in conflation with $R_2P–Y–PR_2$ species that do not contain a P–P bond. This makes an analysis of diphosphane literature more challenging than one would otherwise expect. With this considered, it is possible that some examples have been missed from the following literature review. Regardless, it is clear that examples of functionalised diphosphanes are few and far between. Even when the search is expanded to P(V)–P(V) species and multiple P–P bonded species, the literature remains limited, Figure 5.01.

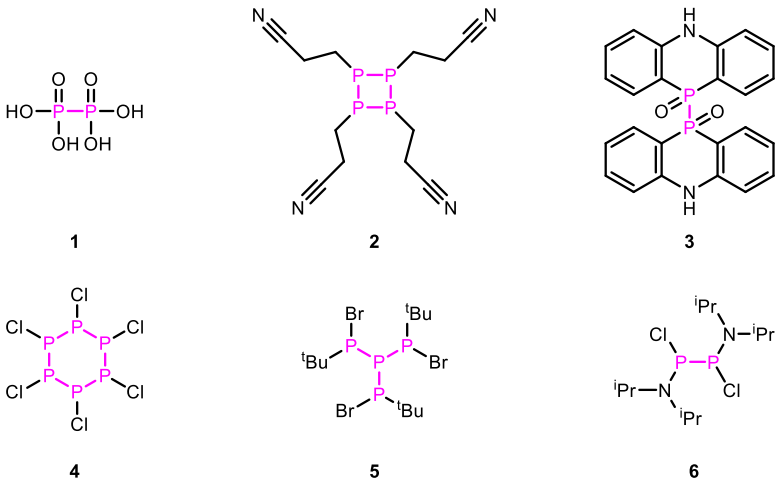

1 **2** **3**

4 **5** **6**

Figure 5.01. Species containing one or more P–P bonds and additional reactive groups.

Hypophosphoric acid (**1**) is a common industrial bleaching agent and likely the most abundant P–P containing species. Theoretically, in having four residual hydroxyl groups this species fits the requirement for additional reactive groups. However, there is no literature concerning the reactivity of this compound beyond its use as an acid. Moreover, when anhydrous, hypophosphoric acid disproportionates with cleavage of the P–P bond.[30]

In 1963, Henderson *et al*.[31] reported the syntheses of several cyclotetraphosphanes including the tetranitrile **2**. In this synthesis, the authors started with the primary phosphine and chlorinated this using phosgene. The resulting dichlorophosphine was then coupled with the primary phosphine to give **2** in a pyridine-chloroform mixture. The reactivity/stability of this compound does not appear to have been investigated.

In 1960, Häring reported the synthesis of **3**,[32] 5H,5'H-[10,10'-biphenophosphazinine]-10,10'-dioxide, from the oxidative coupling of the respective secondary phosphine oxide with iodine. However, this compound was not well characterised. Compounds **4–6** are examples of P–P-containing species which also contain residual P–X (X = Cl, Br) bonds. These compounds should be capable of reacting with strong nucleophiles, though each of these species and their products are likely to be rather unstable. The former two species (**4** and **5**) were reported by Baudler and co-workers.[33,34] **6** was prepared by King and Sadanani from the dichloroaminophosphine via Mg coupling.[35] Though sterically congested by the diisopropylamine groups, it is conceivable that this compound could react with potent organometallic nucleophiles (organolithiums, Grignards etc.).

In summary, the observed dynamic behaviour of diphosphanes, combined with the weakness of the P–P bond (*ca*. 220 kJ mol^{-1}), intermediate between disulfides (*ca.* 260 kJ mol^{-1}) and diselenides (*ca.* 170 kJ mol^{-1}) makes these species promising new candidates for dynamic covalent chemistry. With

appropriate functional groups it may be possible to exploit diphosphane chemistry in similar ways to disulfide/diselenide chemistry (Chapter 4). However, there do not appear to be any examples of ideal target diphosphanes in the academic literature.

5.1.4 Diphosphanes: aims and objectives

In this chapter the key objectives are listed as follows:

- Explore the stability of diphosphanes under various reaction conditions to help identify viable synthetic routes to target functionalised diphosphanes (Section 5.2).
- Synthesise a small series of diphosphanes (Section 5.3) to explore the mechanism of diphosphane exchange (Section 5.4).
- Prepare functionalised diphosphanes with a view to exploring diphosphane exchange in polymers (Section 5.3).
- Investigate mixed (i.e. P–P/S–S and P–P/Se–Se) dynamic systems (Section 5.5).

5.2 Stability and reactivity

To design synthetic pathways to functionalised diphosphanes, a stability study was performed to identify reagents that are compatible or incompatible with P–P bonds. In all cases, tetraphenyldiphosphane (**A_2**) was mixed with an additive in an NMR tube and monitored by $^{31}P\{^{1}H\}$ NMR for approximately 24 h. The results of this study are shown in Table 5.1.

Table 5.1. The stability of tetraphenyldiphosphane in various reaction conditions.

Additive	Additive equivalents	Solvent	Duration / h	Observation	Conclusion
4M $NaOH_{(aq)}$	Large excess	THF[a]	17.5	17% $Ph_2P(O)H$	Good stability
^{n}BuLi	4 eq.	THF	17.5	Negligible change	Good stability
$LiAlH_4$	3 eq.	Et_2O	17	25% Ph_2PH	Moderate stability
$NaBH_4$	3 eq.	THF	20	Negligible change	Good stability
TFA	Large excess[b]	CH_2Cl_2	8	Complete cleavage	Incompatible
HCl	10 eq.	THF/Et_2O[c]	<1	Complete cleavage	Incompatible
TMSBr / sieves	4 eq.	CH_2Cl_2	6.5	Negligible change[d]	Stable when dry
TMSI / sieves	4 eq.	CH_2Cl_2	9	Negligible change[d]	Stable when dry
TBAF	2 eq.	THF[e]	17	1/3 PP remaining	Incompatible
NBS	1 eq.	Toluene	19	1/2 PP remaining	Incompatible
I_2	4 eq.	CH_2Cl_2	<1	Quantitative Ph_2PI formation	Incompatible

[a] biphasic solvent system. [b] to mimic common BOC deprotection conditions. [c] ethereal HCl added to THF. [d] without molecular sieves complete cleavage is observed within 24 h.

From this table, a few gross trends emerge and, assuming that **A_2** is representative of symmetrical diphosphanes more generally, we can make several observations on their stability: (1) Diphosphanes appear to be tolerant of strong bases. A large excess of NaOH resulted in only limited P–P cleavage

over an extended period of time. Consequently, it seems probable that stoichiometric quantities would not affect P–P integrity. The stability towards ^{n}BuLi is even more impressive. Experiments in which diphosphane mixtures are exposed to (2°/3°) amines, discussed later in Section 5.4, confirm that diphosphanes are also tolerant of these bases. (2) Diphosphanes appear to be relatively stable towards reducing agents—the presence of an excess of $LiAlH_4$ results in only modest cleavage after extended periods, and the milder reducing agent $NaBH_4$ has negligible effect on P–P integrity. (3) Diphosphanes appear to be completely incompatible with acids (TFA/HCl). (4) Although P–P bonds appear tolerant of halosilanes—which are commonly used in a variety of deprotection strategies—this is only true in the presence of molecular sieves. The slightest water contamination leads to the formation of HBr/HI, which explains the complete cleavage of the P–P bond in the absence of molecular sieves. Unfortunately, it is often HBr/HI that are the active species in the aforementioned deprotection strategies. (5) Diphosphanes also appear to be incompatible with N-bromosuccinimide (NBS), tetra-butylammonium fluoride (TBAF) and iodine, which have each been used as mild, non-acidic reagents in deprotection strategies.

The aqueous stability of diphosphanes was also investigated. As indicated by the NaOH entry of Table 5.1 and in experiments which will be introduced in Section 5.4, homodiphosphanes appear to be moisture stable. In sharp contrast, solutions of tetraphenyldiphosphane (**A_2**) left open to air exhibit rapid oxidation; complete conversion to a range of oxides (the main product appears to be $Ph_2P(O)H$) is observed in <10 min. Interestingly, when **A_2** is exposed to air in the presence of TEMPO the oxidation process is greatly inhibited, Figure 5.02. Significant inhibition was observed even with stoichiometric quantities of TEMPO. This lends further support to the currently accepted hypothesis of phosphine oxidation being radical-mediated.[36] In this specific case, this may also suggest that phosphinyl radicals (which will be discussed extensively in Section 5.4) are involved in diphosphane oxidation. Importantly, the use of TEMPO to inhibit phosphine oxidation may have wider utility in phosphorus chemistry.

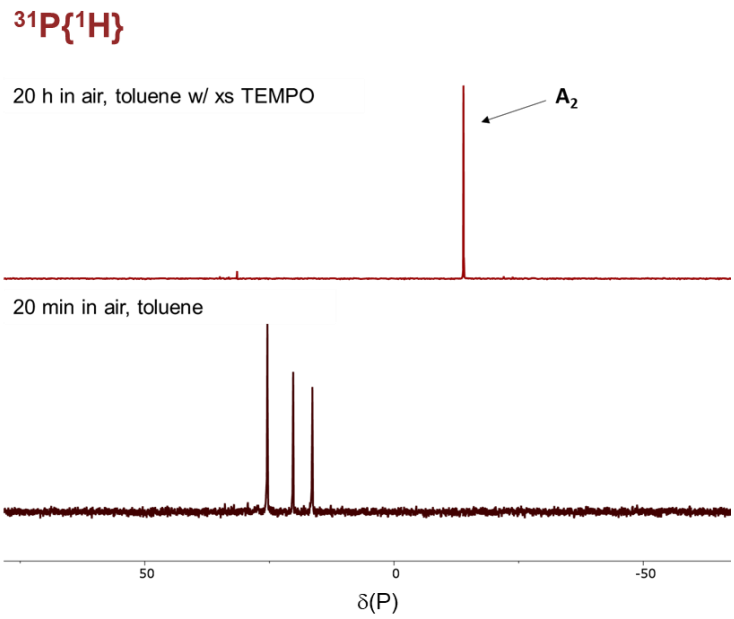

Figure 5.02. $^{31}P\{^{1}H\}$ NMR: the oxidation of **A_2** in stirring toluene (while open to air), with and without 4 equivalents of TEMPO. All diphosphane is consumed by oxidation in <20 min without TEMPO.

One final observation relates to borane protection. The use of borane as a protecting group in phosphorus chemistry is well-known. By complexing the phosphorus lone pair, much of the reactivity of the phosphorus centre can be suppressed. Significantly, borane protection typically makes air-sensitive phosphines air-stable. Additionally, the protection and removal steps are generally facile—as later demonstrated in the preparation of **AE**. However, (di)borane protection of diphosphanes has not previously been reported. This boron chemistry was tested with **A_2** according to Scheme 5.04.

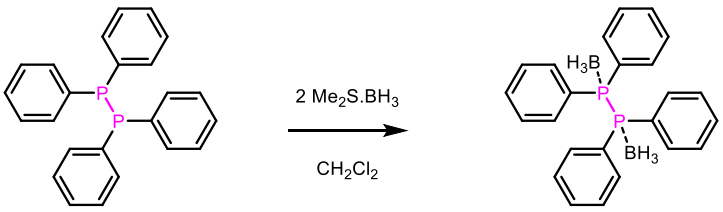

A_2

Scheme 5.04. The attempted borane protection of **A_2**.

This reaction produced a mixture of products, with the expected di-borane diphosphane the dominant species (76%), but with significant contamination with the monoborane and other unidentified species according to ^{31}P NMR. Analysis of the ^{11}B NMR spectrum revealed the presence of significant amounts of borane-dimethylsulfide, suggesting that the monoborane and diborane P–P species were in equilibrium with this borane precursor. In any case, the diborane diphosphane was shown in separate experiments to be reactive both in the presence of deoxygenated water and in the presence of air.

Both experiments produced a large number of ^{31}P NMR resonances, many of which appeared to be P(V) species. It appears the coordination of one phosphorus centre to borane significantly inhibits the coordination of the second borane moiety.

In summary, **A_2** is stable to bases and reducing agents. However, the P–P bond appears to be very sensitive to acids, oxidising agents (including air) and halogenating agents. Accordingly, synthetic procedures devised to prepare functional diphosphanes must be carefully designed to avoid incompatible reagents.

5.3 Synthesis and characterisation of diphosphanes

5.3.1 Tetraaryldiphosphanes

To investigate the mechanism of diphosphane metathesis, five symmetrical tetraaryldiphosphanes were prepared, Figure 5.03. Each of these species were previously reported and therefore were characterised by ^{31}P and ^{1}H NMR spectroscopy only. Tetra(*o*-tolyl)diphosphane (**E_2**) was initially prepared via the classical lithium phosphide–chlorophosphine route in THF, but in a second synthesis it was prepared from the simpler Mg-coupling method (in THF) adapted from the work of Issleib *et al*.[24] and also reported by Grubba *et al*.[5] This Wurtz-type coupling was then extended to **A_2**–**C_2**; however, the preparation of (bis)meta-CF_3 species, **D_2** proved more challenging. With **D_2** and in the attempted synthesis of the para-CF_3 diphosphane (not shown), the chlorophosphine-Mg mixture was observed to rapidly turn purple and then black. Analysis of the resultant ^{31}P NMR spectra revealed two new (broad) resonances at +11.3 and -6.0 ppm and no evidence of the desired diphosphane (i.e. in the absence of signals in the region of -20 ppm). A possible explanation for this could be that the highly electron-poor phosphorus centre may make phospha-Grignard formation preferable to the Wurtz-coupling. Grignard solutions are known to become black with time and this may represent nanoparticulate Mg. In an attempt to circumvent this, the reaction was repeated in Et_2O with more success. However, the coupling reaction was observed to be very slow, with complete conversion not occurring even after 5 days at reflux (35 °C).

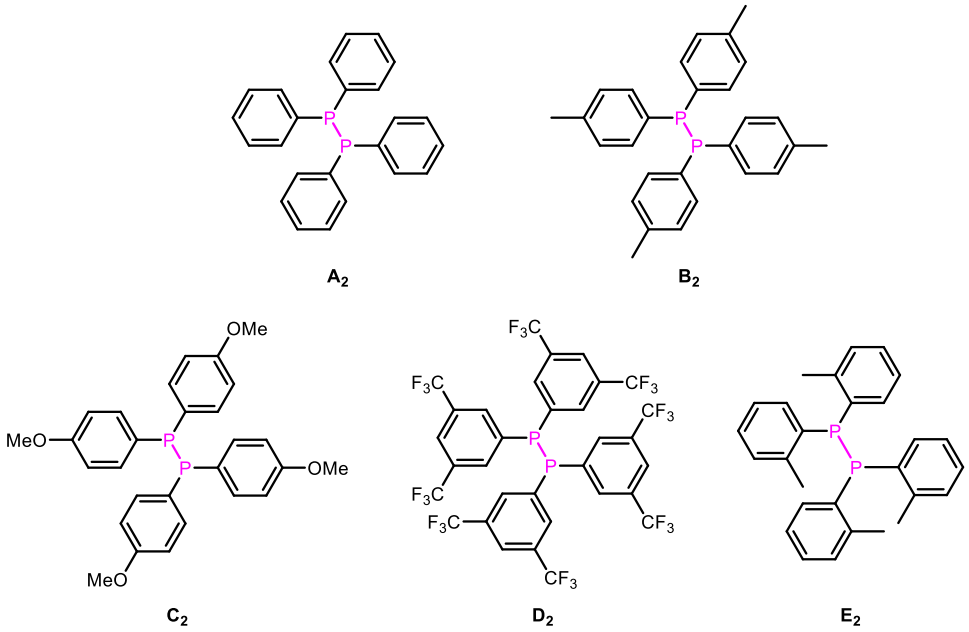

Figure 5.03. Tetraaryldiphosphanes **A_2**–**E_2** used in the metathesis study.

Residual chlorophosphine and secondary phosphine oxide—formed from the reaction of adventitious oxygen/moisture—were easily removed by flushing the ethereal solution through a basic-alumina plug. However, this resulted in enrichment of the other impurity, the secondary phosphine. Despite multiple attempts to purify **D_2** (and two attempts to prepare the related para-CF_3 species) the cleanest sample was contaminated with ~10% secondary phosphine and it was this that was used in further studies. Subsequent testing (Section 5.4) revealed that secondary phosphine has little influence on diphosphane metathesis. Experimental details are given in Section 5.6.

To support the experiments with **A_2–E_2**, the unsymmetrical diphosphane **AE** was prepared. Following the classical lithium phosphide–chlorophosphine protocol of diphosphane synthesis, **AE** was prepared but as an equilibrium mixture with the symmetrical diphosphanes, **A_2** and **E_2**, even when the reaction was maintained at -78 °C throughout, as advised by Grubba *et al*.[5] In an attempt to overcome this and isolate the pure unsymmetrical diphosphane **AE**, the borane-protection method employed by Pringle *et al*.[27] was used instead, Scheme 5.05.

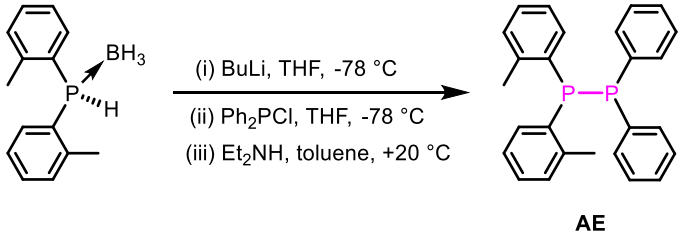

Scheme 5.05. Synthesis of **AE** via borane protection.

Although much improved, this method also produced **AE** contaminated with small quantities (~10% in total) of the symmetrical diphosphanes. However, by recrystallisation from hot MeOH, pure **AE** was isolated for the first time (<3% $\mathbf{A_2}$+$\mathbf{E_2}$ contaminant), Figure 5.04.

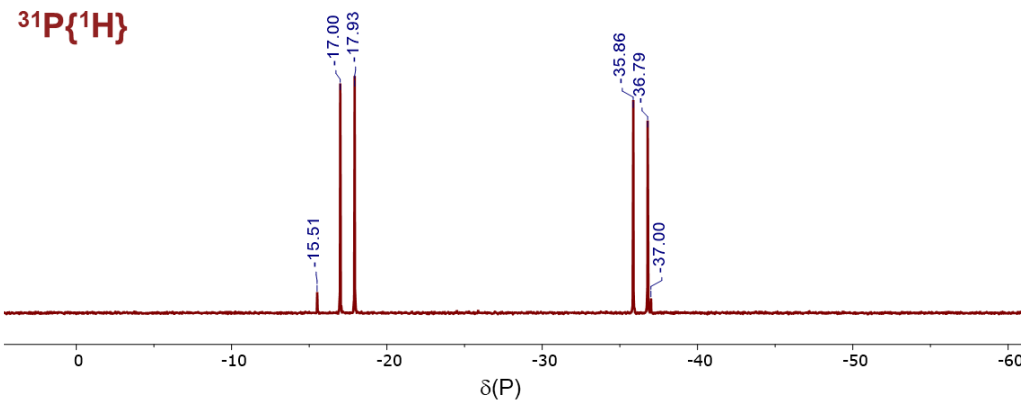

Figure 5.04. The $^{31}P\{^1H\}$ NMR spectrum of **AE** in C_6D_6. The $\mathbf{A_2}$ and $\mathbf{E_2}$ resonances are just visible at -15.5 and -37.0 ppm respectively (~1.5% each).

5.3.2 Functionalised diphosphanes

None of the literature compounds shown in Figure 5.01 are ideal target compounds for incorporation into a polymer. However, the nitrile-functionalised cyclotetraphosphane **2**, the dichloro-diamino diphosphane **6** and the P(V) diphosphane **3** were considered interesting prospects. Although, later experiments would demonstrate that P(V)–P(V) diphosphanes are incapable of the metathesis reactions observed with P(III)–P(III) species.

The literature procedure for the preparation of **3** is shown in Scheme 5.06.[32] Several attempts at reproducing this process were unsuccessful; the majority of the product obtained was insoluble in all common organic solvents, suggesting polymer formation. The limited material that was solubilised was a complex mixture of unidentified species according to ^{31}P NMR spectroscopy.

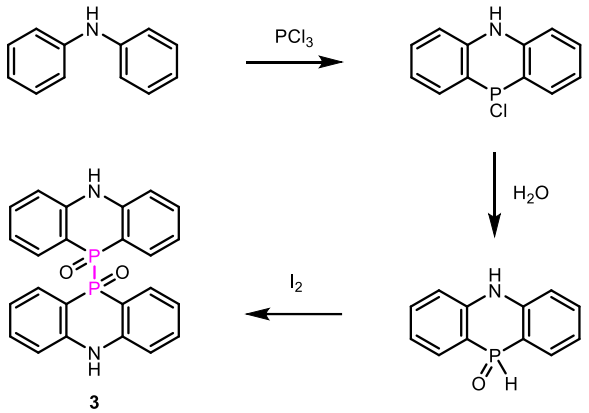

Scheme 5.06. The synthesis of **3** as reported by Häring in 1960.[32]

A series of target compounds were devised through this project, though only a few syntheses were attempted. Some of the most desirable targets are shown in Figure 5.05.

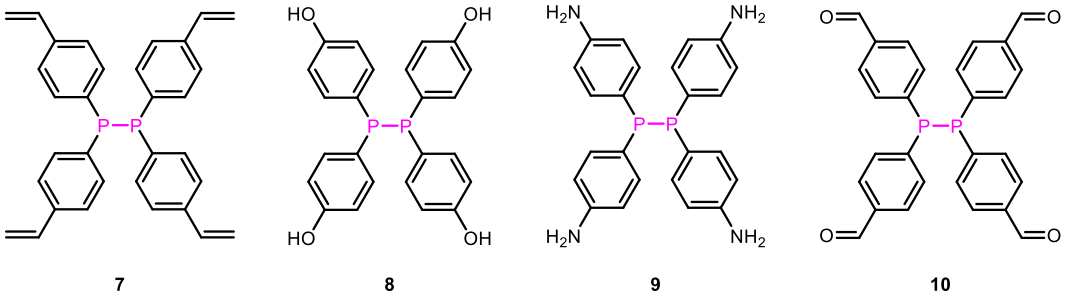

Figure 5.05. Target functionalised tetraaryldiphosphanes: **7** – styrene-, **8** – phenol-, **9** – aniline- and **10** – benzaldehyde-functionalised diphosphanes. None of which have been previously reported.

The strategy for the synthesis of **7** is shown in Scheme 5.07. This procedure follows a general protocol that can be applied for the synthesis of chlorophosphines and then secondary phosphines, though is limited in terms of functional group tolerance: the functional groups must be tolerant of organolithium/Grignard species in the first step, tolerant of HCl in the second and $LiAlH_4$ in the third—all highly reactive compounds. The chlorophosphine itself may be used to prepare the corresponding diphosphane directly via the Mg-coupling, or reduced to the secondary phosphine for use in the chlorophosphine–lithium phosphide route.

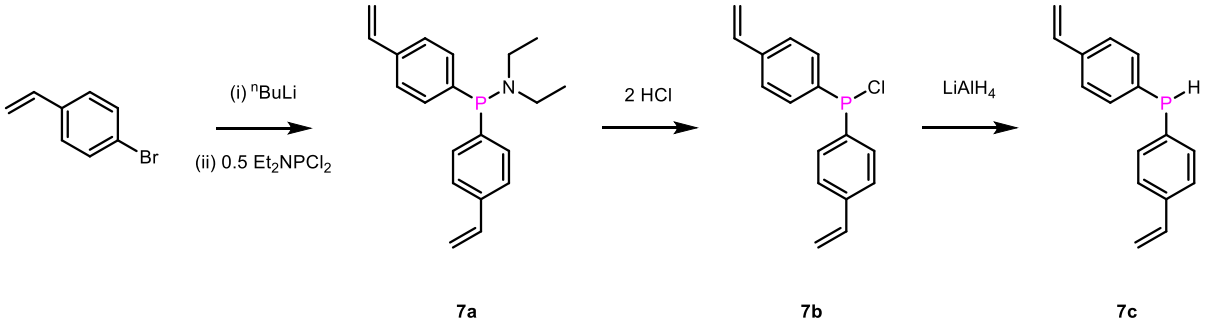

Scheme 5.07. The synthesis of intermediates **7a**-**7c** in the synthesis of 7.

In the preparation of **7** the first reaction to form **7a** works well, and although the Grignard may also be used, the organolithium species was found to react more cleanly. Small amounts of residual chloro(amino)phosphines can easily be removed with a celite plug, readily affording the pure aminophosphine, Figure 5.06 (top). The conversion of **7a** to **7b** is also a robust reaction, provided fresh ethereal HCl was used, Figure 5.06 (upper-middle). However, treatment of **7b** with $LiAlH_4$, and the standard aqueous sodium hydroxide work-up, gave inconsistent results. When the reduction was left for 1 h, analysis of the post–work-up solution revealed the desired secondary phosphine **7c** (-42.4 ppm) and contamination with some secondary phosphine oxide at +16.5 ppm, Figure 5.06 (lower-middle). Critically, when this mixture was subsequently filtered through an alumina plug, the

phosphine polymerised. Styrene forms linear radical addition polymers, difunctional styrenes such as **7a–7c**, would thus be expected to form densely-packed styrene networks with the phosphorus centres as crosslinkers. Polymerisation was also observed when **7b** was heated during solvent removal. Surprisingly, when the reduction of **7b** was left for extended periods (~60 h) the outcome was very different, producing what appears to be the target diphosphane **7** as the major product at -14.8 ppm, Figure 5.06 (bottom). Despite this success, this synthesis was not further pursued due to polymerisation concerns.

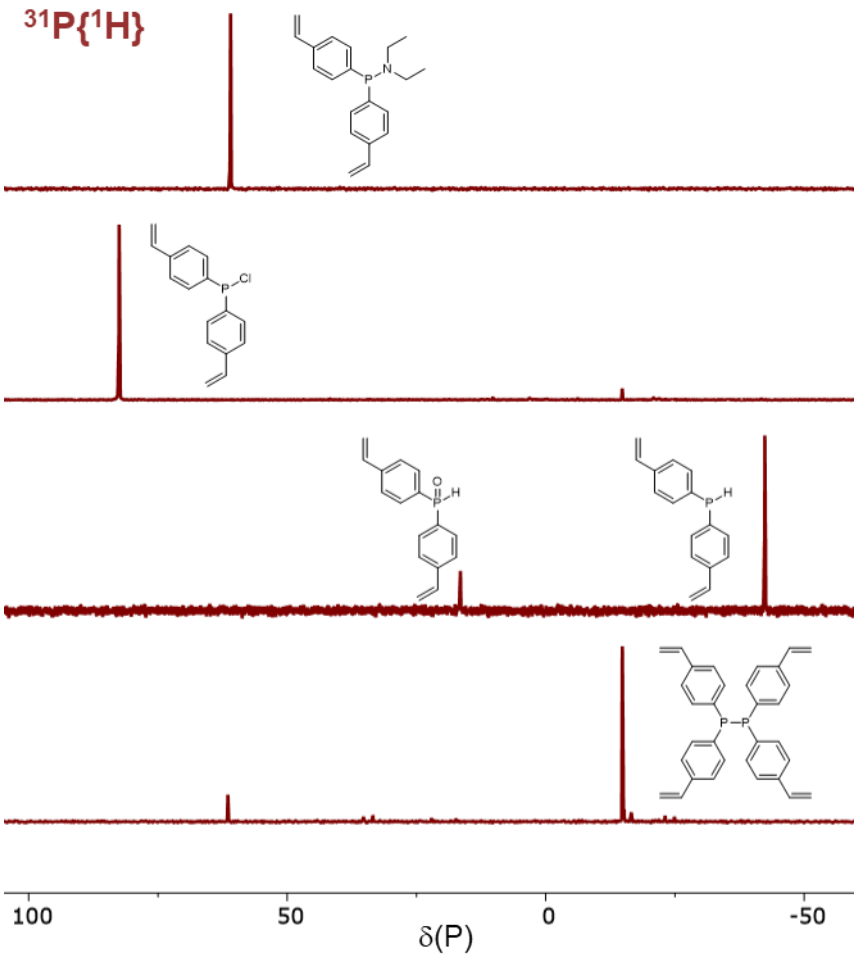

Figure 5.06. $^{31}P\{^{1}H\}$ NMR spectra of the intermediates **7a** (top), **7b** (upper-middle), crude **7c** (lower-middle) and crude **7** (bottom).

A similar method for preparing **8** was devised, Scheme 5.08, using MOM protecting groups. However, this route was tested by H. Yeo (MSci student, University of Bristol) and proved challenging. Attempts were made to make the aminophosphine, although the chlorination was not tested. Conventional MOM-deprotection conditions are acidic, so are likely incompatible with the diphosphane bond. It was hoped that the HCl step (chlorophosphine formation) would simultaneously cleave the MOM

groups and the P–N bond. Alternatively, the TMSBr method of MOM-deprotection reported by Dufresne *et al*.[37] could be used at the end of the synthesis, after diphosphane formation. From the chlorophosphine, a Mg-coupling would be the ideal method of P–P formation.

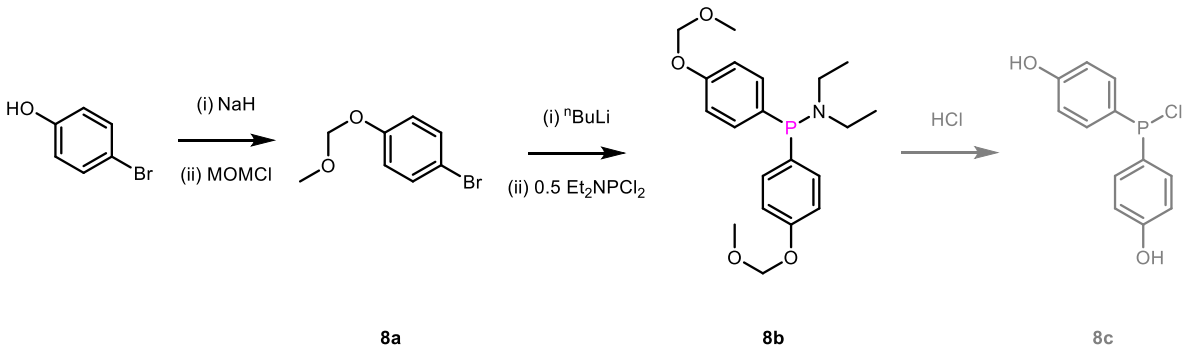

8a **8b** **8c**

Scheme 5.08. The proposed synthesis of **8** using a MOM protection strategy. The formation of **8c** remains untested.

An alternative, simpler method was conceived, starting from tetra(*p*-anisyl)diphosphane (**C_2**, synthesis described in Section 5.3.1), which has previously been reported.[19,38] Of the more common methods of demethylating methyl ethers, sodium ethanethiolate seemed a promising reagent, Scheme 5.09.

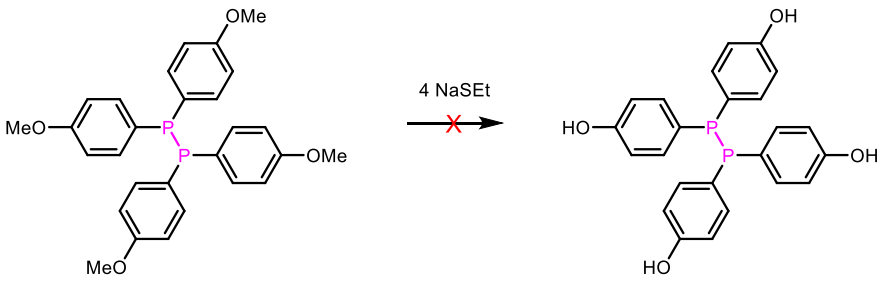

C_2 **8**

Scheme 5.09. Proposed demethylation of **C_2**.

This experiment was performed by H. Yeo, who observed the slow formation of a complex mixture of diphosphanes, secondary phosphines and secondary phosphine oxides by ^{31}P NMR, which appeared to represent a combination of protected and deprotected groups. The major products were the secondary phosphines, indicating substantial diphosphane cleavage had occurred, possibly due to phenolysis (of the P–P bond). Though it is possible that the NaSEt is responsible for the cleavage, it appears from these initial experiments that due to its acidity, **8** has an intrinsically unstable structure possibly due to self-reaction (addition of an O–H bond across the P–P bond).

Synthetic routes to **9** and **10** were also devised and are outlined in the future work section of Chapter 6.

These results clearly demonstrate that the preparation of functionalised diphosphanes is non-trivial.

5.4 Diphosphane homometathesis

5.4.1 Background

In this study, the metathesis reactions of tetraaryldiphosphanes (Scheme 5.10) were explored using a combination of $^{31}P\{^{1}H\}$ NMR spectroscopy and DFT calculations (performed by T. Young), with a view to finding new insights into the dynamic nature of the P–P bond.

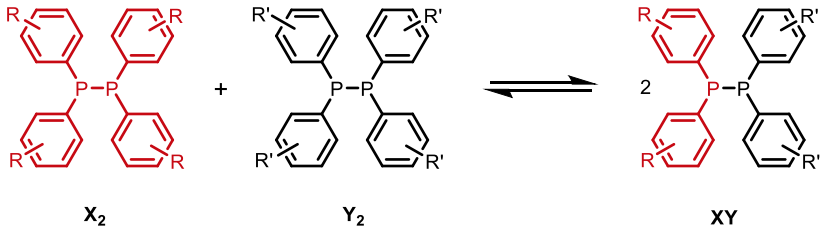

Scheme 5.10. The metathesis reaction between two tetraaryldiphosphanes **X_2** and **Y_2**.

The diphosphanes in this study (**A_2**-**E_2** Figure 5.03) were selected to sample a range of different steric/electronic environments around P–P bonds. They are all previously reported compounds and their synthesis was discussed in Section 5.3.1, experimental details are given in Section 5.7. Diphosphane **D_2** contained significant (~10%) secondary phosphine, although none of the five diphosphanes contain a detectable quantity (<0.05%) of chlorophosphine—the significance of this observation will become apparent in Section 5.4.4. When two of the diphosphanes were mixed in $CDCl_3$ at ambient temperature, a reaction ensued which gave an equilibrium mixture of the parent homodiphosphanes (**X_2** and **Y_2**) and the heterodiphosphane (**XY**).

5.4.2 Equilibria

In a typical procedure, 0.025 mmol (~10 mg) of each diphosphane, **X_2** and **Y_2**, were added to an oven-dried NMR tube under an Ar atmosphere. The sealed NMR tube was then removed from the glovebox and cycled onto the Schlenk line. Thereafter, 0.5 ml of dry, deoxygenated solvent ($CDCl_3$, CD_2Cl_2, C_6D_6, PhMe, PhCl, PhF or THF) was added creating an **X_2** + **Y_2** solution. The NMR tube was then sealed and the cap covered with parafilm to slow the ingress of air. An initial $^{31}P\{^{1}H\}$ NMR experiment was then performed within 20 min of solvent addition. The solution was then re-analysed at intervals until no further change in the ratio of diphosphane resonances was observed. Using the ^{31}P NMR integrals to estimate concentration, the equilibrium constants were calculated according to Equation 5.1.

$$K = \frac{[\mathbf{XY}]^2}{[\mathbf{X_2}][\mathbf{Y_2}]} \qquad \text{Eq. 5.1}$$

For a statistical mixture, i.e. 1 mol **X_2**, 1 mol **Y_2** and 2 mol **XY**, the equilibrium constant *K* = 4. The data for each of the 10 metathesis equilibria are collated in Table 5.2.

Table 5.2. Data for the metathesis equilibria shown in Scheme 5.10

Reaction	X_2	Y_2	*K*	Time[a] / min	^{31}P NMR data for **XY**		
1[b]	$\mathbf{A_2}$	$\mathbf{B_2}$	4	30	-14.9	-16.4	J_{PP} = 162 Hz
2[c]	$\mathbf{A_2}$	$\mathbf{C_2}$	5	20	-15.9	-18.4	J_{PP} = 159 Hz
3[d]	$\mathbf{A_2}$	$\mathbf{D_2}$	30[e]	90	-15.9	-8.5	J_{PP} = 177 Hz
4[d]	$\mathbf{B_2}$	$\mathbf{C_2}$	4	15	-16.8	-18.8	J_{PP} = 156 Hz
5[b]	$\mathbf{B_2}$	$\mathbf{D_2}$	15	20	-11.7	-15.7	J_{PP} = 165 Hz
6[b]	$\mathbf{C_2}$	$\mathbf{D_2}$	3	20	-10.5	-15.4	J_{PP} = 173 Hz
7[c]	$\mathbf{A_2}$	$\mathbf{E_2}$	4	700	-16.6	-35.3	J_{PP} = 152 Hz
8[c]	$\mathbf{B_2}$	$\mathbf{E_2}$	4	1000	-19.1	-36.2	J_{PP} = 149 Hz
9[c]	$\mathbf{C_2}$	$\mathbf{E_2}$	4	2800	-19.0	-36.9	J_{PP} = 148 Hz
10[c]	$\mathbf{D_2}$	$\mathbf{E_2}$	30	4000	-17.9	-29.5	J_{PP} = 156 Hz

[a] Time at which *K* was calculated, after the solvent was added to the diphosphanes. [b] In THF. [c] In $CDCl_3$. [d] In C_6D_6. [e] Estimated value (no residual $\mathbf{D_2}$ was observed so its integral was approximated as 1% of the total spectrum). **Aryl substituent key:** A – H (phenyl), B – *p*-CH_3, C – *p*-OCH_3, D – *m*-CF_3 (bis), E – *o*-CH_3.

The chemical shifts of the doublets in the mixed species are generally within 2–6 ppm of the parent diphosphanes and have $^1J_{PP} \simeq 160$ Hz. The reaction scheme and spectrum of the $\mathbf{B_2}$/$\mathbf{C_2}$ reaction (Table 5.2, Entry 4) is given as an example in Figure 5.07: the singlets of the parent diphosphanes are evident alongside the 'AB pattern' of the mixed species, **BC**.

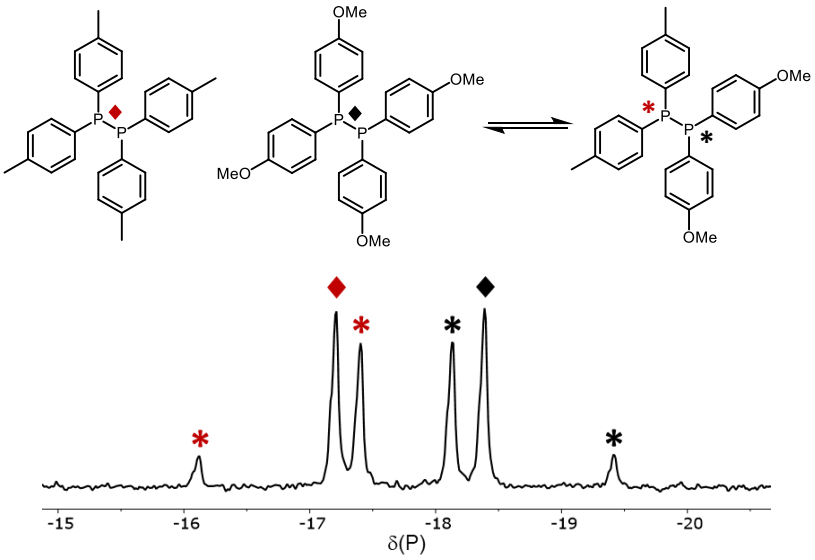

Figure 5.07. The $^{31}P\{^{1}H\}$ NMR spectrum of the metathesis reaction between **B_2** and **C_2**.

The equilibrium constants (*K*) for these exchange reactions are within the range of 3–30 (Table 5.2). This corresponds to ΔG between -0.5 and -2 kcal mol^{-1} (Equation 5.2), indicating that these diphosphanes are very close in energy and insensitive to the steric and electronic effects of the aryl substituents. In general, the timescale of the reactions that do not involve **E_2** are very similar, each resulting in rapid establishment of equilibrium (<10 min) despite the low concentration (~12.5 mM). This means tetraaryldiphosphanes are potentially useful new candidates for dynamic covalent chemistry. Those reactions involving **E_2** are significantly slower, which will be discussed later.

$$\Delta G = -RT\ln K \qquad \text{Eq. 5.2}$$

A series of 22 metathesis reactions were modelled by DFT calculations (performed by T. Young, University of Oxford). The calculated ΔG of the **A_2/E_2** reaction is 1.2 kcal mol^{-1}, which is very close to the experimentally observed -0.8 kcal mol^{-1}. From these results it appears that there is a strong bias towards the **XY** species when there is a significant difference in either steric bulk or electronegativity. The most favoured reaction of those calculated is the reaction between $^{t}Bu_2P–P^{t}Bu_2$ and $F_2P–PF_2$ (-15.4 kcal mol^{-1}). In this case there are both factors: (1) electronegativity difference—between the electron-rich $^{t}Bu_2P$ and electron-poor F_2P centres—and (2) steric relief; the large steric clash of $^{t}Bu_2P–P^{t}Bu_2$ is relieved in the mixed diphosphane $^{t}Bu_2P–PF_2$. Accordingly, species such as this and some of those diphosphanes reported by Grubba *et al.*,[5] should be thermally stabilised with respect to the corresponding symmetrical diphosphanes. This would explain why in their work they were able to avoid using borane protection when synthesising their unsymmetrical diphosphanes.

5.4.3 Mechanistic investigations by DFT

In their 2016 computational study,[4] the lowest energy pathway that Gilheany and co-workers could find involved the ionic triphosphorus intermediate shown in Scheme 5.11. However, they acknowledged that the calculated barrier of 36.5 kcal mol^{-1} could not account for the rapid exchange observed (under ambient conditions) experimentally.

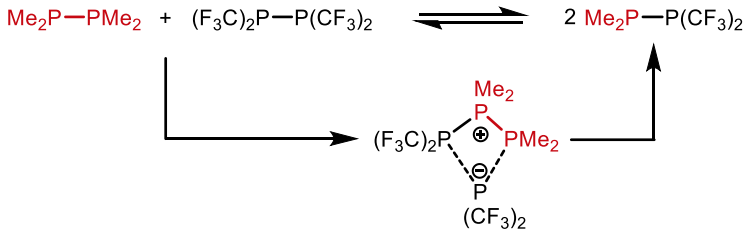

Scheme 5.11. The Gilheany mechanism of diphosphane metathesis.

In a series of further calculations, T. Young explored the viability of three different mechanistic pathways that we proposed for the thermal rearrangement of the degenerate $Me_2P–PMe_2/Me_2P–PMe_2$ system, Scheme 5.12. Each of the proposed mechanisms **i–iii** are plausible and are consistent with some experimental observations as will be discussed later. Mechanism (**i**) is a concerted [2+2] pathway with a 4-membered transition state/intermediate. Mechanism (**ii**) is nucleophilic attack of one diphosphane on another, which produces an ionic intermediate. Mechanism (**iii**) is a radical chain process.

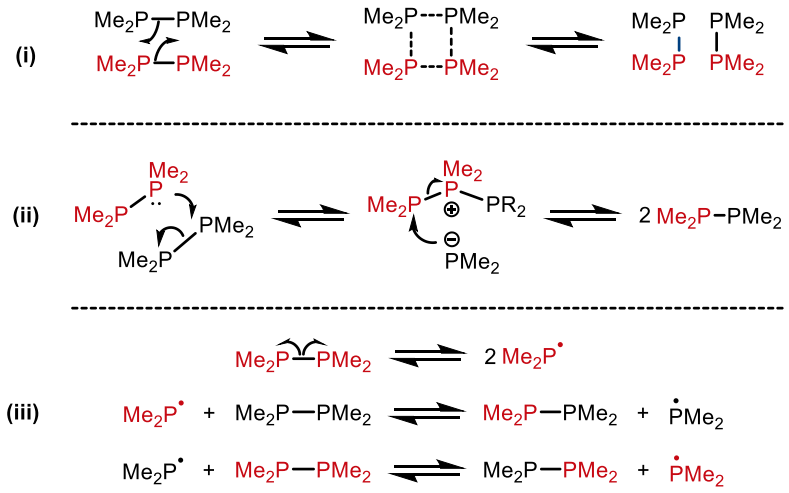

Scheme 5.12. Mechanisms of diphosphane metathesis.

Computational attempts to find a synchronous σ-bond metathesis pathway corresponding to (**i**) were unsuccessful, as similarly reported by Ruipérez *et al.*[39] in their calculations concerning disulfide metathesis. Calculations exploring pathway (**ii**) support the findings of Gilheany and co-workers;[4] the ionic intermediate, at 44.1 kcal mol^{-1}, is too-high in energy to be thermally accessible. When the

calculation was repeated for tetraphenyldiphosphane (**A_2**), the analogous intermediate was found to be lower in energy (38.1 kcal mol^{-1}), but still incompatible with experimental observation (rapid, spontaneous reaction). Pathway (**iii**) requires homolysis of the P–P bond; however, thermolysis of this bond is also not feasible under ambient conditions. With bond enthalpies on the order of 50 kcal mol^{-1}, P–P bonds are weak when compared to many covalent bonds but this is still well above the threshold of a process that is feasible at room temperature. Nevertheless, DFT calculations on **A_2** suggest that excitation from $S_0 \rightarrow S_1$ and $S_0 \rightarrow S_2$ would result in rapid homolysis of the P–P bond, yielding phosphinyl radicals ($Ar_2P\bullet$) via intersystem crossing from S_1 or S_2 to the first excited triplet state (T_1) of **A_2**. The T_1 state is dissociative, and would lead to spontaneous radical formation. These excitations roughly correlate to $n \rightarrow \pi^*$ and $\sigma \rightarrow \sigma^*$ processes as indicated by transition electron density difference plots (calculated using time-dependent DFT), Figure 5.08. From these plots it is evident that in both transitions a significant amount of electron density is migrates from the phosphorus lone pairs and becomes dissociated throughout the molecule. Crucially these calculations explain both where phosphinyl radicals may originate from and why P(V)–P(V) species have not been observed to undergo metathesis.

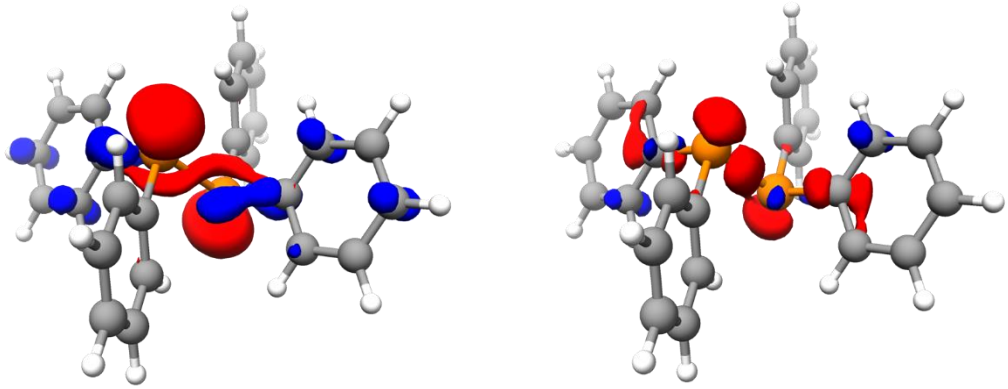

Figure 5.08. Transition electron density difference plots calculated with orca_plot by T. Young with the CAM-B3LYP/def2-TZVPP//PBE0-D3BJ/def2-SVP level of theory. Left, S_0-S_1 and right, S_0-S_2. Red and blue correspond to depleted and excess electron density respectively. Isosurface plotted at a contour of 0.003 au.

Attack of the phosphinyl radical (**X•**) on an intact diphosphane (**Y_2**)—leading to formation of an unsymmetrical **XY** diphosphane and **Y•**—is associated with an energy barrier of only ~5 kcal mol^{-1}. This implies that any generation of phosphinyl radicals would lead to a rapid chain reaction towards the equilibrium mixture.

These results strongly suggest that the photolytic generation of phosphinyl radicals is the most likely mechanism of diphosphane metathesis.

5.4.4 Mechanistic investigations by NMR

The tetraaryldiphosphane metathesis reactions between combinations of **A_2**, **B_2**, **C_2** and **D_2** are extremely rapid under ambient conditions, with equilibrium reached within <10 min in all tested organic solvents (C_6D_6, THF, toluene, fluorobenzene, chlorobenzene, $CDCl_3$ and CD_2Cl_2). In contrast, those reactions between the *o*-tolyl substituted **E_2** and another diphosphane were much slower in $CDCl_3$ (eqm. reached in 6–12 h) and CD_2Cl_2 (eqm. reached in >24 h) and were essentially inert in other solvents. This solvent sensitivity, though unusual, was reported before in similar experiments by Harris and Norval.[3]

A general procedure for the following experiments is given in Section 5.7.3.

The general case (**A_2**-**D_2**). When cold (-78 °C) solutions of **B_2** and **C_2** were mixed and the metathesis monitored by variable temperature (VT) ^{31}P NMR spectroscopy, negligible reaction was observed at -80 °C. After raising the temperature by increments of 20 °C it was found that the reaction at -20 °C proceeded at a convenient rate for study (eqm. established in ~2 h, Figure 5.09). Although a detailed kinetic study was not attempted, the data are not consistent with 0, 1st, 2nd or ½-order kinetics, though the rate appears to be independent of diphosphane concentration during the early stages of reaction.

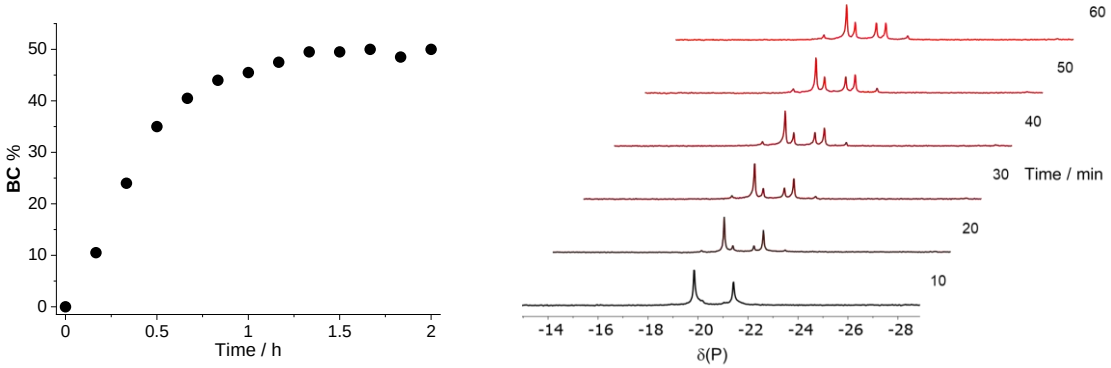

Figure 5.09. Left, plot of heterodiphosphane **BC** formation as a function of time for the full 2 h. Right, ^{31}P{^{1}H} NMR spectra of the reaction between **B_2** and **C_2** at -20 °C in THF, shown in 10 min increments over the course of 1 h (with inverse-gated decoupling).

Two major pieces of experimental evidence support the hypothesis that radicals are involved in the metathesis mechanism:

(1) The radical scavengers TEMPO (2,2,6,6-tetramethyl-1-piperidinyloxy) and TTBP (tri(*t*-butyl)phenol) greatly inhibit the rate of metathesis.

In the metathesis of **A_2** with **C_2** in $CDCl_3$ at -20 °C, the reaction proceeds to equilibrium in approximately 2 h, with 35% **AC** within 1 h. In contrast, an equivalent reaction in the presence of 5 equiv. of TEMPO produced undetectable amounts of **AC** within 1 h. Even after the TEMPO-inhibited reaction was warmed to room temperature, <10% **AC** was observed after 16 h. At room temperature, this reaction

would otherwise be expected to have reached equilibrium (~50% **AC**) within 10 min. Furthermore, two singlet ^{31}P resonances were observed at +30.5 and +31.5 ppm (9% combined integral after 16 h) that are consistent with the formation of TEMPO-P adducts, Scheme 5.13, which have previously been reported from the reaction of TEMPO with secondary phosphines.[40]

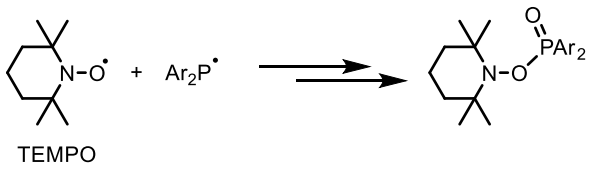

Scheme 5.13. TEMPO-P adduct formation.

(2) Metathesis is slowed in the dark (and accelerated by UV).

In the metathesis of $\mathbf{A_2}$ with $\mathbf{B_2}$ in THF in a conventional NMR tube, equilibrium is established at ambient temperature within ~15 min. However, when an equivalent $\mathbf{A_2}$/$\mathbf{B_2}$ solution was mixed in an amberised NMR tube—designed to minimise the transmittance of both UV and visible radiation—equilibration took ~150 min. This strongly suggests that photodissociation is a limiting factor in the metathesis rate. The UV-vis spectra of $\mathbf{A_2}$, $\mathbf{C_2}$ and $\mathbf{E_2}$ are shown in Figure 5.10. Each of these diphosphanes exhibit the same pattern: (1) a strong absorption in the 230–250 nm region that corresponds to a $\pi\rightarrow\pi^*$ excitation, which unsurprisingly appears sensitive to the aryl substituents. (2) a weaker shoulder absorption at approximately 270 nm that is common to each species but is most pronounced for $\mathbf{E_2}$. From the computational results discussed previously, it is proposed that the major $\pi\rightarrow\pi^*$ absorption is coincident with the $S_0\rightarrow S_2$ ($\sigma\rightarrow\sigma^*$) transition. The shoulder most likely corresponds to the $S_0\rightarrow S_1$ ($n\rightarrow\pi^*$) transition, both of which lead to P–P scission.

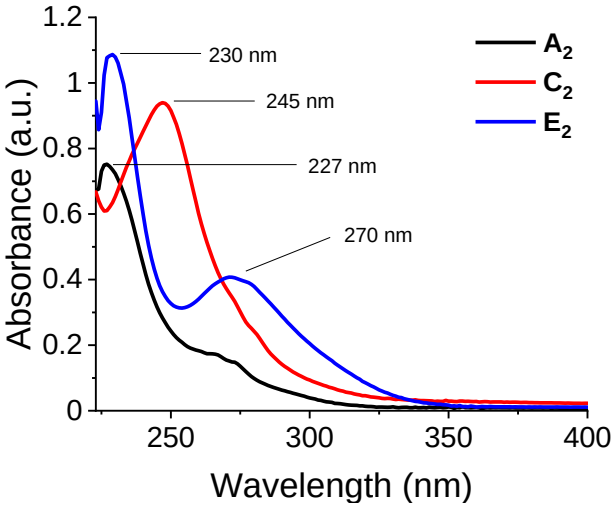

Figure 5.10. UV-vis spectra of $\mathbf{A_2}$, $\mathbf{C_2}$, and $\mathbf{E_2}$ in CH_2Cl_2 (20 μM).

This combination of observations and calculations suggests a radical chain mechanism of the form shown in Scheme 5.14.

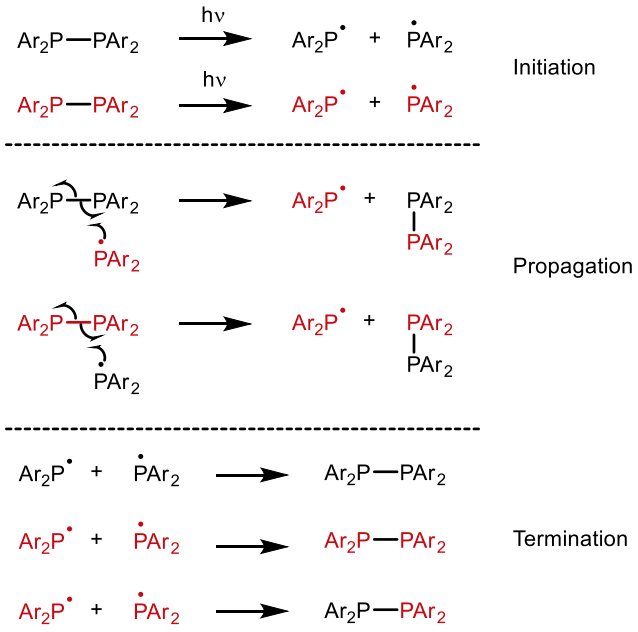

Scheme 5.14. Proposed radical mechanism of diphosphane metathesis.

The initiation, being a photodissociative step, requires UV radiation; however, it appears that there is sufficient ambient UV to induce the reaction in the laboratory. As indicated by DFT calculations, thermolysis is not feasible at ambient conditions, but importantly—since it could have ramifications for materials applications—metathesis can take place in the melt phase, as will be discussed again in the context of metathesis with **E_2**. The degenerate propagating steps ($R_2P\bullet$ + $R_2P–PR_2$, which simply regenerate the starting diphosphanes) are omitted for clarity. Similarly, the reverse process (from photodissociation of $R_2P–PR'_2$) is also possible but is not included in the scheme. These metathesis reactions generally proceed with high selectivity, although secondary phosphine resonances are often observed in the ^{31}P NMR spectra especially after prolonged reaction times, which presumably indicate an alternative termination step whereby a phosphinyl radical abstracts a proton from the solvent.

Overall, this mechanism and these findings share many similarities with disulfide metathesis, which is covered in detail in two papers in *Physical Chemistry Chemical Physics* by Ruipérez *et al.*[39] and Asua *et al.*,[41] which were reviewed in Chapter 4.

In the former study, Ruipérez *et al.*[39] use DFT and MD calculations to model two mechanisms of (aromatic) disulfide exchange: [2+2] concerted metathesis, and [2+1] reaction mediated by the sulfanyl radical. Similar to our findings with diphosphanes above, those authors could not find a plausible transition state for the [2+2] process. The authors were successful in finding suitable 3-membered transition states for the radical process, which had enthalpies of the order of 10 kcal mol^{-1} higher than the starting materials. Through considering the BDEs and the first electronic excitation energy, the authors concluded that the formation of sulfanyl radicals would generally be caused by thermal dissociation because the first excitation energies correspond to UV wavelengths. However, with BDEs of the order of 40–50 kcal mol^{-1}, spontaneous thermolysis seems unlikely under ambient conditions.

In the latter study, Asua *et al*.[41] explored the mechanism of disulfide exchange experimentally using the model system of diphenyl disulfide and di(4-aminophenyl) disulfide which proceeds spontaneously to an equilibrium in *ca*. 12 h. These authors found that the addition of TEMPO as a radical scavenger completely inhibited their model exchange reaction and the reverse effect was observed when a radical initiator (V70) was used. Furthermore, UV-acceleration was also observed, consistent with the radical mechanism. Interestingly, solid-state EPR measurements revealed a resonance for one of their tested disulfides but not the other, suggesting that the radical concentration is near the limit of sensitivity. The observations of these disulfide studies and those of similar diselenide studies,[42] are very similar to ours. Although the authors do not explicitly state that ambient UV is responsible for the spontaneous metathesis reaction, their findings seem to imply this. In any case, there are evidently significant parallels between diphosphanes and disulfides.

Metathesis with E_2. As previously alluded to, the four reactions between tetra(*o*-tolyl)diphosphane (**E_2**) and the other diphosphanes exhibited somewhat different behaviour to the more general metathesis, Figure 5.11. These reactions do not appear to proceed at all in THF, fluorobenzene, chlorobenzene, toluene or C_6D_6 under ambient conditions (up to 72 h), though the reactions do proceed in CH_2Cl_2 and $CHCl_3$ (and the deuterated analogues), though much slower than the other metatheses (see Table 5.2). Accordingly, this process was explored in more detail, starting from both the **A_2**/**E_2** system and pure **AE**.

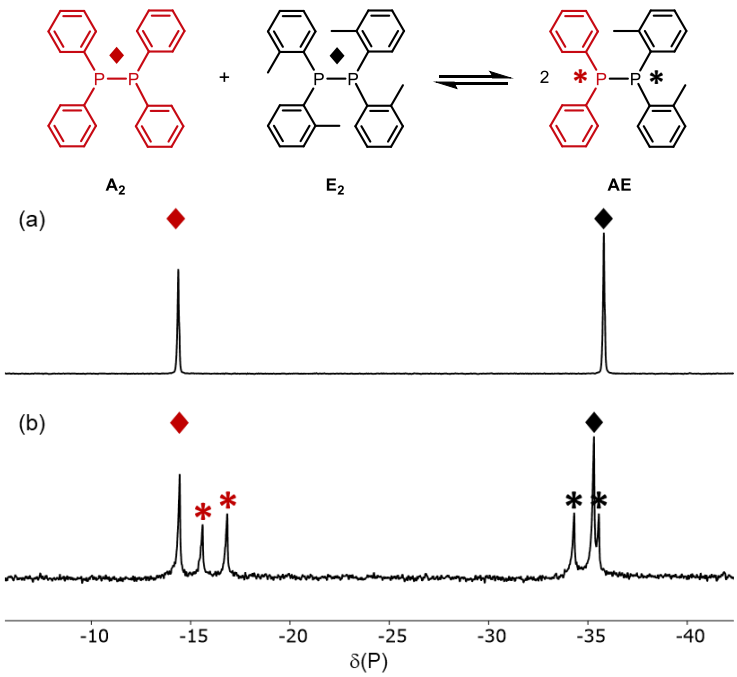

Figure 5.11. The NMR spectra of the **A_2/E_2** system: (a) in toluene after 48 h and (b) in $CDCl_3$ after 6 h.

The kinetics of this reaction were also investigated by ^{31}P NMR spectroscopy (details in Section 5.7.2). The progress of **A_2/E_2** metathesis was probed at 10 min intervals for 12 h (at room temperature). Integration of the diphosphane resonances Figure 5.12 (right) allowed the construction of the plot Figure 5.12 (left). Analysis of this process revealed that the kinetics were not consistent with integrated rate equations for reaction order 0, ½, 1 or 2; indicating that the kinetics are complex, expected where multiple mechanistic pathways are competing. Interestingly, the rate of **AE** formation is fastest between t_0 and the time of the first spectrum (10 min) and then the rate declines significantly. This might be attributable to the decreased light intensity within the spectrometer.

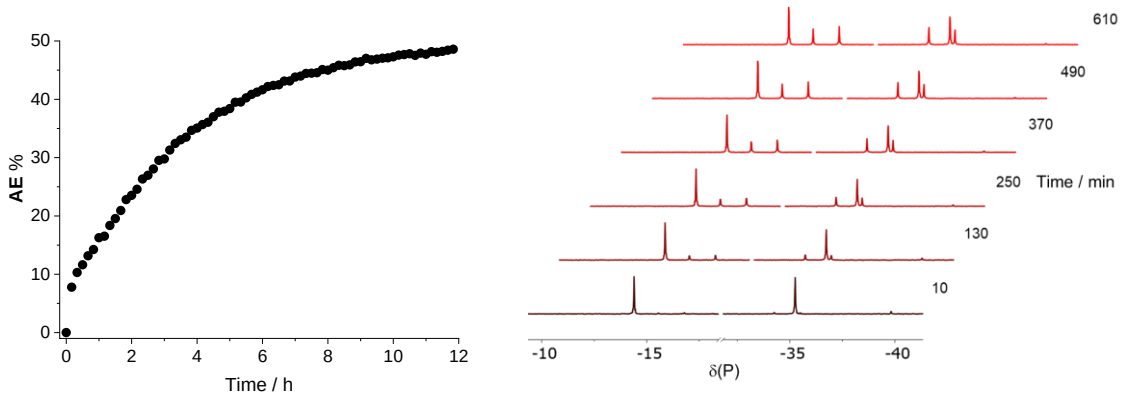

Figure 5.12. Left, plot of the data obtained from integration of the diphosphane resonances in the 72 $^{31}P\{^1H\}$ NMR spectra in $CDCl_3$ between **A_2/E_2**. Right, the associated $^{31}P\{^1H\}$ NMR spectra with a 2 h sampling up to 12 h.

As in the general case, there is good evidence of radical involvement in reactions involving **A_2**/**E_2** as outlined below.

(1) Whereas after 72 h, an **A_2**/**E_2** mixture in THF gave no reaction, when the same solution was irradiated with a handheld UV lamp for 2 h, the reaction proceeded to 30% **AE**. Similarly, starting from pure **AE**, no evidence of reversion to the symmetrical diphosphanes was observed after 72 h; however, the reaction did proceed (to ~50% **AE** and ~50% **A_2**/**E_2** after 1 h) under UV irradiation. This suggests that the photodissociative step in Scheme 5.15 is viable for metathesis with **E_2**, but implies that more intense radiation is required. Indeed, as we can see from Figure 5.10, the UV-vis spectrum of **E_2** seems to show stronger absorption (than **A_2** and **C_2**) in the bands that DFT calculations suggest lead to P–P scission. This indicates that photodissociation should still be possible with this species and it is unclear why more intense irradiation is required. Given the intensity of the transitions in question, it is possible there is more photodissociation with **E_2** compared with other diphosphanes. If true, there must be another reason behind the observed decrease in reactivity. It is possible that there is a mechanism by which **E_2** is excited but does not undergo the same relaxation pathway that leads to photodissociation.

(2) The slow formation of **AE** from **A_2**/**E_2** mixtures in $CDCl_3$ (equilibrium reached in ~12 h) was stopped entirely in the presence of four equivalents of TEMPO or TTBP (no **AE** observed after 16 h).

(3) Pulse-sonication (20 kHz) at 0 °C of $CHCl_3$ or CH_2Cl_2 solutions of **A_2**/**E_2** reduced the time to equilibrium from >12 h to <1 h. However, no reaction was induced in analogous experiments in THF or toluene. This is in agreement with the observations of Fritze and von Delius who reported the sonochemical metathesis of aromatic disulfides.[43] These authors suggested that RS• species were the active intermediates in this process, and these were formed through reaction of the disulfides with chloroform degradation products (e.g. Cl•). This would explain some of the solvent sensitivity, since most solvents are less susceptible to degradation than chloroform.

(4) In the reverse process, the onset of equilibration from **AE** is associated with an induction period of the order of ~6 h, prior to which there is little evidence of metathesis. The fact that the rates of this process and the forward reaction vary between 6–12 h, is also consistent with radical processes.[44]

In addition to the evidence for radical intermediacy, there is also evidence of chlorophosphine involvement in these reactions as follows.

(1) Under the conditions where a mixture of **A_2** and **E_2** in $CDCl_3$ would typically reach equilibrium in ~12 h, in the presence of a large excess of water (*ca*. 100 eq.), the reaction was suppressed such that there was <1% **AE** formed within 20 h. ^{31}P NMR resonances at +23.5 and +21.4 ppm corresponding to the respective secondary phosphine oxides ($Ar_2P(O)H$) were observed, which might be representative

of chlorophosphine formation and subsequent hydrolysis (due to the slow ingress of air into the NMR tube).

(2) When a solution of **A_2/E_2** in $CHCl_3$ is irradiated with UV, ~10% conversion to Ar_2PCl is observed by ^{31}P NMR spectroscopy.

(3) The stoichiometric reaction of **A_2** with $(o\text{-Tol})_2PCl$ in $CHCl_3$ resulted in rapid formation of a mixture of **A_2**, **AE**, Ph_2PCl and $(o\text{-Tol})_2PCl$ as well as some unidentified species, Scheme 5.16. After 4 h, some **E_2** was observed alongside Ph_2PH and $(o\text{-Tol})_2PCl$. This confirms that chlorophosphines are plausible promoters of diphosphane metathesis.

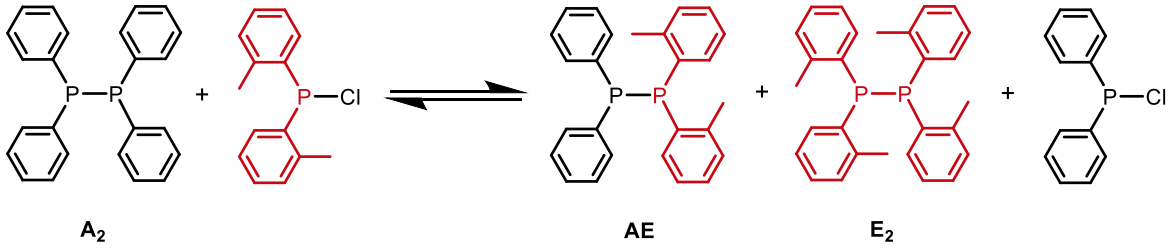

Scheme 5.16. The reaction between **A_2** and $(o\text{-Tol})_2PCl$.

To test if chlorophosphine could *catalyse* diphosphane metathesis, a sub-stoichiometric amount (~5 mol%) of Ph_2PCl was added to a chloroform solution of pure **AE**. This reaction was then compared with a control (with no Ph_2PCl). With no chlorophosphine, the reaction reached equilibrium in ~70 h; in the presence of 5 mol% chlorophosphine, this reaction time was reduced to just 7 h, Figure 5.13.

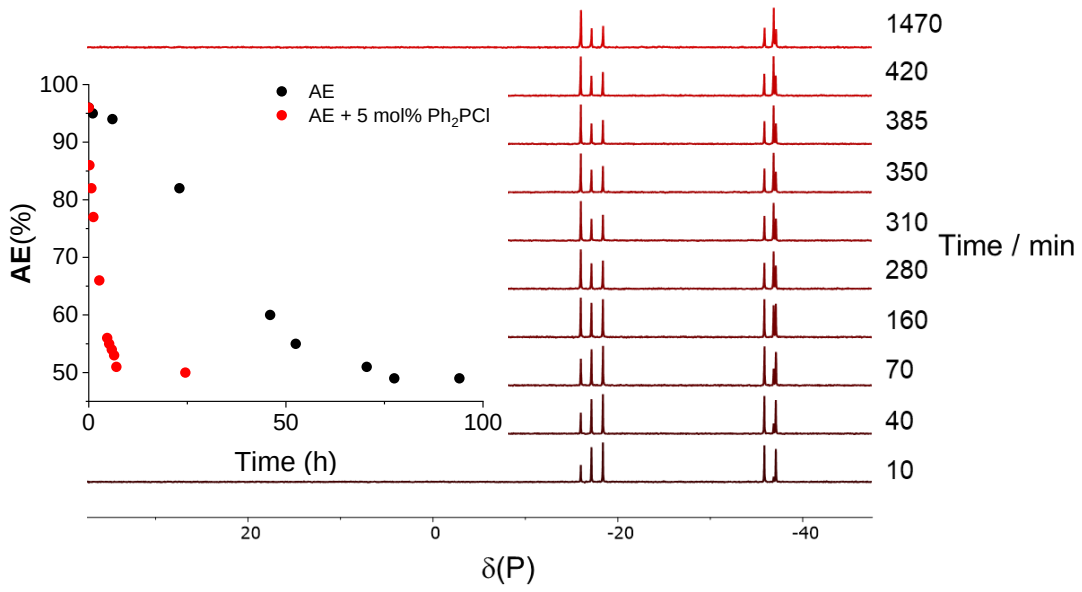

Figure 5.13. Reverse metathesis of **AE** (10 mg) in $CDCl_3$ catalysed with 5 mol% Ph_2PCl.

Thus the key observations concerning the **A_2/E_2** reaction are as follows:

(1) The choice of solvent ($CHCl_3$ or CH_2Cl_2) is critical for the reaction to proceed under ambient conditions.

(2) As in the metathesis more generally, the reaction has the characteristics of being radical initiated.

(3) Chlorophosphine can catalyse the metathesis, and hence it is important to note that no chlorophosphine was detected by ^{31}P NMR in the spectra of the pure diphosphanes.

It is well-documented that $CHCl_3$ can be a source of radicals, particularly under irradiation or sonolysis. Accordingly, the mechanism in Scheme 5.17 has been devised to explain these observations with di(*o*-tolyl)diphosphane (**E_2**) metathesis. In this mechanism, Cl• or other radical fragments produced from $CHCl_3$/CH_2Cl_2 degradation, have the dual role of generating chlorophosphine, which has been demonstrated to catalyse diphosphane exchange, and in forming Ar_2P• (phosphinyl radicals) that may react through the mechanism previously described in Scheme 5.14. DFT calculations suggest that attack of Cl• on Ar_2P–PAr_2 is feasible: ΔG_r = –35.3 kcal mol^{-1} and $\Delta G^{\ddagger}$ = 3.4 kcal mol^{-1} (from the Ph_2P–PPh_2…Cl• association complex).

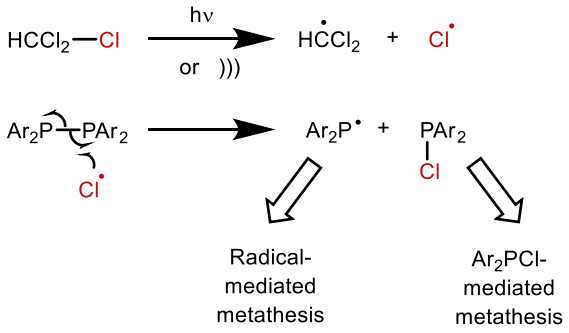

Scheme 5.17. The role of chlorinated solvents in diphosphane metathesis.

The reason for the observed decrease in rate of the metathesis with **E_2** compared to those *without* **E_2**, has not yet been considered. As discussed when the UV-vis spectra were introduced, **E_2** absorbs UV at wavelengths anticipated to result in P–P scission. However, it is possible that scission to (*o*-Tol)$_2$P• is less likely due to a competitive H-abstraction mechanism. Preliminary DFT calculations indicate that intramolecular H-abstraction (of the benzylic protons) may be feasible from the T_1 (diradical) state of **E_2**, which is reached by intersystem crossing from either the S_0 or S_1 states. This mechanism is also consistent with the experimental observation that solutions of **AE** preferentially form *o*-Tol_2PH (over Ph_2PH) during metathesis. A simplified form of this tentative mechanism is shown for the analogous phosphinyl radical in Scheme 5.18. The proximate H atoms could be abstracted to 'quench' the reactivity of the phosphinyl radical (as shown) or the T_1 radical before it can undergo further reaction,

Scheme 5.18. At this stage, prior to dissociation, the T_1 species has an excess energy of *ca*. 33 kcal mol^{-1} which could facilitate such a process. Accordingly, calculations suggest that H-abstraction of this sort is feasible for the T_1 diphosphane but not the phosphinyl radical (shown in Scheme 5.18). Unfortunately, such a mechanism is not straightforward to examine experimentally and thus remains speculative.

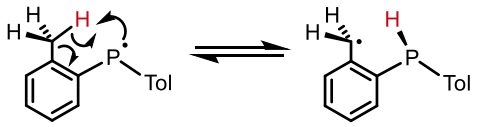

Scheme 5.18. The proposed mechanism of proximal benzylic proton abstraction shown for (*o*-Tol)$_2$P• as a substitute for the more complicated, intact T_1 state of **E_2**.

An alternative explanation for the lower reactivity of **E_2** may lie in steric crowding from the *o*-CH_3 groups. However, DFT suggests that the reaction of (*o*-Tol)$_2$P• with an intact diphosphane should remain feasible; the difference in energy between the transition states in **E_2** metatheses and **A_2** metatheses is minimal (and within computational noise). Only when the *ortho* group is modelled as a *t*-butyl moiety is there a large destabilisation of the R_2P•…R_2P–PR_2 transition state.

Ultimately, it seems likely that there is a steric contribution to the decreased reactivity of **E_2** to diphosphane metathesis, though this may be subtle.

Two further experiments have significance for the application of diphosphanes in polymeric materials.

(1) When **A_2** and **E_2** are melted together at 150 °C for 5 min and then dissolved in THF (a solvent in which these diphosphanes do not undergo metathesis). ^{31}P NMR spectroscopy revealed that the brief melt reaction had been sufficient to establish equilibrium with **AE**. The implication of this is that diphosphane metathesis could be viable in polymer melts.

(2) Mixtures of [$Me_2P(=S)]_2$ and [$Et_2P(=S)]_2$ (i.e. P(V)–P(V) species) were not observed to undergo metathesis in any solvent or in the melt phase; moreover, no reaction was evident when the solutions were treated with AIBN. Although alkyl (and not aryl like the P(III) diphosphanes in this study), these observations suggest that P(V) diphosphanes cannot undergo metathesis reactions. This is consistent with the observation that the phosphorus lone pairs are essential for the electronic excitation that leads to P–P scission. Accordingly, oxidation of P(III)–P(III) materials would be expected to erode their reactivity.

5.5 Heterometathesis: reactions of P–P bonds with other E–E species

In Section 5.4 it was reported that tetraaryldiphosphanes homolyse both in solution and melt phases, resulting in metathesis reactions. This observation combined with our interest in diselenides (Chapter 4)—which are well-known to homolyse under mild conditions[42,45]—led us to speculate on the potential heterometathesis reaction between diphosphanes and diselenides.

5.5.1 Background

In recent decades, phosphorus-sulfur and phosphorus-selenium compounds have attracted increasing research interest, in no small part due to the popularity of Lawesson's reagent and the selenium analogue, Woollins' reagent, which been widely applied in synthesis.[46–48] A plethora of unusual molecules have emerged from this chemistry, notably the complex heterocycles of the Woollins group.[49–51] Further research has led to the development of PS/PSe compounds for applications as diverse as thin film semiconductors and pesticides.[52] However, despite this growing interest there has been surprisingly little attention given to the simplest P(III) compounds, those of the type R_2P–ER (E = S, Se), thiophosphanes and selanylphosphanes, respectively.

According to McLean, the earliest examples of such compounds are the alkylthiodiphenylphosphanes, first reported by Arbuzov in 1910.[53] In 1966, McLean reported the first arylthiodiphenylphosphanes and later the analogous selenium compounds; however, to the best of our knowledge these species were not further tested or characterised.[54]

McLean prepared diphenyl(phenylthiol)phosphane (**11**) via the reaction of Ph_2PCl and sodium thiophenolate in diethyl ether (at 0 °C, with 80–90% yield). The preparation of diphenyl(phenylselanyl) phosphane (**12**), was achieved via the reaction of Ph_2PCl with benzeneselenol in the presence of a slight excess of triethylamine in -10 °C diethyl ether (in 50% yield). More recently, Cui *et al*.[55] prepared 4-((diphenylphosphaneyl)thio)aniline (**13**) as part of their synthesis of a trimetallic iron-iridium photosensitiser via a similar method (in 78% yield), Scheme 5.19.

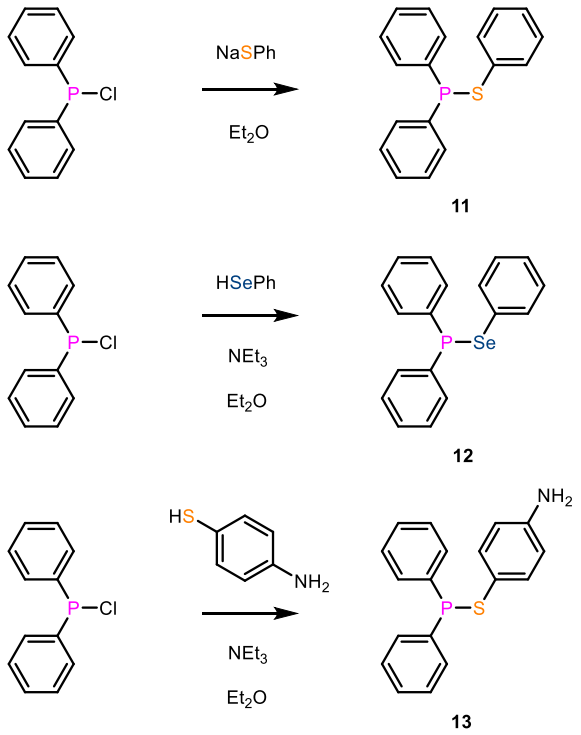

Scheme 5.19. The synthesis of the three literature thio/selanylphosphanes discussed above.[54,55]

5.5.2 Selanylphosphanes

Gratifyingly, on mixing equimolar quantities of tetraphenyldiphosphane (**A_2**) and diphenyldiselenide (Scheme 5.20) in tetrahydrofuran, a new singlet resonance was observed by $^{31}P\{^{1}H\}$ NMR spectroscopy at +29.4 ppm, Figure 5.14. Solvent removal under a reduced atmosphere afforded a colourless oily solid (**12**) in 92% yield. Inspection of subsequent $^{31}P\{^{1}H\}$ NMR spectra revealed that the product resonance had ^{77}Se satellites with J_{PSe} = 229 Hz. Although it was initially difficult to obtain a ^{77}Se NMR signal, by using a 60° pulse, relaxation delay of 30 s and 1000 scans, a well-resolved $^{77}Se\{^{1}H\}$ spectrum was recorded (Figure 5.14), revealing a doublet at 307.5 ppm (J_{PSe} = 229 Hz). Compound **12** was then further characterised by ^{1}H and $^{13}C\{^{1}H\}$ NMR, which showed the expected resonances, and positive-ion APCI mass spectrometry, which showed the expected $[M+H]^+$ peak, 343.0140 m/z. The structure of **12** was then unambiguously confirmed after crystals suitable for single-crystal X-ray diffraction were grown by CH_2Cl_2-hexane vapour diffusion, Figure 5.15.

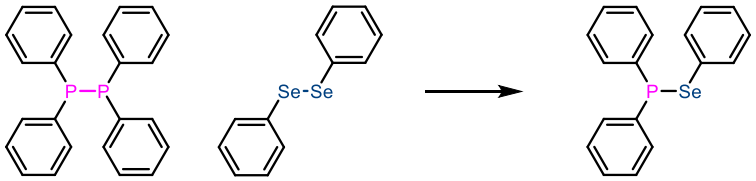

Scheme 5.20. The synthesis of diphenyl(phenylselanyl)phosphane (**12**).

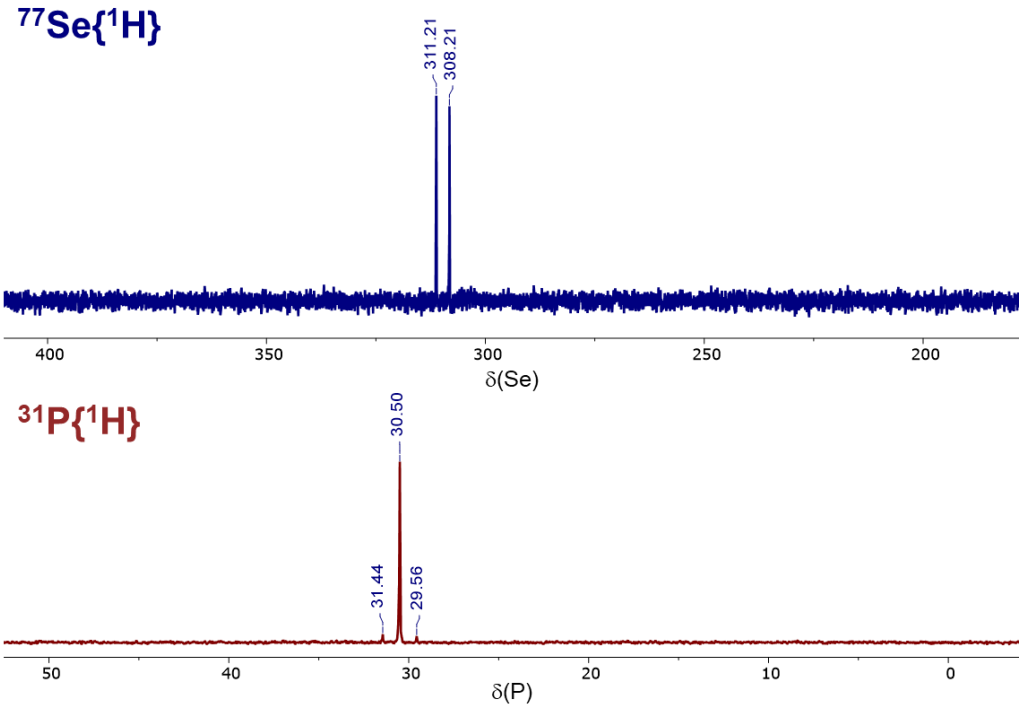

Figure 5.14. The $^{77}Se\{^{1}H\}$ and $^{31}P\{^{1}H\}$ NMR spectra of diphenyl(phenylselanyl)phosphane (**12**) in $CDCl_3$.

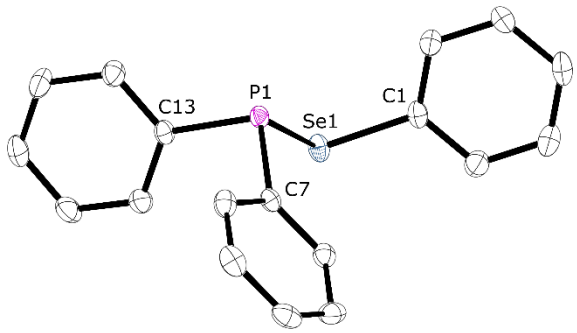

Figure 5.15. Thermal ellipsoid (50% probability) representation of the crystal structure of diphenyl(phenylselanyl)phosphane (**12**), hydrogen atoms omitted for clarity. Selected bond lengths [Å]: P1–Se1 2.262, P1–C7 1.842, P1–C13 1.834, Se1–C1 1.932.

From this initial reaction, the substrate scope was expanded to several other P–Se and P–S species (Scheme 5.21). The mechanism has been briefly investigated and some further reactions of these compounds are explored. Note that no reaction was observed when **A_2** was reacted with other E–E species, including an O–O bond (*t*-butylperoxide), an N–N bond (diphenylhydrazine), a Te–Te bond (diphenyl ditelluride) or an Sn–Sn bond (hexamethylditin); these reactions will not be discussed further.

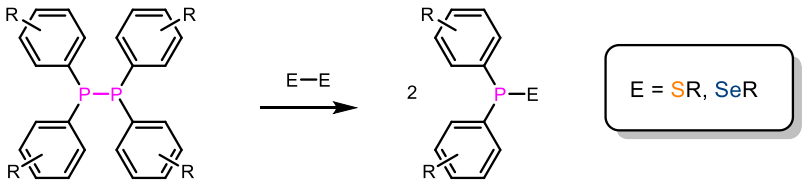

Scheme 5.21. The general concept of this P–S and P–Se metathesis.

The P–Se heterometathesis reaction has been extended to a few other substrates which led to the successful synthesis of compounds **14–17** from their respective combinations of diphosphane and diselenide, Figure 5.16. Each of these compounds was produced in good isolated yield (quantitative yields observed by spectroscopy) as either an oil or oily solid and characterised by $^{31}P\{^{1}H\}$, $^{77}Se\{^{1}H\}$, ^{1}H, $^{31}C\{^{1}H\}$ and APCI mass spectrometry, summarised in Table 5.3. These reactions were either performed in THF, CH_2Cl_2 or toluene; in no case was the solvent observed to affect the rate or outcome of the reaction, which in all cases had proceeded to completion within <10 min—indeed, all reactions had proceeded to completion prior to measurement of the first $^{31}P\{^{1}H\}$ NMR spectrum.

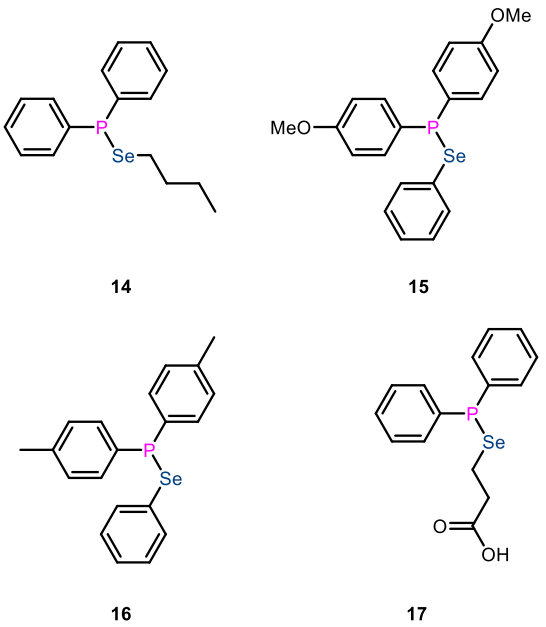

Figure 5.16. Selanylphosphanes **14**–**17**.

Table 5.3. Characterisation data for selanylphosphanes **14–17** ($CDCl_3$). All MS experiments were APCI+ with the exception of **17** which was APCI-.

Compound	^{31}P δ (ppm)	^{77}Se δ (ppm)	J_{PSe} (Hz)	$[M+H]^+$ Theor. / $[M+H]^+$ Obs.
12	30.6	309.6	229	343.0149 / 343.0140
14	22.1	169.5[a]	243	323.0462 / 323.0450
15	29.8	317.1	223	403.0361 / 403.0362
16	30.2	311.5	225	371.0462 / 371.0468
17	23.7	237.8	233	339.0048 / 339.0034

a – measured in toluene

To shed light on the reaction mechanism, $\mathbf{A_2}$ and diphenyldiselenide were mixed in the presence of four molar equivalents of TEMPO, prior to the addition of THF. As we reported in Section 5.4, TEMPO inhibits the metathesis of diphosphane mixtures, presumably via scavenging phosphinyl radicals. In Section 5.2, we reported that TEMPO also inhibits diphosphane oxidation. Similarly, the $Ph_2P–PPh_2$ / PhSe–SePh heterometathesis reaction was also inhibited by the presence of TEMPO, with the reaction rate decreasing from the order of seconds/minutes to hours. This strongly suggests that radicals are involved in (or prior to) the rate determining step of the mechanism. Consequently, it is unlikely that a direct metathesis-type process (Scheme 5.22, i) or an S_N2-type process (Scheme 5.22, ii) are significant in this reaction. In addition, it might be expected that the S_N2 process would show significant solvent-sensitivity (due to charge stabilisation in more polar solvents), which was not observed. Accordingly, the radical processes (Scheme 5.22, iii and iv) are more probable, particularly when considering the known susceptibility of diselenides to photolysis and thermolysis.

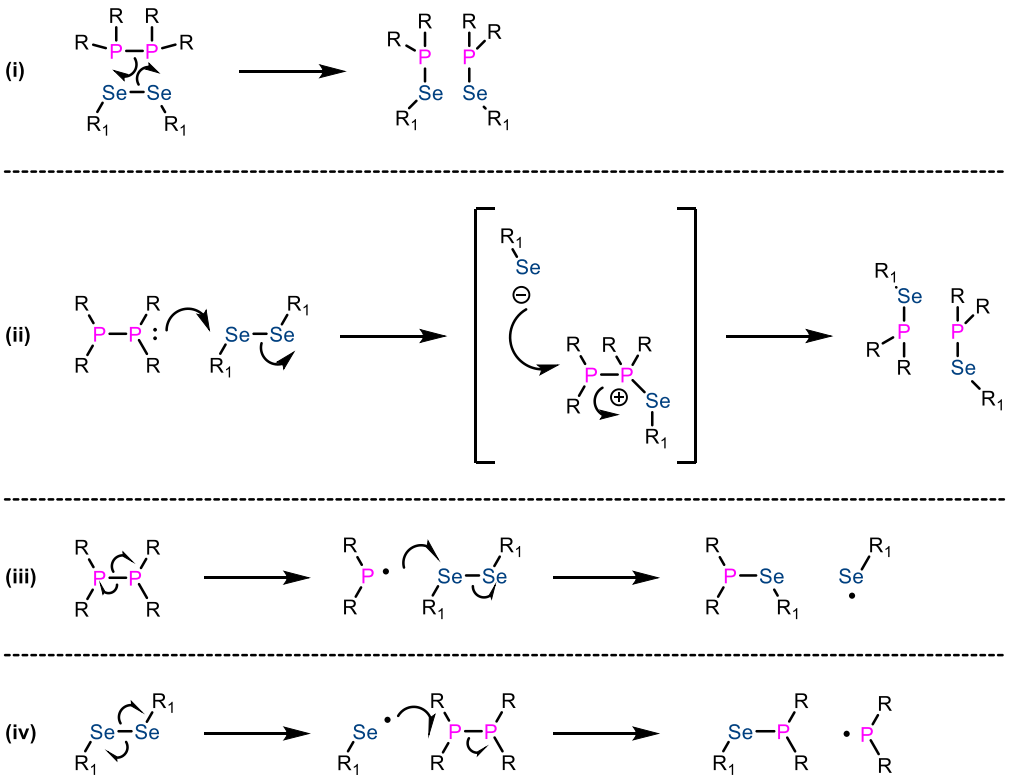

Scheme 5.22. Possible mechanisms of diphosphane-diselenide exchange. (i) – concerted metathesis, (ii) – bimolecular nucleophilic substitution, (iii) – diphosphane homolysis and (iv) – diselenide homolysis.

To the best of our knowledge selanylphosphanes have not previously been tested as ligands, though the juxtaposition of two contrasting donor atoms in P and Se may yield metal complexes with interesting characteristics. Indeed, a variety of different phosphorus- *and* selenium-containing compounds have been used as ligands before.[56–58]

Upon reaction of two equivalents of selanylphosphane **12** with $[Mo(CO)_4(nbd)]$ (nbd = norbornadiene) in CD_2Cl_2, two new compounds were observed by $^{31}P\{^1H\}$ NMR spectroscopy and have been tentatively assigned as shown, Figure 5.17.

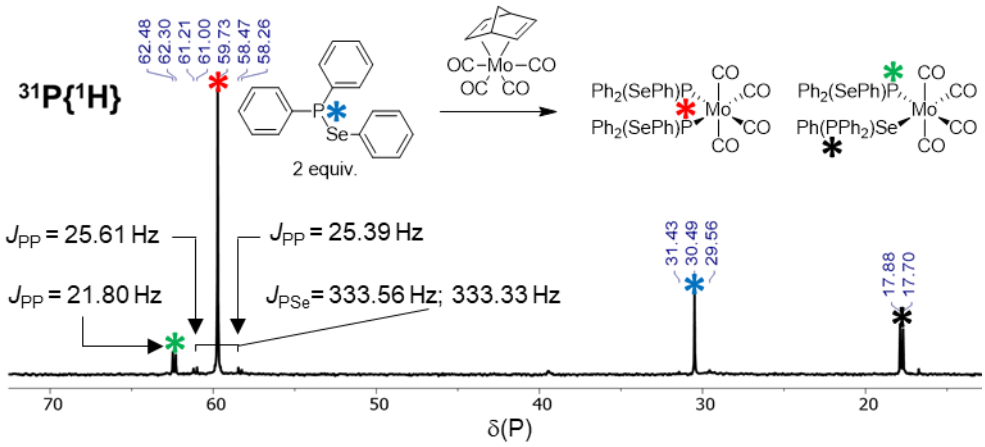

Figure 5.17. The coordination reaction of diphenyl(phenylselanyl)phosphane **12** in CD_2Cl_2 on a molybdenum tetracarbonyl core.

The major product is a singlet at +59.7 ppm with ^{77}Se satellites (J_{PSe} = 333 Hz) that are themselves split into doublets (J_{PP} = 25 Hz). Presumably this inequivalence is the result of a loss of symmetry, in the ^{77}Se isotopologue. Some free ligand is also visible at +30.5 ppm. The major product is associated with a coordination shift of approximately +30 ppm from the free ligand. The other two major peaks are a doublet at +62.4 ppm and a doublet at +17.8 ppm (J_{PP} = 22 Hz). This coupling suggests that two very different phosphorus atoms are present and that is consistent with this second species being an isomer of the first, in which one ligand is coordinated through phosphorus and one ligand is coordinated through selenium as shown. The small value of J_{PP} indicates cis geometry and the presence of several peaks in the carbonyl stretching region of the IR spectrum also supports the hypothesis that these species are cis isomers. When the solution was heated to 50 °C, within a few hours the species giving rise to doublets in the ^{31}P NMR spectrum became the dominant complex in solution, and amongst the emergence of several minor resonances, a significant increase in free ligand was also detected by ^{31}P NMR. A repeated FTIR experiment revealed the presence of a similar pattern of at least four peaks within the carbonyl region, suggesting that both major species have cis configuration.

The selanylphosphanes appear to oxidise upon exposure to moist air. Indeed, single crystals of diphenylphosphinic acid (Cambridge Crystallographic Database deposition number 1145369) formed over the course of approximately three weeks due to the slow ingress of air into an NMR tube containing **12** in THF. Surprisingly, the presence of excess water in anoxic conditions only resulted in very slow hydrolysis of **12**. Moreover, samples of **12** stored under argon have shown negligible thermal degradation in over 2 months. Thus, although selanylphosphanes undergo rapid thermal degradation at 100 °C—as reported by McLean[54]—they are relatively stable species when compared to other P(III)–E-bonded compounds. This has some potential significance since this methodology may be used to

easily furnish phosphines with pendent functional groups (demonstrated with a carboxylic acid, **17** and a primary amine, **13**); moisture sensitivity would otherwise greatly limit the scope of application.

The molybdenum complexes of **12** were not observed to undergo any changes when exposed to excess water.

5.5.3 Thiophosphanes

The P,P–Se,Se heterometathesis reaction was then extended to disulfides via reaction of $\mathbf{A_2}$ with diphenyl disulfide and 4-aminophenyl disulfide, giving the previously reported **11** and **13** respectively, Figure 5.18. In contrast with the analogous diselenide heterometatheses, the disulfide reactions were comparatively sluggish—taking ~20 h to reach completion—and resulted in the production of side products, notably the rearrangement P(V) products **18** and **19**, Figure 5.18. These side products could be removed via elution through an alumina plug though this resulted in a substantial decrease in yield.

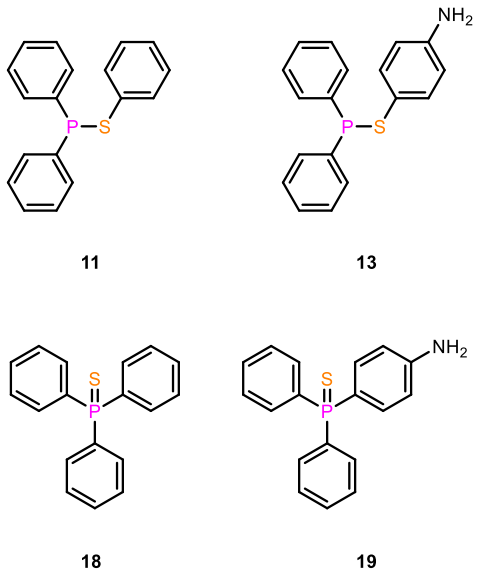

Figure 5.18. Thiophosphanes **11** and **13**, and their respective thermal rearrangement products, phosphine sulfides **18** and **19**.

As with diphosphane-diselenide metathesis, diphosphane-disulfide metathesis was tested for radical inhibition using an excess of TEMPO (four equiv.). In a similar fashion to P–P/Se–Se and P–P/P–P metathesis, P–P/S–S exchange was also greatly slowed, suggesting that radicals play a critical role in the reaction mechanism, which again may feasibly react through analogous pathways to those shown in Scheme 5.22. The fact that the disulfide reaction is at least an order of magnitude slower than the analogous diselenide reaction also implies information about the reaction mechanism. The simplest explanation for this lower reactivity lies in the comparative bond energies involved: diselenides are much weaker and thus much more likely to form radicals in solution (that could attack a diphosphane).

5.6 Summary

In this chapter, the solution metathesis of diphosphanes under ambient conditions is reported. A range of new experimental and computational evidence has revealed that the reaction most likely proceeds through a radical chain process after UV-photolysis of the P–P bond (which generates phosphinyl radicals). With most tetraaryldiphosphanes this reaction is rapid at room temperature, with a mixture of two diphosphanes $\mathbf{X_2}$ and $\mathbf{Y_2}$ generating an equilibrium mixture within minutes, suggesting that the small amount of ambient UV light is sufficient to initiate the reaction. The kinetics and thermodynamics of these reactions were also investigated. Those reactions with tetra(*o*-tolyl)diphosphane ($\mathbf{E_2}$) were much slower, which is attributed to inhibition by the o-CH_3 groups due to radical quenching or through steric effects. However, the deliberate UV-photolysis of these solutions markedly increases the rate of reaction. The reactions with $\mathbf{E_2}$ are also solvent sensitive, which is because of the radical degradation products of $CHCl_3$/CH_2Cl_2 which can initiate metathesis. This solvent degradation occurs spontaneously but can be accelerated with sonication or UV irradiation. These new findings show strong parallels between dynamic diphosphane chemistry and the much more established field of dynamic disulfide chemistry.

Significantly, $\mathbf{A_2}$/$\mathbf{E_2}$ metathesis has also been observed in the melt state—this means that metathesis is likely feasible in polymer melts.

Diphosphane stability was tested with respect to a variety of reaction conditions, with a view to synthesising a P–P-containing compound with pendent functional groups. It was found that diphosphanes are unstable with respect to many reagents and are only reliably tolerant of bases and nucleophiles: even mild acids result in rapid P–P cleavage. Importantly, diphosphanes are extremely air-sensitive, with their solutions oxidising in air within minutes. However, this process can be greatly inhibited in the presence of the radical scavenger TEMPO, which suggests that the formation of radicals is crucial to P–P oxidation. With this knowledge in hand, several syntheses have been designed in attempt to prepare a functionalised diphosphane, though none were successful. The most likely candidate is the tetra(*p*-styrenyl)diphosphane (**7**), though this species was observed to spontaneously polymerise during its synthesis. The synthesis of functional diphosphanes will be expanded upon in the conclusions and future work chapter (Chapter 6).

Finally, at a confluence of the research described in Chapters 4 and 5, a new reaction was discovered: the heterometathesis of diphosphanes with diselenides/disulfides. The reaction of diphosphanes with diselenides proceeds rapidly and chemoselectively, with conversion to the selanylphosphane in 100% atom economy. The presence of TEMPO greatly inhibits these reactions, which strongly suggests the heterometathesis proceeds through a radical pathway. Selanylphosphanes have been previously

reported,[54] but have remained hitherto unexplored. This heteromethathesis reaction was also extended to thiophosphanes, which is less selective, with some formation of the P(V) rearrangement product observed. Importantly, both reactions have been used to create phosphines with pendent functional groups, that could be used for further chemistry. Moreover, these species exhibit surprising levels of moisture tolerance. A first attempt at metal coordination using a selanylphosphane (and a $Mo(CO)_4$ core) has revealed binding through both P and Se atoms.

5.7 Experimental

5.7.1 General considerations

Unless otherwise specified, all reactions were performed under an inert atmosphere of dry nitrogen using standard Schlenk technique. Schlenk flasks and other glassware were dried with a heat gun at ≥600 °C under vacuum (flame-dried), or oven dried prior to use. Dry Et_2O, CH_2Cl_2, THF and toluene was collected from a Grubbs-type solvent purification system and deoxygenated using the freeze-pump-thaw method. Dry MeOH was stored over 3 Å molecular sieves for at least 24 h prior to use, and degassed via N_2-sparging. Deionised (DI) water was collected from a millipore dispenser system and N_2-sparged prior to use. CD_2Cl_2, $CDCl_3$ and C_6D_6 were also degassed with freeze-pump-thaw cycles and dried over 4 Å molecular sieves. 1,4-dioxane was purchased from Alfa Aesar dried over 4 Å molecular sieves and sparged prior to use. Diisopropylamine and triethylamine were purchased from Alfa Aesar and dried over 4 Å molecular sieves. Magnesium, iodine, TEMPO, TTBP, NCS, $LiAlH_4$, borane-dimethyl sulfide, dichloro(diethylamino)phosphine, 2 M ethereal HCl, 4-bromostyrene, diphenyl diselenide, diphenyl disulfide, di(*o*-tolyl)phosphine and the five chlorophosphines were purchased either from Sigma-Aldrich (Merck Chemicals) or Alfa Aesar and used as received. Dithiodianiline was purchased from TCI and used as received. Diethylamine was purchased from Sigma-Aldrich (Merck Chemicals) and dried over 4 Å molecular sieves prior to use.

As discussed in Chapter 4 (see Section 4.6 for details), 1,2-dibutyldiselane (dibutyldiselenide) was prepared from bromobutane and sodium diselenide according to the literature method of J. Scianowski.[59] 3,3'-diselanediyldipropionic acid was prepared from 3-chloropropanoic acid and sodium diselenide according to the literature procedure of V. Nascimento *et al*.[60]

NMR experiments were conducted with Norrell 'standard series' NMR tubes (wrapped with parafilm around the cap to delay oxidation onset) or amberised 500 MHz tubes (where stated) and performed on Jeol ECS300, Jeol ECS400, Bruker Nano400 or Varian ECZ400 spectrometers. $^{31}P\{^1H\}$ spectra are referenced to 85% H_3PO_4 (aq). Low temperature and kinetics experiments were performed on a Jeol ECS300 spectrometer, with inverse-gated decoupling in the case of kinetics experiments. MS experiments were performed by the University of Bristol Mass Spectrometry Service using either a Thermo Scientific Orbitrap Elite (APCI, LC-Orbitrap), Bruker micrOTof II (ESI, TOF) or Waters Synapt G2S (Nanospray, IMS-Q-TOF). FTIR experiments were performed using a Perkin Elmer Spectrum Two (solid state).

UV-Vis experiments were performed with an Agilent Technologies Cary 300 UV-Vis in double beam mode (absorption). 20 µM solutions of diphosphane in CH_2Cl_2 were prepared under a dry nitrogen atmosphere and baselined with respect to a CH_2Cl_2 blank.

Photolysis experiments were performed with a NightSearcher handheld LED UV lamp (5 W, 365 nm).

Note: 'ambient', 'room temperature' or 'RT' corresponds to approximately 20 °C (293 K) throughout this chapter.

5.7.2 Diphosphane synthesis

The synthesis of diphosphanes **A_2**–**C_2** and **E_2** was performed as exemplified by the synthesis of tetraphenyldiphosphane, **A_2**:

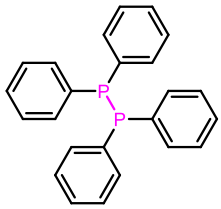

A_2

Magnesium (440 mg, 18.1 mmol) and two crystals of iodine (*ca*. 10 mg) were added to a Schlenk flask. The flask was then flame-dried under vacuum, vaporising the iodine. THF (30 ml) was added and the mixture was stirred vigorously at room temperature for 30 min. Chlorodiphenylphosphine (2.00 g, 9.05 mmol, 1.63 ml) was added dropwise and left to stir overnight. The solution was then filtered from the excess magnesium via cannula, and the THF removed *in vacuo*. Toluene (30 ml) and 1,4-dioxane (1.54 ml, 18.1 mmol) were added and the resultant solution stirred vigorously for 5 min, and then left to stand for 5 h. The solution was cannula filtered again, and the toluene removed under reduced pressure yielding the product **A_2** as a white powder (1.26 g, 75% yield). ^{1}H NMR (400 MHz, CD_2Cl_2): 7.37 (m, 8H, Ar*H*), 7.21 (m, 12H, Ar*H*). $^{31}P\{^{1}H\}$ (162. MHz, CD_2Cl_2): -15.5 (s). NMR data matches that of an authentic sample of **A_2** purchased from Sigma-Aldrich (Merck).

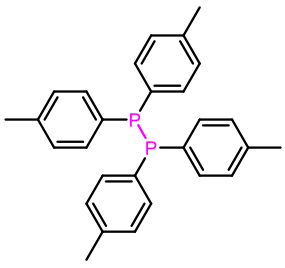

B_2

B_2 was prepared in analogous fashion. The crude product was filtered through a basic alumina plug to remove residual chlorophosphine. Pure **B_2** was isolated as a white powder (540 mg, 64% yield). ^{1}H NMR (400 MHz, $CDCl_3$): 7.25 (m, 8H, Ar*H*), 7.00 (d, J_{HH} = 7.7 Hz, 8H, Ar*H*), 2.28 (s, 12H, CH_3). $^{31}P\{^{1}H\}$ NMR (162 MHz, $CDCl_3$): -18.7 (s). NMR data is in good agreement with the literature.[19]

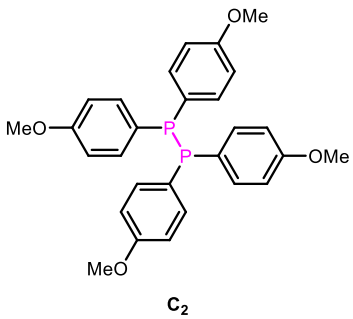

C_2

C_2 was prepared in analogous fashion and isolated as a pale yellow powder (939 mg, 87% yield). ^{1}H NMR (400 MHz, CD_2Cl_2): 7.94 (d, J_{HH} = 8.5 Hz, 8H, Ar*H*), 6.78 (d, J_{HH} = 8.6 Hz, 8H, Ar*H*), 3.75 (s, 12H, OCH_3). $^{31}P\{^{1}H\}$ NMR (162 MHz, CD_2Cl_2): -15.2 (s). NMR data is in good agreement with the literature.[38]

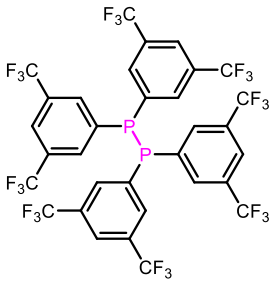

D_2

D_2 was prepared via a similar process, though in refluxing Et_2O for 5 days. The crude product was isolated as above, then filtered through an alumina plug to remove residual chlorophosphine and secondary phosphine oxide. The final product was isolated as an oily solid (214 mg, 23% yield) containing ~10% secondary phosphine side product. $^{31}P\{^1H\}$ NMR (162 MHz, THF): -12.6 (s). NMR data is in good agreement with the literature.[38]

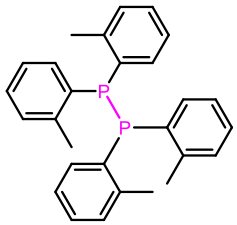

E_2

E_2 was prepared in analogous fashion to **A_2–C_2** and isolated as a white powder (406 mg, 62% yield). ^1H NMR (400 MHz, $CDCl_3$): 7.50 (d, J_{HH} = 7.6 Hz, 4H, Ar*H*), 7.16 (m, 8H, Ar*H*), 7.05 (m, 8H, Ar*H*), 1.93 (s, 12H, C*H*$_3$). $^{31}P\{^1H\}$ NMR (162 MHz, $CDCl_3$): -35.3 (s). NMR data is in good agreement with the literature.[19]

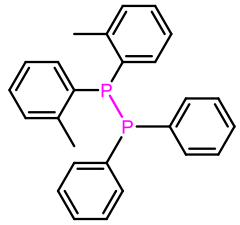

AE

Synthesis of AE:

Di(*ortho*-tolyl)phosphine (258 mg, 1.20 mmol) was added to a Schlenk flask and dissolved in CH_2Cl_2 (5 ml). This solution was then cooled to 0 °C prior to the slow addition of borane-dimethylsulfide complex (1.23 ml, 100 mg, 1.32 mmol). After 1.5 h the solvent was removed *in vacuo*. The residue was then triturated with hexane (5 ml), that was removed *in vacuo* prior to the addition of tetrahydrofuran (5 ml). The resultant borane-protected phosphine solution was cooled to -78 °C prior to the dropwise addition of *n*-butyllithium (0.83 ml, 1.32 mmol, 1.6 M), which resulted in the formation of a deep orange solution. After 35 min, chlorodiphenylphosphine (0.216 ml, 266 mg, 1.20 mmol) was added dropwise and the reaction was left to stir at -78 °C for 5 h. The rection mixture was then allowed to warm to room temperature and diethylamine (0.5 ml, 354 mg, 4.83 mmol) added. After 1 h, volatiles were removed *in vacuo* affording a white powder. The crude product was then filtered by cannula to a second Schlenk flask in toluene (3 x 10 ml), yielding the unsymmetrical diphosphane **AE** in 80% purity. This product was then recrystallised from hot methanol (30 ml) affording the pure product **AE** as a colourless crystalline solid (65 mg, 14% yield). ^1H NMR (400 MHz, C_6D_6): 7.88 (m, 2H, Ar*H*), 7.49 (m, 4H, Ar*H*), 6.96 (m, 10H, Ar*H*), 6.84 (m, 2H, Ar*H*), 2.07 (s, C*H*$_3$). $^{31}P\{^1H\}$ NMR (162 MHz, C_6D_6): -35.1 (d, J_{PP} 150.4 Hz, *P*(Ph)); -16.3 (d, J_{PP} 150.4 Hz, *P*(*o*-Tol). MS (APCI+) m/z: $[M+H^+]$ 399.1412 (theor. 399.1426).

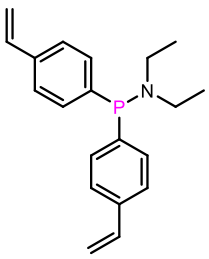

7a

7 (7a, 7b and 7c – attempted synthesis):

A solution of 4-bromostyrene (2 g, 10.8 mmol, 1.40 ml) in THF (17.0 ml) was prepared in a Schlenk flask and cooled to -78 °C. To this solution, *n*-butyllithium (1.6 M in hexanes, 9.8 mmol, 6.13 ml), which turned the solution pale-yellow. Dichloro(diethylamino)phosphine (853 mg, 4.9 mmol, 0.70 ml) in THF (5 ml) was slowly added to the lithiated styrene solution maintained at -78 °C. Residual aminophosphine solution was added to the reaction mixture with a further 2 ml of THF. Upon complete addition, the resulting solution was allowed to warm to ambient temperature. After 2 h the crude mixture was filtered through a celite plug, and either isolated by removal of the volatiles under reduced pressure to give **7a** as an off-white oily solid [$^{31}P\{^{1}H\}$ (162 MHz, THF): +61.0 (s)], or cooled to 0 °C and reacted without further treatment.

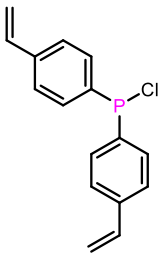

7b

Thereafter, HCl (2 M in Et_2O, 9.8 mmol, 4.9 ml) was added dropwise to the cooled filtrate and after complete addition the reaction was allowed to warm to room temperature. The solvent was removed under reduced pressure and the residue filtered by cannula (3 x 20 ml toluene washes) into a separate Schlenk flask. Removal of the solvents under reduced pressure revealed **7b** as a pale-yellow oil (1.14 g, 4.19 mmol, 86% overall yield). $^{31}P\{^{1}H\}$ NMR (162 MHz, C_6D_6): +82.5 (s). Under an Argon atmosphere **7b** (200 mg, 0.73 mmol) was added to a Schlenk flask and then dissolved in a mixture of Et_2O (15 ml) and THF (1 ml). In a separate Schlenk, $LiAlH_4$ (28 mg, 0.73 mmol) was added and cooled to 0 °C. The chlorophosphine solution was added dropwise to the $LiAlH_4$ and left to stir for 30 min. Thereafter, the $LiAlH_4$ was quenched via the following protocol: DI water (0.1 ml) was added and stirred into the reaction mixture. After 10 min, aqueous NaOH (4 M, 0.1 ml) was added and stirred into the reaction mixture. After 10 min, a further aliquot of DI water (0.3 ml) was added. After 10 min, the solution was filtered by cannula to a Schlenk flask containing $MgSO_4$ (2 g), with Et_2O washes (3 x 10 ml). The solution was filtered by cannula into another Schlenk flask. To separate **7c** from oxides the crude product was then flushed through an alumina plug; however, this resulted in polymerisation.

5.7.3 Diphosphane metathesis mechanistic studies

Kinetics studies

The following procedure outline of the **A_2/E_2** reaction was also extended to the **B_2/C_2** and **AE** reverse-kinetics studies.

To an NMR tube, 10 mg (0.025 mmol) of **A_2** and 11.5 mg (0.025 mmol) of **E_2** were added under an Ar atmosphere. 0.5 ml of solvent ($CDCl_3$ or toluene) was added. In the $CDCl_3$ case, the solution was immediately cooled to -78 °C using a dry ice/acetone bath. The cooled $CDCl_3$ sample was loaded into a JEOL ECS300 spectrometer and allowed to warm to ambient temperature. A 64 scan $^{31}P\{^1H\}$ NMR spectrum was then recorded at 10 minute intervals for 12 h, using inverse-gated decoupling. In the toluene case, the reaction was left at ambient temperature and remained unchanged, but for minor oxidation (due to air ingress), after a period of 3–4 days.

Further mechanistic investigations

Reactions involving additive inhibitors (e.g. water, $^{i}Pr_2NH$, TEMPO) or other non-diphosphane metathesis partners (e.g. Ar_2PCl/Ar_2PH) were performed in a similar fashion to the aforementioned kinetics studies via the following procedure.

To an oven-dried NMR tube 0.025 mmol of **X_2** and 0.025–0.1 mmol of **Y_2** (or Ar_2PCl/Ar_2PH) was added under an Ar atmosphere. A 1:1 stochiometric balance was used unless otherwise stated. At this stage, any solid additives (e.g. TEMPO, TTBP) were added in excess (0.1–0.2 mmol) were also added. The NMR tube was then sealed, removed from the glovebox and cycled onto a Schlenk line under a dry N_2 atmosphere. At this stage, any liquid additives (e.g. H_2O, $^{i}Pr_2NH$) were syringed into the NMR tube prior to the addition of 0.5 ml of dry, degassed solvent ($CDCl_3$, CD_2Cl_2, C_6D_6, PhMe, PhCl, PhF or THF). The NMR tube was then re-sealed with a parafilm wrap around the cap to slow the ingress of air into the tube. Generally, a $^{31}P\{^1H\}$ NMR spectrum was recorded within 20 min of solvent addition.

In photolysis experiments, the NMR tube was wrapped illuminated with a 5 W, 365 nm handheld UV lamp. Control experiments were wrapped in aluminium foil and placed in a dark cupboard.

In sonication experiments with the **A_2/E_2** system, the following procedure was employed:

Under an Ar atmosphere, **A_2** (93 mg, 0.25 mmol) and **E_2** (107 mg , 0.25 mmol) were added to a Schlenk flask and dissolved in 5 ml of solvent (CH_2Cl_2, $CHCl_3$, THF or PhMe). Immediately thereafter the reaction was syringed into a custom-built Suslick vessel (which had undergone three successive cycles of being evacuated and refilled with nitrogen) whilst under a positive pressure of N_2. The Suslick vessel was sealed and then sonicated in pulse mode (1 s on, 1 s off) at 20 kHz at 0 °C for 9 h. 0.5 ml aliquots of

the reaction mixture were then removed from the reaction mixture at regular intervals into oven-dried tubes for $^{31}P\{^{1}H\}$ NMR examination.

5.7.4 Selanylphosphane and sulfanylphosphane synthesis

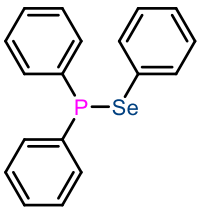

12

Diphenyl(phenylselanyl)phosphane (12):

Tetraphenyldiphosphane (190 mg, 0.513 mmol) and diphenyl diselenide (160 mg, 0.513 mmol) were added to a Schlenk flask and dissolved in THF (10 ml), immediately creating a pale-yellow solution, which was left to stir for 10 min. The solvent was then removed *in vacuo* affording **12** as an almost-colourless oily solid (323 mg, 92% yield). After storage under argon overnight the oily solid partially crystallised. Crystals suitable for single-crystal X-ray crystallography were grown over 1 week via CH_2Cl_2-hexane vapour diffusion. ^{1}H NMR (400 MHz; $CDCl_3$): 7.57 (6H, m, Ar*H*), 7.34 (6H, m, Ar*H*), 7.22 (3H, m, Ar*H*). $^{31}P\{^{1}H\}$ NMR (162 MHz; $CDCl_3$): +30.5 (s, J_{PSe} = 229.0 Hz). $^{77}Se\{^{1}H\}$ NMR (76 MHz; $CDCl_3$): +309.7 (J_{SeP} = 229.0 Hz). $^{13}C\{^{1}H\}$ NMR (101 MHz; $CDCl_3$): 137.1 (d, J_{CP} = 27.4 Hz), 133.9 (d, J_{CP} = 5.8 Hz), 133.5 (s), 133.3 (s), 129.3 (s), 129.3 (s), 128.7 (d, J_{CP} = 6.3 Hz), 127.6 (s). HRMS (APCI+): Found $[M+H]^+$: m/z 343.0140 (343.0149).

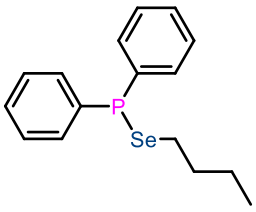

14

(Butylselanyl)diphenylphosphane (14):

Tetraphenyldiphosphane (166 mg, 0.488 mmol) and di(*n*-butyl) diselenide (122 mg, 0.488 mmol) were added to a Schlenk and dissolved in THF (15 ml), which gave a pale-yellow solution that was left to stir for 20 min. The reaction mixture was then filtered through a basic alumina plug. The solvent was removed under reduced pressure affording **14** as a colourless oil (138 mg, 48% yield). ^{1}H NMR (301 MHz; $CDCl_3$): 7.55 (m, 4H, Ar*H*), 7.31 (m, 5H,m, Ar*H*), 2.79 (q, 2H, J_{HH} = 7.72 Hz, CH_2), 1.69 (m, 2H, CH_2), 1.37 (m, 2H, CH_2), 0.86 (t, 3H, J_{HH} = 7.38 Hz, CH_3). $^{31}P\{^{1}H\}$ NMR (162 MHz; $CDCl_3$): +22.1 (s, J_{Pse} = 241.8 Hz). $^{77}Se\{^{1}H\}$ NMR (76 MHz; toluene): +169.5 (d, J_{SeP} = 243.3 Hz). $^{13}C\{^{1}H\}$ NMR (101 MHz; $CDCl_3$): 138.5 (d, J_{CP} = 26.02 Hz), 133.4 (d, J_{CP} = 20.61 Hz), 129.2 (s), 128.8 (d, J_{CP} = 6.27 Hz), 34.4 (d, J_{CP} = 4.45 Hz), 27.0 (d, J_{CP} = 20.61 Hz), 23.2 (s), 13.7 (s). HRMS (APCI+): Found $[M+H]^+$ m/z 322.0450 (323.0462).

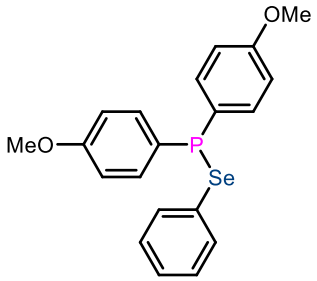

15

Bis(4-methoxyphenyl)(phenylselanyl)phosphane (15):

Tetra(*p*-anisyl)diphosphane (150 mg, 0.305 mmol) and diphenyl diselenide (95 mg, 0.305 mmol) were added to a Schlenk flask, dissolved in THF (10 ml), and stirred for 10 min. The solvent was removed under reduced pressure affording **15** as a yellow oil (114 mg, 79% yield). ^{1}H NMR (400 MHz; $CDCl_3$): 7.54 (m, Ar*H*), 7.23 (m, Ar*H*), 6.91 (m, Ar*H*), 3.82 (s, 6H, C*H*$_3$). ^{31}P{^{1}H} NMR (162 MHz; $CDCl_3$): +29.8 (s, J_{PSe} = 223.2 Hz). ^{77}Se{^{1}H} NMR (57 MHz; $CDCl_3$): +317.1 (d, J_{SeP} = 223.4 Hz). ^{13}C{^{1}H} NMR (100 MHz; $CDCl_3$): 160.8 (s), 134.8 (d, J_{CP} = 22.2 Hz), 133.8 (d, J_{CP} = 5.0 Hz), 131.7 (s), 129.2 (s), 128.1 (d, J_{CP} = 25.6 Hz), 127.3 (s), 114.4 (d, J_{CP} = 7.1 Hz), 55.4 (s). HRMS (APCI+): Found $[M+H]^+$ m/z 403.0362 (403.0361)).

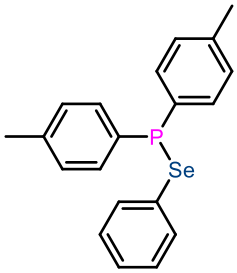

16

(Phenylselanyl)di-*p*-tolylphosphane (16):

Tetra(*p*-tolyl)diphosphane (150 mg, 0.350 mmol) and diphenyl diselenide (110 mg, 0.350 mmol) were added to a Schlenk flask, dissolved in THF (10 ml) and then stirred for 20 min. The solvent was removed under reduced pressure affording **16** as a yellow oil (221 mg, 90% yield). ^{1}H NMR (400 MHz; $CDCl_3$): 7.50 (m, 6H, Ar*H*), 7.19 (m, 7H, Ar*H*), 2.36 (s, 6H, C*H*$_3$). ^{31}P{^{1}H} NMR (162 MHz; $CDCl_3$): +30.2 (s, J_{PSe} = 225.2 Hz). ^{77}Se{^{1}H} NMR (57 MHz; $CDCl_3$): +311.4 (d, J_{SeP} = 225.4 Hz). ^{13}C{^{1}H} NMR (101 MHz; $CDCl_3$): 139.4 (s), 133.9 (s), 133.7 (d, J_{CP} = 5.9 Hz), 133.6 (s), 133.3 (d, J_{CP} = 21.0 Hz), 129.5 (d, J_{CP} = 6.65 Hz), 129.2 (s), 127.3 (s), 21.5 (s). HRMS (APCI+): Found $[M+H]^+$ m/z 371.0468 (371.0462).

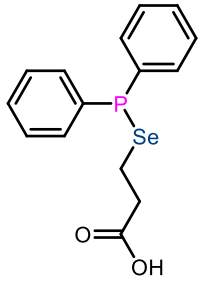

17

3-((diphenylphosphaneyl)selanyl)propanoic acid (17):

Tetraphenyldiphosphane (100 mg, 0.270 mmol) and 3,3'-diselanediyldipropionic acid (82 mg, 0.270 mmol) were added to a Schlenk flask, dissolved in THF (10 ml) and then stirred for 20 min. The solvent was removed under reduced pressure affording **17** as a colourless oil (93 mg, 51% yield). ^{1}H NMR (400 MHz; $CDCl_3$): 10.6 (bs, COO*H*), 7.19–7.51 (m, 10H, Ar*H*), 2.91 (q, 2H, J_{HH} = 7.7 Hz), 2.75 (t, 2H, J_{HH} = 7.3 Hz). ^{31}P{^{1}H} NMR (162 MHz; $CDCl_3$): +23.0 (s, J_{PSe} = 235.7 Hz). ^{77}Se{^{1}H} NMR (57 MHz; $CDCl_3$): +394.3 (d, J_{SeP} = 237.8 Hz). ^{13}C{^{1}H} NMR (101 MHz; $CDCl_3$): 177.8 (s), 137.25 (d, J_{CP} = 25.6 Hz), 133.2 (d, J_{CP} = 20.6 Hz), 129.2 (s), 128.7 (d, J_{CP} = 6.3 Hz), 36.5 (d, J_{CP} = 4.8 Hz), 19.7 (d, J_{CP} = 22.5 Hz). HRMS (APCI+): Found $[M+H]^+$ m/z 339.0034 (339.0048).

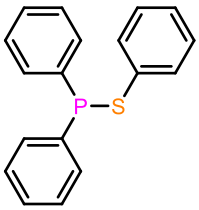

11

Diphenyl(phenylthiol)phosphane (11):

Tetraphenyldiphosphane (300 mg, 0.81 mmol) and diphenyl disulfide (219 mg, 0.81 mmol) were added to a Schlenk flask, dissolved in THF (15 ml) and then stirred for 2 h. The solution was then filtered through two basic alumina plugs to remove residual P(V) species. The solvent was removed under reduced pressure affording **11** as a colourless oily solid (205 mg, 40% yield). ^{1}H NMR (301 MHz; $CDCl_3$): 7.61 (m, 4H, Ar*H*), 7.53 (m, 2H, Ar*H*), 7.38 (m, 6H, Ar*H*), 7.24 (m, 3H, Ar*H*). $^{31}P\{^{1}H\}$ NMR (162 MHz; $CDCl_3$): +32.7 (s). $^{13}C\{^{1}H\}$ NMR (101 MHz; $CDCl_3$): 137.6 (d, J_{CP} = 23.2 Hz), 135.2 (d, J_{CP} = 14.1 Hz), 132.9 (d, J_{CP} = 20.9 Hz), 132.0 (d, J_{CP} = 7.9 Hz), 129.5 (s), 129.1 (s), 128.7 (d, J_{CP} = 6.5 Hz), 127.1 (d, J_{CP} = 1.7 Hz). HRMS (APCI+): Found $[M+H]^+$ m/z 295.0695 (295.0705).

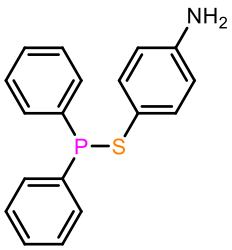

13

4-((diphenylphosphaneyl)thio)aniline (13):

Tetraphenyldiphosphane (287 mg, 0.775 mmol) and 4,4'-dithioaniline (265 mg, 0.775 mmol) were added to a Schlenk flask, dissolved in CH_2Cl_2 and then the resultant lime green solution was stirred for 1.5 h. The solution was then filtered through a basic alumina plug and the solvent removed under reduced pressure affording **13** as an almost colourless oily solid (186 mg, 34% yield). ^{1}H NMR (400 MHz; CD_2Cl_2): 7.58 (m, 4H, Ar*H*), 7.37 (m, 6H, Ar*H*), 7.21 (m, 2H, Ar*H*), 6.56 (m, 2H, Ar*H*), 3.77 (bs, 2H, N*H*$_2$). $^{31}P\{^{1}H\}$ NMR (162 MHz; CD_2Cl_2): +37.2 (s). $^{13}C\{^{1}H\}$ NMR (101 MHz; CD_2Cl_2): 146.9 (s), 138.1 (d, J_{CP} = 25.2 Hz), 134.8 (s), 134.8 (s), 129.2 (s), 132.7 (d, J_{CP} = 20.8 Hz), 128.5 (d, J_{CP} = 6.4 Hz), 115.4 (s). HRMS (APCI+): Found $[M+H]^+$ m/z 310.0802 (310.0814).

5.8 References

1 C. Branfoot, T. A. Young, D. F. Wass and P. G. Pringle, *Dalton Trans.*, 2021, **50**, 7094–7104.

2 H. C. E. McFarlane and W. McFarlane, *Chem. Commun.*, 1972, 1189–1190.

3 R. K. Harris, E. M. Norval and M. Fild, *Dalton Trans.*, 1979, 825–831.

4 A. Molloy, G. Sánchez-Sanz and D. Gilheany, *Inorganics*, 2016, **4**, 36.

5 N. Szynkiewicz, Ł. Ponikiewski and R. Grubba, *Dalton Trans.*, 2018, **47**, 16885–16894.

6 S. Kawaguchi, S. Nagata, T. Shirai, K. Tsuchii, A. Nomoto and A. Ogawa, *Tetrahedron Lett.*, 2006, **47**, 3919–3922.

7 N. Szynkiewicz, L. Ponikiewski and R. Grubba, *Chem. Commun.*, 2019, **55**, 2928–2931.

8 T. Shirai, S. Kawaguchi, A. Nomoto and A. Ogawa, *Tetrahedron Lett.*, 2008, **49**, 4043–4046.

9 N. A. Giffin, A. D. Hendsbee, T. L. Roemmele, M. D. Lumsden, C. C. Pye and J. D. Masuda, *Inorg. Chem.*, 2012, **51**, 11837–11850.

10 W. Kuchen and H. Buchwald, *Chem. Ber.*, 1959, **92**, 227–231.

11 S. J. Geier and D. W. Stephan, *Chem. Commun.*, 2008, **054**, 99–101.

12 A. D. Gorman, J. A. Cross, R. A. Doyle, T. R. Leonard, P. G. Pringle and H. A. Sparkes, *Eur. J. Inorg. Chem.*, 2019, **2019**, 1633–1639.

13 G. Fritz, in *Advances in Inorganic Chemistry*, eds. H. J. Emeleus and A. G. Sharpe, Academic Press, 1987, vol. 31, pp. 171–214.

14 A. K. King, A. Buchard, M. F. Mahon and R. L. Webster, *Chem. Eur. J.*, 2015, **21**, 15960–15963.

15 R. Waterman, *Organometallics*, 2007, **26**, 2492–2494.

16 V. P. W. Böhm and M. Brookhart, *Angew. Chem. Int. Ed.*, 2001, **40**, 4694–4696.

17 M. C. Fermin and D. W. Stephan, *J. Am. Chem. Soc.*, 1995, **117**, 12645–12646.

18 S. Molitor, J. Becker and V. H. Gessner, *J. Am. Chem. Soc.*, 2014, **136**, 15517–15520.

19 L. Wu, V. T. Annibale, H. Jiao, A. Brookfield, D. Collison and I. Manners, *Nat. Commun.*, 2019, **10**, 1–10.

20 F. W. Bennet, H. J. Emelius and R. N. Haszeldine, *J. Chem. Soc.*, 1953, 1565–1571.

21 W. Hewertson and H. R. Watson, *J. Chem. Soc.*, 1962, 1490–1494.

22 H. Niebergall and B. Langenfeld, *Chem. Ber.*, 1962, **95**, 64–76.

23 H. Noth and H.-J. Vetter, *Chem. Ber.*, 1961, **94**, 1505–1516.

24 K. Issleib and W. Seidel, *Chem. Ber.*, 1959, **92**, 2681–2694.

25 K. O. Feldmann and J. J. Weigand, *J. Am. Chem. Soc.*, 2012, **134**, 15443–15456.

26 A. H. Cowley, *Chem. Rev.*, 1965, **65**, 617–634.

27 D. L. Dodds, M. F. Haddow, A. G. Orpen, P. G. Pringle and G. Woodward, *Organometallics*, 2006, **25**, 5937–5945.

28 D. L. Dodds, J. Floure, M. Garland, M. F. Haddow, T. R. Leonard, C. L. McMullin, A. G. Orpen and P. G. Pringle, *Dalton Trans.*, 2011, **40**, 7137–7146.

29 S. Katsyuba and R. Schmutzler, *Sect. Title Gen. Phys. Chem.*, 2008, 1465–1470.

30 N. N. Greenwood and A. Earnshaw, *Chemistry of the Elements*, Butterworth-Heinemann, 2nd edn., 1997.

31 W. A. Henderson, M. Epstein and F. S. Seichter, *J. Am. Chem. Soc.*, 1963, **85**, 2462–2466.

32 M. Häring, *Helv. Chim. Acta*, 1960, **43**, 1826–1840.

33 M. Baudler and J. Hellmann, *Zeitschrift für Anorg. und Allg. Chemie*, 1982, **18**, 11–18.

34 M. Baudler, D. Grenz, U. Arndt, H. Budzikiewicz and M. Feher, *Chem. Ber.*, 1988, **121**, 1707–1709.

35 R. B. King and N. D. Sadanani, 1985, 1719–1722.

36 B. Stewart, A. Harriman and L. J. Higham, *Organometallics*, 2011, **30**, 5338–5343.

37 S. Hanessian, D. Delorme and Y. Dufresne, *Tetrahedron Lett.*, 1984, **25**, 2515–2518.

38 S. Molitor, C. Mahler and V. H. Gessner, *New J. Chem.*, 2016, **40**, 6467–6474.

39 J. M. Matxain, J. M. Asua and F. Ruipérez, *Phys. Chem. Chem. Phys.*, 2016, **18**, 1758–1770.

40 T. Heurich, Z.-W. Qu, S. Nožinović, G. Schnakenburg, H. Matsuoka, S. Grimme, O. Schiemann and R. Streubel, *Chem. Eur. J.*, 2016, **22**, 10102–10110.

41 S. Nevejans, N. Ballard, J. I. Miranda, B. Reck and J. M. Asua, *Phys. Chem. Chem. Phys.*, 2016, **18**, 27577–27583.

42 S. Ji, W. Cao, Y. Yu and H. Xu, *Angew. Chem. Int. Ed.*, 2014, **53**, 6781–6785.

43 U. F. Fritze and M. von Delius, *Chem. Commun.*, 2016, **52**, 6363–6366.

44 X. Xu and P. D. Pacey, *Phys. Chem. Chem. Phys.*, 2001, **3**, 2836–2844.

45 M. Irigoyen, A. Fernández, A. Ruiz, F. Ruipérez and J. M. Matxain, *J. Org. Chem.*, 2019, **84**, 4200–4210.

46 T. Ozturk, E. Ertas and O. Mert, *Chem. Rev.*, 2007, **107**, 5210–5278.

47 I. P. Gray, P. Bhattacharyya, A. M. Z. Slawin and J. D. Woollins, *Chem. Eur. J.*, 2005, **11**, 6221–6227.

48 M. Jesberger, T. P. Davis and L. Barner, *Synthesis (Stuttg).*, 2003, 1929–1958.

49 G. Hua, R. A. M. Randall, A. M. Z. Slawin and J. D. Woollins, *Tetrahedron*, 2013, **69**, 5299–5305.

50 L. Ascherl, A. Nordheider, K. S. A. Arachchige, D. B. Cordes, K. Karaghiosoff, M. Bühl, A. M. Z. Slawin and J. D. Woollins, *Chem. Commun.*, 2014, **50**, 6214–6216.

51 G. Hua, Y. Li, A. M. Z. Slawin and J. D. Woollins, *Chem. Commun.*, 2007, **83**, 1465–1467.

52 R. Davies and L. Patel, in *Handbook of Chalcogen Chemistry: New Perspectives in Sulfur, Selenium and Tellurium*, eds. F. Devillanova and W.-W. Du Mont, Royal Society of Chemistry, 2nd edn., 2013, pp. 238–306.

53 A. Arbuzov, *J. Russ. Phys. Chem. Soc.*, 1910, **42**, 549.

54 R. A. N. N. McLean, *Inorg. Nucl. Chem. Lett.*, 1969, **5**, 745–747.

55 H. Cui, M. Hu, H. Wen, G. Chai, C. Ma, H. Chen and C. Chen, *Dalton Trans.*, 2012, **41**, 13899.

56 R. C. S. Wong and M. L. Ooi, *Inorganica Chim. Acta*, 2011, **366**, 350–356.

57 L. Y. Goh, W. Chen and R. C. S. Wong, *Organometallics*, 1999, **18**, 306–314.

58 M. Di Vaira, I. de los Rios, F. Mani, M. Peruzzini and P. Stoppioni, *Inorg. Chem. Commun.*, 2002, **5**, 879–880.

59 J. Ścianowski, *Tetrahedron Lett.*, 2005, **46**, 3331–3334.

60 V. Nascimento, N. L. Ferreira, R. F. S. Canto, K. L. Schott, E. P. Waczuk, L. Sancineto, C. Santi, J. B. T. Rocha and A. L. Braga, *Eur. J. Med. Chem.*, 2014, **87**, 131–139.

Chapter 6: Conclusions and future work

6.1 Diels-Alder CANs

6.1.1 Diels-Alder CANs – conclusions

In Chapters 2 and 3, a previously reported family of Diels-Alder epoxies were developed into a second generation of materials. The primary goal of that work was to take an established dynamic chemistry and apply it in fibre reinforced polymer composites, i.e. to explore the value of CANs in composites. In principle, the use of CANs as FRP matrices should lead to more sustainable composites by bestowing them with added functionality—notably self-healing and recyclability. Although there is some literature overlap between FRPs and CANs, there are few examples at present.

The new series of Diels-Alder epoxies were thoroughly characterised through a combination of chemical, thermal and mechanical techniques. This revealed that these polymers are highly dynamic and due to their capacity to melt, are capable of exotic processes including powder-compression moulding, self-healing and solvent-assisted recycling. In Chapter 3, the ability to manufacture healable and recyclable FRPs with these polymers was clearly demonstrated. However, the mechanical performance of these polymers was poorer than expected. Although the stiffness of the DA CANs remained in the expected region for DGEBA-based epoxies, both the strength and failure strains were very low. These characteristics are manifestations of the extreme brittleness (or low toughness) of these materials. An assessment of each of the tested materials led to the conclusion that the most likely explanation for this brittleness is a less-than-expected crosslink density. When fibre-reinforced, the brittleness is much less pronounced; nonetheless, it is important that if this class of materials is to be used as composite matrices going forward, they should be developed to be less brittle.

In some preliminary tests discussed in Chapter 3, a few methods of reducing brittleness were explored. Since the low crosslink density is largely a product of the very short length of oligomer chain (from which the CANs are made), one obvious strategy for increasing the toughness is increasing the chain length. This can easily be achieved by varying the ratio of the amines and epoxides used in the synthesis of the prepolymer. However, by increasing the length of the prepolymer the ‘dynamic activity’ (manifested in terms of ‘melt-ability’) is reduced. Accordingly, it would be prudent in future work to prepare DA CANs which contain a mixture of long-chain oligomers/polymers (for toughness) and short-chain oligomers for dynamic activity. Other approaches were considered, and one that was deemed most promising was substitution of the prepolymer end-capping units. In the current generation of DA CANs, these end-caps are inert dicyclohexylamine groups; however, as also discussed

in Chapter 3, it should be possible to substitute these groups for furyl groups, which could participate in crosslinking/chain-extension—this should result in a large increase in apparent crosslink density, with only a minor change to the melt behaviour. The initial findings of this work were inconclusive and it would be advisable to carry out a more extensive study of this end-capping process. Ideally, a robust method of using the thiol-epoxy reaction to achieve this furyl end-capping should be explored, Figure 6.1.

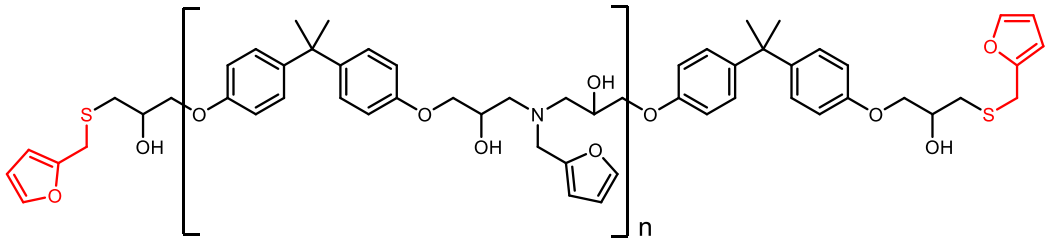

Figure 6.1. The proposed use of furfuryl mercaptan (thiol) end-capping units (highlighted red) in DA CANs.

The nature of the crosslinking unit in the Diels-Alder reaction, the bismaleimide (BMI) was also explored in a preliminary study. One of the limitations of the current iteration of DA CANs is their stability at elevated temperature. The viscosity of the CANs gradually increases with time, which leads to a reduction in dynamic performance. This is attributed to a combination of gradual homogenisation and the occurrence of undesired side-reactions which lead to permanent crosslinking. The most important of these side-reactions is BMI homopolymerisation (HP). Since HP typically occurs above the melting point of the BMI, one method of increasing high temperature stability may be to use higher-melting BMIs, such as BMI3 (Figure 6.2). This compound does appear to polymerise at significantly higher temperature (than those used herein); accordingly, the use of this compound should be further tested—isothermal rheology experiments would be a good way to determine any improvement in performance.

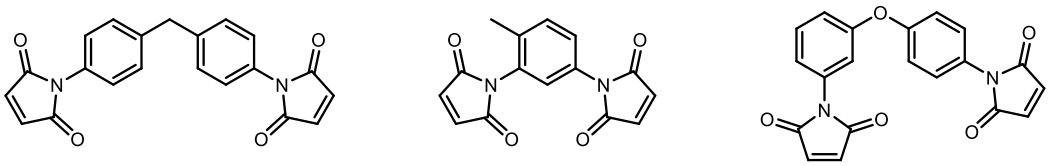

BMI1 **BMI2** **BMI3**

Figure 6.2. The structure of the bismaleimides reported in Chapters 2 and 3.

Alternative strategies involving the use of bisitaconimides (BIIs) and biscitraconimides (BCIs) were also explored, Figure 6.3. However, the former class of compounds appears to polymerise at lower temperature than BMIs so were ruled-out for this reason. A range of BCIs were successfully prepared and early results, in agreement with literature findings, suggest that these compounds undergo HP at

much higher temperatures than BMIs. However, unfortunately, no evidence of a successful Diels-Alder reaction between these compounds and furans was observed. Accordingly, these compounds do not appear to be viable.

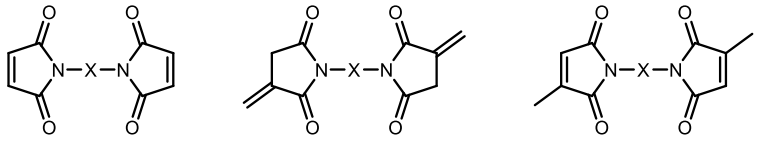

Figure 6.3. Bismaleimides, bisitaconimides and biscitraconimides (where X could be any molecular backbone).

The use of DA CANs as thermoreversible adhesives was also tested in a preliminary lap-shear study. The results of this experiment (derived from a comparison of high-temperature and room temperature shear strengths) show that these polymers indeed have potential as reversible adhesives. However, several refinements to the methodology of testing are advisable including: (1) substrate surface preparation—the substrate surface should be more thoroughly keyed to create a more consistent bond line and (2) thermal equilibration—specimens should be given more time to equilibrate with the high temperature environment to ensure the polymer has reached the desired temperature. This should also improve consistency. The logical next steps in this work are to use composite substrates and to explore different (preferably localised) mechanisms of applying heat, perhaps through resistive heating.

6.1.2 Diels-Alder CANs – future work

The future work concerning the Diels-Alder CANs can be straightforwardly separated into studies concerning the neat polymer—notably the design of an improved next generation of DA materials (Section 6.1.2)—and studies concerning composite testing and characterisation (Section 6.1.3).

As discussed in Section 6.1.1, there are two main limitations with the Diels-Alder CANs presented in this thesis: high temperature stability and brittleness.

Preliminary studies with the use of high-melting crosslinkers (i.e. BMI3) show that this material is a promising candidate for creating DA materials which are less prone to the BMI HP reaction. DSC confirmed that HP occurs at a significantly higher temperature with BMI3 than BMI1 and BMI2, those used to make the CANs discussed in this thesis. In future work, new DA CANs should be made in two versions, one with BMI1 and one with BMI3 to compare performance. Isothermal rheology experiments would be particularly useful for comparing the high-temperature stability.

One alternative method of increasing high temperature stability is by directly inhibiting the HP reaction. Since BMI homopolymerisation is believed to proceed via a radical mechanism, radical scavengers (such as TEMPO) could inhibit the reaction. Although radical scavengers can be very

effective in solution reactions, it remains unclear if this inhibitory activity would translate into polymer melts (and/or the solid state). A sensible way to bind TEMPO into a polymer network for such a purpose would be through reacting a primary amine (such as furfurylamine) with 4-oxo-TEMPO.[1] This would ensure that the inhibitor remains bound into the polymer, Scheme 6.1.

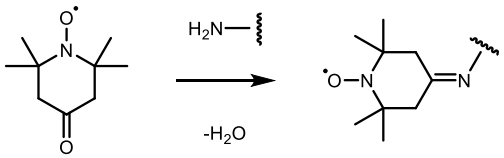

Scheme 6.1. The formation of a polymer-bound radical scavenger by imine formation from of 4-oxo-TEMPO and a polymer-bound primary amine.

To improve the brittleness of DA CANs, there are two main methods which can be employed: (1) the addition of toughening agents and (2) the redesign of the polymers.

The addition and dispersion of nanoscale toughening agents such as clay particles or graphene oxide particles throughout a polymer is a well-known method of improving polymer toughness,[2] so would be worth exploring in future work. However, a redesigned, new generation of DA CANs with a combination of short oligomers (for processability) and long oligomers (for toughening) is likely to produce a greater improvement. For this reason, a range of new DA polymers should be prepared which span a variety of prepolymer/oligomer lengths. Moreover, the use of furan end-caps (e.g. 2-furfurylmercaptan, as mentioned above) should be explored further. Any means of increasing both the number of intermolecular and intramolecular (crosslinks) should result in a more mechanically robust material. New generations of DA CANs made in such a way should then be moulded and characterised through 3-point bend (3pb) testing and compared with DA1, DA2 and DA0.5. Moreover, *in situ* polymerisation methods should be investigated, since this may maintain one of the key advantages of thermosets over thermoplastics (fibre impregnation), which is not currently a feature of these powdered DA CANs.

6.1.3 Diels-Alder composite – future work

Although the value of DA CANs in composites has been demonstrated, more studies regarding composite manufacture and healing/recycling characterisation are required. Ideally, the fibre volume fraction of 12plyDA0.5 should be determined by microscopy and the self-healing/recycling experiments performed on 8plyDA1 should be extended to this composite. However, it is worth noting that it was difficult to consistently damage composite specimens via 3pb testing without significant fibre damage. For this reason, the values of self-healing appear deceptively low. With hindsight, a more robust method of investigating self-healing may be to forgo specimen-specimen comparison

(before/after repair) and instead use average results for quantifying healing. In doing this, the same specimens do not need to be used for each series of experiments. For example, with three series of specimens, one series could be used to determine pristine ultimate strength. A second series could be used to determine damaged strength via loading to a set strain (e.g. 4%), unloading the specimens and then re-testing to failure. The third series of coupons could be tested to the previous strain value, repaired and then finally also tested to failure. This methodology would allow average values of ultimate strength to be calculated for each series and compared between each of the three states (pristine, damaged, and repaired). This should make the data more reliable at the slight cost of increasing the number of specimens (and thus laminate area) required. Alternative mechanical tests could also be investigated in the future, one of the most promising candidates being compression after impact (CAI) testing. This test provides particularly valuable information given that impact damage is realistic of many real-world applications. The downside with CAI is it requires thicker laminates (more polymer) and is more complicated to perform. For further investigating the viability of the proposed recycling process, the fibre surfaces should be examined by microscopy for evidence of surface damage after treatment. In addition, a more critical analysis of the economics of different recycling processes should be performed; it is possible that using steam or supercritical fluids as alternatives to conventional solvents could be an improvement.

6.2 Disulfides and diselenides

6.2.1 Disulfides and diselenides – conclusions

The primary objective of this sub-project was to explore the use of diselenide crosslinkers in CANs and attempt to compare their activity with disulfides. As a benchmark, the disulfide CAN reported by Odriozola *et al*.[3] was prepared and characterised. As an associative (vitrimeric) CAN, this material had strongly contrasting behaviour to the Diels-Alder CANs discussed in Chapters 2 and 3. Surprisingly, the 'weak' disulfide linkage was observed to have only a minor effect on the mechanical performance of the host polymer. This suggests that, when designed appropriately, the inclusion of dynamic moieties within polymer networks does not have to significantly compromise mechanical performance.

A range of diselenides containing different functional groups were prepared and fully characterised, including one (**BOCDS**) which had potential as a latent epoxy curative. The metathesis of these species was explored and found to be extremely rapid and crucially, spontaneous at room temperature. These diselenides were then tested in small-scale polymerisation reactions. However, there is much research still to be performed on these materials.

Unfortunately, subsequent testing revealed that **BOCDS** is not stable at the high temperatures required to remove the BOC protecting groups. A comparison of disulfide- and diselenide-containing polymers by DSC indicates that diselenides have a lower thermal stability and likely decompose above 200 °C. However, this should not be a problem for most target applications.

6.2.2 Disulfides and diselenides – future work

It would be desirable to continue researching methods of deprotecting **BOCDS** with a view to preparing the original target compound **ADS**, Scheme 6.2. The conformational flexibility produced by the benzylic (CH_2) units combined with the aromatic rigidity would be expected to yield a high-performance epoxy crosslinker.

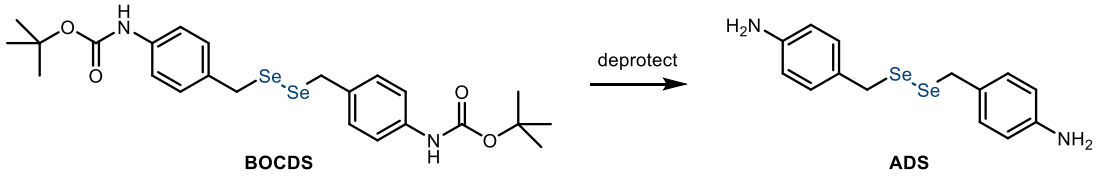

Scheme 6.2. **BOCDS** and **ADS**, the highest priority target of this sub-project.

With **ADS**/**BOCDS** and each of the other diselenides (Figure 6.4), it would be prudent to explore their reactions in forming linear polymers before returning to network polymers (CANs). Although CANs are the ultimate goal of this research, the formation of linear polymers is generally both simpler and more controlled. Accordingly, such studies would likely be a more informative means of testing polymerisation and would still allow the dynamic behaviour to be explored. Moreover, the use of linear (non-crosslinked) polymers facilitates the use of rheology to probe the dynamic behaviour. Initial experiments reacting either **CDS** and **PEDS** with TDI (toluene diisocyanate) to prepare a polyamide and a polyurethane were unsuccessful and thus these experiments were not included in Chapter 4. In hindsight, the attempted polyurethane/polyamide syntheses would certainly have benefitted from being tested in linear polymers first—it seems likely that these syntheses were unsuccessful due to the use of glycerol as a crosslinker. Glycerol is highly hygroscopic and any water content could easily have consumed the isocyanates, preventing the expected polymerisation. Accordingly, the simple reactions of both of these diselenides with TDI should be tested and the resultant linear polymers tested for dynamic behaviour either by DMA, rheology or both.

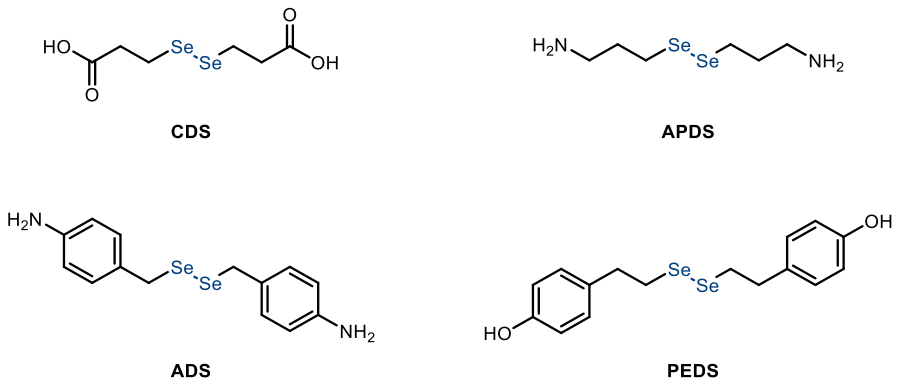

Figure 6.4. The four diselenides investigated as crosslinkers in Chapter 4.

Because diselenide and disulfide exchange operates through an additive radical mechanism, when used in network polymers (as CANs), the resulting polymers are best described as vitrimers. Accordingly, these materials cannot melt and thus the characterisation of the dynamic behaviour with rheology is essentially impossible. However, this makes analysis of these materials via DMA ideal. As such stress relaxation–based DMA experiments should be priority characterisation experiments with all of these diselenide polymers in the future.

The potential of diselenide CANs to create visible light–activated functional composites means that these materials are certainly worth pursuing in the future.

6.3 Diphosphanes

6.3.1 Diphosphanes – conclusions

The primary objective of this sub-project was to determine the viability of using P–P bonds in dynamic materials such as CANs. With a long history of unexplained dynamic behaviour, diphosphanes appeared to represent a hitherto unexplored source of dynamic covalent bonds. An extensive investigation into the underlying mechanism of diphosphane exchange (homometathesis) revealed new insights into this chemistry, most importantly that radical species are the key intermediates—a strong parallel with dynamic disulfide and diselenide chemistry.

Crucially, tetraaryldiphosphanes are capable of rapid metathesis at room temperature and are also capable of metathesis in the melt. This means it is highly likely that aromatic diphosphanes within a polymer network would be capable of undergoing exchange under the right conditions. Since this reaction appears to be UV-initiated, this could be exploited to create UV-responsive CANs. However, in a series of attempted syntheses and an associated stability/reactivity study, it was observed that diphosphanes are highly reactive species and accordingly are not tolerant of many types of reaction environment. Acidic and oxidising environments are particularly problematic, though the

diphosphanes showed good tolerance toward reducing agents and bases, which gives hope that a functionalised diphosphane—that could be incorporated within a polymer network—can be prepared.

The selanylphosphane/thiophosphane species introduced in Chapter 5 (heteromethathesis) are included for completeness and interest, since they do not seem to exhibit the dynamic behaviour of their parent species (diphosphanes and diselenides/disulfides). However, these species may have wider significance in phosphorus chemistry since—particularly in the case of selanylphosphanes—they provide an atom-efficient and robust route to creating functionalised phosphines. Accordingly, further exploration of their reactivity, particularly in their coordination to transition metals is advisable. The potential to coordinate both through the phosphorus and selenium (or sulfur) atoms is highly unusual and thus would be important to confirm.

6.3.2 Diphosphanes – future work

Since the characterisation of diphosphane stability and metathesis has been largely completed, the majority of the future work associated with this sub-project concerns the synthesis of functionalised diphosphanes, in order to bind a diphosphane moiety within a polymer.

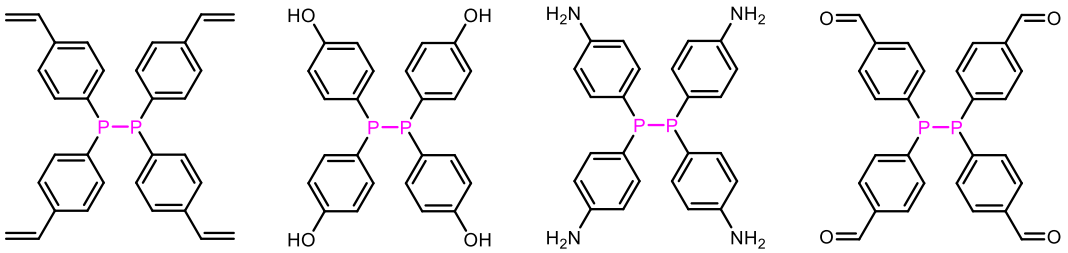

Figure 6.5. The target functional diphosphanes discussed in Chapter 5: **7** – styrene-, **8** – phenol-, **9** – aniline- and **10** – benzaldehyde-functionalised diphosphanes. None of which have been previously reported.

Of the target functionalised diphosphanes discussed in Chapter 5 (Figure 6.5), **8** the phenolic diphosphane, seems likely to be intrinsically unstable due to the mildly acidic phenol moieties. **7**, the styrenyl diphosphane certainly seems a more viable candidate. When the synthesis of **7** was first tested, the author was unaware of the simple Mg-coupling method of P,P-formation. Accordingly, with hindsight, it seems quite likely that **7** could be isolated via such a reaction, since the chlorophosphine precursor (**7b**) has been cleanly prepared. Whether this compound could be successfully incorporated into a polymer network remains unclear. With the knowledge that diphosphane metathesis is radical-mediated, it is possible that the diphosphane would be cleaved during incorporation with radical polymerisations—it is these processes, such as through polymerisation with acrylates, which would be the most straightforward way of integrating **7** into a polymer network, Scheme 6.3. Nevertheless,

there is a chance that a significant proportion of **7** would remain intact in such a polymerisation; this is certainly worth exploring.

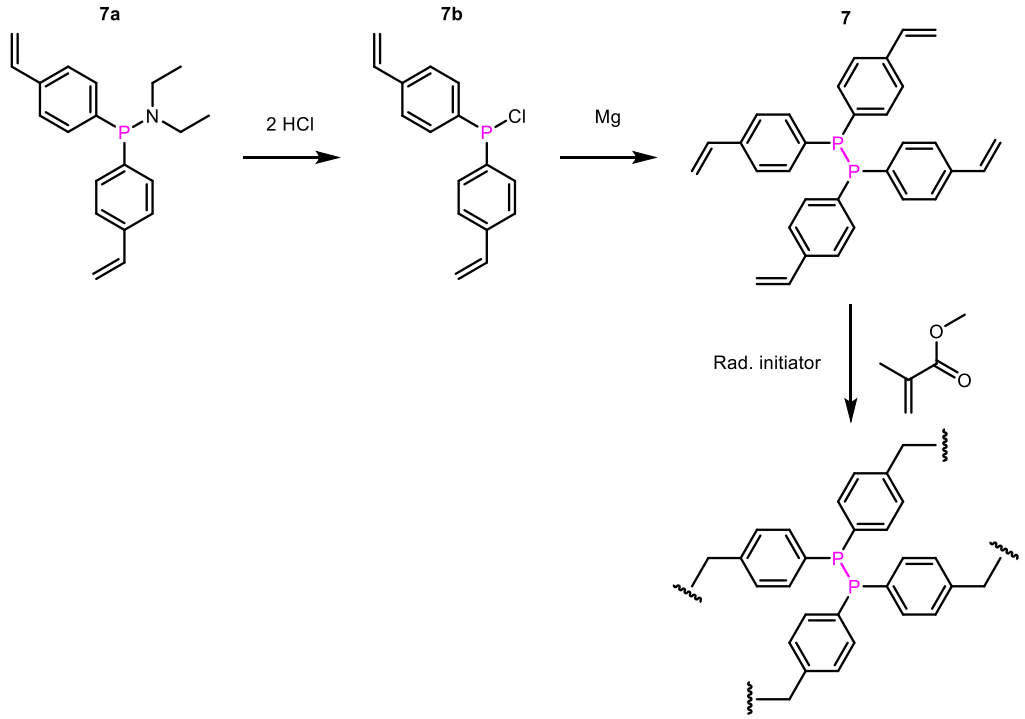

Scheme 6.3. A revised synthesis and method of polymerising **7** with acrylate chemistry.

Of the literature compounds referred to in Chapter 6, whose syntheses were not attempted, **2** and **6** are the most viable candidates, Figure 6.6. The tetraphosphane **2**,[4] could feasibly be reduced at the nitrile positions using SmI_2 (to primary amines),[5] and then reacted into a polymer network, perhaps through epoxy chemistry. However, it is unclear if the cyclotetraphosphane unit would have the same reactivity as aromatic diphosphanes. Compound **6** is perhaps the most promising candidate,[6] as a relatively simple (though non-aromatic) diphosphane, it would be expected to have a similar susceptibility to metathesis as those compounds discussed in the homometathesis study. P–Cl bonds are generally highly reactive and would be expected to react with a range of nucleophiles, including amines and organometallic species.

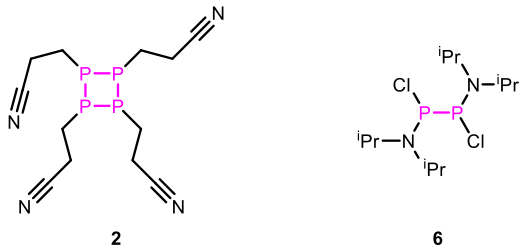

Figure 6.6. Literature examples of P–P-containing species with pendent functional groups.

Multiple potential synthetic schemes for the preparation of **9** and **10** were conceived, though none were tested. These are some of the most desirable targets discussed in Chapter 5, particularly the primary amines (of **9**), which would be expected to easily crosslink epoxies. A proposed synthesis of **9** is outlined in Scheme 6.4. More labile protecting groups, including BOC/FMOC units, were deemed likely to be cleaved during one or more of the proposed reaction steps. The required tolerance of any functional group (for diphosphane synthesis) that is particularly challenging to achieve, is tolerance to organometallic reagents such as Grignards and organolithiums. One such group is the benzylic groups proposed. However, these groups are generally only removable using H_2 with Pd/C—the stability of diphosphanes in such an environment is unknown.

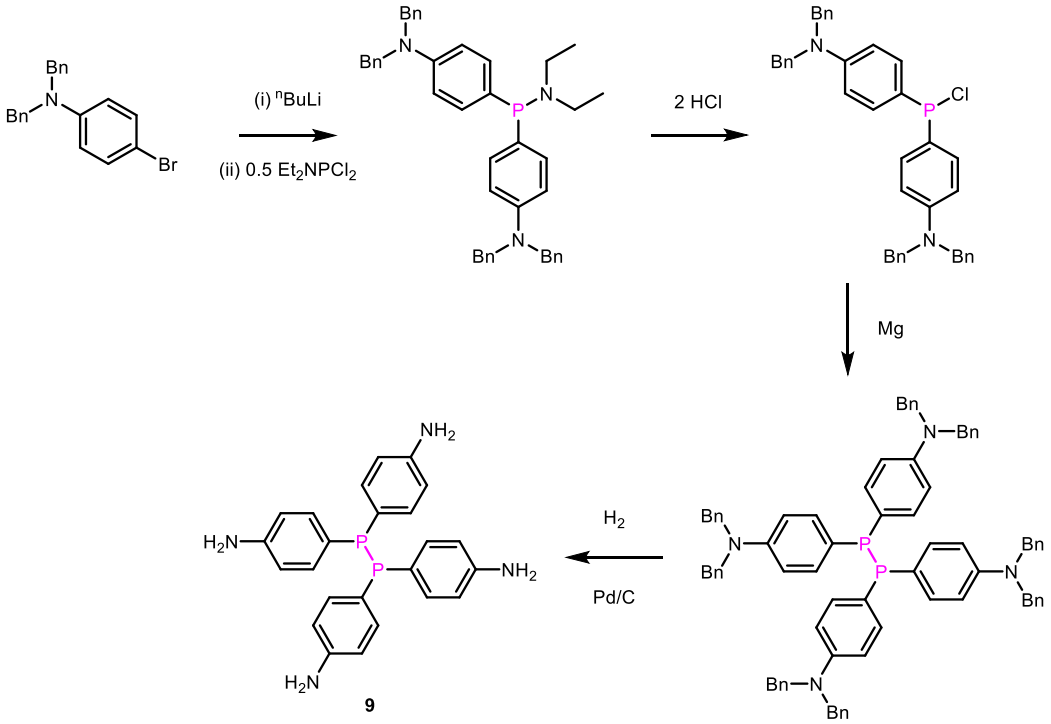

Scheme 6.4. The proposed synthesis of the tetra-aniline diphosphane **9** using benzyl protecting groups.

The proposed synthesis of **10** may have a higher chance of success, Scheme 6.5; the aldehyde moieties could feasibly be incorporated into a polymer network via imine formation (reaction with amines), though this is often acid-catalysed, which would not be feasible here. Alternatively, the reaction with an organometallic reagent, such as Grignard (producing a 2° alcohol) could be exploited. In this proposed synthesis, since the acetals should be stable to the organometallics, the most likely source of problems is the HCl (chlorination) step—the standard method of removing acetals is in aqueous acid. Nevertheless, since this process should be completely anhydrous the acetals should not be cleaved.

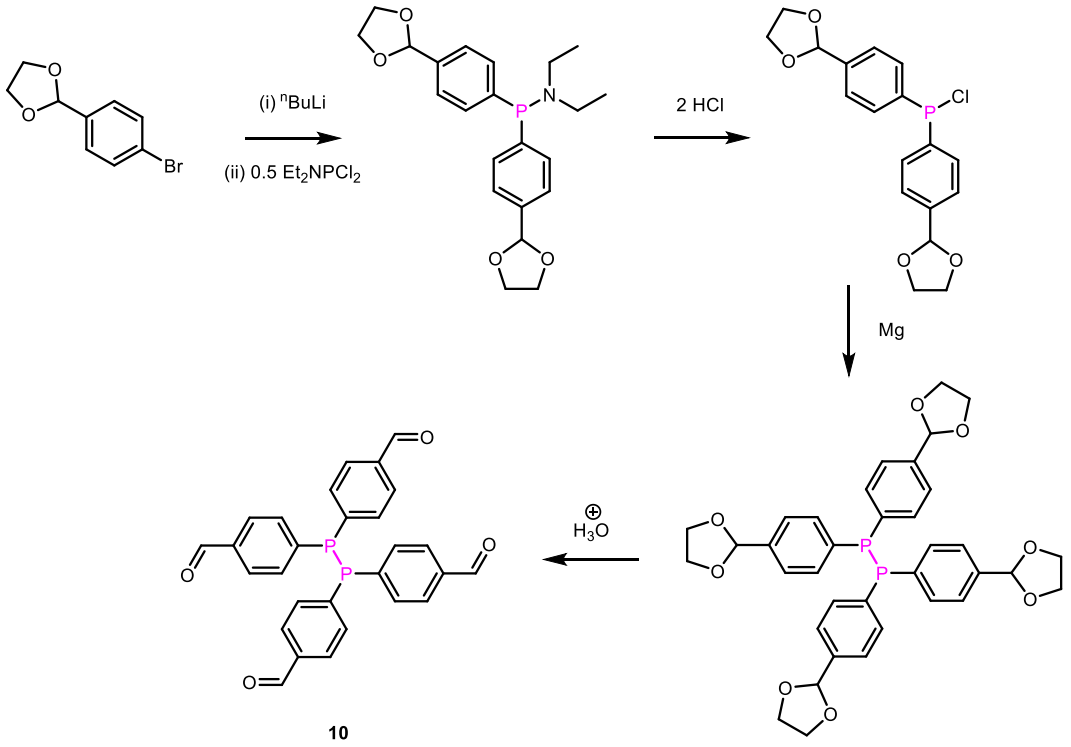

Scheme 6.5. The proposed synthesis of the tetra-aldehyde **10**.

In addition to the major challenges in preparing functional diphosphanes, the secondary challenge with implementing this exchange in polymers is the oxygen sensitivity of these species. Diphosphanes readily oxidise in air. Although this was not discussed in detail during Chapter 5, there are no literature examples of metathesis occurring in the oxidised (P(V)–P(V)) form of diphosphanes. Indeed, in the few experiments performed in the course of this work, no reaction was observed between the diphosphanes shown in Scheme 6.6. Despite this, due to steric shielding, it would be expected that diphosphanes would be considerably more resilient to oxidation when bound within polymer networks. Moreover, radical scavenger species such as TEMPO were shown in Chapter 5 to inhibit diphosphane oxidation and thus could be used as polymer additives to further improve oxidative stability in P–P polymers. This should be the subject of future research if diphosphanes are successfully integrated within polymers.

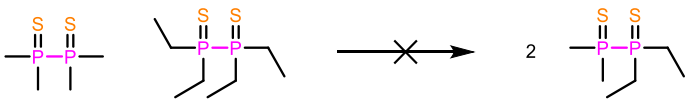

Scheme 6.6. No metathesis reaction is observed between P(V)–P(V) diphosphanes.

6.4 Concluding remarks

In this thesis the author has attempted to demonstrate the value of covalent adaptable networks (CANs) in fibre-reinforced polymer composites (FRPs), particularly with respect to their potential to improve sustainability. These improvements may be manifested through a combination of phenomena which serve to increase composite lifetime (via straightforward repair) and reduce waste (through novel manufacture methods and end-of-life recycling). These concepts were explored with a new generation of Diels-Alder materials prepared in collaboration with TNO Eindhoven (Chapters 2 and 3). Although presently these materials exhibit some mechanical limitations, namely brittleness, they clearly demonstrate the value that CANs may contribute to the future of FRPs. It is hoped that future iterations of these materials may find a useful compromise between mechanical performance and dynamic activity.

In Chapters 4 and 5, new dynamic chemistries were explored with a view to their eventual development into functional CANs. In Chapter 4, several new diselenides were prepared and initial investigations into their application within polymers explored. With some refinement concerning polymerisation method, and characterisation using DMA, some of these materials have potential significance in the field of CANs, with the epoxy (EpxSeSe1) prepared from the dialkylamino diselenide (AADS) a particularly promising candidate. In Chapter 5, a new avenue within dynamic chemistry was explored using diphosphanes (P–P bonds). As a result of this research, the exchange reaction between these species is now well-understood and due to their highly dynamic behaviour, diphosphanes could have significance in the field of dynamic covalent chemistry.

6.5 References

1 B. K. Hughes, W. A. Braunecker, A. J. Ferguson, T. W. Kemper, R. E. Larsen and T. Gennett, *J. Phys. Chem. B*, 2014, **118**, 12541–12548.

2 X. Wang, J. Jin and M. Song, *Carbon*, 2013, **65**, 324–333.

3 A. Ruiz de Luzuriaga, R. Martin, N. Markaide, A. Rekondo, G. Cabañero, J. Rodríguez and I. Odriozola, *Mater. Horizons*, 2016, **3**, 241–247.

4 W. A. Henderson, M. Epstein and F. S. Seichter, *J. Am. Chem. Soc.*, 1963, **85**, 2462–2466.

5 M. Szostak, B. Sautier, M. Spain and D. J. Procter, *Org. Lett.*, 2014, **16**, 1092–1095.

6 R. B. King and N. D. Sadanani, *J. Org. Chem.*, 1985, **50**, 1719–1722.